ornl

ORNL/TM-12220

OAK RIDGE NATIONAL LABORATORY

MARTIN MARIETTA

Fuel-Coolant-Interaction Modeling and Analysis Work for the High Flux Isotope Reactor Safety Analysis Report

R. P. Taleyarkhan
V. Georgevich
C. W. Nestor
S. J. Chang
J. Freels
U. Gat
B. L. Lepard
R. C. Gwaltney
C. Luttrell
J. Kirkpatrick

MANAGED BY
MARTIN MARIETTA ENERGY SYSTEMS, INC.
FOR THE UNITED STATES
DEPARTMENT OF ENERGY

ORNL/TM-12220

500
2

FUEL-COOLANT-INTERACTION MODELING AND ANALYSIS WORK FOR THE HIGH FLUX ISOTOPE REACTOR SAFETY ANALYSIS REPORT

R. P. Taleyarkhan
V. Georgevich
C. W. Nestor
S. J. Chang
J. Freels
U. Gat
B. L. Lepard
R. C. Gwaltney
C. Luttrell
J. Kirkpatrick

July 1993

Prepared by the
OAK RIDGE NATIONAL LABORATORY
Oak Ridge, Tennessee 37831
managed by
MARTIN MARIETTA ENERGY SYSTEMS, INC.
for the
U. S. DEPARTMENT OF ENERGY
under Contract No. DF-AC05-84OR21400

ACRONYMS AND INITIALIZATIONS

ANS	Advanced Neutron Source
ASME	American Society of Mechanical Engineers
CVOID	Ratio of Volume of Vapor to Volume of Liquid
CCFL	Counter-Current-Flow Limitation
DOE	Department of Energy
ETD	Engineering Technology Division
FCI	Fuel Coolant Interaction
HFIR	High Flux Isotope Reactor
LWR	Light Water Reactor
MPa	Megapascals
ORNL	Oak Ridge National Laboratory
PRA	Probablistic Risk Analyses
RCS	Reactor Coolant System
RPV	Reactor Pressure Vessel
RRD	Research Reactor Division
RSS	Reactor Safety Study
SAR	Safety Analysis Report
SNL	Sandia National Laboratory

TABLE OF CONTENTS

TABLE OF CONTENTS (continued)

LIST OF TABLES

LIST OF FIGURES

LIST OF FIGURES (continued)

LIST OF FIGURES (continued)

LIST OF FIGURES (continued)

LIST OF FIGURES (continued)

LIST OF FIGURES (continued)

LIST OF FIGURES (continued)

LIST OF FIGURES (continued)

ACKNOWLEDGMENTS

Several individuals contributed to the timely completion of the work presented in this report. Consulting advice and transmittal of several computer codes by M. L. Corradini of the University of Wisconsin and E. Hertell of Sandia National Laboratory are acknowledged. Consulting advice provided by Professor M. Z. Podowski regarding core melt progression is also acknowledged. Insights gained from the many interactions with members (Lap Cheng, Jim Close, Richard Moore, Phil Ellison, Lee Hyder, Kevin O'Kula, Lloyd Nelson, Marshall Berman, Dave Beck, Lou Baker, and Dae Cho) of the national committee, "Fuel-Coolant-Interactions Issues Resolution for U-Al Fueled Reactors," played an important role. The assistance provided by Doug Leader of Savannah River Laboratory for manufacturing and shipment of the depleted High Flux Isotope Reactor fuel material to enable performance of experiments is greatly appreciated.

Work for this report was conducted as a significant team effort. Individuals whose technical work has been included in this report are: J. Freels, S. Chang, R. Gwaltney, J. Kirkpatrick, C. Luttrell, C. W. Nestor, V. Georgevich, and R. P. Taleyarkhan.

Finally, the authors gratefully acknowledge the sponsorship, critique, management, and active support for this work provided by Dave Cook, Uri Gat, Lamar Lepard, and George Flannagan of Oak Ridge National Laboratory's Research Reactor Division.

EXECUTIVE SUMMARY

This progress report provides an overview perspective on the status of Fuel-Coolant-Interaction (FCI) issues research at the Oak Ridge National Laboratory's (ORNL's) High Flux Isotope Reactor (HFIR).

In Sect. 1, the general subject of steam explosions is introduced. A brief historical background and a description of the necessary short- and long-term task plan development efforts for effective closure of this important safety issue for HFIR are given. Short-term aspects deal with FCI issues experimentation, modeling, and analysis for the flow-blockage-induced steam explosion events in direct support of the Safety Analysis Report (SAR) that was completed in October 1992. Long-term aspects deal with addressing FCI issues resulting from other accidents in conjunction with issues dealing with aluminum ignition, which can result in an order of magnitude increase in overall energetics.

In Sect. 2, the specific aspects dealing with problem formulation, mathematical modeling, and computer code simulation for the various phases of steam explosion analyses are described. Core melt initiation aspects, which use the RELAP5 code, are described. The evaluation of core melt propagation and melt superheat are described, with related efforts concerning structural failure of individual plates. The development and use of ADINA code models for the purpose of determining plate failure are introduced.

Core debris coolability, heatup, and melting/freezing aspects have been studied via use of the two-dimensional melting/freezing analysis code 2DKO, which was also benchmarked with MELCOR code predictions. Descriptions are provided for the UWHM, UWHUGO, FCIMOD, and CTH computer codes that have been implemented on the IBM RISC/6000 workstation. These codes are used for studying steam explosion energetics from the standpoint of evaluating bounding loads by thermodynamic models or

best-estimate loads (with fluid-structure-interactions) from one- and two-dimensional simulations of steam explosion energetics.

Models were developed for evaluating failure characteristics of the HFIR vessel using the principles of fracture mechanics in conjunction with finite-element structural mechanics codes such as ADINA. This model formulation is described. A simple conservatively scoped model was also developed for determination of failure characteristics of bolts in the HFIR top-head and is also described in Sect. 2. Finally, a description is given for a one-dimensional mathematical model, which was developed for evaluating missile dynamics (viz., top head missile evolution through the large reactor pool). This model accounts for viscous dissipation, virtual mass effects, and material inertia.

Section 3 provides the results of analysis work that has been done for HFIR. Previous HFIR accident analysis work for the evaluation of the degree of core melt fraction from small and large flow blockages had determined these amounts to be about 10% and 24% respectively. These fractions were evaluated on the degree of fuel and coolant heatup necessary for causing a one-dollar reactivity change before the control system caused a scram to occur. A renewed attempt to conservatively evaluate with simple postulate (of plate collapse upon melting onto adjacent plates) and hand calculations led to the conclusion that a maximum of 14% of core plates would melt from a localized melting event. Current HFIR analysis using RELAP5 indicated that fuel melting would not occur until more than 92% of the flow channel area for multiple channels was blocked over a period of 0.1 s. For only one flow channel blocked, no fuel melting will occur. Although the RELAP calculations are one-dimensional in nature, they do account for two-phase flow effects. As such, they represent the best-effort thermal-hydraulic analyses for evaluation of fuel heatup from flow blockages for HFIR.

The analysis of aspects concerning core melt propagation indicated that several physical scenarios can be postulated that can cause fuel melting damage to propagate

when a certain region of the HFIR core experiences fuel melting from a core flow blockage. Thermal hydraulic conditions for these various scenarios have been developed for use in evaluating fuel plate structural response using the ADINA code. It was determined that plate collapse from buckling, because of increased coolant velocity through unblocked channels will not occur. The degree of melt propagation from localized steam explosions was analyzed using a combination of results from ADINA and FCIMOD.ORNL calculations for plate structural response from localized pressure spikes. These results indicated that in-core steam explosions caused by individual fuel plate melting would have a high likelihood to generate sufficiently energetic pressure pulses to cause adjacent plate collapse and, therefore, melt propagation to occur.

Debris heatup calculations using 2DKO indicate that a significant potential exists for melt superheat to occur if the core debris melts and relocates to the lower shield plug region. This potential is a function of several parameters, viz. debris power density upon release of fission products, aluminum ignition, amount of debris discharged, etc. These calculations indicate that the potential for an energetic steam explosion over the shield plug region of the HFIR vessel cannot be overlooked.

The preliminary analysis of steam explosion energetics from thermodynamic models resulted in pressurization levels that varied from 60 mega pascals (MPa) to several hundred MPa with the conversion ratio ranging from low values to about 45%. Significant reductions were observed for the same conditions when a one-dimensional best-estimate simulation was conducted using the FCIMOD.ORNL code. Results of FCIMOD.ORNL calculations were used to generate energy source term rate values for multidimensional CTH calculations. CTH calculations in conjunction with results of structural response calculations based on fracture mechanics determined that for thermally driven steam explosions, the HFIR confinement would be able to withstand loads generated from melting of about 65% of the core. With about 65% of the HFIR core participating in a thermally-driven steam explosion consisting of about 65 MJ of

energy, loads on the upper head would be enough to cause the bolts to shear off and cause a missile to form and reach the confinement roof .ssile dynamics calculations were conducted parametrically, which showed that the entire top head would need to be accelerated with an initial velocity of about 35 m/s to cause it to rise up to the HFIR confinement boundary. From a conservative standpoint, it is judged that a thermally-driven steam explosion with more than 65 MJ of thermal energy insertion over a period of a few milliseconds would be needed to cause a sufficiently energetic missile with a capacity to cause confinement failure.

Based upon the front-end work evaluating the level of core melting from flow blockage events, it is considered highly unlikely that 65% or more of the HFIR core can melt and materially participate in a steam explosion event. Further, based upon past experiences with uranium-aluminum fueled reactors undergoing fuel melting accidents from flow blockages, aluminum ignition simultaneous with steam explosions was assumed to be an unlikely event for HFIR SAR purposes. This aspect is currently under research for most of DOE reactors and also for HFIR. It is expected that these studies will demonstrate the unlikely nature of chemical reactions occurring on an explosive time scale in HFIR to significantly alter the dynamic characteristics demonstrated so far. Therefore, based on the available evidence, it is judged that the HFIR pressure vessel and top head structure will be able to withstand loads generated from thermally driven steam explosions initiated by any credible flow blockage.

Section 4 provides a brief description of open issues, the resolution of which would aid in considerably improving the analyses of FCI events in HFIR. The triggering characteristics of HFIR fuel need to be evaluated based upon the unique characteristics of U_3O_8-Al cermet-type fuel, which may indicate a very low propensity of undergoing steam explosions. The aspect of core-melt progression during FCI events needs to be looked at more carefully to evaluate more accurately the degree to which damage can propagate.

It was mentioned earlier that pressure loads caused from localized melting events have the capacity to cause adjacent plates to fail. What was not possible to evaluate is the degree to which propagation can occur and the effect of such a propagation mode. A third area needing further study relates to steam explosions in the shield plug region. Because of time constraints, it was not possible to look into this mode of FCI occurrence, and the effects of resulting energetics on vessel failure and missile generation. Also, as mentioned in Appendix D, the FCIMOD calculations were conducted with a model essentially set up for analyzing FCI events in power reactors. For FCI events in a closed-system (i.e., full of water) such as HFIR, the feedback mechanism of the elastic system boundaries needs to be accounted for. Finally, a critical open issue that needs to be resolved deals with the degree of aluminum-water reactions during steam explosion events in HFIR for events that are not driven by large quantities of reactivity insertion (as for SPERT, BORAX, and SL-1 incidents). It is expected that scoping studies for each of these areas will lead to significant confirmation for the various assumptions made in making the safety case for HFIR from FCI events.

A review study was conducted on FCI analysis for HFIR in the past, as documented in ORNL-3573. This is described in Appendix A. Several shortcomings in the past analysis are described, and recommendations offered. Overall, it was found that the authors of ORNL-3573 did a fairly thorough job based upon the information they had.

Appendix B provides a description of thermal-hydraulic conditions, which were evaluated for the postulated scenarios that may lead to fuel melt propagation during fore flow blockage events in the HFIR. Appendix B provides supporting information for Appendix D related to fuel plate temperature distributions during accident conditions.

Appendix C describes the analysis conducted with RELAP5, which attempts to evaluate from a best-estimate standpoint the likelihood of melting initiation. As mentioned previously, even though the RELAP5 calculations are based on a

one-dimensional model, the effects of phase change and axially distributed heat transfer variation with time are accounted for.

Appendix D provides a summary of the analyses performed in conjunction with fuel plate failure initiation and propagation. Various different boundary conditions were studied to develop failure envelopes to be used with loads determined using FCIMOD.ORNL calculations. The analyses for fuel plate buckling from increased velocities in channels is also shown. As mentioned previously, the analysis shows that for the range of velocities expected during flow blockage events, fuel plate buckling instabilities will not occur.

Appendix E provides a summary of the modeling and analysis performed to evaluate debris coolability characteristics for steam explosion calculations in the shield plug region.

Appendix F provides a summary of the modeling and analysis work performed for evaluating energetics calculations with HM, BH, and FCIMOD.ORNL codes. Variation of energetics with variations in ambient pressure and temperature, fuel temperature, thermal penetration depth, and also in the inertial constraint are described. In addition, FCIMOD.ORNL calculations are presented for evaluation of pressure pulse dynamics from localized explosions which may be caused from fuel plate melting in blocked channels. These results (i.e., from localized loads) were evaluated to judge the likelihood of damage propagation in the core region.

Appendix G provides a summary of the modeling and analysis work performed for evaluating shock wave physics, phase transformation, multi-material motion, and fluid-structure interactions with CTH. Various cases evaluated with CTH with varying levels of sophistication in the system geometry are described here, along with sensitivity studies conducted with varying levels of energy level and rate insertion.

Appendix H provides a summary of the modeling and analysis performed to evaluate the failure characteristics of the HFIR vessel using the principles of fracture

mechanics. Results are presented from a conservative perspective using ASME guidelines, as well as from a probabilistic view. Appendix H also provides a summary of the work conducted to evaluate failure characteristics of the bolts on the top head of the HFIR.

Appendix I provides a summary of the modeling and analysis work performed to evaluate missile energetics calculations.

Finally, an experimental effort has been undertaken to investigate the propensity of molten HFIR fuel at various levels of superheat to undergo steam explosions and to evaluate propagation and energy conversion aspects. These tests are being conducted at the University of Wisconsin in conjunction with ORNL efforts for the Advanced Neutron Source (ANS) Project. In addition to these tests, mathematical models are being developed to evaluate the triggering characteristics of HFIR fuel. The model for triggering characteristics will take into account the effects of material viscosity, surface tension, and crust formation. Aspects dealing with aluminum ignition will also be addressed. It is expected that the results of these tests and modeling efforts will provide a basis for using lower values for thermal-to-mechanical energy conversion during steam explosions, and also demonstrate the low propensity of triggering and ignition onset for HFIR fuel.

ABSTRACT

This progress report provides an overview perspective on the status of Fuel-Coolant-Interaction (FCI) work conducted for Oak Ridge National Laboratory's (ORNLs) High Flux Isotope Reactor (HFIR) Safety Analysis Report (SAR).

A brief historical background and a description of short- and long-term task plan development for effective closure of this important safety issue for the HFIR are given. Short-term aspects deal with FCI issues experimentation, modeling, and analysis for the flow-blockage-induced steam explosion events in direct support of the SAR. Long-term aspects deal with addressing FCI issues resulting from other accidents in conjunction with issues dealing with aluminum ignition, which can result in an order of magnitude increase in overall energetics.

Problem formulation, modeling, and computer code simulation for the various phases of steam explosions are described. The evaluation of core melt initiation, propagation, and melt superheat are described. Core melt initiation and propagation have been studied using simple conservative models as well as from modeling and analysis using RELAP5. Core debris coolability, heatup, and melting/freezing aspects have been studied by use of the two-dimensional melting/freezing analysis code 2DKO, which was also benchmarked with MELCOR code predictions. Descriptions are provided for the HM, BH, FCIMOD, and CTH computer codes that have been implemented for studying steam explosion energetics from the standpoint of evaluating bounding loads by thermodynamic models or best-estimate loads from one- and two-dimensional simulations of steam explosion energetics. Vessel failure modeling and analysis was conducted using the principles of probabilistic fracture mechanics in conjunction with ADINA code calculations. Top head bolts failure modeling has also been conducted, where the failure criterion was based upon stresses in the bolts exceeding the material yield stress for a given time duration. Missile transport modeling and analysis was

conducted by setting up a one-dimensional mathematical model that accounts for viscous dissipation, virtual mass effects, and material inertia.

From a conservative standpoint (but assuming the absence of aluminum ignition on an explosive time scale), it is judged that a thermally driven steam explosion with more than 65 MJ of thermal energy insertion in the core region over several milliseconds would be needed to cause a sufficiently energetic missile with a capacity to cause confinement failure. This amounts to approximately 65% of the HFIR core mass melting and participating in a steam explosion event. Based on front-end work to evaluate the level of core melting from flow blockage events, it is considered that an upper bound value for the fraction of HFIR core melting and propagation during flow blockage events amounts to approximately 24%. It is judged that the HFIR pressure vessel and top head structure will be able to withstand loads generated from thermally driven steam explosions initiated by any credible flow blockage event.

An experimental effort has been implemented to investigate the propensity of molten HFIR fuel at various levels of superheat to undergo steam explosions and to evaluate propagation and energy conversion aspects. These tests are being conducted at the University of Wisconsin in conjunction with ORNL modeling and analysis efforts.

1. INTRODUCTION

1.1 GENERAL ASPECTS

It is important to recall that the very idea of an energetic steam explosion stems principally from experiences with destructive steam explosions in plate-type, aluminum-clad research reactors undergoing prompt critical nuclear excursions. This evidence includes the SL-1 incident[1] and both the BORAX-1 and SPERT-1 destructive tests.[2,3] The characteristics of the High Flux Isotope Reactor (HFIR) core closely parallel those of the previously mentioned reactor cores; therefore, it is important to evaluate the threat to pressure boundaries from steam explosions in HFIR. For power reactors, this issue gained initial prominence through the so-called Reactor Safety Study (RSS) or WASH-1400.[4]

In 1975, the RSS concluded that, based upon probabilistic risk analyses (PRA), Light Water Reactor (LWR) core-meltdown accidents were the dominant risk contributors to public health and safety. One prime reason for this conclusion was that containment failure and subsequent radioactivity release could be caused by steam explosions, also commonly called Fuel-Coolant-Interactions (FCIs). The analytical model used to calculate the rupture of pressure vessels in the RSS was based principally on extrapolated experience from small test reactors undergoing steam explosions (that is, BORAX and SPERT tests and the SL-1 incident). Furthermore, industrial experience with steam explosions caused by accidental spills of molten material into water in metal foundries and in the pulp and paper industry were cited as general support that large-scale steam explosions could occur.

The RSS gave rise to an extensive experimental and analytical research program that has evolved over the past 15 yrs. This program has led to a greater understanding of the conditions required for large-scale steam explosions to occur. These studies have

generally concluded that steam explosions are physical phenomena that result from an extremely rapid thermal energy transfer between two intimately mixed liquids at different temperatures. The temperature of the hotter liquid, usually a molten metal or refractory material, must be far above the normal boiling point of the second liquid to produce explosive vaporization rates that generate pressures and shock waves characteristic of an explosion. However, it is important to note that even though steam explosions result in high pressures, they are quite different from chemical "detonations." For a description of the salient differences see Ref. 5. To properly introduce the modeling and analytical material presented in subsequent sections, it is important to appreciate the several stages of steam explosions. These stages are:

1. Fuel coolant mixing. The molten fuel and liquid coolant become intermixed on an explosive time scale, whereas the heat-transfer mode is relatively quiescent. This process provides enough surface area of contact between the molten fuel and coolant to sustain the required high heat-transfer rates.
2. Triggering. The fuel and coolant are brought into near liquid-liquid contact. Thereafter, rapid heat transfer begins. Triggers can be spontaneous or from external stimuli, such as exploding wires or minidetonators.
3. Explosion propagation. The heat-transfer process rapidly escalates as more of the molten material is fragmented and as more high-pressure coolant vapor is generated. This phenomenon ensures that a sizable fraction of the available explosive work is used. Note that at this stage, significant, potentially destructive, pressure pulses are generated in the millisecond duration range.
4. Expansion. The high-pressure vapor expands against the surroundings with the potential for destructive mechanical work, such as rupturing the reactor pressure vessel (RPV).

1.2 TASK PLAN DEVELOPMENT

The task plan for addressing FCI- related issues for HFIR is described in several stages. First, a brief background is given to highlight the many associated phenomena and initiating accidents that need to be accounted for in the closure process. Thereafter, a brief description is given on the consideration of special effects that potentially can cause significant changes in perceptions and predicted loads.

Descriptions for the various elements of the task plan follow.

1.2.1 Background

The study of FCIs, of which steam explosions are a part, comprise specific efforts that are not directly addressed by other HFIR safety analysis efforts. Explosive severe accident analysis and the FCI issue in particular are conventionally separated from normal severe accident analysis tasks related to the PRA because of its significance and difficulty of resolution. Several aspects need to be considered for effective closure of the FCI-related issues for HFIR. These aspects are described briefly in subsequent paragraphs.

1.2.1.1 Initiating Accidents

The initiation of a steam explosion requires the existence of molten aluminum in a steam-water environment. Hence, the obvious initiating accident scenarios will be those that cause significant core melting in the presence of water or those in which molten core debris relocates into a pool of water. Several accident conditions can possibly lead to core melting in the presence of water. Based upon recommendations from Oak Ridge National Laboratory (ORNL's) Research Reactor Division (RRD), for in-vessel HFIR FCI analysis three different accident scenarios will be considered for the overall closure

process. Only the first one was addressed to the extent possible for the Safety Analysis Report (SAR). These scenarios are:

1. Core Flow Blockage Events (only ones for HFIR SAR consideration),
2. Large-Break LOCA Events, and
3. Reactivity Excursion Events.

Selected aspects related to each of the above accident events will need to be evaluated with a focus on the principal parameters on which steaming, hydrogen production, and fission product release amounts depend. Table 1.1 lists these important parameters. To determine these parameters, various levels of sophistication can be applied related to core melt progression. It was recommended that a staged approach should be followed, which uses simple techniques at first to evaluate such important parameters as maximum melt temperatures and material relocation, to judge whether predicted loadings on system boundaries can be tolerated. Improved sophistication should be introduced on an as-needed basis to reduce conservatisms, in conjunction with approaches used and methods developed elsewhere.

Initiating accident scenarios for ex-vessel events should be considered only if circumstances indicate that fuel can relocate outside the reactor coolant system (RCS). An estimate should be made of this possibility and FCI analyses conducted thereafter as necessary.

1.2.1.2 FCI Loads and System Response

In essence, the resolution of FCI-related issues for HFIR will entail showing that loads generated are acceptable for a variety of accident scenarios. The loads to be considered are:

1. Pressure pulses from steam explosions that follow after the mixing and triggering phases.
2. System pressurization and structural response resulting from the expansion phase when the high pressure steam expands. This phase can also lead to energetic slugs or missiles if a void volume is present above the explosion zone.
3. Possible detonation loads resulting from hydrogen generation as a result from exothermic aluminum-water reactions.
4. Fission product inventory release in various system compartments where steam explosions can possibly occur.

The evaluation of loads from a steam explosion can be conducted in several ways, ranging from the use of empirical models to the use of fairly sophisticated codes. Section 2 of this report provides a description of the various tools that can be used for modeling and numerical simulation. Again, the evaluation of structural response can also be performed by the use of simple correlations, solutions to analytical derivations, and codes such as ADINA.[6] A review of available techniques and an investigation for the sources of relevant information have already been completed for a scoping study that was done for the Advanced Neutron Source (ANS). The study included evaluations for pressure pulses, system pressurization, and structural response. Results have been documented in a report entitled "Steam Explosion Safety Considerations for the ANS Reactor at ORNL," ORNL/TM-11324, by R. P. Taleyarkhan.[5]

To evaluate loads from possible hydrogen detonation or deflagration resulting from FCI events, amounts of hydrogen generated should be used in conjunction with containment transport code (such as MELCOR)[7] calculations. These code calculations would give an indication of whether detonatable concentrations can be reached in the first place. Thereafter, wave codes such as CTH (see Sect. 2) or TNT-equivalence techniques

may be used (as done for the previous HFIR SAR, ORNL-3573)[8] to evaluate structural response characteristics.

The determination of fission product inventory release during FCI events should be coupled with evaluations from mathematical models for prediction of such releases from HFIR fuel and TREAT[9] data. Thereafter, containment transport codes should be used for evaluation of off-site release amounts.

1.2.2 Consideration of Special Effects

Certain effects that can have a pronounced influence on FCI-related issues require special attention. Special effects related to HFIR are judged to be:

1. Behavior of HFIR fuel and,
2. Onset of aluminum ignition.

Currently no information exists on the propensity of molten U_3O_8-Al fuel mixtures to undergo steam explosions. It is well-known that the triggering energy necessary for initiating steam explosions in different mixtures can range from essentially none (that is, spontaneous explosions) to extremely large (that is, more than the energy content of the molten mixture). Because of its cermet composition, it is likely that HFIR fuel may require unrealistically large energy levels to initiate steam explosions in the first place. As a consequence, ORNL's RRD, in conjunction with the Engineering Technology Division (ETD), has put in place an experimental program at the University of Wisconsin to evaluate the steam explosion triggerability and propagation characteristics of HFIR fuel. However, in the absence of such information the assumption has to be made that sufficient trigger energies will be available to initiate a steam explosion.

Another effect that can have a pronounced effect on loads generated from steam explosions is the aspect of simultaneous aluminum ignition. As is well-known, this

process can add up to 17 MJ/kg of aluminum consumed and also cause significant amounts of hydrogen generation. Recent Sandia National Laboratory (SNL) tests have indicated the possibility of aluminum ignition at temperatures as low as 850°C. It is generally accepted that this is a scale dependent process wherein the ignition threshold temperature drops with increasing aluminum mass. This issue is still under debate, and it is being followed carefully. For HFIR, it is clear that this aspect will need to be taken into account in varying degrees, depending upon the maximum fuel temperature and the aluminum particle sizes evaluated from the melt progression analyses.

1.3 DEVELOPMENT OF PLAN FOR CLOSURE OF FCI-INDUCED THREATS IN HFIR ISSUE

With the above background, a task plan was developed for attaining closure of the FCI issue for HFIR. The basic strategy for attaining closure is outlined in Fig. 1.1 As noted, the closure process consists of first determining goals for acceptability. It is recommended that the initial acceptability goal for HFIR is that for conceivable steam explosions occurring in-vessel, the reactor pressure vessel and maybe even the RCS boundary will be able to contain the pressurization loads. Such a goal would then build on what was conducted previously for the HFIR accident analysis report.

1.3.1 Task 1

Thereafter, scenarios or events would be identified, and melt conditions at the inception of steam explosions would be evaluated using conservative assumptions (similar to that documented in the HFIR accident analysis report). This task would include a review of past ANS and HFIR work for relevance, applicability, and further development. Estimates would be made for pressure pulse magnitudes, energetic missile evolution, and system pressurization from steam explosion events. Estimates would also be made for structural response of the RCS, especially the reactor pressure vessel. If it is

determined that the loads are sustainable, the in-vessel FCI-related issue may be considered closed. This piece of work would constitute Task 1 of the task plan, and is the essence of what is presented in this report (see Sects. 2 and 3).

1.3.2 Task 2

If the immediate acceptability goal is not met from the above-mentioned conservative analysis, two avenues may be open. First, the acceptability goal could be revised to prove that the confinement does not get breached, or if it does, that off-site dose consequences are not exceeded. Thereafter, the confinement response would be evaluated using the results of the first phase of the task plan. This could be done in conjunction with use of accident management techniques that may involve procedural or structural modifications. Secondly, one could initiate efforts to reduce the conservatisms inherent in the methods and analysis bases used for Task 1. Once again, if acceptability goals are achieved, then closure would be obtained.

Technical aspects to be considered in this task would entail the setting up of models for evaluation of melt progression phenomena such as debris relocation, debris dispersal, and debris mixing (with water). The work in this area would include more sophisticated structural ablation calculations than those performed for Task 1 (and described in Sects. 2 and 3 of this report) to evaluate the likelihood of the HFIR core debris to relocate outside of the RCS (e.g., to the sub-pile room).

1.3.3 Task 3

If closure is not obtained from Tasks 1 and 2 mentioned above, it may become necessary to reduce conservatisms regarding triggering, conversion efficiency and ignition by selected experimentation to support analytical assumptions. The aspects of confinement failure from missile penetration or ex-vessel FCI phenomena may need to be modeled if estimates indicate that a high probability exists for the core debris to relocate

out of the RCS or if the energetics of the explosion process indicate reactor vessel or RCS failure to occur with a high enough likelihood.

The work associated with further experimentation, sophisticated modeling, and ex-vessel analysis would constitute Task 3 in the overall closure process.

For work conducted for the HFIR SAR, the event under consideration involves the occurence of a sufficiently large core flow blockage to cause fuel plate melting under full power conditions. The mode of analysis is as described for Task 1 above. The basic approach consisted of evaluating what fraction of the HFIR core could realistically melt from the occurrence of small or large core flow blockages. Simultaneously, a comprehensive analytical framework was developed to evaluate the energetics of a resulting steam explosion coupled with an analysis of HFIR vessel and top head bolt failure characteristics. A key assumption for modeling and analysis of steam explosion energetics involved neglecting chemical energy sources from aluminum ignition in water. It is then shown that for realistic upper bound values of core melting, the resulting steam explosion loads are tolerable, in the sense they do not compromise the integrity of the reactor vessel, or the top head bolts. Thereafter, the margin to safety is evaluated by analyzing for that core melt fraction participating in a steam explosion which is energetic enough to cause vessel and/or top head bolt failure, and the generation of a missile with the capacity of breaching the confinement. The overall calculation process is shown in a flow chart format in Fig. 1.2. Chapter 2 provides a description on aspects dealing with problem formulation, modeling and simulation of the various processes involved during steam explosion events cause from flow blockages. Thereafter, Chapter 3 describes the specific analyses that have been conducted (and are to be addressed in future) for the HFIR.

TABLE 1.1

Important Parameters for Fuel-Coolant-Interaction Anlayses

1) Droplet Sizes (available surface area)

2) Rate of surface cooling

3) Rate of heat production (e.g., exothermic reactions between metals & water, decay heat)

4) Initial & boundary conditions for melt and coolant ambient

- melt mass
- melt volume
- melt composition
- melt temperature
- melt entry velocity
- melt pour diameter
- vessel geometry
- degree of vessel confinement
- presence and nature of melt flow restrictions, and other structures
- water mass
- water volume
- water depth
- water temperature
- ambient pressure
- coolant void fraction
- melt contact mode (jet, water over melt, reflood, etc.)
- wettability of surfaces
- trigger occurence and strength

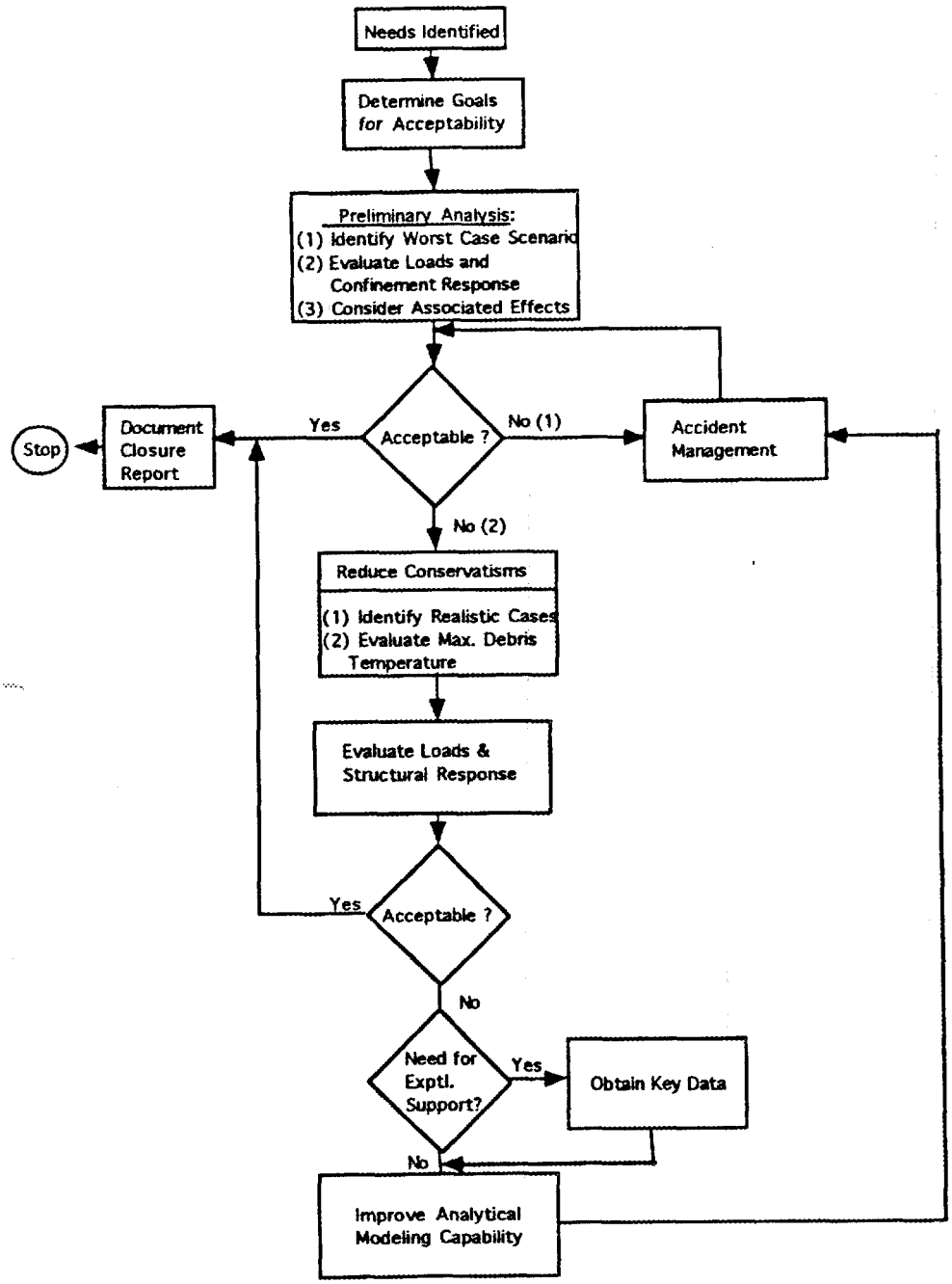

Fig. 1.1 HFIR Fuel-Coolant-Interaction Issue Resolution Framework and Strategy

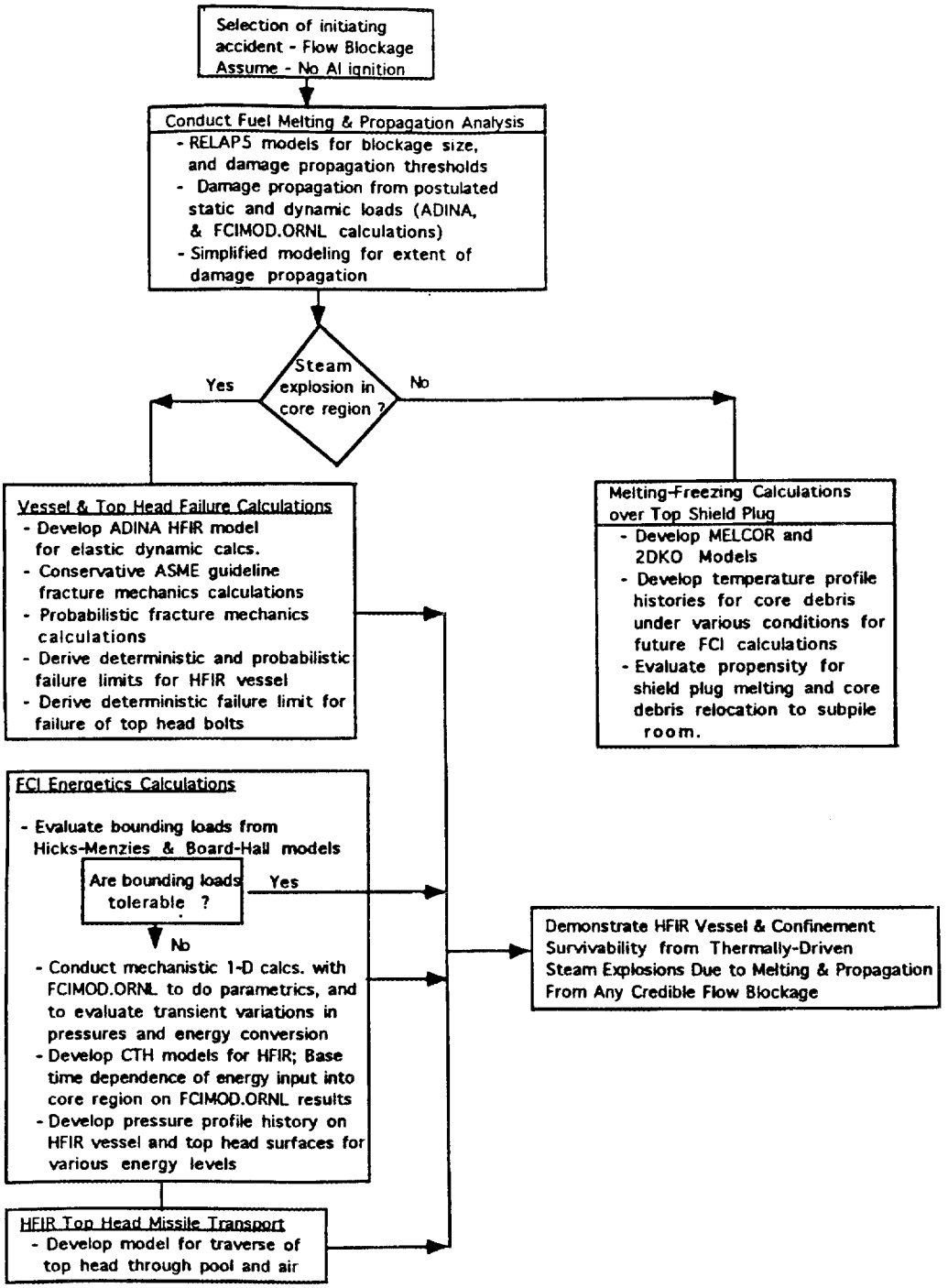

Fig. 1.2 FCI Work Elements and Framework for HFIR SAR

2. PROBLEM FORMULATION, MODELING AND COMPUTER CODES FOR FCI ANALYSIS

In this section we provide a brief description of several aspects dealing with problem formulation, modeling, and codes for FCI analysis during flow blockage events. The overall problem consists of several different complex phenomena such as eutectic formations, fission product release, heatup, melting, propagation of melting, fuel plate dispersion into the coolant, pressure pulse generation and interaction with structures, missile generation during the expansion phase, etc. A long-term objective should thus be to develop an integrated modeling approach that takes all such phenomena into account simultaneously. However, because of the short time available for evaluating the threat to HFIR from possible energetic FCIs it was decided to analyze the overall problem from several different angles so as to reasonably account for the most important parameters. This approach is discussed below.

The approach followed in this initial effort towards developing a modeling framework for the FCI issue in HFIR arising from flow blockage is to break down the problem into the following components:

- Plate melting and damage propagation in the core region.
- Core debris heatup, melting, and freezing after relocation onto the lower shield plug region of HFIR.
- Evaluation of bounding loads that can be generated if a steam explosion occurs either in the core region or when the core debris has relocated onto the lower shield plug region.
- Evaluation of multidimensional steam explosion energetics in the explosion zone.
- Evaluation of vessel and bolts failure characteristics.
- Evaluation of missile evolution and transport characteristics.

- Incorporation of special effects such as aluminum ignition, eutectic formation, and impact on triggerability, fission product release, etc.

A brief description is given for the first six components previously outlined, and how a suitable modeling approach has been utilized.

2.1 MODELING FOR FUEL MELTING AND DAMAGE PROPAGATION IN THE CORE REGION

Two parameters play a key role in evaluating the energetics of steam explosions — fuel material mass and temperature when interaction occurs with the coolant. These parameters are also quite difficult to estimate in the absence of a suitable mechanistic core melt progression modeling capability. The approach used in evaluating the maximum possible mass of core material and the temperature of such material is to combine previous analyses reported in ORNL-3573 (see Appendix A) with scoping calculations being conducted using hand calculations and codes such as RELAP5,[10] MELCOR, 2DKO,[11] and ADINA. A brief description of the overall problem formulation scheme is provided in this section, whereas, additional details are provided in Appendices A through D. Because the RELAP5, MELCOR, and ADINA codes are sufficiently well known, no details will be given regarding capabilites of these codes. However, the 2DKO code capabilities will be summarized.

A modeling framework was established to evaluate the size of flow blockage necessary to initiate fuel melting in the HFIR core under full-power conditions. That is, models of various levels of sophistication were set up to find out what amount of coolant channel area would need to be blocked before fuel plate melting would initiate, and thereafter, to propagate to other fuel plates. This process was conducted systematically as follows.

To begin with, the previous HFIR modeling postulates for core material melting from flow blockages was examined. This modeling scheme is described in ORNL-3573, and key elements are summarized in Appendix A. ORNL-3573 analysts recognized two types of flow blockages — small and large. The basic postulate of the model for evaluation of core damage (i.e., fuel melt fractions) is based upon evaluation of the degree of fuel and coolant heatup necessary for causing a one-dollar reactivity change before the control system causes a scram to occur. It is assumed that fuel melting is simultaneous in all affected plates, and no credit is taken for scram signal initiation because of fission product detection in the coolant stream downstream. Melt propagation aspects are not modeled.

A method (Model A) was devised[22] to evaluate via scoping hand calculations, the minimum necessary flow blockage area for multiple blocked channels that would lead to fuel plate melting. A postulate is made that the critical blockage size would be related to a certain critical mass flow rate. This critical mass flow rate is that which leads to complete vaporization of all the coolant channel liquid normally flowing through an unblocked coolant gap. The corresponding critical steam velocity is evaluated from the simple expression,

$$Vc = \dot{m}_c / (\rho A)$$

where, $\dot{m}_c$ is the critical mass flow rate, ρ is the steam density, and A is the coolant channel flow area. Vc is used to evaluate a corresponding critical channel pressure drop (ΔPc) across the length of the core. Thereafter, the critical blockage size area Ac is that size which leads to an increase in the channel inlet loss coefficient (ΔKc) such that the pressure drop across the blocked channel is the same as that across the entire core (as a result of the so-called parallel channel condition), viz., 0.75 MPa (107.14 psid).

To confirm the hypothesis and postulate associated with the above-mentioned method for evaluating the required minimum flow blockage area to cause melting, a more detailed 10-channel model (viz., Model B) was set up using the RELAP5 code. Figure 2.1 provides the salient details of the RELAP5 model. As seen from Fig. 2.1, the base model (i.e., Model B) represents ten different coolant flow channels (referred to as pipe volumes) connected between two plena (tdv-001 and tdv-002). Heat structures representing the fuel plates adjacent to every flow channel have also been represented. These heat structures are referred to as hs-001 to hs-999 in Fig. 2.1.

A separate RELAP5 calculation using a new code model (viz., Model C) was set up to estimate the effect of complete flow blockage of adjacent flow channels. This was essentially done using the representation of Fig. 2.1 and setting the appropriate valve openings at the channel entrances to zero.

To evaluate the propensity for core damage propagation another RELAP5 model (viz., Model D) was set up. This model endeavors to reveal whether a series of melted plates could lead to additional melting of (previously unmelted) adjacent plates. Model D was designed such that a core symmetry plane is created around the "melted box" consisting of a set number of plates that have melted and have fused together. A conservative assumption is made such that the heat flux from the melted box to the flow channel adjacent to the next unmelted fuel plate is a multiple of the nominal heat flux. This multiple essentially corresponds to the number of melted plates contained in the "melted box." The aim of this calculation is to evaluate at what multiple does the heat transfer condition in the fluid channel adjacent to the next unaffected plate deteriorate enough to cause melting to initiate. It is clear that this calculational scheme would tend to provide conservative estimates for damage propagation because no credit is taken for possible steam cooling of melted plates, and also the possibility of melted plates relocating away from the core region. Details of the RELAP5 modeling are reported elsewhere[22] and are also summarized in Appendix C.

Model D using the RELAP5 code would tend to provide an estimate for the approximate amount of initial plate melting necessary in the core regions (that is, inner or outer fuel elements). However, these calculations do not provide an estimate of how many plates would melt once propagation does occur under full-power conditions. A simple model was developed[33] for this purpose. This model postulates that any plate once melted would slump onto its neighbor. Thereafter, the fused plates would heat up together until the reactor is scrammed. The time limit available for this domino-effect to keep propagating is set as three seconds, based upon the transit time for a fluid particle to reach regions where high radiation level detection can take place, which then initiates a scram signal. Once again, this is a highly conservative method for evaluating the degree of melt propagation. The size of a flow blockage will determine how many plates get melted simultaneously before propagation occurs. However, because of the absence of a priori knowledge of this parameter, it is assumed that at first one fuel plate will melt and slump onto its neighbor. Appendix C and Ref. 33 provide additional detail.

The problem formulation for investigating melt propagation also involved investigation of additional scenarios. Melt propagation could occur because of static or dynamic loads that may be generated from unique situations in the core region. It should be recognized that the initiation of steam explosions is not well understood from an analytical standpoint, and hence the occurrence is somewhat stochastic in nature. For some situations, it may be possible that localized fuel melting leads to steam explosions that may damage adjacent unmelted plates. Keeping such conditions in mind, the following scenarios are postulated depicting situations with and without the occurrence of steam explosions in the core region.

Scenario 1

Experiments show that melting aluminum in a flowing medium can get dispersed and get carried away by the coolant. If a steam explosion does not occur simultaneously,

then molten fuel plates may essentially disappear from the core region. This causes an enlargement of the hydraulic diameter and flow area of the new coolant channel that is created. For example, if only one fuel plate melts and gets carried away, the new hydraulic diameter and flow area are approximately three times the corresponding values for a normal coolant channel. Using the parallel channel condition, the velocity of flow in the enlarged channel will be ~1.73 times the velocity of coolant in the balance of the system coolant channels. For a case where two fuel plates get ablated, the resulting flow velocity in the enlarged channel is ~2.2 times the velocity of coolant in the balance of the system coolant channels. As the velocity of coolant in enlarged channels keeps increasing, a buckling instability may set in, which needs to be characterized. Simultaneous with the increased velocity (and therefore flow) in the enlarged coolant channels, flow reduction necessarily has to occur in the balance of the coolant channels. This would lead to further erosion in margins to the onset to nucleate boiling. Of course, beyond a certain point the parallel channel condition will no longer hold. It should also be recognized, however, that this type of damage propagation will necessarily be arrested once radiation detectors cause a scram signal to get initiated.

Before launching out into a research effort to characterize the thermal-hydraulics of the situation further, the structural response behavior was investigated first. This investigation was initiated on the possibility that plate collapse from higher velocities in enlarged flow channels is real (that is, is it really a problem?). To solve this problem an exact analytical formulation was developed to evaluate critical flow velocities. Details of the model development are given in Appendix D.

Scenario 2

The second scenario concerns plate deformation from static and dynamic pressure loadings, once again neglecting steam explosion occurrence in regions where plate

melting (but not ablation) has occurred. Two different cases are considered, as described below.

The first case considers a situation where a coolant channel gets blocked and causes almost total flow starvation (that is, from the onset of Leddinegg[21] instability). Thereafter, an axially-varying radial pressure gradient will get established across adjacent fuel plates. As an approximation, the gradient across the plate will vary linearly from zero at one end to a maximum of about 0.7 MPa (i.e., core pressure drop) at the other. We need to know whether such a pressure gradient can cause sufficient bending of plates (adjacent to the flow-starved channel), which will result in the onset of boiling conditions in the adjacent channels. If so, damage propagation will likely result. A finite element code, ADINA, was used to evaluate deformations under the postulated thermal-hydraulic conditions given in Appendix B.

Scenario 3

The third scenario concerns possible plate failure from dynamic pressure loadings resulting from localized steam explosions, in regions where plate melting occurs becasue of flow blockage in channels. In this instance, large pressure pulses will be generated in the millisecond time range. For damage propagation to occur, the pressure pulse from steam explosions should be in a position to cause sufficient plate deformation to cause steaming in adjacent channels and therefore lead to the possibility of propagating steam explosions. Because of the various possible magnitudes of pulses that can be generated under different thermal-hydraulic conditions, it is necessary that a failure envelope be generated for the response characteristics of fuel plates adjacent to the explosion zone. A series of finite element models with the ADINA code are used for evaluating failure curves from dynamic loads for single and multiple fuel plates in the HFIR core. These models were developed with varying levels of sophistication. Failure was judged to occur if the material stresses in the plates exceeded the yield stress when subjected to

dynamic pressure pulses on the plate surface of a given magnitude and duration. The models ranged from a single fuel plate to a cluster of several plates supported at their ends by the fuel supports. Details are given in Appendix D. Results from the FCIMOD.ORNL code (described in a later section) were used to evaluate whether localized melting caused steam explosion loads are sufficiently large to damage adjacent fuel plates.

In the absence of a mechanistic model of damage propagation, the results from the previously mentioned analyses were used in arriving at estimates of how much of the core fuel material would be involved in a steam explosion. The question of what temperature the melt is likely to reach before an energetic FCI occurs is more difficult to answer because of the possibility for the onset of aluminum ignition, which can release an order of magnitude of more energy than the thermal content of the molten fuel itself. Because of this uncertainty (which is also the target of nation-wide research for U-A1 fueled reactors), it was decided to model the FCI process first without aluminum ignition. The effects of aluminum combustion on the progression of the explosion should be accounted for later. Because of several uncertainties, it was decided that evaluating fuel melt temperatures for the core region would best be done parametrically.

2.2 MODELING OF CORE DEBRIS HEATUP, MELTING, AND FREEZING AFTER RELOCATION TO THE LOWER SHIELD PLUG REGION OF THE HFIR

As mentioned previously, the occurrence of steam explosions in the core region is considered to be somewhat stochastic in nature (due primarily to a lack of understanding). Under some circumstances, the core material may melt and then relocate (most likely) onto the steel shield plug in the HFIR pressure vessel. The core debris could then heat up, melt, and undergo a steam explosion. It is thus important to evaluate the possibility of debris coolability and the extent of melt superheat that is possible. Models were

developed using the 2DKO and MELCOR computer codes. The MELCOR code is reasonably well known and is thus not described further. The model used in the 2DKO computer code accounts for two-dimensional (2-D) phenomena related to simultaneous heat transfer and phase change (melting/freezing) between hot liquids and relatively cold solids. Various applications of the mathematical model include the melting of a solid structure when in contact with a continuously delivered liquid, melting of a solid plate subjected to an impinging jet of hot liquid, and the melting of a vertical wall in contact with a liquid pool.

The 2DKO model has been validated against experimental data and showed good agreement. This code is useful for the present analysis of debris heatup or coolability because it also allows for transient debris deposition on a plate. The physical boundary value problem is depicted in Fig. 2.2 (in Cartesian coordinates). The user can specify boundary conditions for each of the four sides. In addition, the debris layer height is allowed to vary based on a time-dependent delivery rate.

The 2DKO code model was also compared against the results of a one-dimensional (1-D) heat transfer model developed using the CVH and HS modules of the MELCOR code. The sample problem was set up to evaluate the transient thermal response of a two-slab system consisting of molten superheated aluminum debris on a cold HFIR shield plug. Boundary conditions were set on all four sides to be adiabatic for the sample comparison calculation. MELCOR's HS module was employed to simulate the two-slab geometry, and the specific heat capacity of each material was modified to account for the effects of melting and freezing. That is, the specific heat capacity of each slab material is increased by the latent heat of fusion on the material over a 5°K temperature range centered around the material's melting temperature. This modification was necessary because MELCOR does not allow for "heat" structures to melt. The surface control volumes modeled the HFIR reactor vessel volume and the air cavity below the shield plug region. For the MELCOR calculations the additional shield plug

below the shield plug in contact with the core debris was included (to take into account possible radiative losses if the shield plug temperature becomes high enough). The water and atmosphere in the two control volumes receive heat via convection and radiation. The MELCOR and 2DKO models are shown in Figs. 2.3 and 2.4 respectively. Transient temperature profiles generated for the case of adiabatic surface conditions are shown in Fig. 2.5. The two models give essentially similar results (considering the basic differences involved in the two codes) and are in good agreement with one another. This comparison of 2DKO against MELCOR, coupled with the comparison of 2DKO against experimental data, provides reasonable confidence that 2DKO can be applied to provide credible evaluations of debris coolability. The MELCOR model will be used later on also for another case to assist in providing boundary conditions for further 2DKO calculations detailed in Chap. 3.

As a final note, we provide the following basic assumptions made for conducting debris heatup or coolability calcualtions:

- Multidimensional thermal-hydraulic effects are negligible.
- Core debris spreads uniformly and instantaneously over the top shield plug.
- Transient variations in fission product or aerosol release are negligible.
- Eutectic formations and their effects on melting/freezing are neglible.
- Aluminum does not undergo oxidation or ignition.
- The core debris mass is 100 kg of aluminum into which decay power is distributed uniformly.

Limitations imposed from the use of the previously mentioned assumptions should be kept in mind when forming judgements on debris coolability or heatup and structural melting or freezing.

2.3 MODELING FOR EVALUATION OF BOUNDING LOADS THAT CAN BE GENERATED IF A STEAM EXPLOSION OCCURS EITHER IN THE CORE REGION OR WHEN THE CORE DEBRIS HAS RELOCATED ONTO THE LOWER SHIELD PLUG REGION

It is well known that an energetic FCI has been a concern in nuclear reactor safety because of its potential for destructive mechanical energy release. To properly assess the hazard from an FCI event, it is necessary to accurately estimate the conversion efficiency of the thermal energy to mechanical energy. However, in the absence of a complete model to determine the FCI explosive energy yield, one needs to rely on deriving an idea of the upper bound using a thermodynamic model. Such a model is relatively more straightforward to formulate in comparison to mechanistic models and is a useful tool to have.

A thermodynamic model describes the mixing and explosion expansion phases of steam explosions connecting the three points that describe (1) the initial coarse mixture, (2) the equilibrium high-pressure state, and (3) the final expanded state. Because work done during the expansion is a path-dependent quantity, the path of constant entropy can provide the maximum work output as proposed by Hicks and Menzies.[13] The thermodynamic path in their model assumes that equilibrium mixing occurs between the fuel and coolant adiabatically without volume change and then expands isentropically to a specified end state. Unlike the Hicks-Menzies model that provides an estimate for the maximum work output, the model proposed by Hall[14] is commonly used to predict the lower limit. Hall's model consists of two adiabatic processes: (1) constant-volume mixing of fuel and coolant to a final system pressure, and (2) constant-pressure expansion to a specified final volume. The limitations of this model deal with the fact that it is only applicable for the case of a known final volume and that the final pressure can generally be different depending on the path chosen. Another model that provides an estimate for the maximum work output was proposed by Board and Hall[15] by using an analogy to chemical detonations. Subsequently, Bang and Corradini[16] developed a theoretical

prediction of the explosion pressure and propagation velocity by applying the model proposed by Board and Hall with the classical theory of detonation in chemically reactive flows to the 1-D case of a plane explosion front propagating through a coarsely mixed region of fuel and coolant. The thermodynamic paths followed by the various models is shown schematically in Fig. 2.6. For further details, consult the original references previously cited.

Several computer programs were obtained from the University of Wisconsin for use in evaluating maximum pressurization, and work output from thermodynamic considerations. These are: (1) UWHM,[17] (2) UWHUGO,[18] and (3) STEAM.[19] The UWHM code provides estimated maximum work output and pressure buildup using the Hicks-Menzies model, whereas, the UWHUGO provides the same estimates using the shock-adiabatic model proposed by Board and Hall. STEAM is a subrouting package for evaluating steam and water properties and is used by UWHM and UWHUGO. These programs are operational on our IBM/RISC-6000 workstation. Predictions for the conversion ratio and pressurization for a sample problem are shown in Figs. 2.7–2.10. These figures show that the pressure levels and conversion ratios predicted via thermodynamic evaluations can be quite high. Further discussion of results from these programs will be given in Sect. 4 on analysis for HFIR FCI studies.

2.4 EVALUATION OF MULTIDIMENSIONAL STEAM EXPLOSION ENERGETICS IN THE EXPLOSION ZONE

As mentioned in Sect. 2.3, using bounding thermodynamic-based models can give rise to pressure levels and conversion ratios that may be intolerable from the standpoint of qualifying the containment potential of pressure boundaries. They do, however, provide a ceiling or upper bound. Considerable reduction in the pressurization and conversion ratio is possible to achieve by going in for reducing levels of conservatism through best-estimate modeling of the various phases of the steam explosion process. Energetics of

the steam explosion process can be evaluated in either one, two, or three dimensions using increasing levels of sophistication.

Because of the early stages of this analytical model development, it is assumed that the fuel-coolant mixture can be triggered into an explosive FCI.

Again, Fig. 2.8 shows that the amount of molten fuel that mixes intimately with a certain amount of coolant in the explosion region plays an important role in evaluating how much thermal-to-mechanical energy conversion occurs. As noted from Fig. 2.8, the maximum conversion ratio usually occurs when the volume ratio is close to one. In the absence of a mechanistic core melt progression capability, it is herein conservatively assumed that for preliminary HFIR analysis, equal volumes of fuel and coolant will mix intimately during steam explosion events. This reasoning has a certain physical basis also, because the design of the HFIR core is such that the fuel and coolant volume fractions therein are both 50% each. Further, by design, the fuel and coolant in the core region also constitute a well-mixed state. For these reasons, it was decided that it would not be wise to expend scarce time and resources for developing a sophisticated mixing model, especially for this preliminary study.

For best-estimate energetics calculations we have obtained the FCIMOD[20] and CTH[8] computer codes from the University of Wisconsin, and Sandia National Laboratory (SNL) respectively. Brief descriptions on the capabilities of each of these codes are given below.

2.4.1 FCIMOD Code for Evaluating 1-D Energetics

The FCIMOD computer code models a 1-D FCI in the geometry shown schematically in Fig. 2.10. We assume that there is a mixing zone at the bottom of the system under consideration where molten fuel is fragmented into small particles and mixed with liquid coolant. The shaded area depicts an enlarged view of a molten fuel particle, surrounded by a vapor blanket. Above the mixing zone, there is a region called

the slug zone, filled with coolant, which will be accelerated upward by the expanding vapor generated in the mixing zone. The slug is free to travel upward into the expansion zone. We have shown a planar mixing zone-slug interface; although the code can treat the case of a hemispherical slug, the planar slug usually leads to higher peak pressures. The entire assembly is a right circular cylinder. Most of the essential physics for evaluating steam explosion energetics has been included in FCIMOD. To summarize, the model is a lumped-parameter formulation that treats the whole fuel-coolant mixture as one control volume with another control volume modelling the inertial constraint of an overlying slug. The expansion dynamics is treated in a 1-D fashion either in a planar or hemispherical geometry with possible entrainment of the liquid slug into the mixture because of Rayleigh-Taylor instabilities with associated slug breakup. The fuel fragmentation process is postulated to be controlled by coolant jet penetration of the fuel droplet surface during film collapse.

A fair amount of comparison against integral steam explosion test data taken at SNL has been performed previously by Corradini et al. using FCIMOD.[20] The results indicate good agreement where the various key input parameters are known. Wide variations can be expected when key parameters such as void fraction and mixing volumes for fuel and coolant were not known with sufficient accuracy. Overall, good qualitative agreement was obtained.

Corradini has benchmarked[52] FCIMOD calculations for conversion ratio and pressurization against two experiments that seem to represent the most carefully characterized explosion experiments to date. The first experiment was the last in a test series of experiments (C-16) involving molten tin (~1 kg) poured into a water column. The second experiment was also the last of a test series (KROTOS-21) involving a larger mass of molten tin (~8 kg) poured into a water column. We found that FCIMOD did a reasonably good job of predicting the correct scale of explosion pressure and yield for both experiments. Details of the benchmarking process have been published.[52]

Upon conducting parametric calculations (for HFIR FCI analysis) with FCIMOD, we found that for certain combination of operating conditions unusual and nonphysical results were predicted. That is, for some combination of input parameters coolant freezing was predicted. This was traced to the particular treatment of the modeling for the thermal penetration depth in the liquid coolant. The FCIMOD model had introduced a counter-current-flow limitation (CCFL) correlation for evaluating vapor generation. For certain conditions, the correlation predicted exaggerated values for steam production, which leads effectively to cooling of the liquid. A more mechanistic formulation was developed and implemented into the code, which was renamed FCIMOD.ORNL.

The FCIMOD code will be used to show the possible levels of pressurization and conversion ratio for a wide range of accident conditions in HFIR in Chap. 3. Again, FCIMOD calculations provide a means for estimating the rate of energy deposition into the coolant in the explosion zone. This information is then used for evaluating complex wave propagation dynamics in the internals of HFIR using the sophisticated CTH code.

2.4.2 CTH Code for Evaluating Wave Propagation in Multi-Material Mixtures

As mentioned above the FCIMOD code is used to build a model for evaluating energetics of possible steam explosions in the explosive region. In most cases, these pressure levels would most likely not be possible to tolerate if applied directly to the vessel walls, which would represent a highly conservative approach. For flow blockage events where a steam explosion may be occurring in the core region, substantial mitigation of mechanical energy transfer can be expected because of multi-phase mixture formation in the explosion region, and also because of absorption of energy by mechanical structures. In addition, the HFIR vessel-internals geometry is complex, and clearly requires at least a 2-D simulation, (if not three). This calls for a fairly sophisticated analytical capability.

To meet the demands of the situation, we have acquired the large, highly sophisticated CTH computer code package from SNL. The key features of CTH are outlined in Fig. 2.12. As noted in Fig. 2.12, CTH simulates shock wave physics and multi-material motion and interactions with any structures in the path in one, two, or three dimensions. It incorporates comprehensive equations of state for single-phase solids, liquid and vapor states, mixed-phase gas-liquid and solid-liquid states, as well as models for material strength, and fracture. The numerical algorithm involves finite difference analogs of Lagrangian equations of momentum and energy conservation with continuous rezoning to construct Eulerian differencing. Because there was no version of the package for the IBM AIX operating system on the IBM RISC/6000 workstation, we have conducted suitable modifications for enabling calculations on a workstation environment.

The CTH system and the RSCORS graphics package are currently operational on the IBM RISC/6000 workstation. The RSCORS package includes post-processors for displaying graphical output on a variety of devices, including X Windows terminals, Tektronix terminals, and PostScript printers. We have run the test problems supplied with the CTH package and find satisfactory agreement with the results from the same problems run at SNL.

For transient evaluations, once a spatial step size is chosen, CTH will adjust the time step so that the finite-difference scheme will satisfy the well-known Courant-Friedrichs-Levy stability criterion. To allow for the fact that nonlinear finite-difference schemes may be unstable, even though the Courant condition is satisfied, CTH reduces the step size to 0.6 of the value satisfying the Courant criterion. Physically, this amounts to ensuring that no shock wave can propagate further than one spatial step in one time step. For our simplified HFIR system (Fig. 2.13) preliminary analysis we have used spatial steps of 2 and 4 cm; aside from the factor of four difference in run time to be expected from halving the spatial step size in a 2-D calculation, there is an additional

factor because of the reduction in the maximum allowable time step. Whereas a case with the 4 - cm spatial step size takes about 30 min on the IBM/RISC 6000, one with a 2-cm spatial step size takes two and one-half hours to simulate six milliseconds of problem time. The time requirements are highly problem-dependent. Examples quoted are for a grossly simplified representation that consisted of energy deposition into a tank of water.

The CTH package also allows the user to specify a number of so-called tracer points, at which material properties will be recorded during the course of the calculation, so that graphical output can be prepared. The tracer points can be either Lagrangian or Eulerian. For the simplified preliminary HFIR model shown in Fig. 2.12, the points labelled with L are Lagrangian; otherwise, points labelled E are Eulerian.

Several models were generated in a systematic fashion. The first model (Model 1) consisted of a tank of water, roughly the size of the HFIR vessel but simplified to a right circular cylinder, containing a cylindrical annulus of beryllium to represent the reflector. In the second model (Model 2), we have added an aluminum pipe inside the reflector, extending from the bottom of the tank to about 1.5 m above the reactor midplane to simulate the control plate supports below the core, the tank and some of the structure of the outer fuel annulus within the core, and the target tower supports and associated structures above the core. In the third model (viz., Model 3, best-estimate representation), a cylindrical steel shell was added with a hemispherical lower section and a thick top plate to represent the pressure vessel and the top head. The three models are shown schematically in Figs. 2.13–2.15. As mentioned previously, the points labelled L1, L2, and so on, are locations where the pressure, temperature, density and other variables are recorded at selected times during the calculation. A constant mesh spacing of 20 mm was used for all calculations. This assumption was checked with a smaller mesh spacing, and found to be good enough in terms of providing an adequate degree of resolution.

We should note that CTH does not incorporate a capability for simulating the details of molten fuel dispersion into a coolant medium The thermal energy imparted to the coolant has to be introduced by the user separately. Based upon thermal-to-mechanical energy conversion ratio variation with time profiles predicted using the FCIMOD.ORNL code, a simple representation for the specific power, r(t), as a function of time was developed as,

$$r(t) = 4\, r_o\, (t/t_o)\, (1 - t/t_o) \qquad (2.1)$$

where t_o is the duration of the energy source and r_o is the peak specific power. Integrating this expression over the duration of the pulse and setting the result equal to the desired energy density allowed evaluation of the peak specific power r_o and to construct a table of specific power values at selected times, as required by CTH. Because of the particular nuance associated with the interpolation scheme utilized in CTH, combined with coolant flashing in the explosion zone the actual energy input is somewhat different from the desired energy input (but not by much). Further details of the modeling process are provided in Appendix G. Results of CTH calculations can be used in conjunction with results of vessel and top head failure analysis models to evaluate HFIR system response characteristics during steam explosion conditions of varying levels of severity. Analysis results are presented in Sect. 3.

2.5 MODELING OF VESSEL AND TOP HEAD BOLTS FAILURE CHARACTERISTICS

During explosion events in the HFIR vessel, it is necessary to know what level of loads are sufficient to cause vessel failure, to gauge the potential for confinement damaging missile generation. For this models were developed separately for evaluating vessel failure and top head bolts failure as described in Sects. 2.5.1 and 2.5.2.

2.5.1 Modeling Vessel Failure

A detailed modeling effort was undertaken to evaluate vessel failure characteristics, both from a conservative deterministic sense and from a probabilistic standpoint. Both approaches are briefly summarized here. They used the principles of fracture mechanics.

To calculate vessel critical stresses, a model was developed in which dynamic pressure pulses were applied over a range of magnitudes and pulse durations. The geometry of the HFIR vessel was modeled using the ADINA code package, with 41 elements in a finite element formulation. Nozzles along the vessel surface were neglected to simplify modeling. To not have to undertake a detailed three-dimensional (3-D) modeling effort and to stay consistent with CTH modeling, a 2-D formulation was developed as shown in Fig. 2.16. Internal pressure is applied uniformly along the inner surface of the vessel for various durations. These calculations allow the derivation of so-called failure envelopes (to be discussed in Sect. 3) which are then used in conjunction with the principles of fracture mechanics to evaluate critical surface dynamic pressure pulses that will cause vessel failure. Using ASME guidelines for specification of cracks and membrane response characteristics, a so-called fracture toughness and geometric factor are evaluated from which an allowable hoop stress is calculated. This model tends to produce conservative results.

A second modeling approach was also developed in which a closed-form expression to calculate the fracture probability of the vessel containing a small fractional number of cracks is derived. In this approach the so-called weakest link hypothesis for strength or Weibull's method for strength are used. This model built upon the data obtained from studies made by Cheverton et al.[36] to evaluate the HFIR vessel steel radiation embrittlement condition and the suitability of the reactor to stay in operation. As opposed to previous studies, the current model used Cheverton's data base in conjunction with a dynamic rather than static stresses using the ADINA code. Further details are given in Ref. 35 and in Appendix H.

2.5.2 Modeling Top Head Bolts Failure

The top head of the HFIR vessel is a complex geometrical structure with multiple penetrations. It is held in place by 44 bolts spaced uniformly around the top head as mentioned in Ref. 53. To conduct a scoping analysis for top head failure from steam explosion loads in the vessel several assumptions had to be made. Details of these assumptions and justifications of the same are given in Appendix H and in Ref. 47. The top head is represented as an equivalent circular disk with a radius of 0.965 m, and a thickness of 0.356 m. Further, it was assumed that the 44 bolts (of diameter 0.076 m) that hold the top head in place will uniformly absorb pressure loads. Thereafter, for a given imposed dynamic pressure of magnitude P, the average stress (s_{av}) on each bolt is calculated from,

$$\sigma_{av} = PA_{head}/(N\,A_{bolt}) + \sigma_t \qquad (2.2)$$

where P is the pressure, A_{head} is the area of the head, N is the number of bolts, Abolt is the area of a bolt, and σ_t is the approximately 210 MPa pretension applied to the top head studs. It is further assumed that the pressure required to break the bolts is that pressure

which gives rise to a value of σav, which exceeds the yield stress (σ_y) of the steel bolts. That is, failure will occur if

$$\sigma_{av} > \sigma_y \tag{2.3}$$

Further details regarding the straightforward modeling for bolts failure and related justifications are given in Appendix H and in Ref. 47.

2.6 MISSILE TRANSPORT MODELING

When the load on the HFIR vessel is found to be high enough, it is possible that energetic missiles may evolve. Any such missiles would need to traverse through the large reactor pool over the HFIR pressure vessel. A likely missile could be the top head once the bolts holding it down are broken. The model formulation for evaluating the top head transport consisted of setting up and solving a pair of ordinary differential equations describing the motion of a disk upwards through a water pool. Details are provided in Appendix I. A momentum balance equation is set up which takes into account viscous drag, inertia, gravitational decelleration, and virtual mass forces. The resulting differential equation set is solved subject to a given initial velocity (v_o). This v_o is calculated from CTH results combined with bolt failure analysis.

A stand-alone FORTRAN program was written to numerically integrate the differential equations. Separately, an exact analytical formulation was developed to predict disk traverse. This analytical solution was used to validate the numerical solution. Excellent agreement was obtained. Details are given in Ref. 50.

Once the disk rises through the water pool, a simple method was used to evaluate how high it might rise above the pool surface. This simple method neglects viscous drag

for a disk traversing in air and thus gives conservative estimates. The rise height above the pool surface is calculated simply from a simple force balance, which yields,

$$h_{rise} = v^2_{exit}/2g \tag{2.4}$$

where h_{rise} is the height above the pool surface, v_{exit} is the velocity of the disk as it exits the pool surface, and g is the gravitational acceleration.

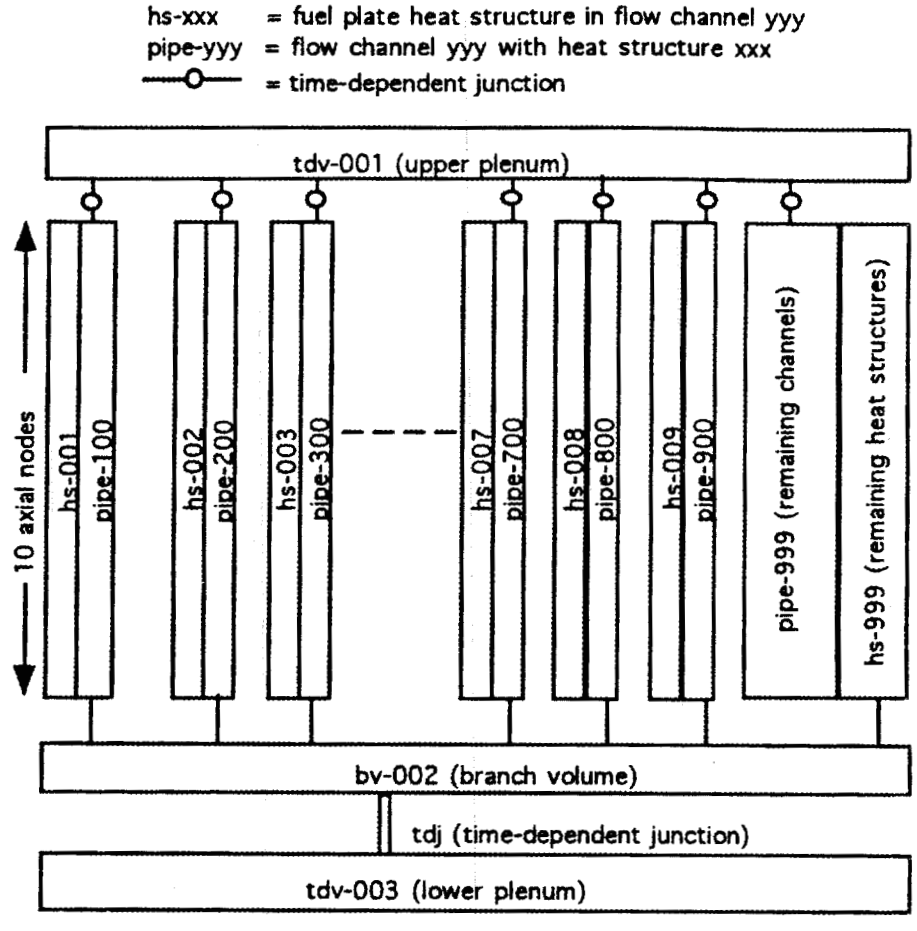

Fig. 2.1 Node map of HFIR FCI flow blockage RELAP5 model

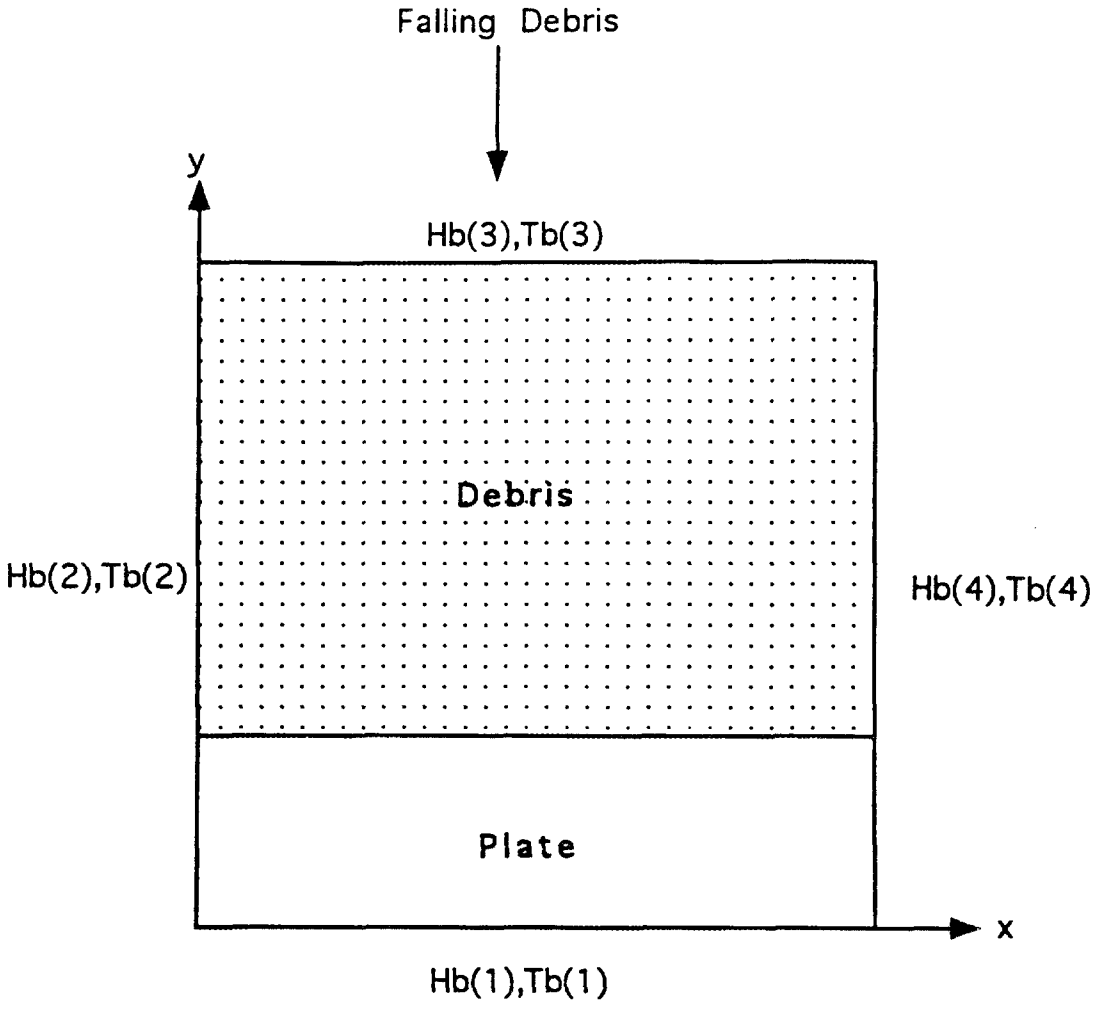

Notes:

1) Hb(i), Tb(i) - Surface Heat Transfer Coefficient & Temperature at Boundary i
2) Ta(i) - Ambient Temperature around Boundary i

Fig. 2.2. 2DKO Model for Debris-Plate Interaction Analysis

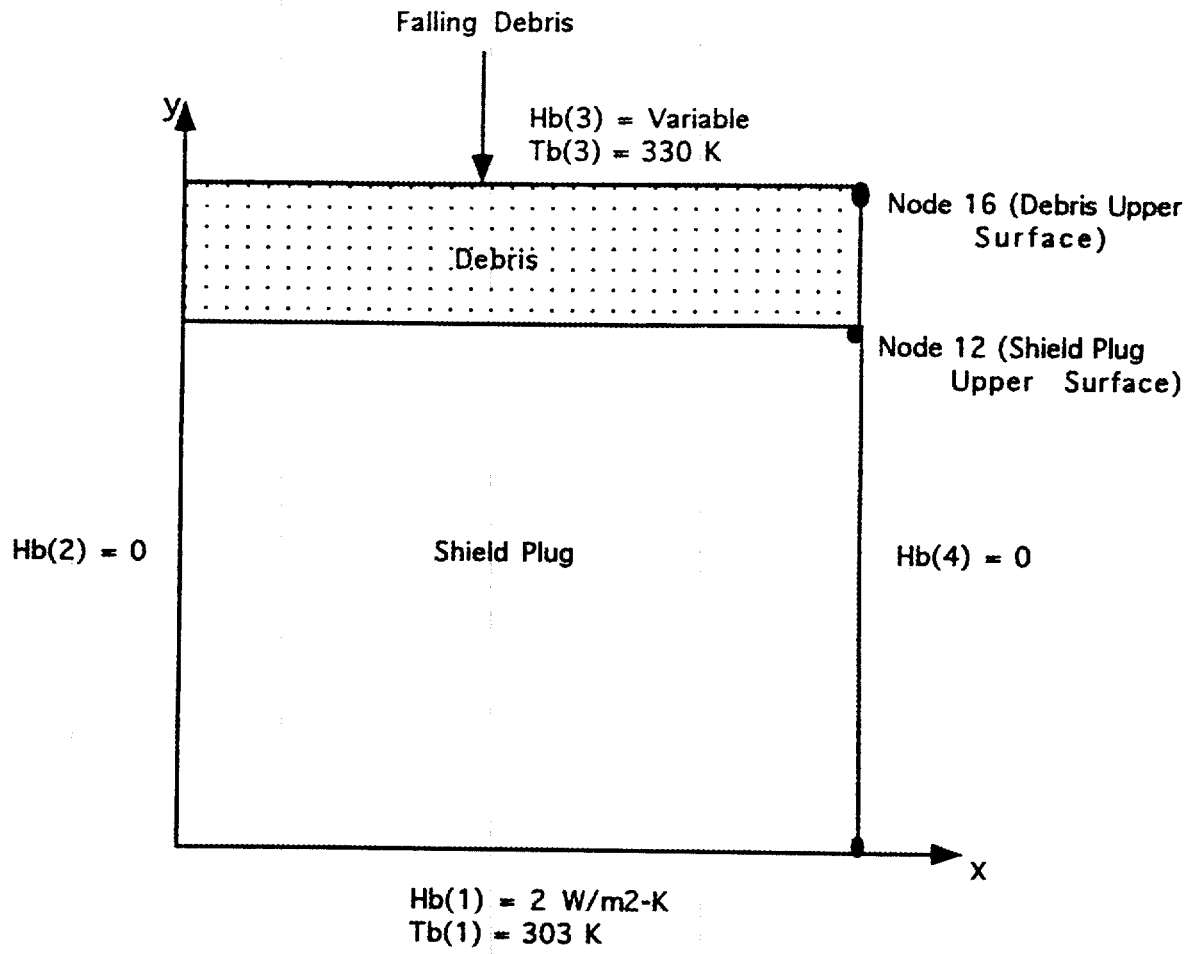

Notes:
1) Hb(i), Tb(i) - Surface Heat Transfer Coefficient & Temperature at Boundary i
2) Ta(i) - Ambient Temperature around Boundary i

Fig. 2.3. 2DKO Model for Debris-Plug Interaction Analysis

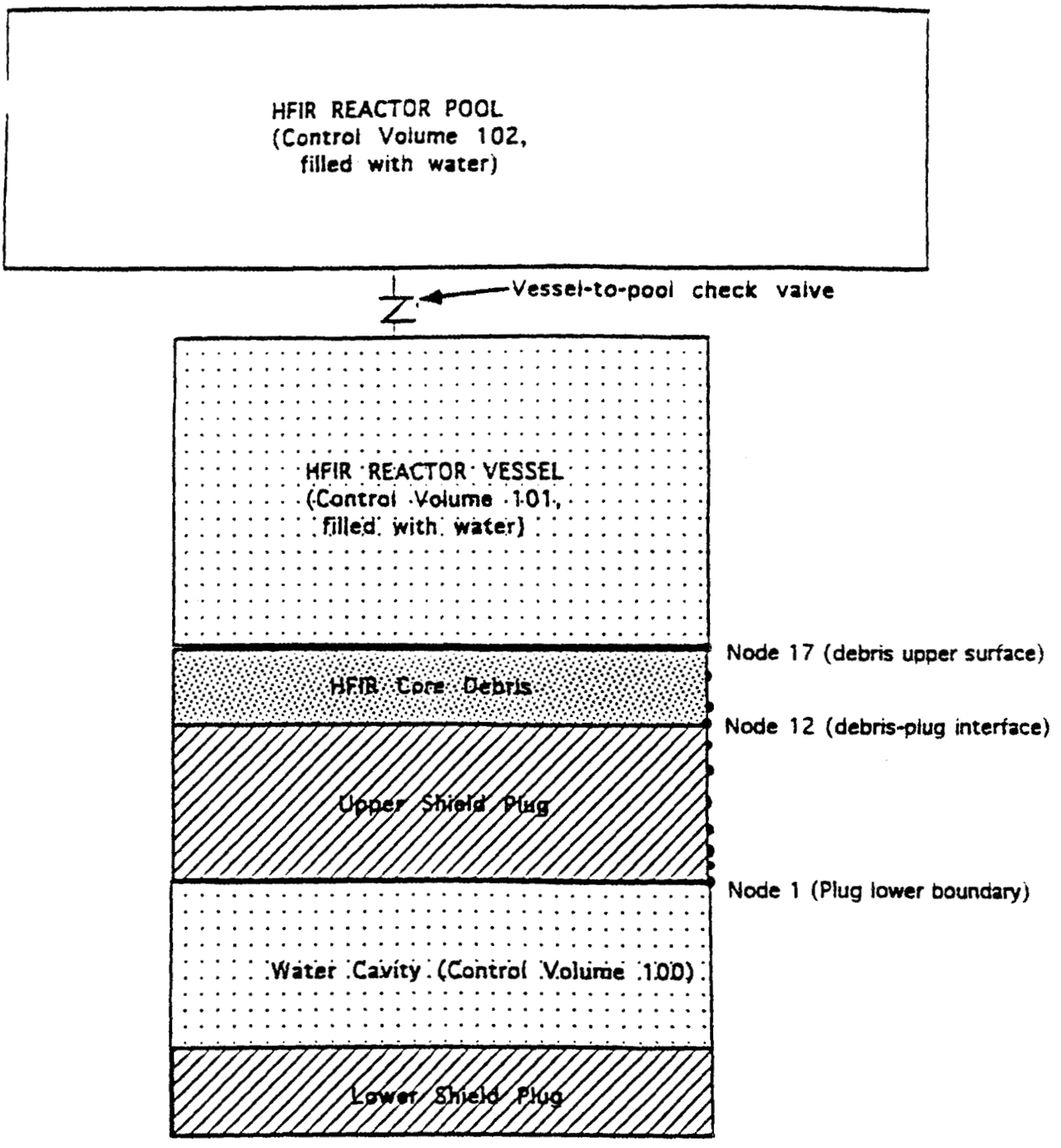

Note

At debris and shield plug interfaces with adjacent atmospheres, heat transfer is due to convection and radiation

Fig. 2.4 MELCOR Model for Debris-Shield Plug Interaction Verification Calculations

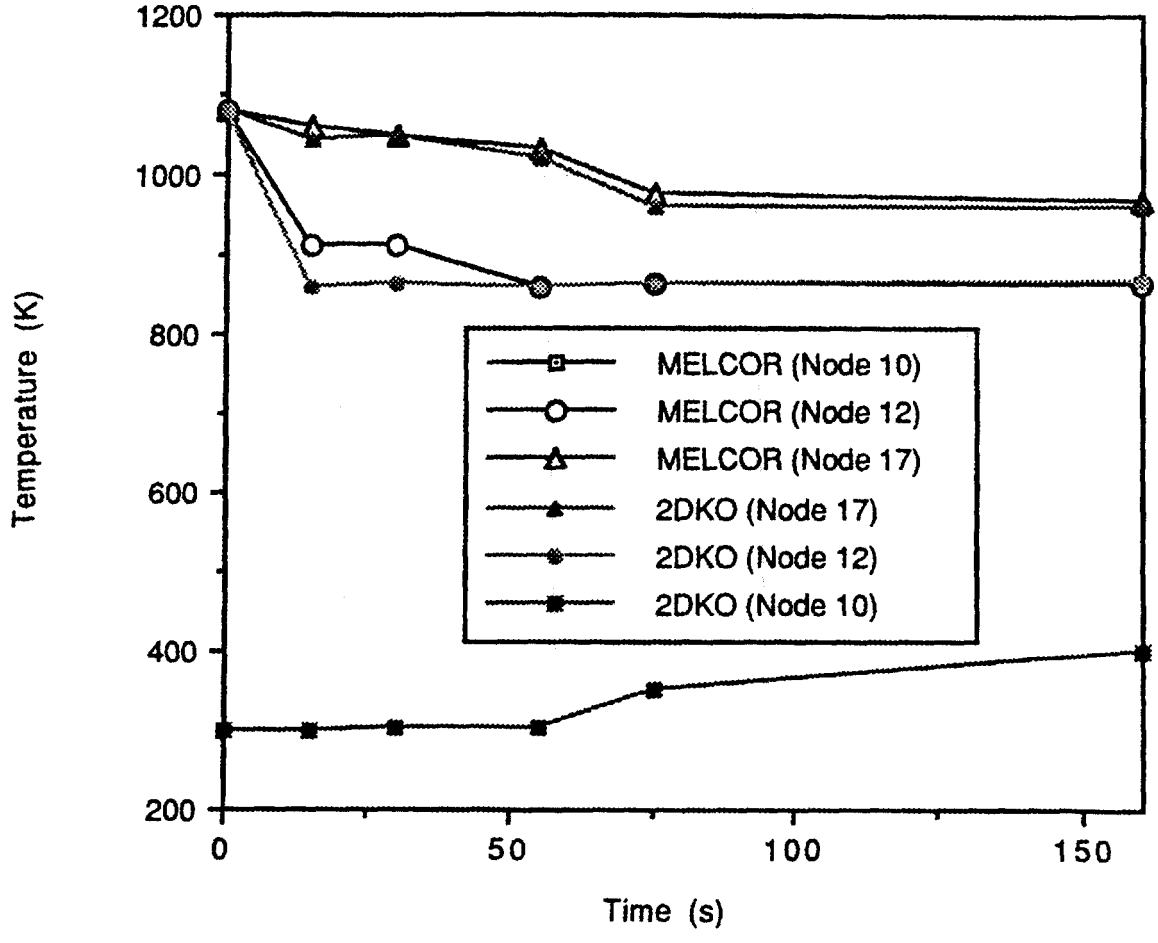

Fig. 2.5 Comparison of Predictions by MELCOR and 2DKO

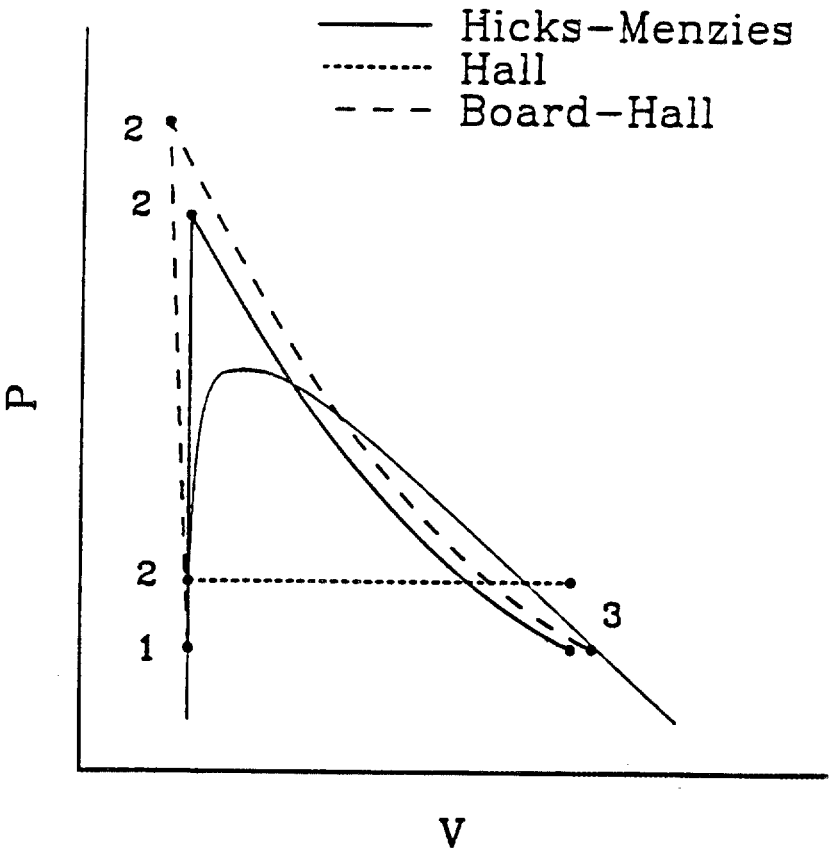

Fig 2.6 P-V Diagrams for Various Explosion Models

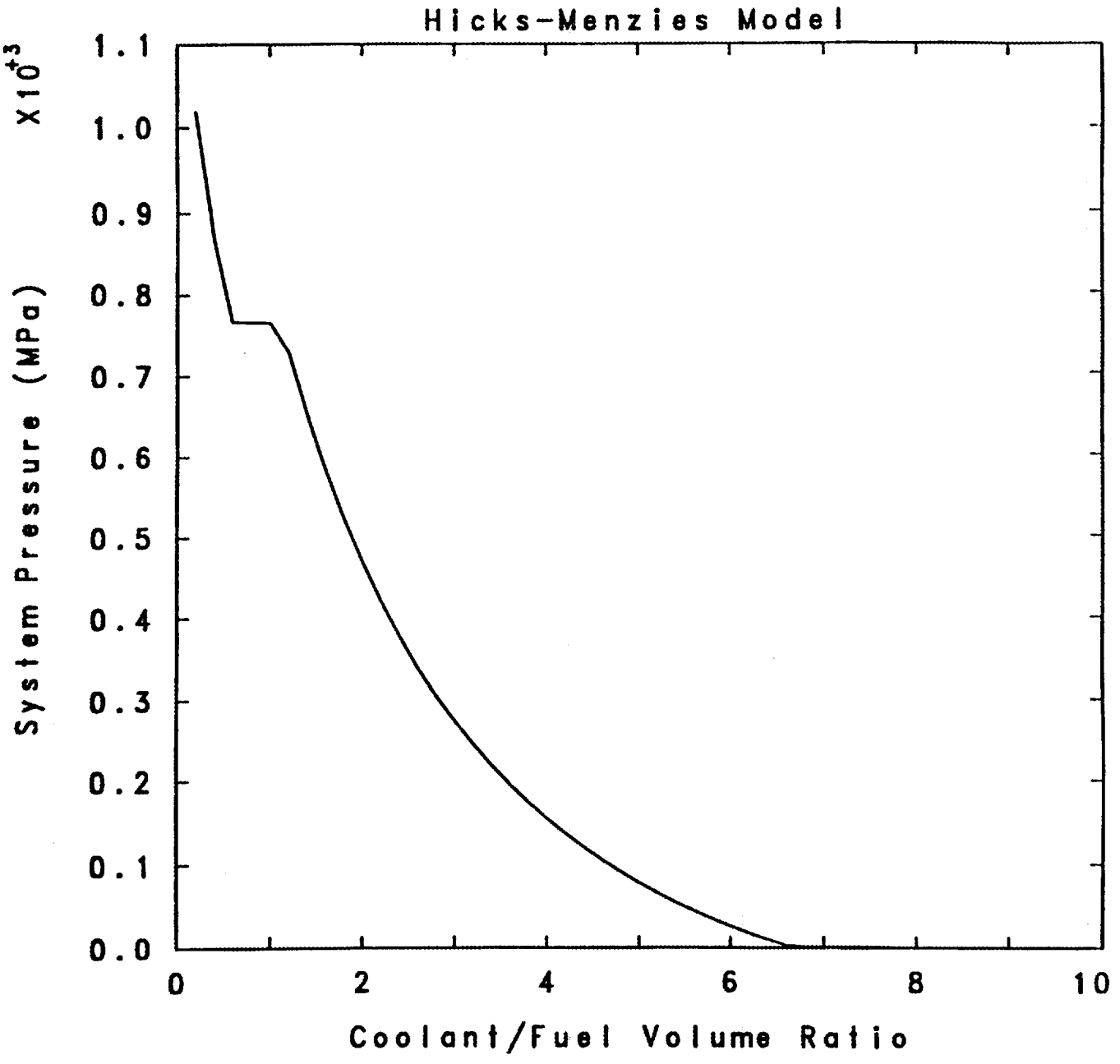

Fig. 2.7 Pressurization versus Coolant-to-Fuel Volume Ratio (Hicks-Menzies Model Predictions)

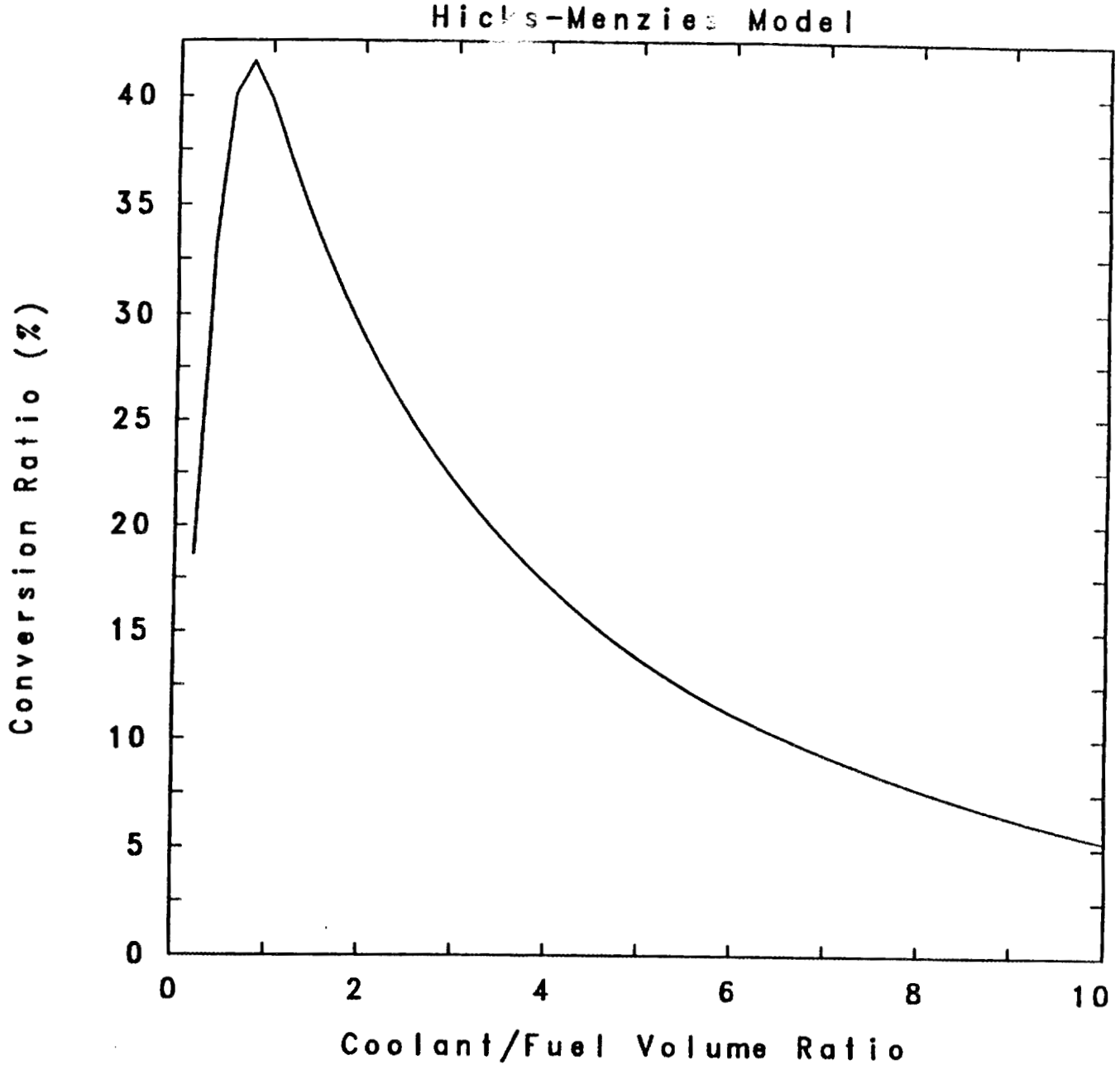

Fig. 2.8 Conversion Ratio versus Coolant-to-Fuel Volume Ratio (Hicks-Menzies Model Predictions)

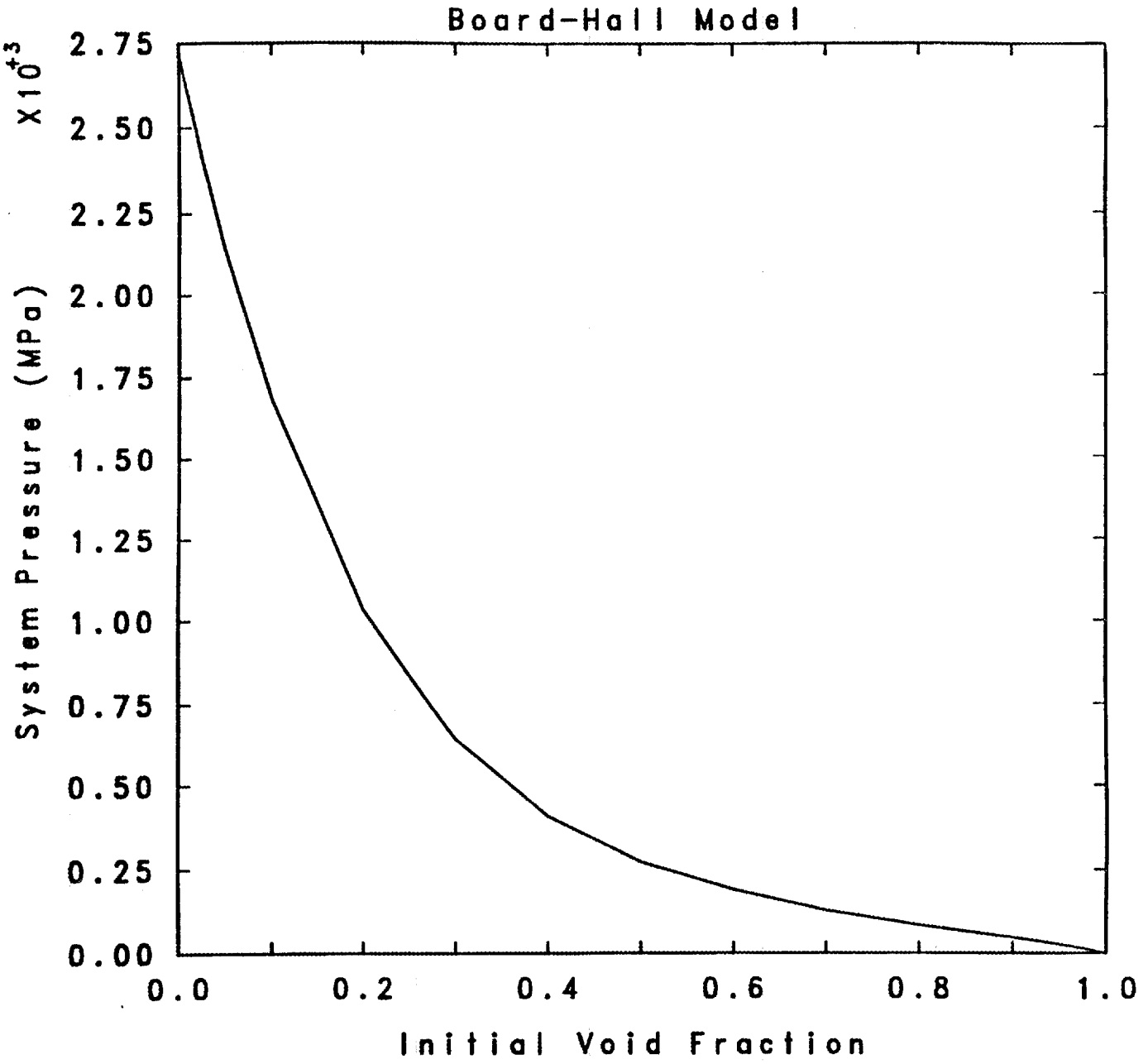

Fig. 2.9 Pressurization versus Coolant-to-Fuel Volume Ratio (Board-Hall Model Predictions)

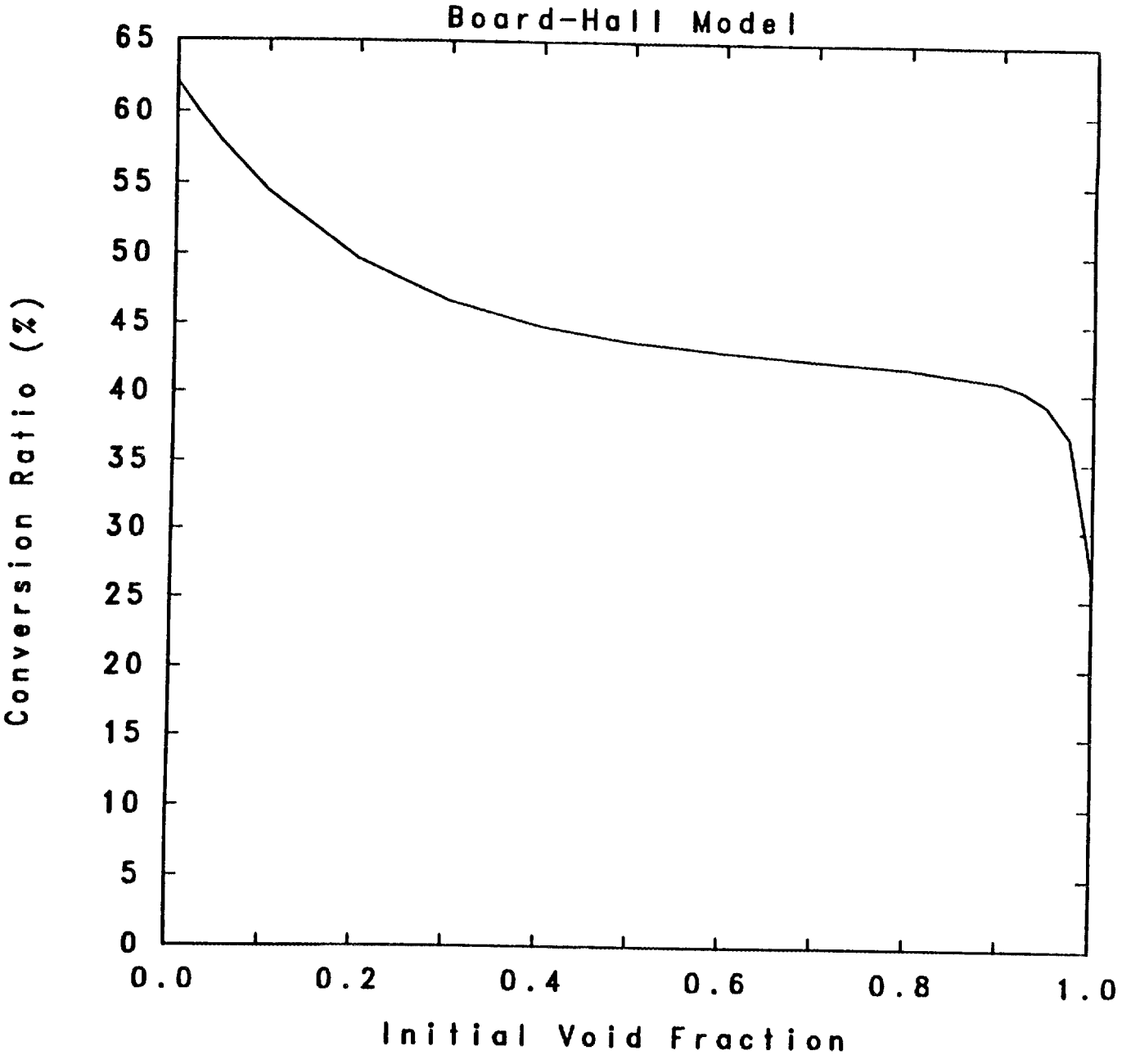

Fig. 2.10 Conversion Ratio versus Initial Void Fraction (Board-Hall Model Predictions)

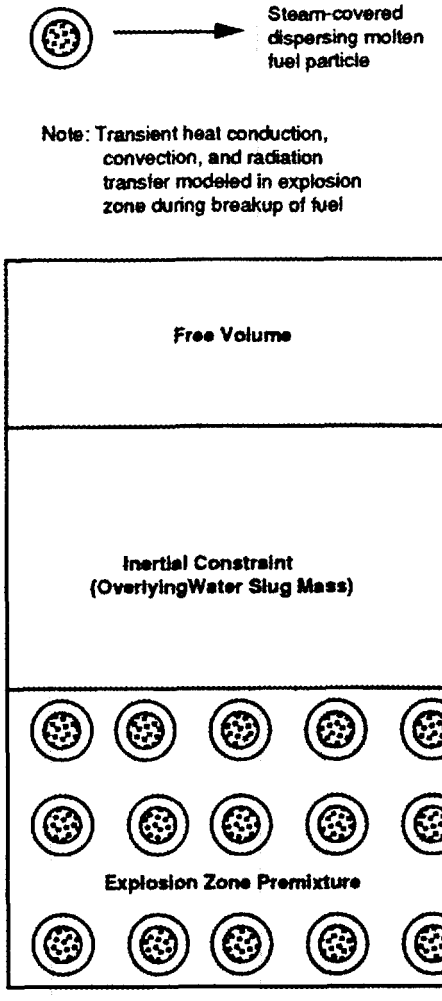

Fig. 2.11 FCIMOD.ORNL modeling geometry

o PRINCIPAL **APPLICATION** FEATURES

- Shock **Wave** Physics Simulations
- Multi-Material Motion & Interactions (Comprehensive equations of state for single-phase solid, liquid & vapor states, mixed-phase gas-liquid **and** solid-liquid states; Models for material strength, fracture, high explosives)
- 1-D, 2-D, 3-D Geometry Simulations

o EXTENSIVE POSSIBLE USES

- Nuclear Reactor Safety Applications (e.g., Steam Explosion Accidents)
- Projectile Evolution, Interaction, & Penetration Studies (100+ km/s)
- Space & Defense Applications (e.g., high velocity **space** debris impact)

o NUMERICS

- Finite Difference Analogs of Lagrangian Equations of Momentum & Energy Conservation with Continuous Re-Zoning **to** Construct Eulerian Differencing

o POWERFUL **SUITE** OF POST-PROCESSING PROGRAMS

- 1-D, 2-D, **3-D** Color Contour Plots; History Plots *of* Thermo-Mechanical Data

OPERATIONAL AT **ORNL** ON IBM RISC/6000 WORKSTATION

Figure 2.12 CTH CODE & ORNL CAPABILITIES

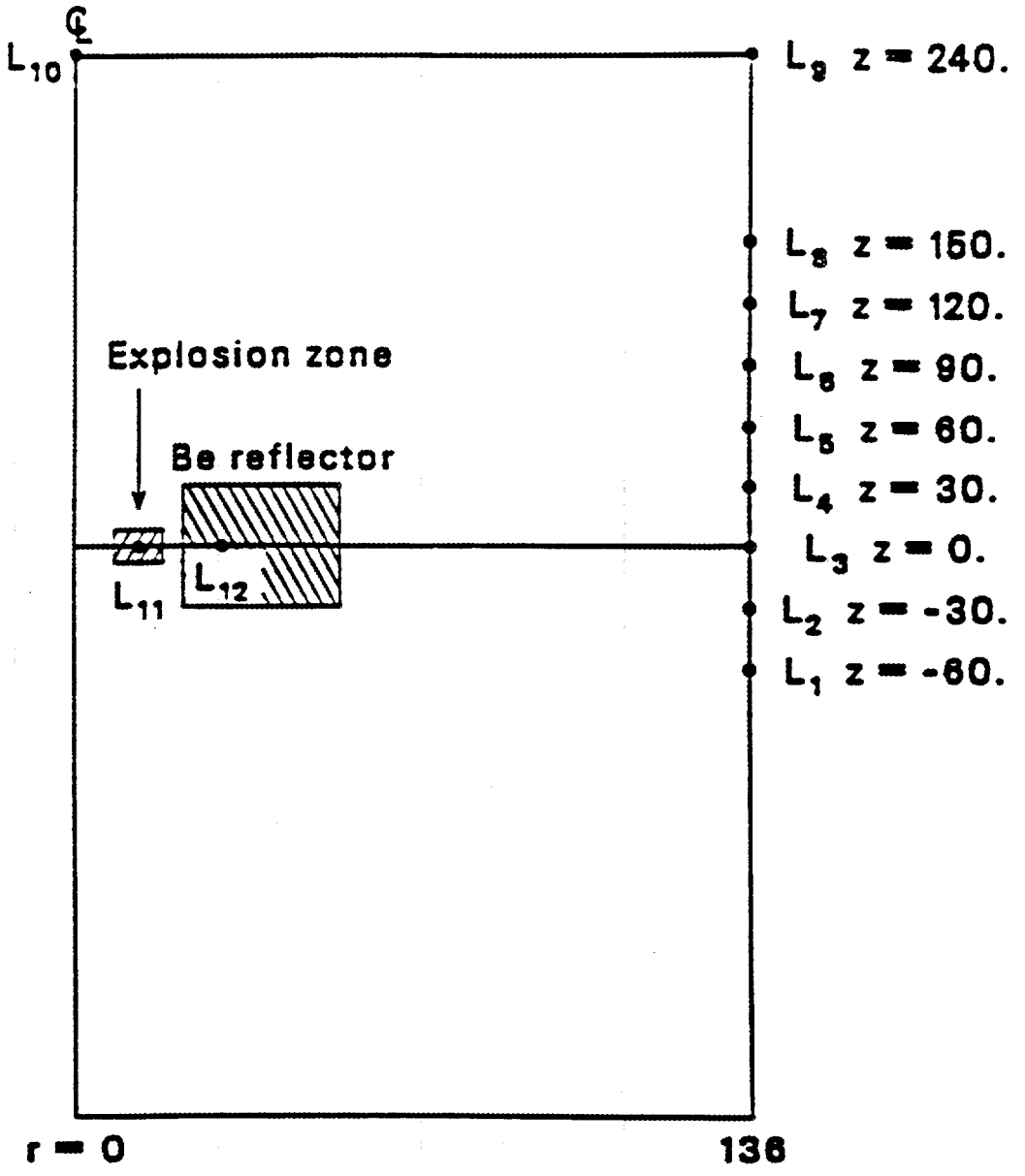

All dimensions in centimeters

Initial Temperature 330 K, Initial Pressure 3.2 MPa

Fig. 2.13 Model 1 of HFIR for CTH Calculations

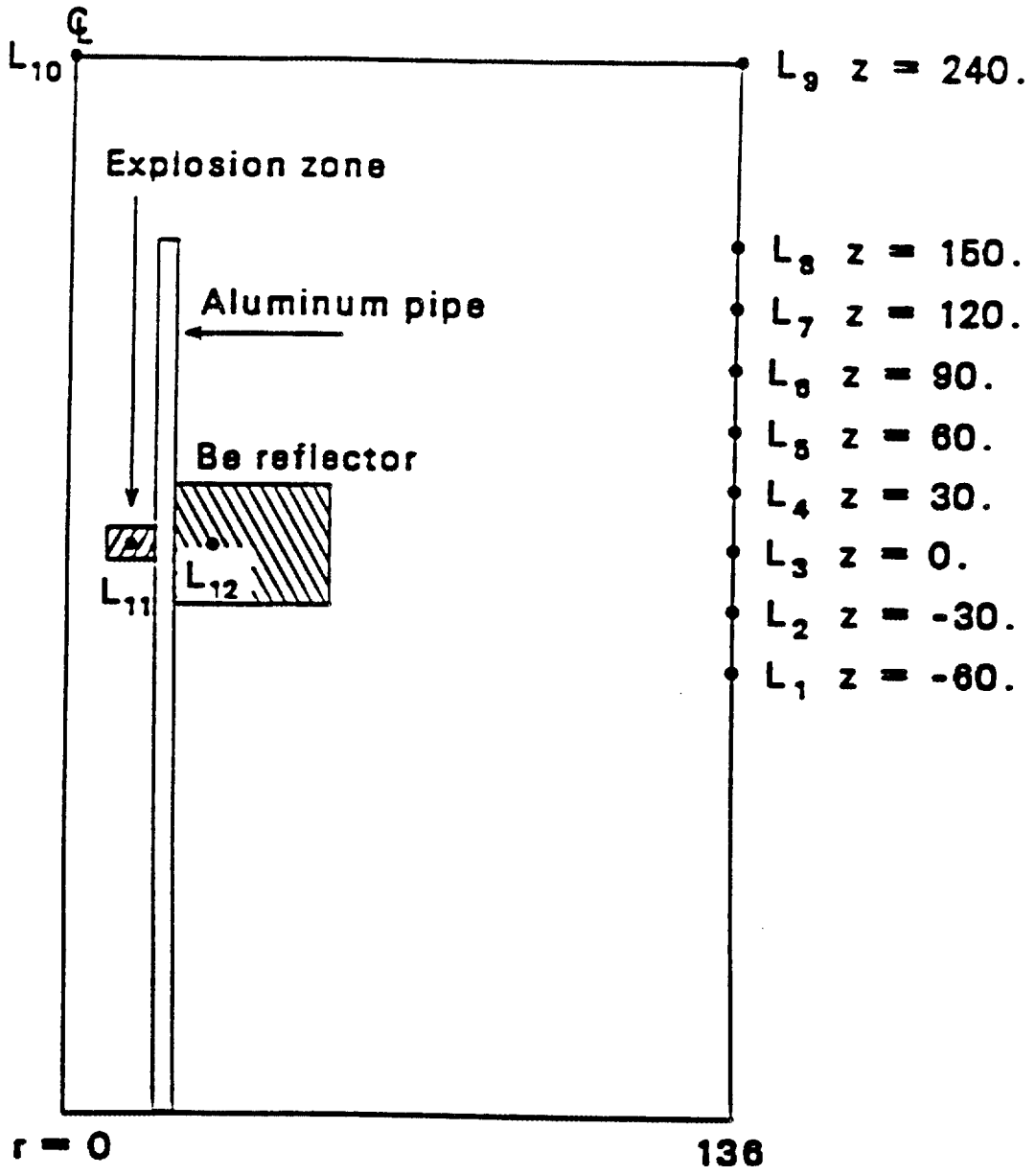

All dimensions in centimeters

Initial Temperature 330 K, Initial Pressure 3.2 MPa

Fig. 2.14 Model 2 of HFIR for CTH Calculations

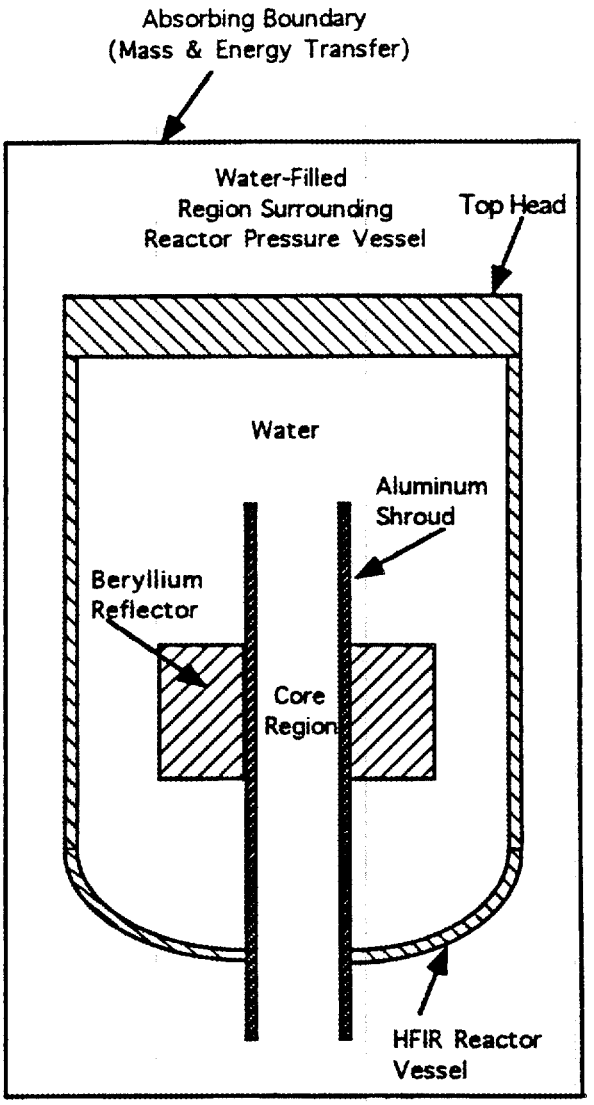

Fig. 2.15a Model 3 of HFIR for CTH Calculations

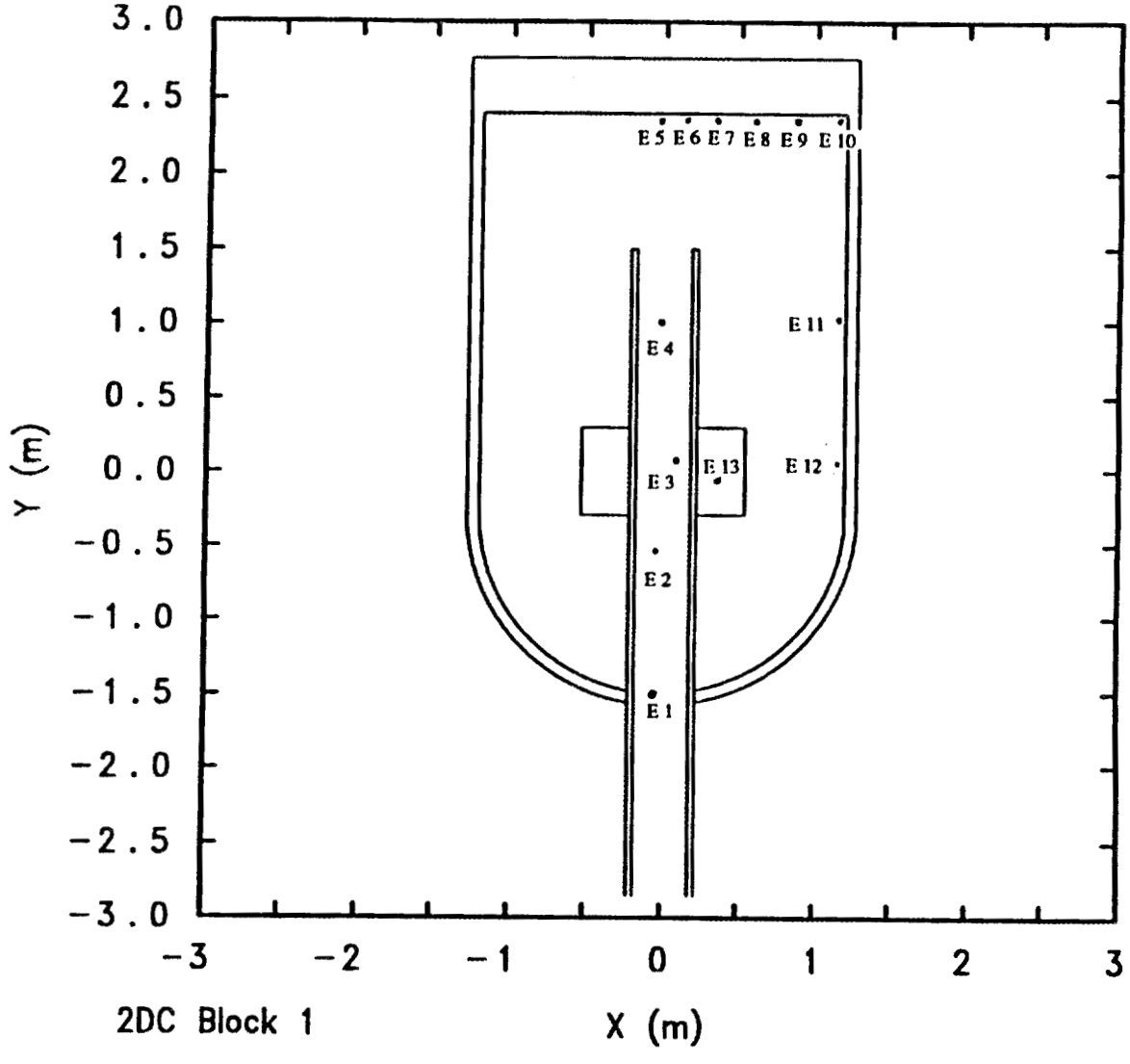

Fig. 2.15b Model 3 of HFIR for CTH Calculations (Location of Lagrangian Points)

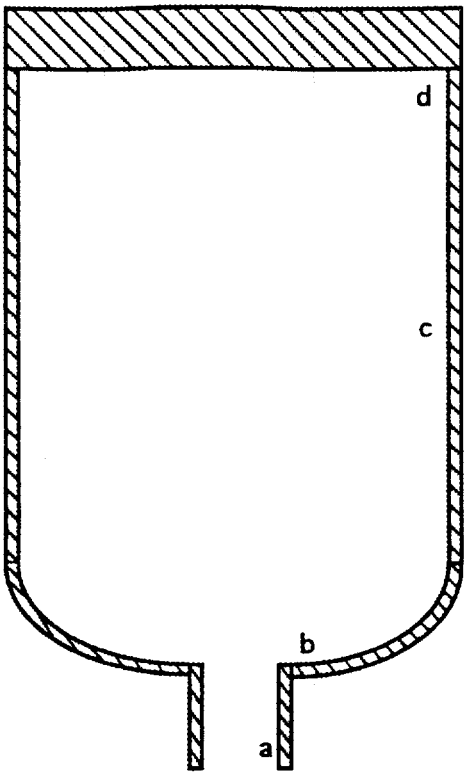

Fig. 2.16 ADINA Model of HFIR Pressure Vessel for Dynamic Calculations

3. STEAM EXPLOSION ANALYSIS FOR HFIR

In this section we describe the spectrum of analyses conducted for addressing the issue of steam explosions in the HFIR vessel region arising from core flow blockage events. The various aspects of analyses are described below:

3.1 IN-CORE MELT INITIATION AND PROGRESSION ANALYSIS

Some of the key aspects concerning steam explosions during flow blockage-induced accidents in the HFIR deal with the questions of damage initiation and propagation, which are a subset of a larger issue dealing with core melt progression and fission product release. The magnitude and duration of dynamic pressure pulses are directly related to, and are very dependent on, the quantity of melt available for explosive interaction. It is thus important to formulate at least a rudimentary mechanistic basis for evaluating the number of fuel plates that can be involved in steam explosions during flow blockage accidents.

Various aspects dealing with melt initiation, propagation modeling, and problem formulation have been described in Sect. 2. These models and postulates were used in deriving preliminary information on core melt initiation and propagation during flow blockage events. Results are described systematically.

3.1.1 Fuel Melt Initiation Analysis

Two models (viz., Model A and Model B) described earlier were used to estimate the degree of core flow blockage necessary to cause melt initiation. Model A utilizes a lumped parameter conservative approach. With Model A, the critical velocity through a blocked coolant channel required to cause saturation conditions at core exit amounts was calculated to be 46.6 m/s (153 ft/s). Such a steam velocity leads to a pressure drop of

about 111 kPa (15.9 psid) across the length of the core in the blocked channel. The nominal core pressure drop across the HFIR core is about 0.749 MPa (107.1 psid). Therefore, the blocked channel area should be such as to cause an entrance pressure drop of 0.638 MPa (91.2 psid, which is equal to 107.1–15.9). An estimate was made of the flow area reduction required at the channel entrance that would lead to the necessary pressure drop using classical sudden contraction correlations. This study led to the conclusion that the channel inlet flow area reduction of 74% or greater could lead to melting of adjacent fuel plates. Further details are given in Appendix C and in Ref. 22.

As mentioned in Sect. 2, Model A (Fig. 2.1) is expected to give rise to conservative estimates for flow blockage fractions necessary for causing fuel plate melting. To refine this estimate from a lumped parameter approach (viz., Model A) to a 1-D multiphase flow analysis, Model B was utilized based on use of the well-known RELAP5 code. Details regarding two-phase flow thermal-hydraulics in the core region are given in Appendix C. Calculations for Model B revealed that blockage of several flow channels below 92% of the collective flow area would be necessary to cause the onset of fuel plate melting. From a 1-D perspective, the Model B calculations were conducted using several conservative assumptions (e.g., axial and radial heat conduction neglected). On the other hand, these calculations did not account for multidimensional thermal-hydraulic effects in the flow channels and also did not account for the effects of hot spots or hot streaks. However, it should be mentioned that these calculations with RELAP5 are not meant to represent an exhaustive best-estimate study. They were conducted to provide an order of magnitude estimate from a 1-D perspective to evaluate the necessary flow blockage area for onset of fuel melting. Model B results indicate that a substantial portion of the inlets to several fuel channels would need to be blocked before fuel melting could ensue.

Two situations were analyzed using Model C based on use of the RELAP5 code. The first situation represents complete blockage of a single channel (via closure of the

A preliminary estimate of the likelihood for damage propagation was made using the "melted box" model (viz., Model D) described in Sect. 2. Model D uses the RELAP5 code with conservative assumptions relating to heat transfer from the so-called "melted box" to the neighboring unmelted fuel plates. Details are provided in Sect. 2 and in Appendix C. Results of the analysis using Model D revealed that up to 9 or 7 fuel plates in the inner or outer fuel element regions, respectively, can melt without causing the neighboring fuel plates to heat up to melting conditions. For any number of plates less than 9 or 7 in the inner and outer fuel elements, sufficient heat transfer is possible around the unmelted plates to prevent temperature rise (all the way to melting conditions).

In Sect. 2 three scenarios were postulated that may lead to the possibility of fuel melting. Scenario 1 considered the possibility of fuel plate ablation from the core region. This would lead to widening of flow channels and to an increase in the flow velocity there. An analytical framework was developed to evaluate so-called critical velocities for the onset of buckling instabilities in fuel plates. This work is summarized in Appendix B. When compared to the velocities necessary for causing fuel plate buckling-induced failure, it was seen that the highest predicted flow velocities in the vicinity of about 45 m/s are lower than the critical flow velocities in the range of 50 to 77 m/s. Because it is highly unlikely that melted fuel plates will completely ablate away, the highest predicted flow velocity in widened flow channels of about 45 m/s represents a conservative upper bound. Therefore, we can conclude that Scenario 1-type situations will not lead to propagation of fuel melting.

For Scenario 2 it was shown (in Sect. 2) that the maximum static lateral pressure difference across a fuel plate in a blocked coolant channel cannot be more than about 0.7 MPa (100 psi). ADINA and ABAQUS codes were used to set up 2-D and 3-D models of HFIR fuel plates as mentioned in Appendix D to evaluate the necessary buckling pressures. Results of these calculations revealed that the necessary buckling loads for the first three buckling modes (for HFIR fuel plates) are in the vicinity of

valve in junction 502 of Fig. 2.1); whereas, the second situation is a full blockage of three flow channels (via closure of valves in junctions 402, 502, and 602 in Fig. 2.1). It was found that a single-channel full-flow blockage did not result in fuel melting. This is because the heat sink available from the adjacent flow channels was sufficient to cool the fuel plates bounding the blocked channel. The multichannel flow blockage did result in fuel melting. This is in relative agreement with results presented earlier using Model B which indicated that partial flow blockages of >92% would lead to fuel melting.

At this stage it is useful to summarize results from previous work conducted for HFIR safety analysis and reported in ORNL-3573.[54] In this previous work, the analysts postulated that small- and large-flow blockages to the HFIR core would result in melting of 10 and 24% of the core fuel plates, respectively. These fractions were evaluated on the degree of fuel and coolant heatup required to cause a one dollar reactivity change before the control system would cause a reactor scram to occur. These estimates were essentially based on overall postulates alone and are deemed to be conservative. The analysis did not deal with details of core melt initiation and propagation, and did not take credit for void-reactivity feedback or even for the possibility of molten fuel material relocation out of the core. Further comments on the ORNL-3573 analyses are given in Appendix A.

3.1.2 Fuel Melt Propagation Analysis

In this section we discuss various aspects of the core melt propagation analysis work done for HFIR. As mentioned in Sect. 2 several models were developed for evaluating various aspects of core melt propagation. Results of analyses with the various models are described sequentially. First, we deal with melt propagation from a static perspective. Thereafter, results are presented on the propensity for damage propagation arising from localized steam explosions.

1.2 MPa. This value is close to twice the maximum possible static pressure difference across a fuel plate surface. Therefore, we conclude that Scenario 2-type situations cannot lead to propagation of fuel melting.

A third scenario (viz., Scenario 3) was postulated in Sect. 2 for addressing the issue of damage propagation, and deals with the possibility of localized steam explosions resulting from melting in selected regions of the core. The dynamic pressure pulses may be large enough to damage adjacent plates to the point of causing flow disruption and melting there. Thereafter, a domino-type effect may take place until the reactor is scrammed. Structural failure envelopes were evaluated for a variety of different boundary conditions and geometrical set-ups, using the ADINA code to evaluate the response of fuel plates to dynamic loads. Failure envelopes were developed for the fuel plate subjected to triangular pulses on the entire surface using a 2-D model, or selectively as a pressure strip or a patch using a 3-D model. Details of the various models developed are given in Appendix D. Models developed ranged in the degree of detail modeled from a single plate with no accounting for fluid inertia of side plates to a representation of two plates with three coolant gaps and side walls to model the complete outer fuel core plates. Additional 2-D confirmatory analyses were conducted with more elements to check for convergence. Results of the additional 2-D analysis and the two 3-D analyses are shown in Fig. 3.1. As seen from Fig. 3.1, the results for the single plate, the single plate with more elements, and the 3-D plate with a pressure strip across the span give essentially the same failure envelopes. Only the 3-D plate model with a pressure patch in the center of the plate gives a somewhat higher failure envelope.

All in all, the results of dynamic structural analyses indicate that for steam explosions with pressure pulses in the millisecond duration range, plate failure will occur if the steam explosion pressure magnitude is above 1.75 MPa (250 psi). To evaluate pressure pulses likely in the explosion zone, FCIMOD.ORNL calculations were

performed. Details of the evaluation process are given in Appendix F. Briefly, two cases were analyzed:

Case 1: One molten fuel plate and water from two coolant channels mix before an explosion, and

Case 2: Two molten fuel plates and water from three coolant channels mix before an explosion.

Results of the FCIMOD.ORNL calculations for the two cases mentioned above are depicted graphically for different assumptions for the coolant void fraction in the explosion zone before an explosion. As seen in Figs. 3.2 and 3.3, depending on the thermal hydraulics of the situation, the pressure pulse magnitude can range from about 6 to about 26 MPa. In all instances, the pressure pulse width is several milliseconds long, and much greater than the required 1.75 MPa pressure level for adjacent plate failure. Therefore, we conclude that damage propagation under full power conditions is likely for Scenario 3-type situations.

The extent of damage propagation is difficult to state with confidence for any of the two cases mentioned above where damage propagation was shown to be a possibility (i.e., from Model D RELAP5 and Scenario 3 analyses). This is essentially due to the absence of a properly validated and integrated melt progression modeling capability. However, based on the HFIR control system design and previous conservative analyses conducted and reported in ORNL-3573, an upper bound may be set at 24%. That is, up to 24% of the core material may be conservatively assumed to melt and participate in a steam explosion event during core flow blockage accidents in HFIR.

3.2 DEBRIS HEATUP/COOLABILITY EVALUATIONS

As mentioned previously, steam explosion occurrence is considered somewhat stochastic. Steam explosions in the core region may not have occurred even upon significant plate melting. Under such circumstances, the fuel plate materials would most likely relocate to the shield plug region separating the sub-pile room from the reactor pool. Debris heatup (on decay heat) and melting/freezing of the debris-steel combination need to be evaluated to provide a structured means for steam explosion energetics calculations for that region.

Evaluations of heatup, melting, and freezing were conducted using the 2DKO and MELCOR codes as described briefly in the previous section. MELCOR code evaluations were used only to provide a means for suitable benchmarking of selected aspects of the 2DKO code, and also for providing an approximate estimate for the surface boundary conditions to be used in 2DKO calculations. This section briefly outlines the test matrix of calculations and the results of the melting/freezing calculations. Details are described in Appendix E and in Refs. 40 and 44.

The test matrix of runs made with MELCOR and 2DKO is shown in Table 3.1. Case 1 was a rudimentary effort to compare results from MELCOR and 2DKO codes. This comparison exercise has been described in Sect. 2. As noted previously, reasonably good agreement was observed in the traces of temperature profiles provided by these two codes. In Table 3.1, the debris height of 0.073 m corresponds to the height of the debris bed corresponding to the whole core (approximated as 100 kg of aluminum) relocating to the shield plug with no porosity. Variations of this height essentially constitute evaluations for different amounts of the core material relocation. The debris decay power level was also parametrically varied to account for reduced core material inventory relocating to the shield plug region (e.g., Case 3), and for situations where debris power reduction occurs due to loss of volatile fission products (e.g., Case 6). The debris

surface-to-pool heat transfer coefficient was estimated at ~3000 W/m^2-K for stable film boiling from MELCOR calculation plots as shown in Fig. 3.4(b) for Case 2. Similarly, the shield plug-to-water connective heat transfer coefficient was estimated as being close to 250 W/m^2-K. The debris surface-to-pool heat transfer coefficient was also parametrically increased to a high value of 4000 W/m2-K to account for possible increases caused by surface churning and radioactive losses (which were accounted for in the MELCOR calculations but are not reflected in the film boiling heat transfer coefficient). Additionally, runs were also made with 2DKO with the assumption that the core debris relocating onto the shield plug would do so over a period of 10 s (as an unverified assumption). These are cases 8, 9, and 10, in Table 3.1. For these runs, the nodalization and problem geometry assumed was as described in Sect. 2.

Results of runs for Cases 2 to 10 are summarized in Table 3.2. As seen in Table 3.2, the maximum debris temperature for Case 2 can get close to 1660 K or even 2065 K, depending on the surface heat transfer conditions. However, this is true only in the extreme case where all of the core debris has relocated instantly and none of the volatile fission products leave the debris bed. Under similar conditions, with the exception that only half of the core relocates down to the shield plug region, the maximum debris temperature reached is lower by about 45% as seen for Case 3. If the surface heat transfer coefficient is higher than thought (i.e., 4000 W/m^2-K instead of 3000 or 2000 W/m^2-K), the corresponding maximum debris temperatures are lowered to 1452 K and 794 K, respectively, as seen for Cases 3 and 4. Cases 3 and 4 are the same as Cases 2 and 3, with the exception of the debris-to-reactor pool heat transfer coefficient.

Starting with Case 2 again, if we now look for the effect of debris power reduction from complete loss of volatile fission products, we see from Case 6 that the reduction in maximum temperature is similar to that seen for Case 3 (where only half the core debris had relocated). If only half of the core debris relocates and, further, all of the volatile fission products are relieved to the reactor pool, no debris heatup is obtained as

seen for Case 7. That is, enough heat transfer capacity is available to prevent debris bed superheating beyond melting. Cases 8 through 10 are the same as Cases 2, 3, and 6, with the exception that the core debris is allowed to relocate onto the upper shield plug over 10 s instead of instantly. The results for maximum temperature rise indicate that the increased time span over which debris relocation occurs does have a beneficial effect. That is, the maximum temperature rise is lower for the case where the debris relocates over a given time period instead of relocating instantly. The amount of temperature lowering is small for the situations being analyzed. Because of the absence of a core melt progression capability, it is difficult to state with confidence what level of temperature lowering one might see in reality. Therefore, for evaluating FCI loads, it is recommended that the results obtained by assuming instant relocation onto the upper shield plug be used.

Further details involving time histories of the key variables (viz., temperatures and melting/freezing fractions) are shown graphically in Appendix E.

3.3 ANALYSIS OF STEAM EXPLOSION ENERGETICS

As mentioned in Sect. 2, the energetics aspects of steam explosions can be evaluated from several different perspectives. That is, one can conduct conservatively bounding (i.e., thermodynamics) calculations using the Hicks-Menzies or Board-Hall approaches, or one can conduct more realistic calculations using either one-, two- or three-dimensional simulations. In this section we show results on steam explosion energetics evaluations from use of the HM/BH (i.e., thermodynamic estimates), FCIMOD (one-dimensional best-estimate simulations), and the state-of-the-art CTH (two-dimensional simulation) codes, the capabilities of which are described earlier in Sect. 2.

A test matrix of desired or targeted calculations was set up for accommodating a wide range of possible combinations of parameters. The test matrix is given in Table 3.3

where a range of possible combinations for key parameters in the explosion zone (i.e., mass of fuel, mass of coolant, coolant initial void fraction, fuel and coolant initial temperatures, inertial constraint, etc.) has been considered.

3.3.1 Results of Thermodynamic Evaluations

As mentioned in Sect. 2, thermodynamic evaluations using either HM or BH approaches necessarily give high end-point estimate values for pressure buildup and thermal-to-mechanical energy conversion. Nevertheless, they serve a useful purpose in evaluating whether system boundaries can withstand such loads. If so, then further evaluation with more sophisticated tools may be safely avoided. Selected results for maximum mixture, pressure buildup in the explosion zone and energy conversion were obtained for certain cases outlined in Table 3.3 using the HM and BH approaches and are presented in Table 3.4 for Cases 2, 5, and 7, respectively. As noted from Table 3.4, significant pressurization (i.e., more than 1000 MPa) can be obtained, and the conversion ratio can be significant. Note the strong variation in pressure buildup and energy conversion with the mass of fuel that mixes and interacts with a given mass of coolant in the explosion zone. Again, the value for pressurization predicted using the BH approach consistently gives larger values when compared to those from using the HM approach. This is attributed to the BH approach which treats the process as being one of detonation. The correct answer from the standpoint of thermodynamic evaluations will lie somewhere in between.

Graphical representations of results for a variety of initial void fraction levels are shown in Fig. 3.5 to 3.8, respectively, assuming that 10 kg of molten aluminum at 1300 K mixes with 10 kg of water at 330 K in the explosion zone. The very strong dependence on void fraction for the pressurization is evident from these diagrams. However, the total work done on surroundings is dictated by the energy conversion ratio, which remains relatively constant at about 23% over a wide range of void fractions.

These results provide useful benchmarks for calculated results obtained using more sophisticated methods described in Sect. 3.3.2. However, further details of the calculation results using these models are given in Appendix F and in Ref. 48.

3.3.2 Results of 1-D Energetics Calculations with FCIMOD

This section describes some of the preliminary results obtained for the energetics of steam explosions in a one-dimensional geometry using the FCIMOD program described in Sect. 2. Briefly, FCIMOD models a one-dimensional FCI in the geometry shown schematically in Fig. 2.11. A mixing zone at the bottom where molten fuel is fragmented into small particles and mixed with liquid coolant is assumed. Above the mixing zone, the slug zone is accelerated by the expanding vapor into the expansion zone. A planar mixing zone is shown in Fig. 2.11 at the slug-mixture interface, although the code can treat the case of a hemispherical slug also. For our situation, the interface was deemed to be best represented by a planar interface. Inertial constraint is another key parameter that needs to be evaluated. For a power reactor scenario, this constraint is essentially the mass of slug over the mixing zone. However, for a solid system such as the HFIR during a flow-blockage accident condition, the proper choice of an inertial constraint is not that clear. Hence, as a first step we have chosen to evaluate the energetics parametrically as depicted in various cases considered in Table 3.3.

Salient results for all 34 test cases are summarized in Table 3.3 (where the test matrix conditions are also given), and shown graphically for some of the test cases in Figs. 3.9 through 3.14. As seen for Cases 1 through 6, the degree of pressurization increases with initial fuel temperature but the conversion ratio ranges from 6% to 8% for all six cases. Actually, the conversion ratio is still increasing up to the point the calculation was run, but from experience should flatten out soon thereafter. In any case, it is noteworthy that the peak pressure values are in the range of 65 to 140 MPa for the first three cases. Specifically for Case 2, a direct comparison can be made with values

obtained from thermodynamic calculations. FCIMOD predictions indicate a pressure rise and conversion ratio of 78 MPa and 8.2%, respectively. These predictions are a lot lower than the corresponding HM calculated values of about 571 MPa and 23%. The degree of conservatism that is reduced from not using thermodynamic maximum values is evident.

Note that for Case 26, a slug breakup condition was encountered wherein the FCIMOD.ORNL code aborted the calculation. The slug breakup occurs when vapor "bubbles out" of the water rather than pushing the slug as a missile. A study of the transient plots of pressure and conversion ratio for the 34 cases provided the following insights:

- An increase in the fuel temperature increases the peak pressure pulse magnitude. This is to be expected because the higher fuel temperatures contribute to the increased energy transfer to the coolant. Fig. 3.15 displays the peak pressure variation by test case and also the fuel temperature.
- An increase in the vapor volume in the explosion zone generally decreased the peak pressure pulse magnitude as can be seen from Fig. 3.16. The size of the pressure shock depends on the vapor generation rate, which is also governed by resistances to energy transfer. Some of the resistances are: fuel, vapor region, and liquid. Of these, the vapor layer contributes the greatest resistance because of its relatively low thermal conductivity.
- An increase of coolant mass in the explosion zone reduces the peak pressure magnitude. This is attributed to the increased energy required to heat up the liquid instead of produce the vapor. Clearly, a tradeoff exists because we have stated earlier that increased vapor production beyond a certain value also decreases pressure pulse generation capability.
- An increase in the ambient pressure does not significantly affect the pressure pulse magnitude; however, the conversion ratio decreases.

- An increase of the slug mass (i.e., inertial constraint) increases the peak pressure pulse magnitude, but also tends to reduce the overall thermal-to-mechanical energy conversion ratio.

A few further observations are in order. The rapid oscillations seen in the pressure in the neighborhood of the critical point (22.055 MPa) for Case 4 are a symptom of difficulty with the NWSTEAM subroutine package in FCIMOD. We plan to replace this with a different package based on relatively new data and fits (National Bureau of Standards). As a result of this problem, the conversion ratio has a maximum value of about 5.4% at about 45 ms, and then begins to decrease. The break in the liquid coolant temperature curve at just past 1 ms indicates the beginning of the transfer of more cool liquid into the mixing zone from the slug.

3.3.2.1 Effect of FCI on Reactor Vessel

Previous FCI work done for HFIR[54] estimated that a uniformly applied internal pressure required to burst the HFIR vessel (from an elastic standpoint) would be 35.7 MPa. FCI energetics calculations reported in this appendix using FCIMOD.ORNL have shown that such a pressure level can certainly be reached and exceeded in the explosion zone (but for short durations only). However, the strain energy required to rupture the vessel was calculated[54] at 200 MJ, which represents the work performed by pressurized fluid expanding in a given volume. It should be noted that the peak pressure predicted by FCIMOD.ORNL is not a static pressure rise. All considered, it was found that based on the predictions of thermal-to-mechanical energy conversion during steam explosions for Cases 1 through 34, the mechanical work performed (see Table 3.3) is not sufficient to cause gross rupture of the vessel. It is recognized that FCIMOD results are from 1-D calculations that cannot be directly compared to the previous calculations for global HFIR vessel failure. The Ref. 54 analyses assumed uniform application of the

200 MJ of energy for HFIR vessel failure. At this stage, it should be mentioned that vessel failure characteristics have been studied with more sophisticated tools, using the principles of fracture mechanics for the current report, and are discussed later in this report.

3.3.2.2 Propagation of Core Damage From Localized Steam Explosions

In the event of the fuel melting of certain fuel plates, it was postulated in Sect. 2 that a localized FCI may produce a large enough pressure pulse to cause damage propagation. As discussed earlier, failure envelopes were developed for the fuel plates in the HFIR core. These failure envelopes indicated that pressure pulses of a magnitude greater than 1.75 MPa (250 psi) and lasting for a milisecond or more would cause plate failure.

To evaluate pressure pulses likely in the explosion zone, FCIMOD.ORNL calculations were performed. Two selected cases given below show that the pressures reached during an energetic FCI under likely thermal-hydraulic conditions can be as high as 25 MPa regardless of whether one or two fuel plates have initially melted. The following two cases were analyzed:

Case 1: One molten fuel plate and water from two coolant channels mix before an explosion, and

Case 2: Two molten fuel plates and water from three coolant channels mix before an explosion.

Input parameters for FCIMOD.ORNL calculations are the mass of fuel, coolant, and slug, and void fraction in the explosion zone. For both cases, a column of water 1.2 m in height (representing water above the core) was used to estimate the slug mass (viz., inertial constraint). The cross-sectional area of the reaction zone is the sum of the

cross-sectional areas of the fuel plate(s) and the cross-sectional area of the coolant flow channels. Two different void fractions were evaluated [viz., 25% (i.e., CVOID = 0.33) and 75% (i.e., CVOID = 3.0), respectively].

Results obtained for the two cases are summarized in this section. Graphical variation of results are given in Appendix F (viz., Figs. F.12 through F.13). For both cases with CVOID = 0.33, peak pressure pulses reached are 23 and 26 MPa, respectively. For the high void fraction situation (i.e., CVOID = 3.0), the respective pressure levels are 6 and 9 MPa. In all instances, the pressure pulse width is several miliseconds long and much greater than the required 1.75 MPa pressure level for adjacent plate failure. We therefore conclude that localized steam explosions in the core region would very likely lead to damage propagation.

3.3.3 Steam Explosion Energetics - Preliminary CTH Analysis

As mentioned in Sect. 2, various models were developed for analyzing multidimensional (i.e., 2-D) steam explosion energetics in the HFIR vessel using the CTH code. These model representations are shown in Figs. 2.13 through 2.15. For all cases, energy deposition in the explosion zone (i.e., core region) was done using the representation of Eq. (2.1).

Enormous quantities of information were generated from these evaluations, for which details exist in Appendix G, calculational notes, and in Refs. 43 and 46.

Using Model 1 (i.e., simple model without aluminum tube), with an initial pressure of 3.2 MPa and an energy source of 15 MJ, it was found that the results for an absorbing and reflecting boundary are quite different. Even though the pressure buildup in the explosion zone is similar for the two boundary conditions, the pressure buildup at the top head lower surface is considerably lower for the case with an absorbing boundary condition. It clearly underscores the importance of appropriate modeling of boundary conditions.

Using Model 2 (i.e., simple model with aluminum tube) with an initial pressure of 3.2 MPa and an energy source of 15 MJ, it was noted that the effect of absorbing versus reflecting boundary conditions is similar to that seen earlier with Model 1. In addition, it was found that having the aluminum tube increases the pressure buildup in the explosion zone, but reduces the pressure buildup at the top head lower surface. This is attributed to greater resistance to energy dissipation from the explosion zone, which causes a higher pressure buildup there. However, the aluminum tube material also acts as an energy-absorbing medium that assists in reducing the shock wave energy levels at the various vessel surfaces.

Calculations were also performed with the various models using the initial system pressure as 0.1 MPa (i.e., atmospheric pressure). However, it was found that both initial system pressures produce about the same pressure rise from initial conditions.

Additional scoping calculations were performed to evaluate the impact of lengthening the time span over which the energy deposition occurs in the explosion zone, from 1 to 2 ms. No discernible differences were observed.

Further details of calculational results obtained with Model 1 and Model 2 are given in Appendix G.

Additional scoping calculations were performed to evaluate the impact of lengthening the time span over which the energy deposition occurs in the explosion zone, from 1 to 2 ms. No discernible differences were observed.

Upon completion of scoping calculations with the simplified models (i.e., Models 1 and 2), the best-estimate model (viz., Model 3) was exercised. Because of the significantly increased machine time requirements for analyzing Model 3, all calculations were conducted with the most realistic (viz., absorbing) boundary condition only. Runs were made with energy deposition levels of 7, 31, 51, and 65 MJ. The cases with 7 and 31 MJ of thermal energy inserted in the explosion zone over 1 ms did not result in sustained pressure levels in excess of failure levels for the vessel or top head (viz., about

21 MPa on the average for greater than 0.6 ms for the reactor vessel, and more than 26 MPa required for failure of top head bolts, as described in Appendices I and J). The case with 31 MJ of energy deposition does give pressure pulses in the centerline region right under the top head greater than 26 MPa. However, these are peak pulse magnitudes and do not last for more than about 0.5 ms. In addition, the pulse magnitude decreases significantly from the centerline to the vessel wall interface region, with the result that vessel failure pressure level (of 21 MPa lasting for more than 0.6 ms) is not reached. These attributes are clearly seen in the sample results displayed in Figs. 3.17(a) and (b) and 3.18(a) and (b) for the two cases under consideration. An important aspect of the situation for these two cases is that the mechanical integrity of the aluminum shroud tube is not affected. This accounts to a large measure for the significant variation in pressure pulse magnitudes from the top head centerline to the vessel wall-top head interface. For these instances, the shroud acts as a channel, directing pressure waves upwards, and thus limits the degree of dissipation in the radial direction. It also serves as an organ pipe, giving rise to significant ringing effects as seen in the high frequency pressure waves being built up as the transient progresses and reflected waves tend to overlap. For the 7 and 31 MJ cases, significant reduction in pressure pulse levels occurs in the radial direction as a result of the gun-barrel effect mentioned earlier.

The two additional cases with 51 and 65 MJ energy insertion did cause the aluminum shroud to rupture from the FCI energetics. This is seen in Figs. 3.19(a) and 3.20(a) for these two cases. The rupture of the shroud allows for increased dissipation of explosion energy in the radial direction, and also leads to significant reduction or even elimination of the buildup of the above-mentioned "organ-pipe" effect. Pressure pulse histories for these two cases (directly beneath the top head in line with the vessel centerline, and also at the interface between the vessel wall and top head) are shown in Figs. 3.19 and 3.20. It was found that the pressure pulse magnitudes underneath the top head display much less variation in the radial direction than that seen for earlier cases

where the shroud had not ruptured. Note that for the 51 and 65 MJ cases, the average pressure below the top head and in the vicinity of the reactor vessel is larger than the required 21 MPa pressure (lasting more than 0.6 ms) required for vessel rupture from fracture, or even the 26 MPa required for failure of bolts, and thereafter, for generation of an energetic missile. These results would indicate that the energy level required for causing imminent vessel failure would amount to a value between 31 and 51 MJ. Engineering judgment indicates that this value is around the 40-MJ energy level. For 51 MJ, the average pressure over the top head under surface amounts to about 30 MPa lasting about 3 ms, whereas the corresponding values for 65 MJ are in the vicinity of about 35 MPa, also lasting for around 3 ms. Further details are given in Ref. 46. Another important result worth noting is the sharp reduction in pressure levels from the explosion zone to the top head and vessel wall boundaries. Figure 3.20(b) provides the pressure history in the explosion zone for the 65 MJ case. As can be seen, pressures in the explosion zone can be higher by a factor of 5 or more than pressures at the system boundary (for the HFIR case).

Additional details of the calculational results are given in Appendix G.

For the cases where vessel or bolt failure may occur, the initial velocity of a missile must be evaluated. If we estimate that an average pressure (P_{av}) acts on the top head for a given time (τ) after the top head has broken loose, the initial upward velocity of the top head is estimated as,

$$V_o = \frac{P_{av} A \tau}{\rho_s A H} \qquad \text{(G.2)}$$

where H, the thickness of the top head is 0.36 m; ρ_s, the density of the steel is 8000 kg/m^3, and τ is the time over which the force acts (beyond the about 0.6 ms required for failing the vessel or bolts via fracture). For the two high energy cases, the initial velocity is then calculated as:

Energy (MJ)	P_{av} (MPa)	τ(ms)	Vo (m/s)
51	30	2.4	25
51	30	3.0	31
65	35	2.4	30
65	35	3.0	37
65	40	2.4	35

The velocities estimated were used to evaluate missile energetics and transport through the reactor pool and high-bay air space.

3.4 VESSEL AND BOLTS FAILURE ANALYSIS

In this section we describe the analysis work for evaluating the loads necessary to cause failure of the HFIR vessel and top head bolts, based on the modeling and problem formulation outlined in Sect. 2, and discussed further in Appendix H.

3.4.1 Vessel Failure Characteristics

As mentioned previously (Sect. 2), the dynamic strength of the HFIR vessel to resist hypothetical accidents was analyzed by using the methods of fracture mechanics. Vessel critical stresses were estimated by applying dynamic pressure pulses of a range of magnitudes and pulse durations. Elastic dynamic ADINA calculations were performed to obtain hoop stress magnitudes at the three locations shown in Fig. 2.16. It was found that the effective stress values at the points "a" and "b" are essentially similar. However, for point "d" the effective stresses in the material were seen to be significantly higher. This is to be expected, since point "d" is at a location where significant stress concentrations can occur. Point "d" values are not considered here because in reality the top head is

bolted to the vessel. Therefore, for evaluating vessel failure, the failure envelopes for the midplane will be taken as the representative ones. It was also noted that the hoop stress does not vary much across the vessel wall, which indicates the absence of significant bending moments to modify the hoop stress variation. So-called failure envelopes generated are shown in Fig. 3.21. These are essentially plots of peak-induced stresses in the vessel wall when subjected to an external pressure pulse (y-axis) of a given magnitude (x-axis). As seen in Fig. 3.21 the failure curves tend to flatten out for pulse durations larger than about 0.6 to 0.8 ms. For analysis purposes this implies that to determine whether a steam explosion will cause vessel failure, one need only determine if the pulse duration in general is larger than about 0.6 to 0.8 ms. The precise value of pulse duration is not as important.

Thereafter, a conservative deterministic estimate[34] was made to evaluate vessel failure loads. This conservative approach was based on American Society of Mechanical Engineers (ASME) guidelines in which a 25.4-mm (1-in.) crack was assumed in conjunction with a factor of safety of 1.0 and an operating temperature of 367 K. This resulted in a failure hoop stress of about 245 MPa (35 ksi). Further details are given in Appendix H.

If the information in Fig. 3.21 is combined with the knowledge of the allowable vessel effective/hoop stress of 245 MPa (35 ksi) lasting for more than about 0.6 ms, the largest pressure pulse that can be tolerated is no more than 10 MPa (1.5 ksi). This approach gives rise to conservative estimates for vessel failure loads because it uses a set of highly conservative ASME guidelines.

To evaluate the best-estimate loads required, a probabilistic framework was also developed. The resulting calculation is probabilistic because the crack depths on the vessel surface have been assumed to follow a probability distribution. A brief description of the process is given in Appendix H and details can be found in Ref. 35. Results obtained from this probabilistic approach are summarized in Fig. 3.22. As can be seen in

the figure the probability of fracture is 7×10^{-6} after 10 EFPYs of embrittlement since 1989 for the stress level of 161 MPa (23 ksi). The probability increases 5×10^{-3} as the stress increases to 518 MPa (74 ksi), which may occur under severe accident loading conditions.

Based on the probabilistic approach results outlined in Fig. 3.22, it is seen that the 10-MPa failure pressure [corresponding to a hoop stress of 245 MPa (i.e., 35 ksi) has a low fracture probability of 10^{-4}]. However, for higher values of hoop stresses, [viz., >500 MPa (>70 ksi)], the corresponding failure pressure rises to about 20 MPa with a much higher fracture probability approaching 10^{-2}. It should be noted that these results are dependent on several parameters, one of which is the crack density in the material. The probabilistic results are based on a best-estimate crack density of 0.0753 cracks/m^2 (0.007 cracks/ft^2). Increasing this parameter proportionally increases the probability of fracture. See Appendix H for further details.

3.4.2 Top Head Bolt Failure Analysis

Based on the model described for top head failure in Sect. 2 and Appendix H, an analysis was conducted to evaluate what level of loads would be sufficient to cause the bolts (holding the top head to the vessel) to fail.

An important feature of the analysis for bolt failure is related to the time duration of the pressure pulse. As is well known, permissible material stress levels can increase quite sharply if the duration of the imposed pressure pulse gets smaller and smaller. Such an evaluation would require a dynamic structural analysis. In the absence of such an analysis, the results of vessel failure analysis shown as failure curves for the HFIR pressure vessel (viz., Fig. 3.21) were used to provide guidance on the time duration of pulses necessary, after which the failure curve tends to flatten out.

With the dimensions of the disk and bolts listed in Appendix H, and using Eq. (2.2) and (2.3) we obtain the ratio of bolt stress to pressure

$$\frac{(\sigma a_v - \sigma_t)}{P} = 24.6 \qquad (3.2)$$

If we take the yield strength of the steel bolts from original HFIR drawing equal to 840 MPa, and account for the 210 MPa pre-tension stress imposed on the bolts, the pressure required to break the bolts is then about 26 MPa.

To determine whether the bolts would fail before the vessel, a probabilistic fracture mechanics study would be required for the bolts region, as was done for the vessel. However, in the absence of such a study, we may concluded that if the pressure level adjacent to the top head lower surface exceeds the level of about 23.3 MPa for more than about 0.6 to 0.8 ms, the bolts would fail. For any extent that the imposed pressure exceeds this range, the effect would tend to be one where momentum transfer occurs to accelerate the top head. In reality, it should be recognized that upon bolts failure and top head rise, pressure relief may also occur to the large reactor pool. This would then tend to lessen the degree of momentum transferred to the top head. A detailed study of such a pressure relief could not be conducted for the work done for the HFIR SAR. Hence, from the standpoint of conservatism, the effect of pressure relief is not taken into account in evaluating missile energetics.

3.5 MISSILE EVOLUTION AND TRANSPORT ANALYSIS

An analysis was conducted to evaluate top head missile energetics for situations where a steam explosion of sufficient intensity causes the bolts to break and to accelerate the top head with an initial velocity, Vo. The model formulation of this phenomenon described in Sect. 2 was used to evaluate top head transport characteristics. The top head is represented as a circular disk, 2.43 m (8 ft) in diameter and 0.36 m (14 in.) thick, with a density of 8000 kg/m^3, launched upward with an initial velocity, V_o. The reactor pool is

4.3 m (14 ft) deep, filled with water with a density of 1000 kg/m^3. Drag coefficients were taken from Ref. 51. The value for C_v is a conservative estimate equal to 0.9. Because the density of water is only one-eighth that of steel, this choice should have only a minor effect on the results.

With the above-mentioned input parameters, the following estimates were made for the break time, exit speeds, and rise height:

Case 1: Drag Coefficient = 1.0

	Initial velocity (m/s)	
	20.0	35.0
t_{break} (s)	0.33	0.18
v_{exit} (m/s)	8.3	16.9
h_{rise} (m)	3.5	14.6

Case 2: Drag Coefficient = 1.4 (best-estimate)

	Initial velocity (m/s)	
	20.0	35.0
t_{break} (s)	0.40	0.21
v_{exit} (m/s)	5.7	12.6
h_{rise} (m)	1.6	8.2

As shown in Sect. 3.4, in a case where about 65 MJ energy level is inserted in the core region, the top head initial velocity would be in the vicinity of 30 to 37 m/s. As seen from the above calculations, if the drag coefficient were 1.0, such an initial velocity may be capable of causing the top head to almost reach the confinement roof, which is about 14 m (48 ft) above the pool surface level (Ref: ORNL-3572, Fig. 3.2.6).

Based on the results presented in this chapter, and using engineering judgment to conservatively account for uncertainties, we thus conclude that to threaten the HFIR confinement and cause bypass of filter banks, about 65 MJ thermal energy would need to be inserted into the reactor core region on an explosive time scale. This further assumes that aluminum temperatures will not rise high enough to cause ignition.

Table 3.1 Test Matrix of Debris Heatup / Coolability Calculations

Case	Code	Debris Ht. (m)	Initial Debris Power Level (Mw and %)	Debris-Pool Ht. Transf. Coeff. (W/m2-K)	Plug-Air Ht. Transf.Coeff. (W/m2-K)	Comments
1	MELCOR/2DKO	0.073	0.0 / 0.0	0	0	Benchmark Calculations
2	MELCOR/2DKO	0.073	85 / 100	2000	2	All Core Debris Relocated on Shield Plug; No Fission Product Escape - Nominal Case
3	2DKO	0.037	42.5 / 100	2000	2	Same as Case 2 but only half of core debris on Shield Plug
4	2DKO	0.073	85 / 100	4000	2	Same as Case 2 but with enhanced heat transfer
5	2DKO	0.037	42.5 / 100	4000	2	Same as Case 3 but with enhanced heat transfer
6	2DKO	0.073	42.5 / 50	2000	2	Same as Case 2 but with 50% of decay power (simulates volatile fission product escape)
7	2DKO	0.037	21.25 / 50	2000	2	Same as Case 3 but with 50% of decay power (simulates volatile fission product escape)
8	2DKO	0.073	85 / 100	2000	2	Same as case 2 but assuming a falling core debris over 10 s.
9	2DKO	0.037	42.5 / 100	2000	2	Same as Case 3 but assuming a falling core debris over 10 s.
10	2DKO	0.073	42.5 / 50	2000	2	Same as Case 6 but assuming a falling core debris over 10 s.

Table 3.2 Results of Debris Heatup / Coolability Calculatio

Case	Debris Ht. (m)	Initial Debris Power Level (Mw and %)	Debris-Pool Ht. Transf. Coeff. (W/m2-K)	Maximum Debris Temperature (K)	Plug Mass Melted (%)	Comments
2	0.073	85 / 100	3000	1660	2.10	Maximum temperature reached in 500 s; No debris freezing.
			2000	2065	10.30	Maximum temperature reached in 500 s; No debris freezing.
3	0.037	42.5 / 100	3000	912	0	Maximum debris temperature reached in 100 s; Complete debris freezing in 1000 s.
			2000	1080	0	Maximum debris temperature reached in 100 s; Complete debris freezing in 4670 s.
4	0.073	85 / 100	4000	1452	2.10	Maximum debris temperature reached in 100 s; No debris freezing
5	0.037	42.5 / 100	4000	794	0 0	Maximum debris temperature reached in 100 s; Complete debris freezing in 622 s.
6	0.073	42.5 / 50	3000	890	0	Maximum debris temperature reached in 100 s; Complete debris freezing in 2772 s.
			2000	1085	0	Maximum debris temperature reached in 500 s; 32% of debris freezes in 5000 s.
7	0.037	21.25 / 50	3000	660	0	Debris freezes continuously; Complete debris freezing within 100 s.
			2000	660	0	Debris freezes continuously; Complete debris freezing within 297 s.
8	0.073	85 / 100	3000	1638	2.10	Characteristics similar as for Case 2.
			2000	2050	9.80	Characteristics similar as for Case 2.
9	0.037	42.5 / 100	3000	733	0	Characteristics similar as for Case 3.
			2000	1042	0	Characteristics similar as for Case 3.
10	0.073	42.5 / 50	3000	861	0	Characteristics similar as for Case 4.
			2000	1077	0	Characteristics similar as for Case 4

Table 3.3 **Test matrix with results of steam explosion energetics calculations**

Case	Mfuel (kg)	Mc (kg)	Tfuel (K)	CVOID	mc/mf	Mtot (kg)	Pinc (kPa)	Conv. rat. %	Peak Press (Mpa)	Pulse width (msec)	Work energy KJ	Case
1	10	1	1100	0.33	0.1	500	101	8	65	0.8	911.4	1
2	10	1	1300	0.33	0.1	500	101	8.2	78	0.8	1081.8	2
3	10	1	1600	0.33	0.1	500	101	8.3	140	0.7	715.2	3
4	10	1	1300	3	0.1	500	101	7	23	8	923.5	4
5	10	3	1300	0.33	0.3	500	101	6	30	2	791.6	5
6	10	3	1300	3	0.3	500	101	3.5	8.5	20	461.7	6
7	10	10	1300	0.33	1	500	101	7	25	20	923.5	7
8	10	3	1300	3	0.3	5000	101	4	17	30	527	8
9	10	10	1300	0.33	1	5000	101	4.5	30	40	503.6	9
10	10	3	1300	0.33	0.3	500	3300	2.5	30	10	329.8	10
11	10	3	1300	3	0.3	500	3300	1.2	11	20	158.3	11
12	10	10	1300	0.33	1	500	3300	2.5	24	15	329.8	12
13	10	10	1300	3	1	500	3300	0.9	6.6	30	1IK.7	13
14	10	3	1300	0.33	0.3	5000	3300	1.6	40	15	211	14
15	10	10	1300	0.33	1	5000	3300	t.5	30	15	197.8	15
16	10	3	1300	3	0.3	5000	3300	4	20	60	527.7	16
17	10	3	1300	3	0.3	5000	3300	4.5	25	70	715.2	17
18	50	5	1100	0.33	0.1	500	101	7	100	5	3987.5	18
19	50	5	1300	0.33	0.1	500	101	8	110	10	5277.2	19
20	50	5	1600	0.33	0.1	500	101	8.5	160	10	5607	20
21	50	5	1300	3	0.1	500	101	7	37	50	4011.5	21
22	50	15	1300	0.33	0.3	500	101	3	27	SO	1978.9	22
23	50	15	1300	3	0.3	500	101	3.5	12	50	2308	23
24	50	50	1300	0.33	1	500	101	1.5	23	80	2968.4	24
25	50	15	1300	3	0.3	500	101	2.5	22	50	1649.1	25
26	50	50	1300	0.33	1	5000	101	<<<<<Slug breakup>>>>>				26
27	50	15	1300	0.33	0.3	5000	3300	1.5	25	50	989.5	27
28	50	15	1300	3	0.3	500	3300	2.1	11	60	1385.3	28
29	50	50	1300	0.33	1	500	3300	2	23	60	1319.3	29
30	50	50	1300	3	1	500	3300	1.2	8	70	791.6	30
31	50	15	1300	0.33	0.3	500	3300	1.1	80	8	725.6	31
32	50	50	1300	0.33	1	5000	3300	0.1	23	40	361.7	32
33	50	15	1300	3	0.3	5000	3300	1.7	23	40	1121.4	33
34	50	15	160	3	0.3	5000	3300	1.7	27	30	1121.4	34

Legend:
Mfuel - Mass of Fuel
Mc - Mass of coolant
Tfuel - Initial Fuel Temperature
Pinc - Initial system pressure

Conv.rat. - conversion ratio
CVOID - Ratio of volume of vapor to volume of liquid
Mtot - Total mass of the fuel coolant and the overlying slug
mc/mf - mass of coolant to mass of fuel ratio

Table 3.4 Results of specific thermodynamic calculations for steam explosion energetics

ase	Fuel mass (kg)	Fuel temperature (K)	Water mass (kg)	Water temperature (K)	Hickes-Menzies Pressure rise (MPa)	Hickes-Menzies Conversion ratio	Board-Hall Pressure rise (MPa)	Board-Hall Conversion ratio
2	10.00	1300.00	1.00	330.00	571.82	0.23	1427.40	0.27
5	10.00	1300.00	3.00	330.00	427.57	0.41	869.80	0.46
	10.00	1300.00	10.00	330.00	57.53	0.23	164.30	0.25

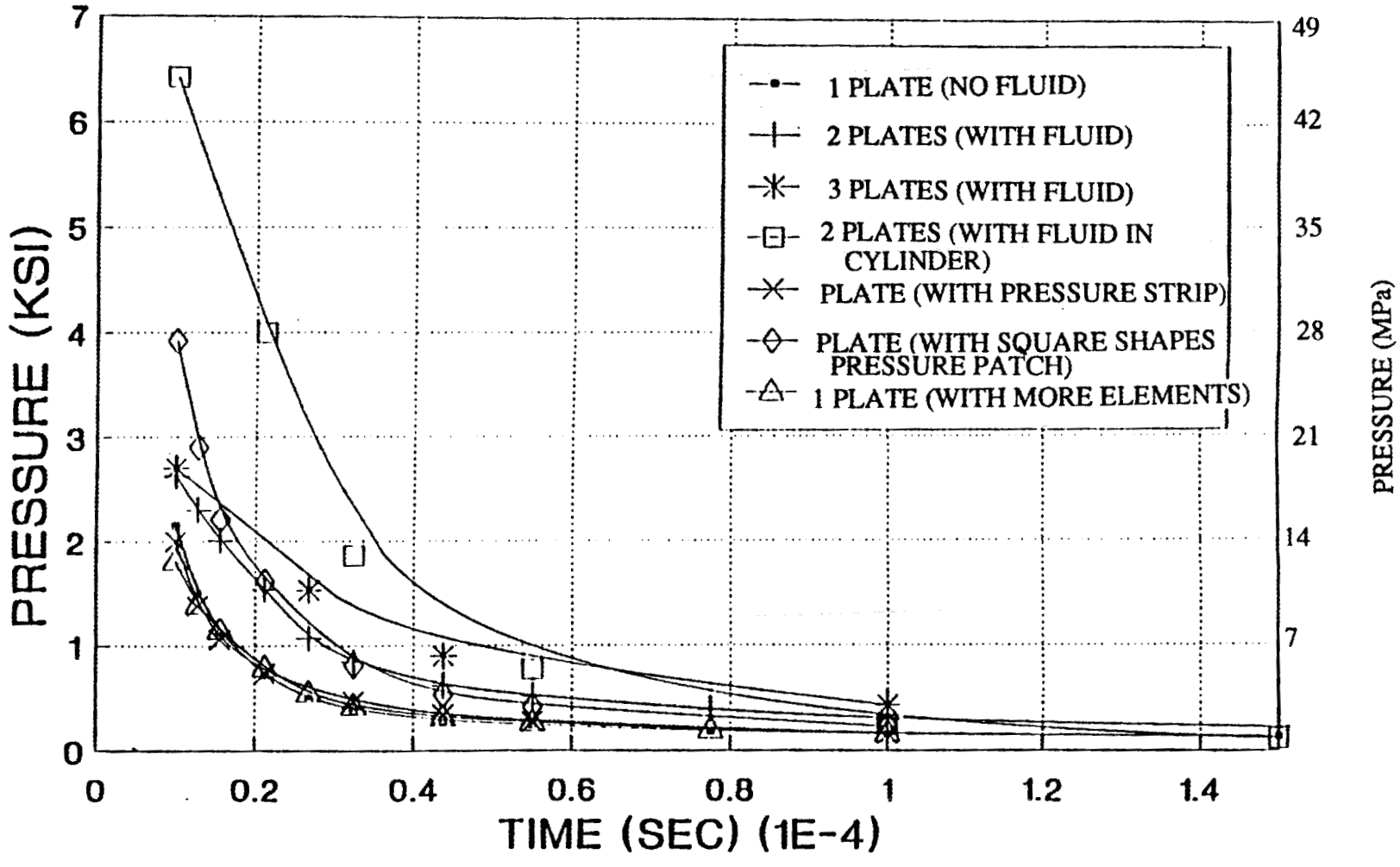

Fig. 3.1 Failure Envelopes for HFIR Outer Fuel Plates

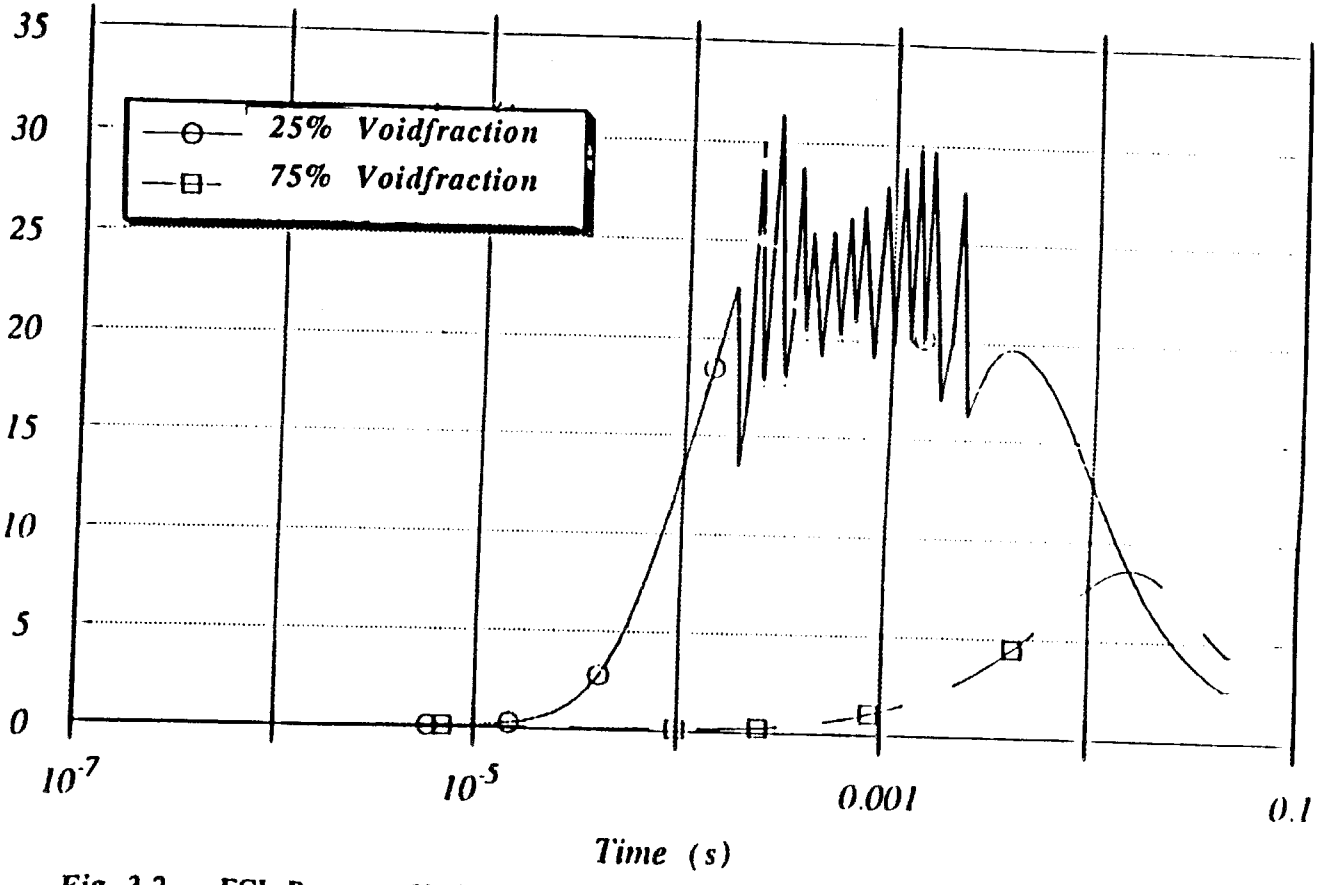

Fig. 3.2 FCI Pressure Variation vs Time (Single Plate Melt Interacting with Water from Two Flow Channels)

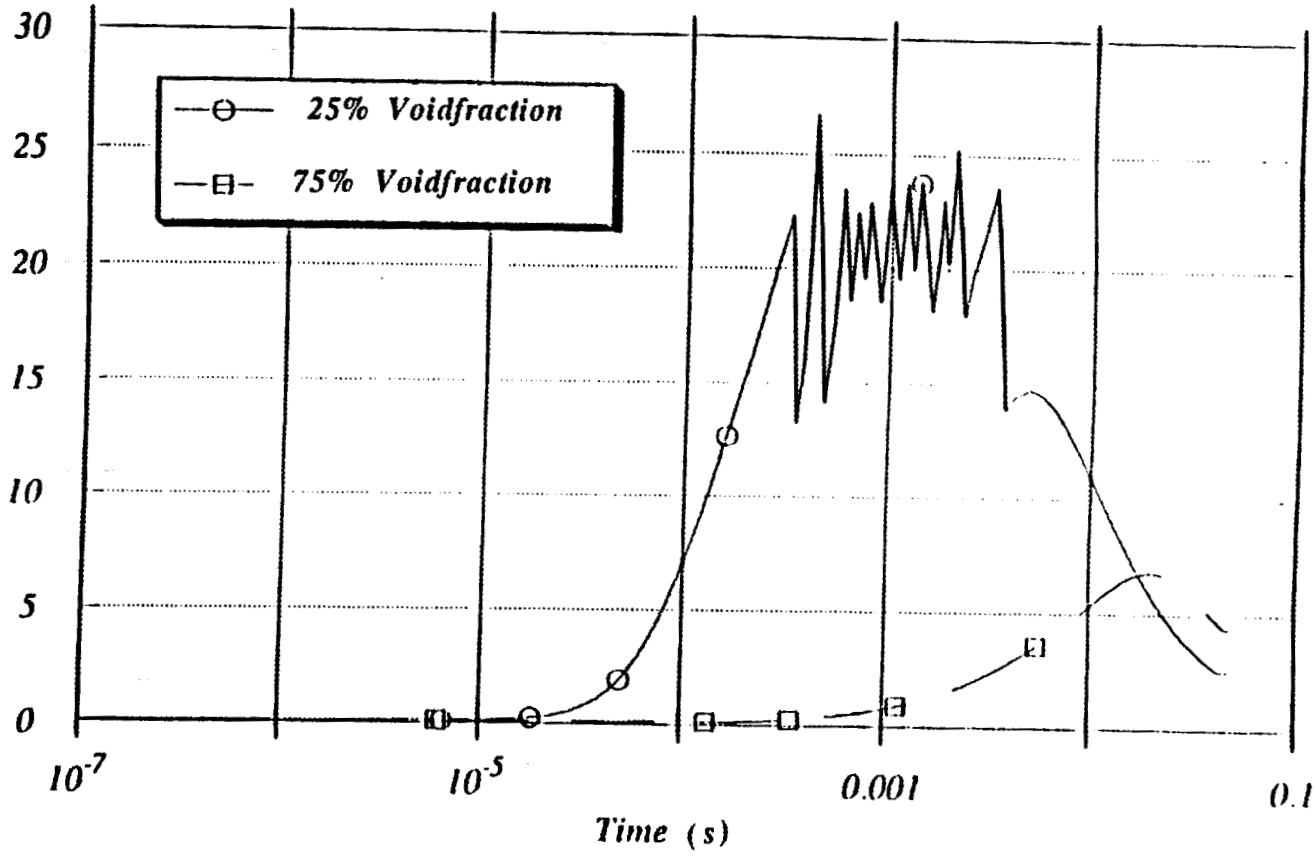

Fig. 3.3 FCI Pressure Variation vs Time (Single Plate Melt Interacting with Water from Three Flow Channels)

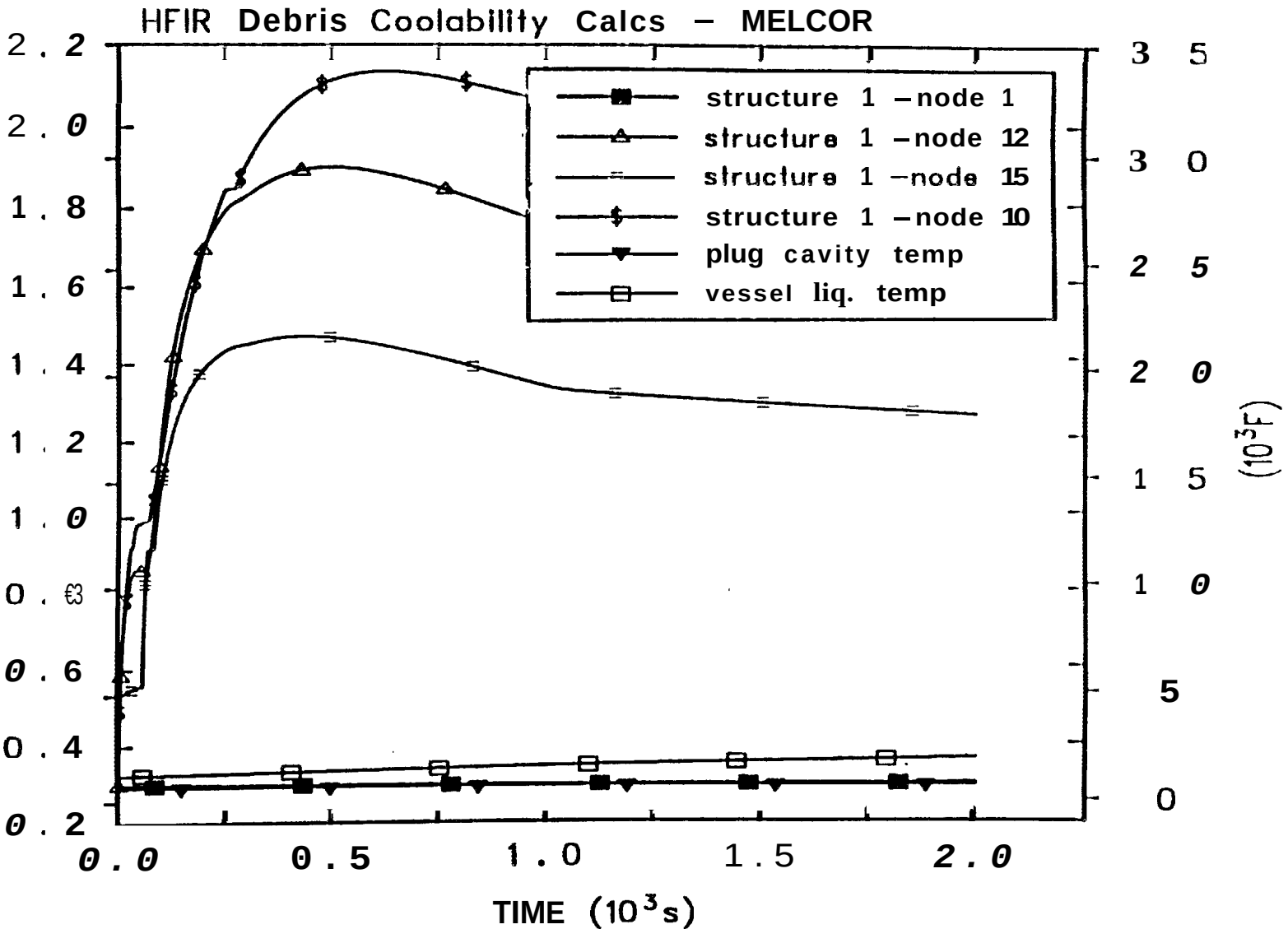

Fig. 3.4a Variation of Debris and Plug Temperature vs Time (MELCOR Results for Case 2)

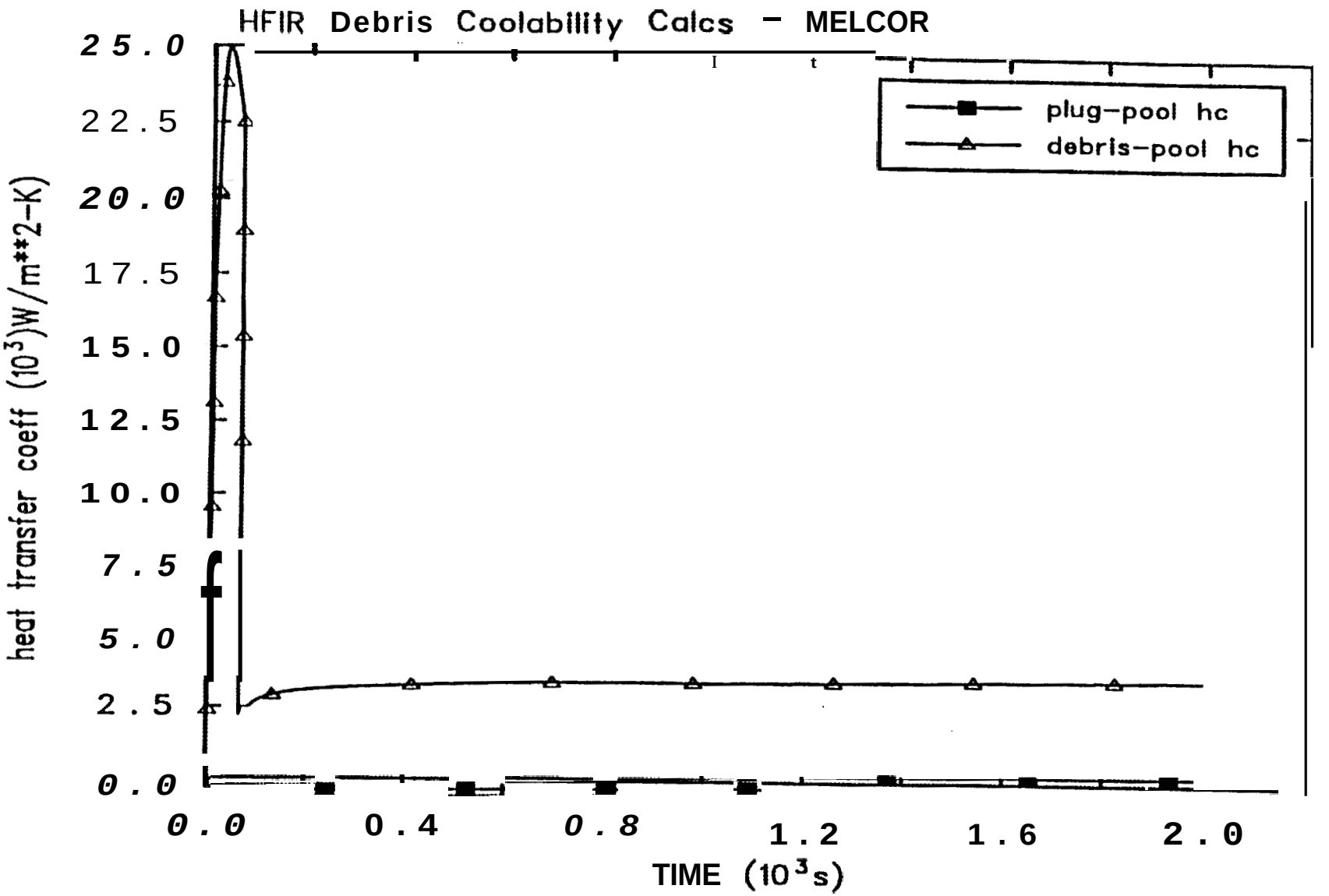

Fig. 3.4b Variation of Debris-to-Pool and Plug-lo-Pool Heat Transfer Coefficients vs Time (MELCOR Results for Case 2)

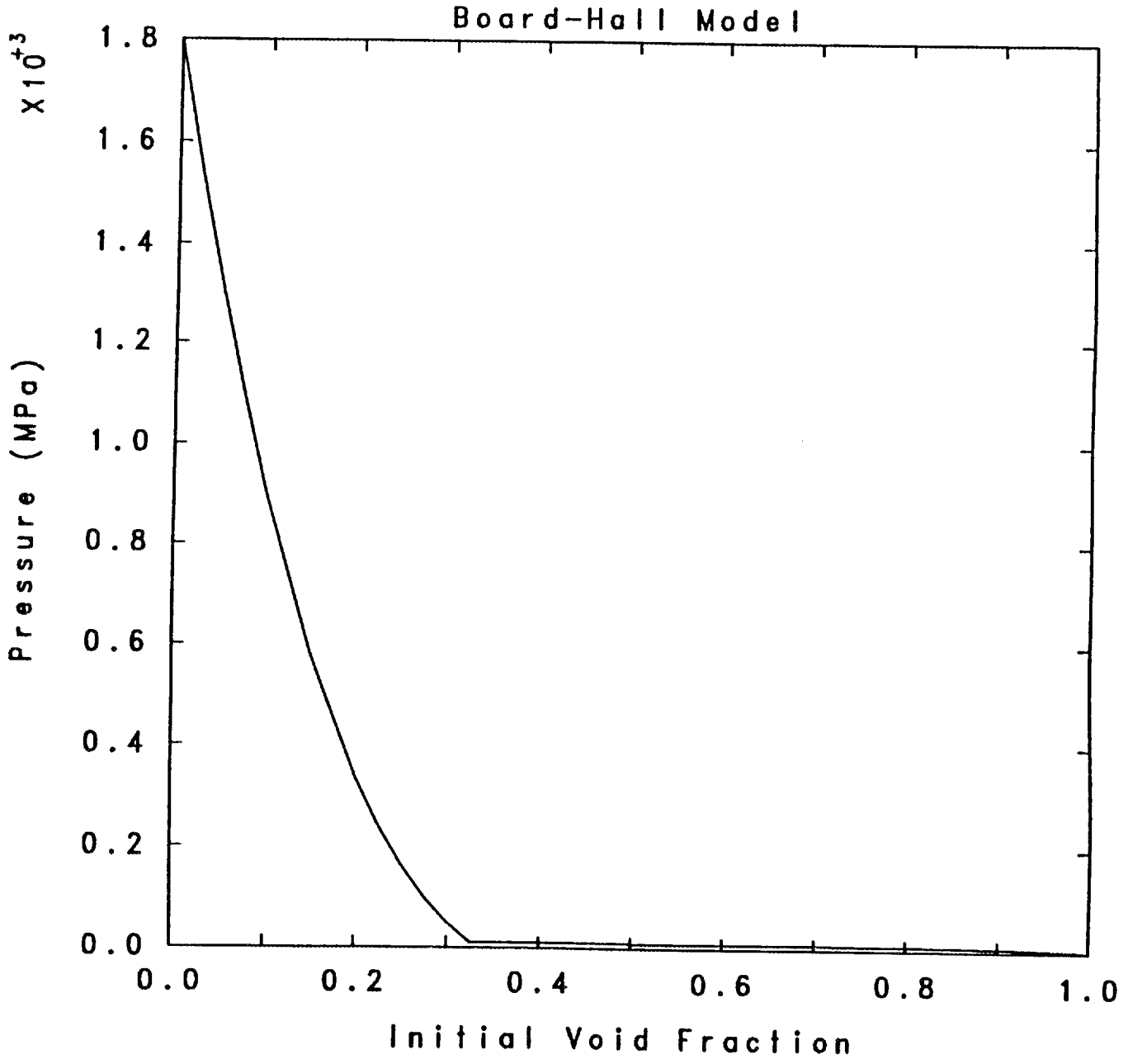

Fig. 3.5 Pressurization versus Initial Void Fraction Predictions (Board-Hall Model)

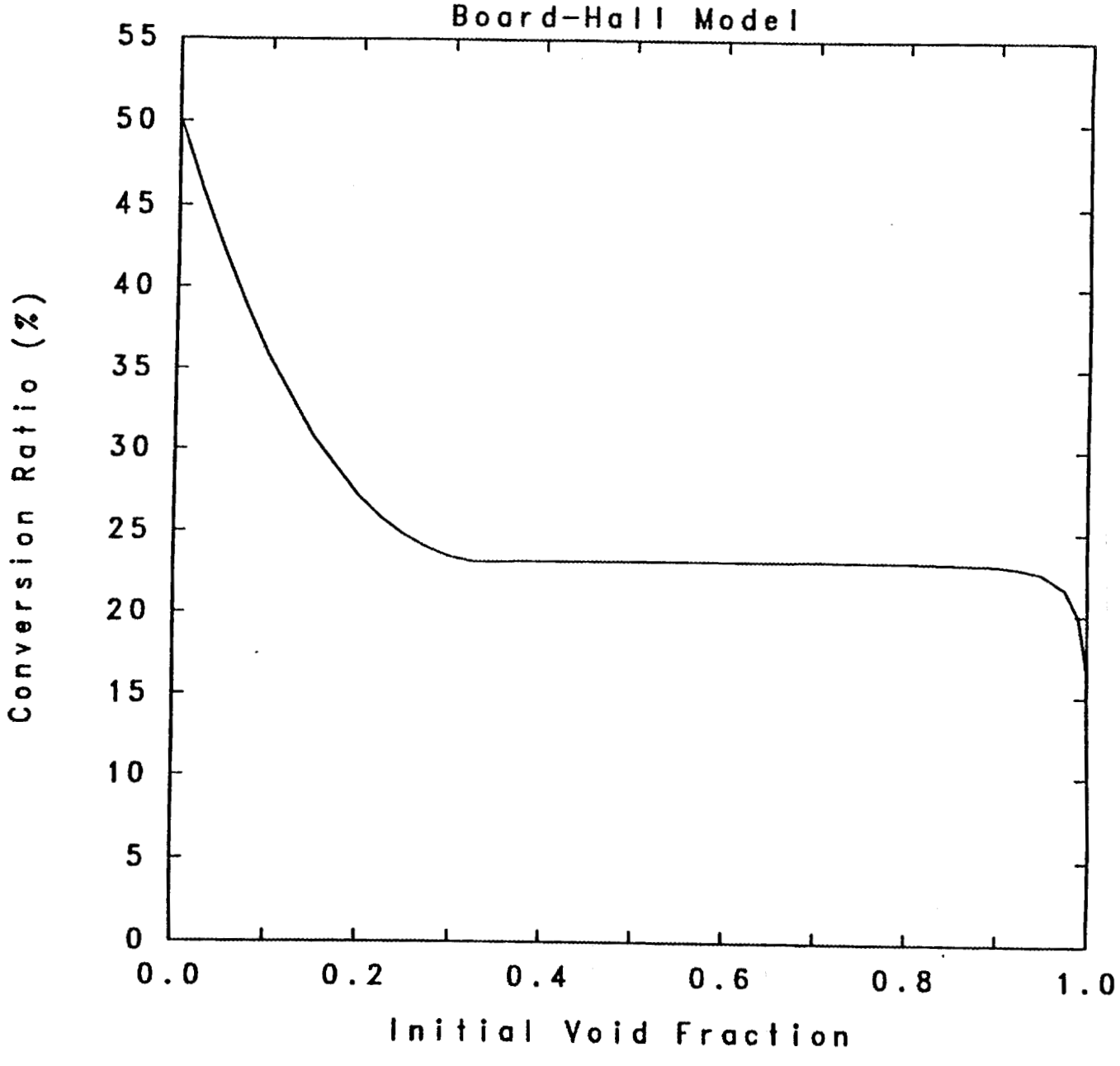

Fig. 3.6 Conversion Ratio versus Initial Void Fraction Predictions (Board-Hall Model)

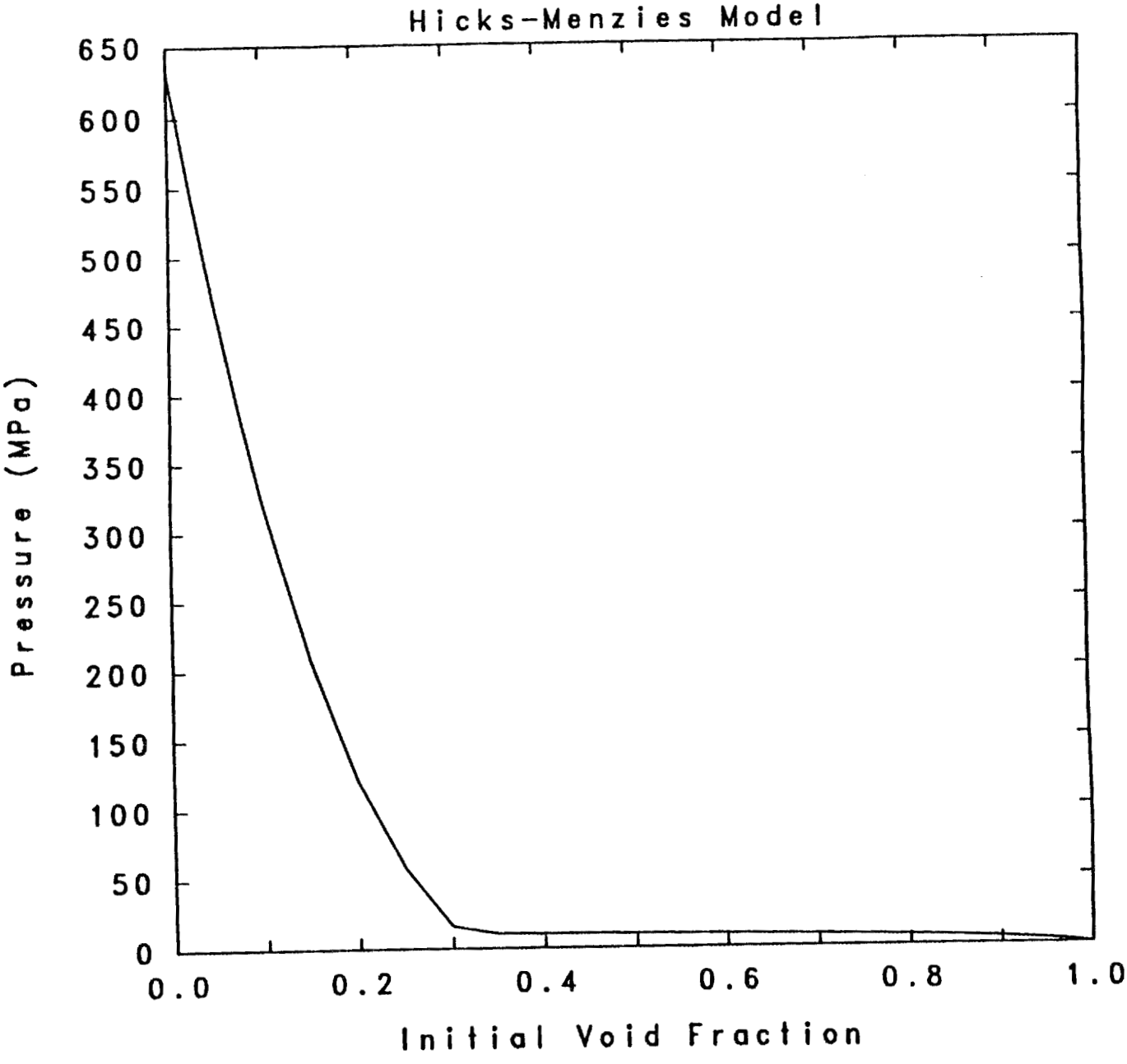

Fig. 3.7 Pressurization versus Initial Void Fraction Predictions (Hicks-Menzies Model)

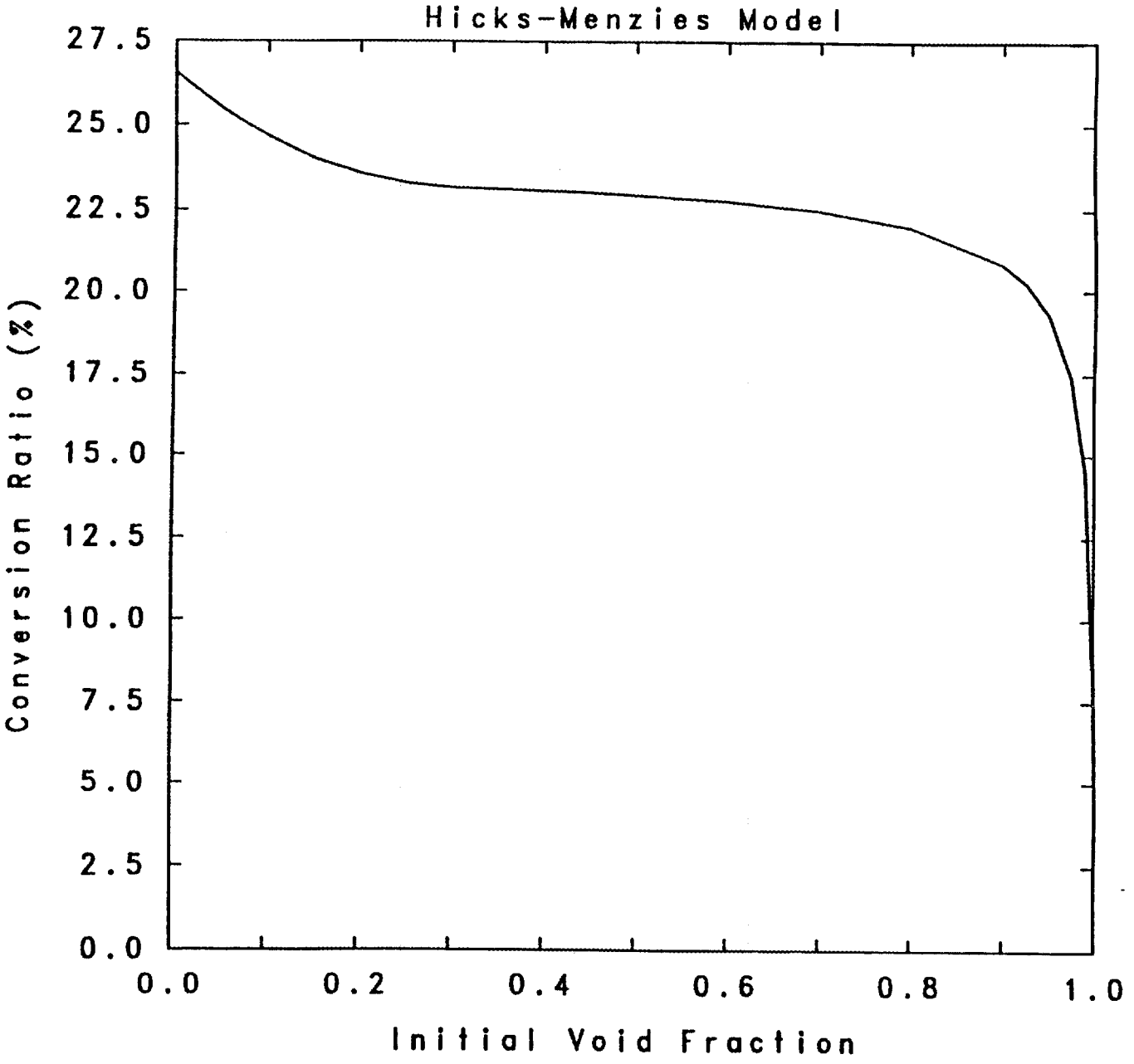

Fig. 3.8 Conversion Ratio versus Initial Void Fraction Predictions (Hicks-Menzies Model)

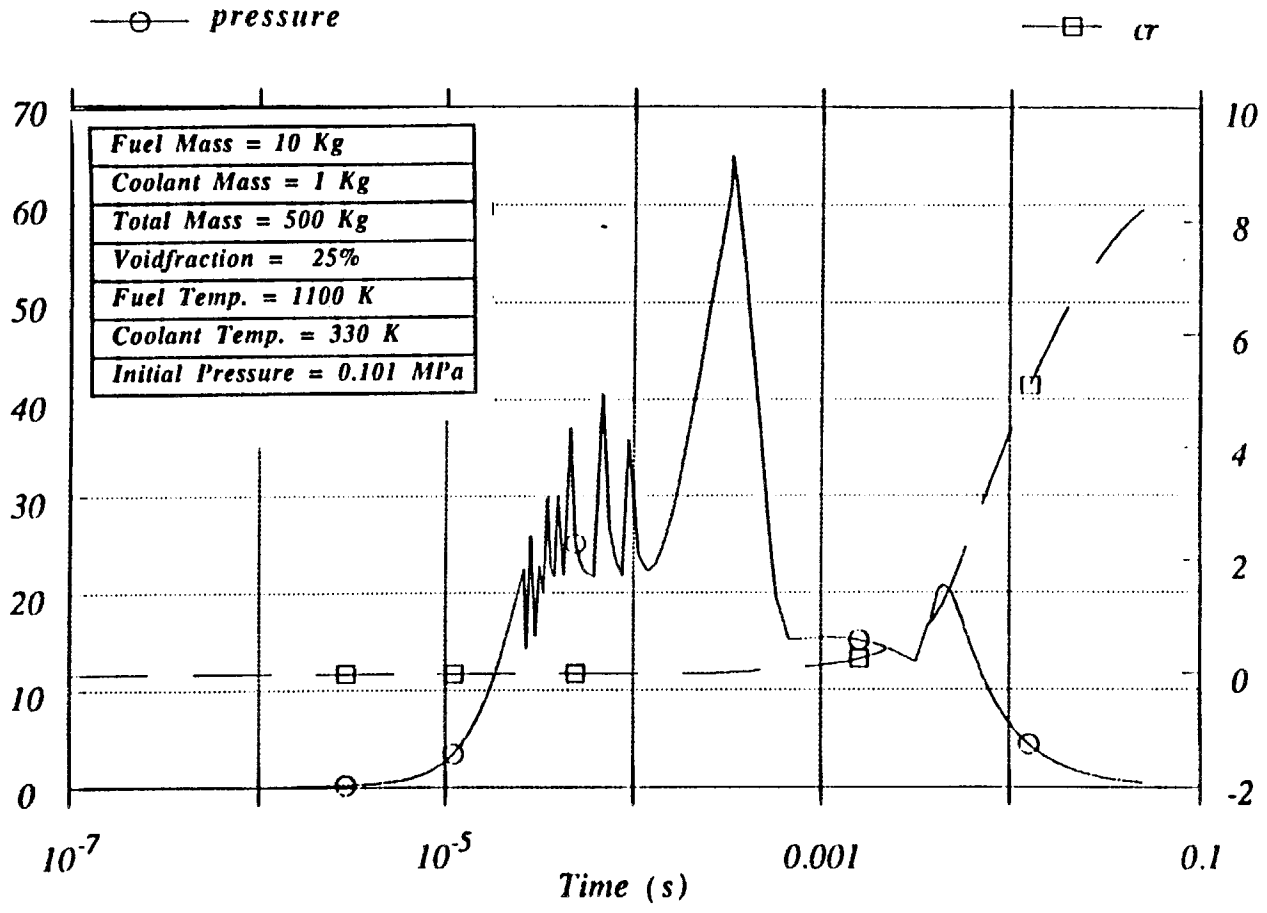

Fig. 3.9 Variation of Peak Pressure and Conversion Ratio vs Time for Case 1

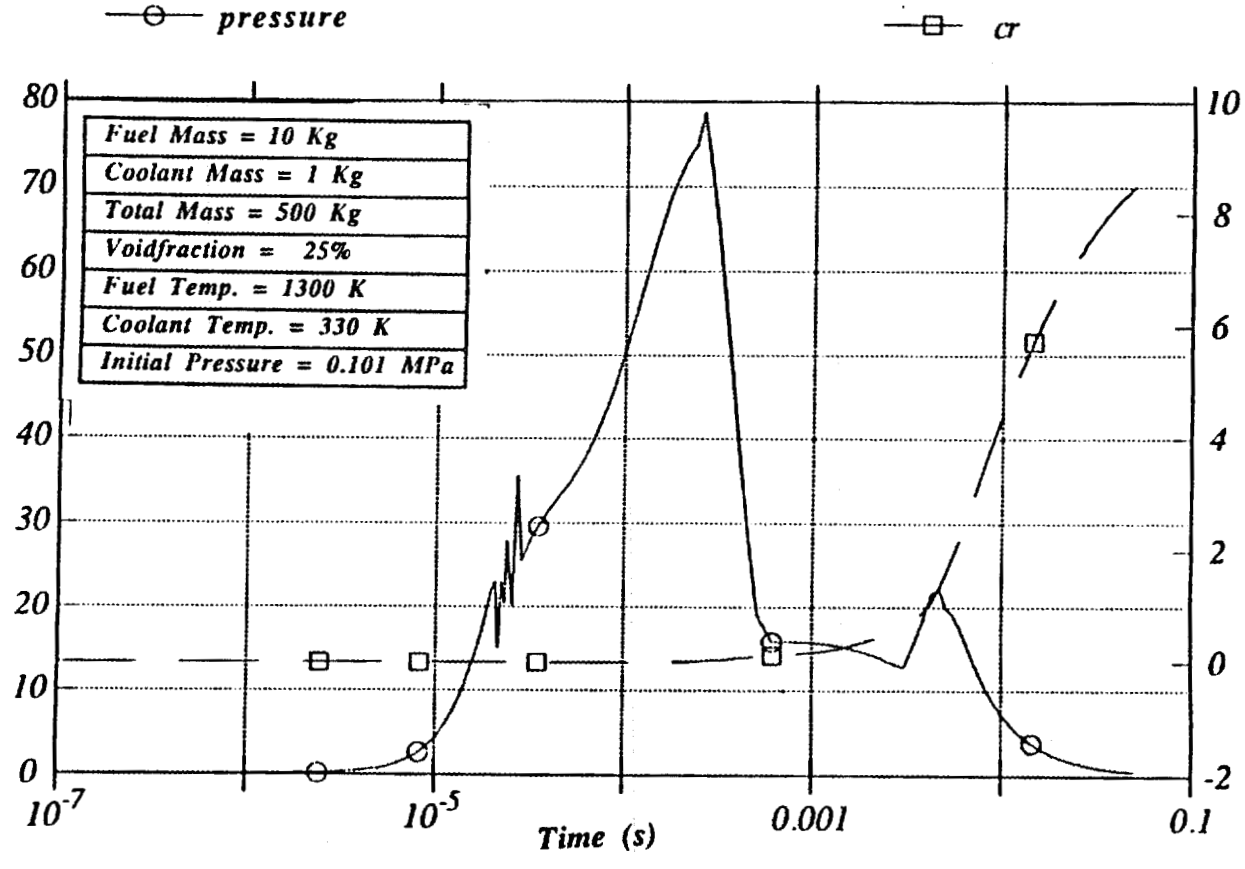

Fig. 3.10 Variation of Peak Pressure and Conversion Ratio vs Time for Case 2

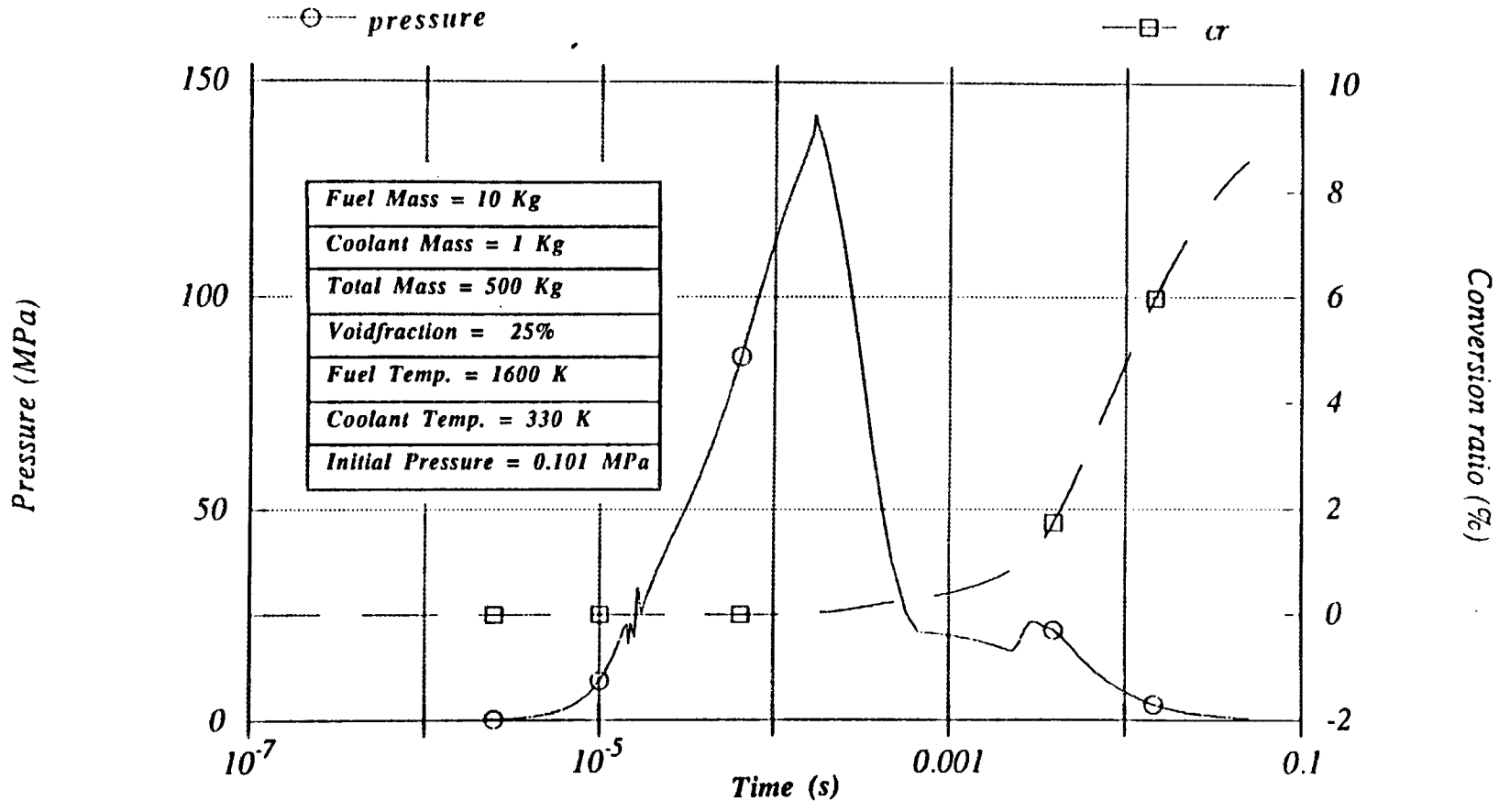

Fig. 3.11 Variation of Peak Pressure and Conversion Ratio vs Time for Case 3

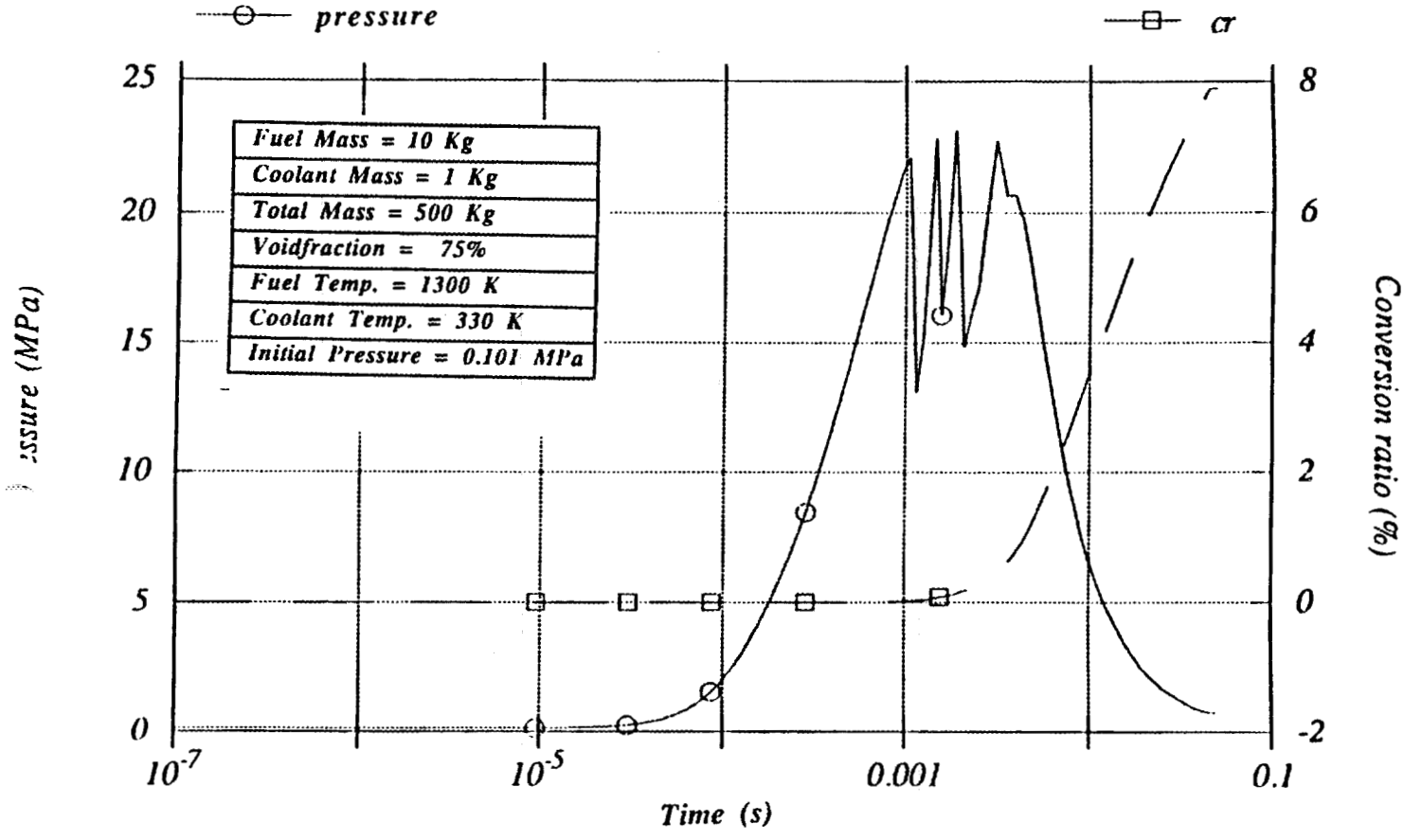

Fig. 3.12 Variation of Peak Pressure and Conversion Ratio vs Time for Case 4

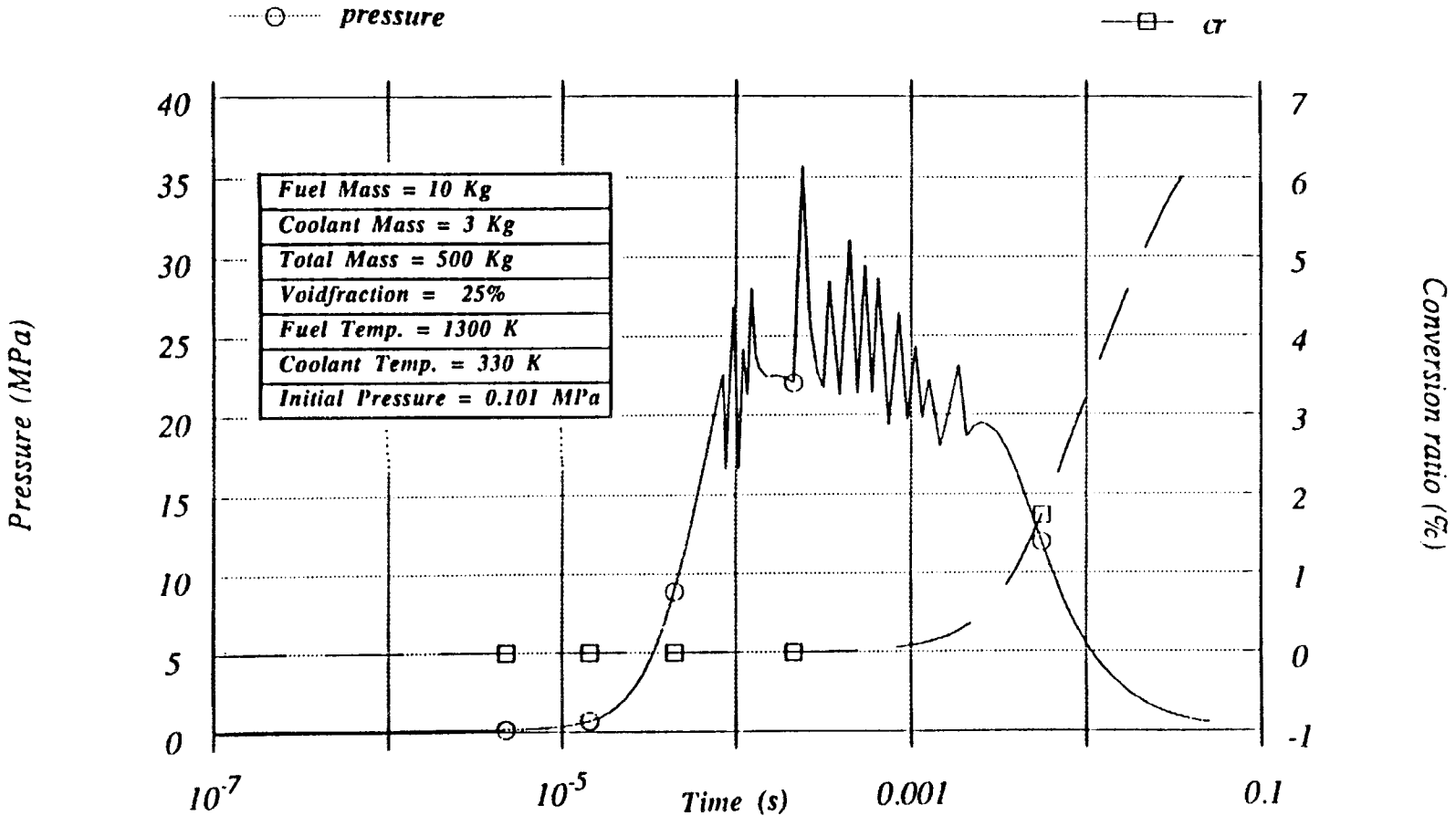

Fig. 3.13 Variation of Peak Pressure and Conversion Ratio vs Time for Case 5

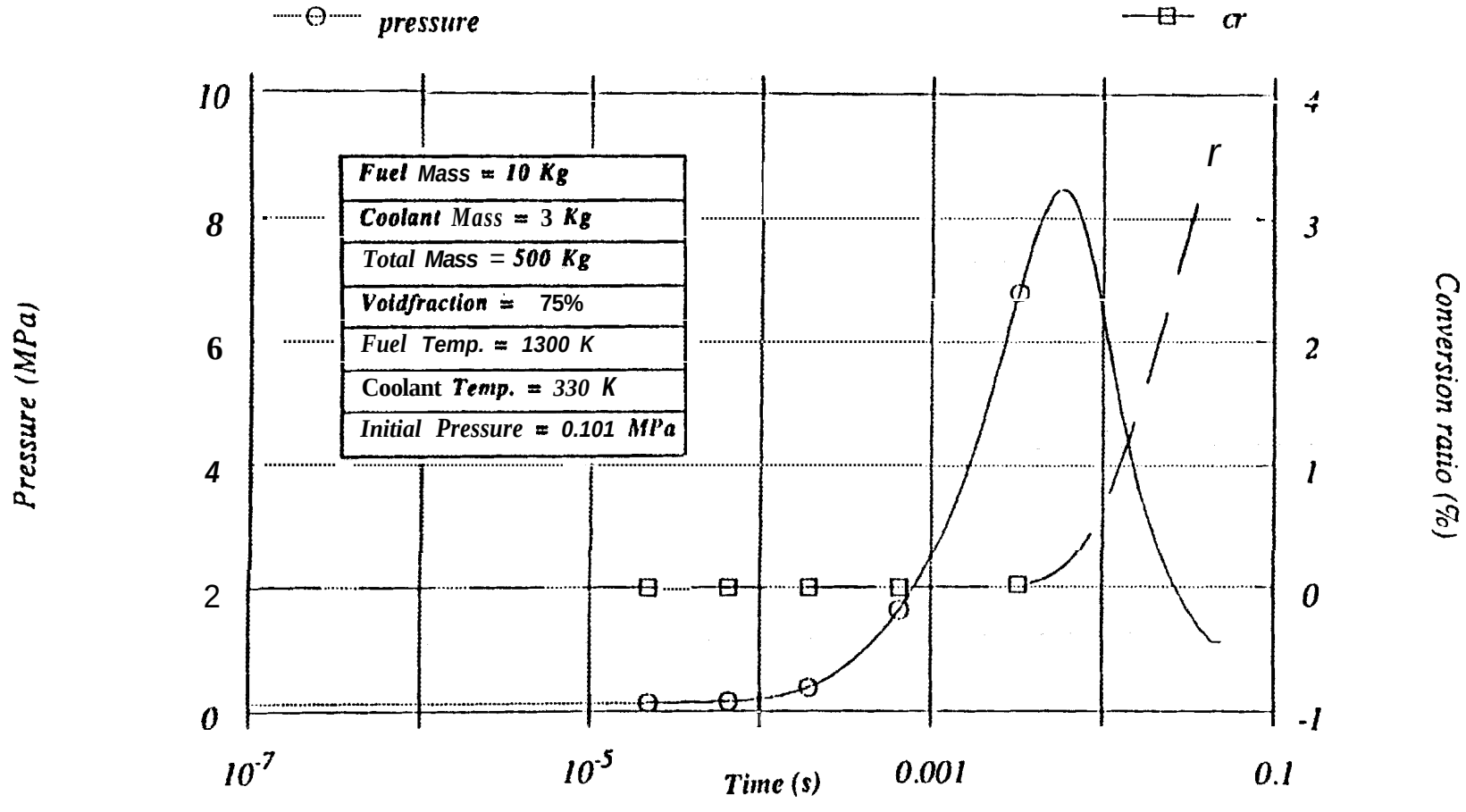

Fig. 3.14 Variation of Peak Pressure and Conversion Ratio vs Time for Case 6

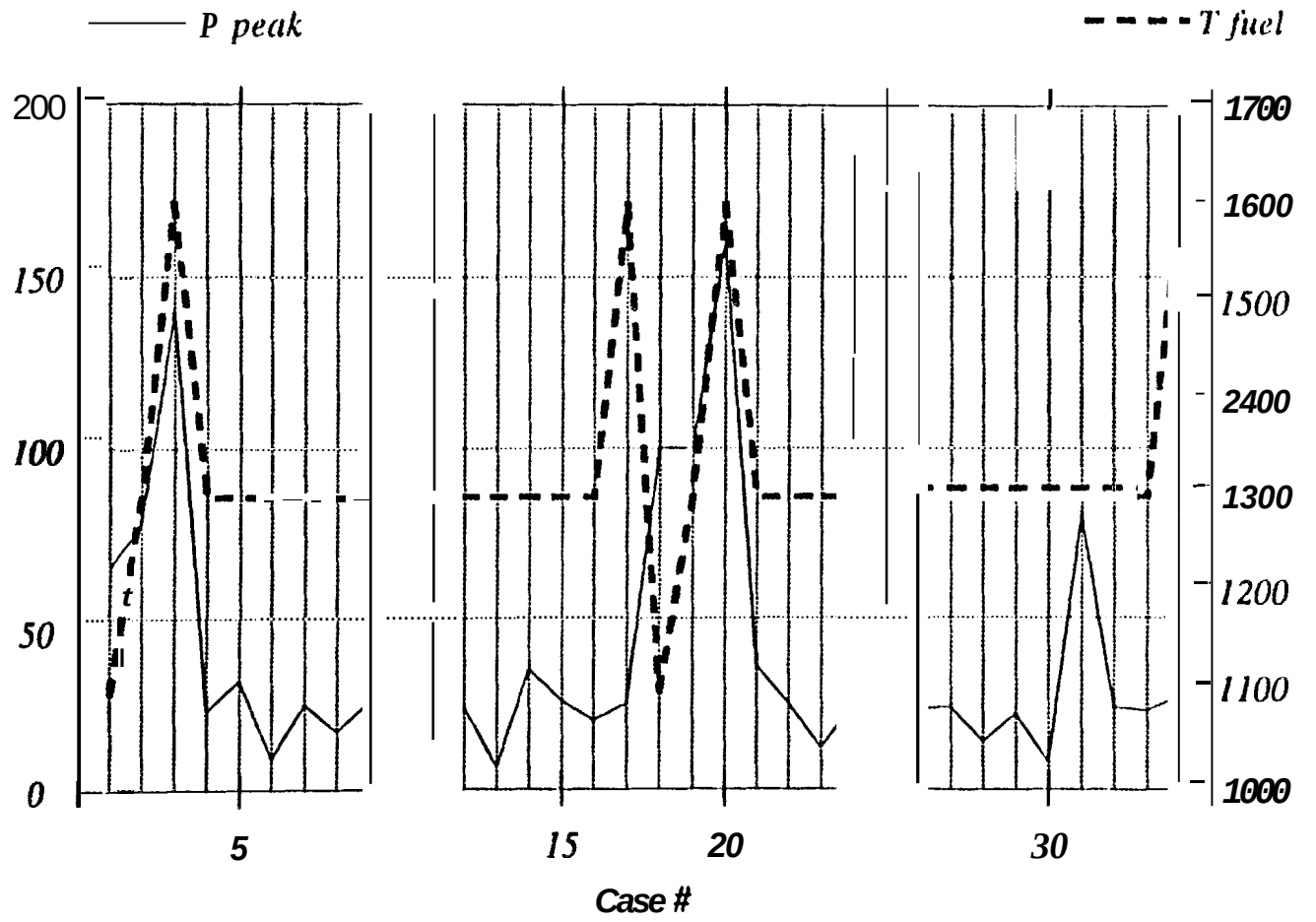

Fig. 3.15 Effect of Fuel Temperature on Peak Pressure Magnitude for Cases 1 lo 35

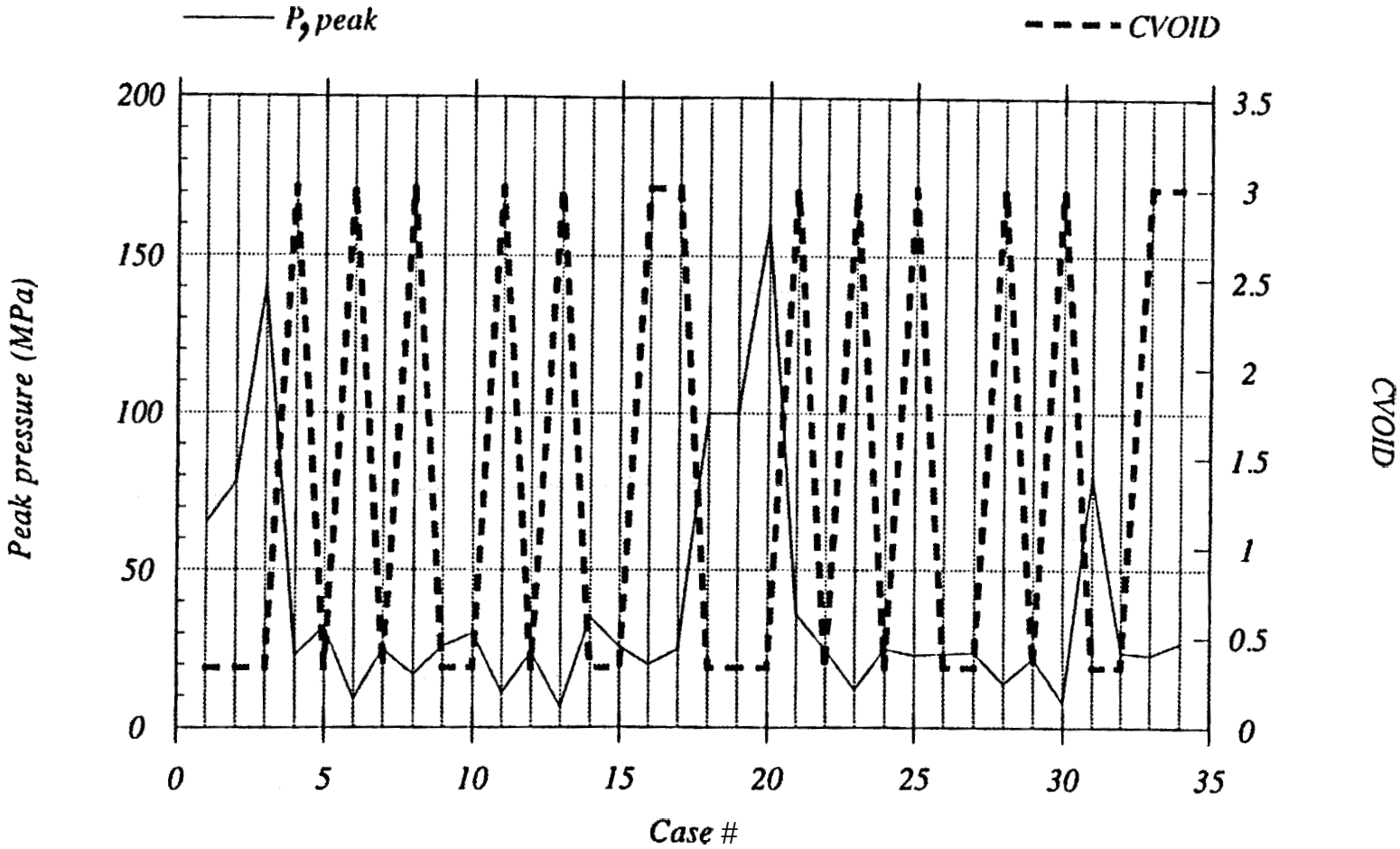

Fig. 3.16 Variation of **CVOID** and Peak Pressure Magnitude for Cases 1 to 35

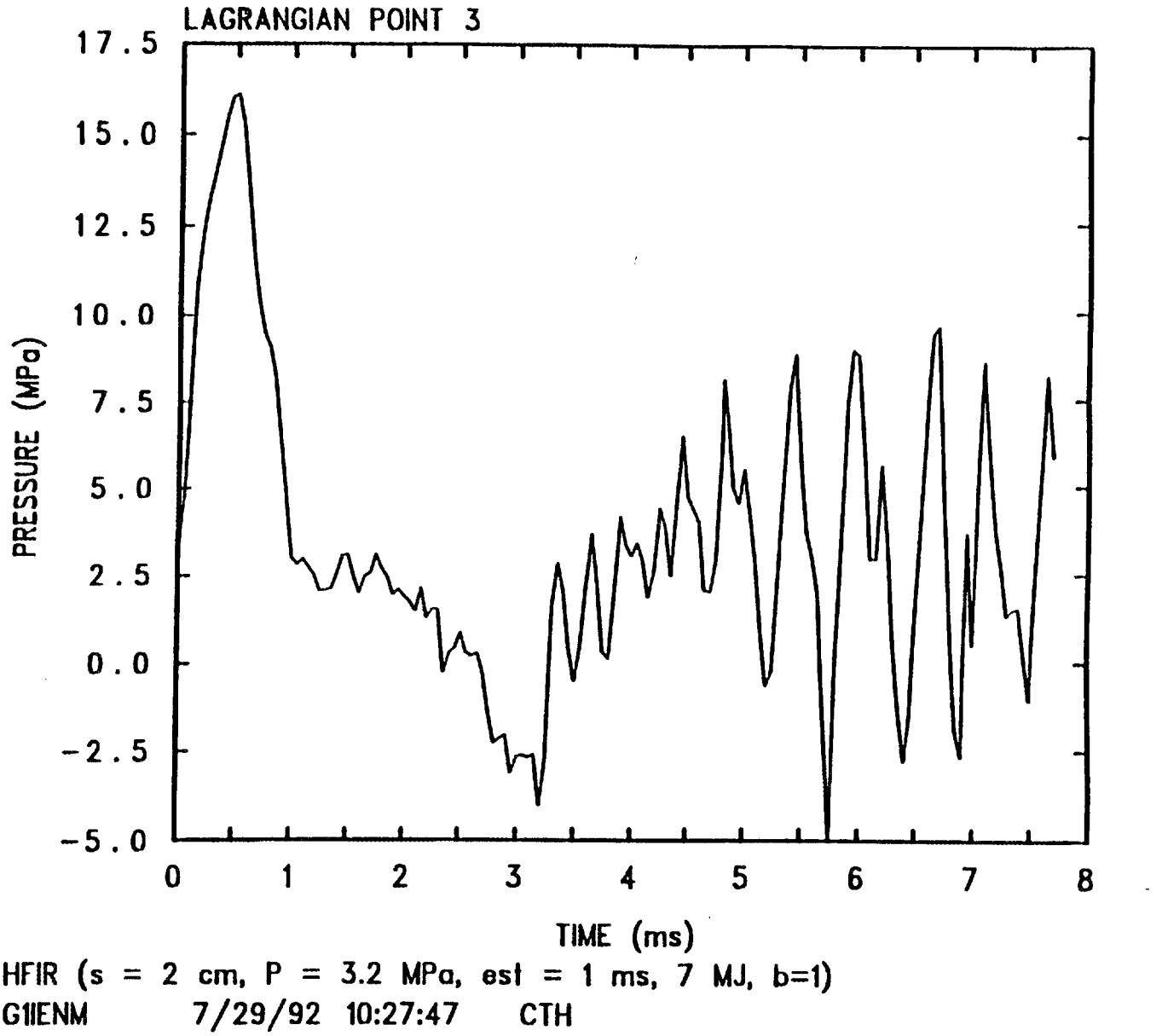

Fig. 3.17a Variation of Pressure vs Time for Model 3 (Lagrangian Point 3, 7 MJ Case)

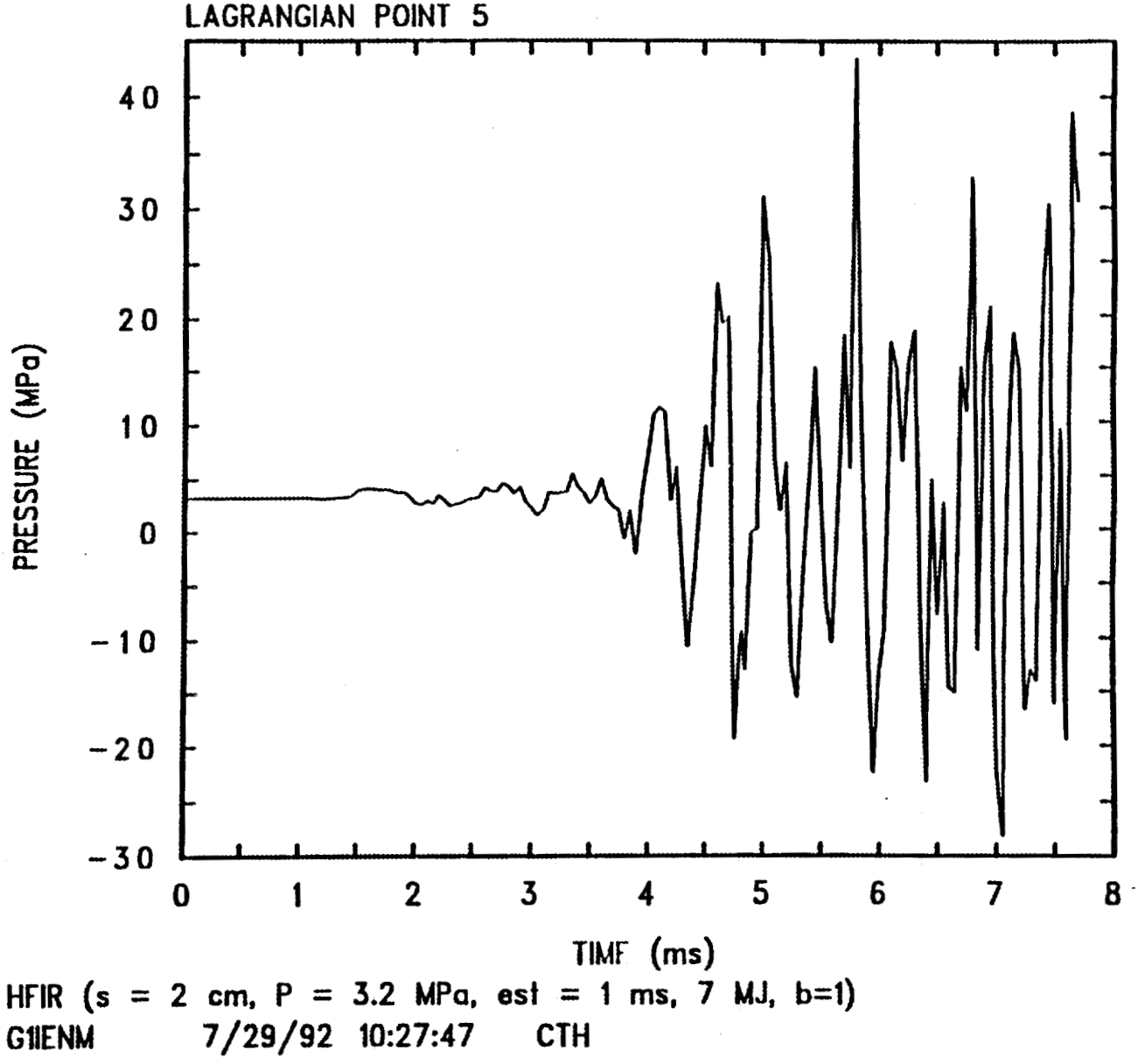

Fig. 3.17b Variation of Pressure vs Time for Model 3 (Lagrangian Point 5, 7 MJ Case)

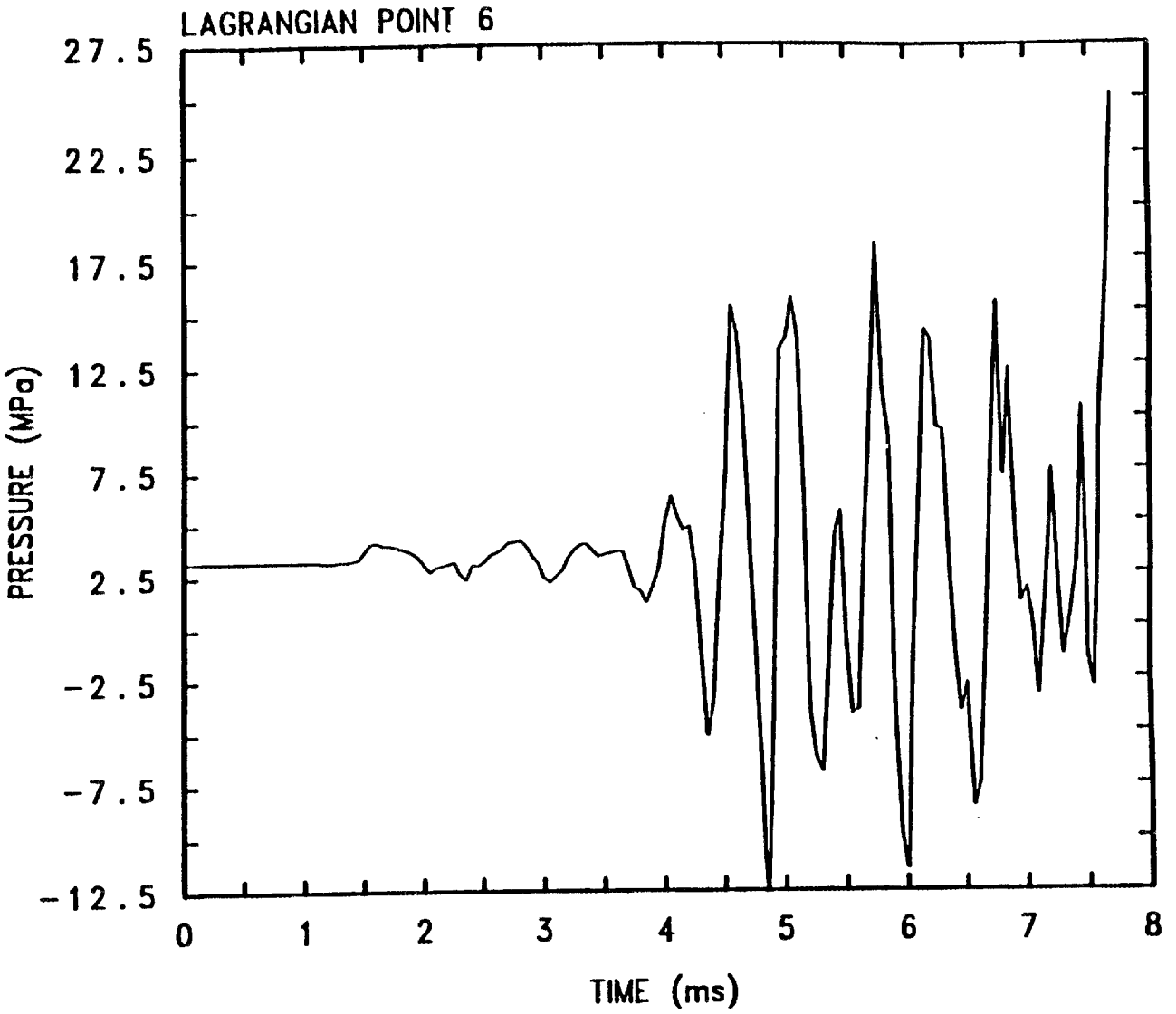

Fig. 3.17c Variation of Pressure vs Time for Model 3 (Lagrangian Point 6, 7 MJ Case)

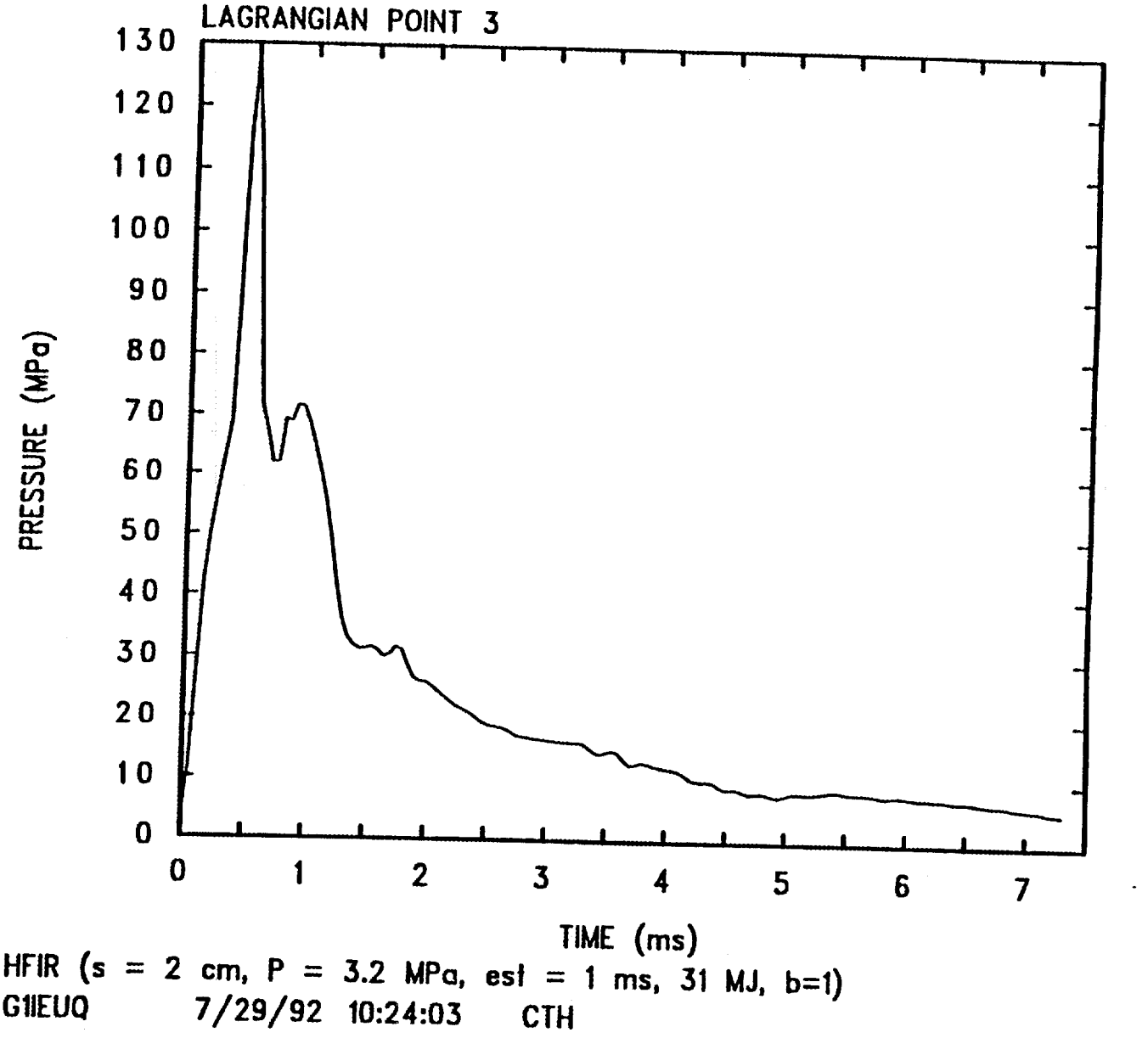

Fig. 3.18a Variation of Pressure vs Time for Model 3 (Lagrangian Point 3, 31 MJ Case)

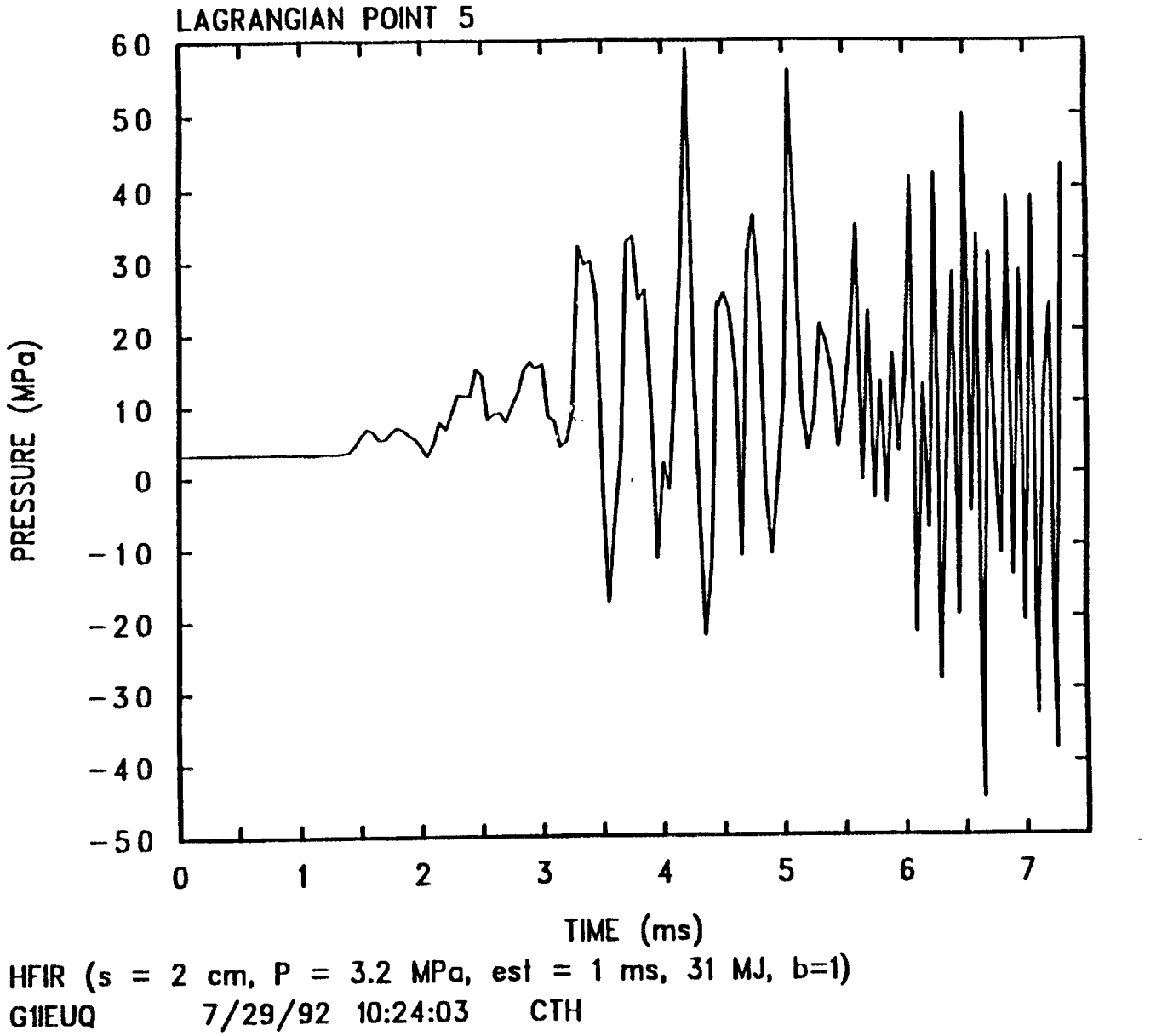

Fig. 3.18b Variation of Pressure vs Time for Model 3 (Lagrangian Point 5, 31 MJ Case)

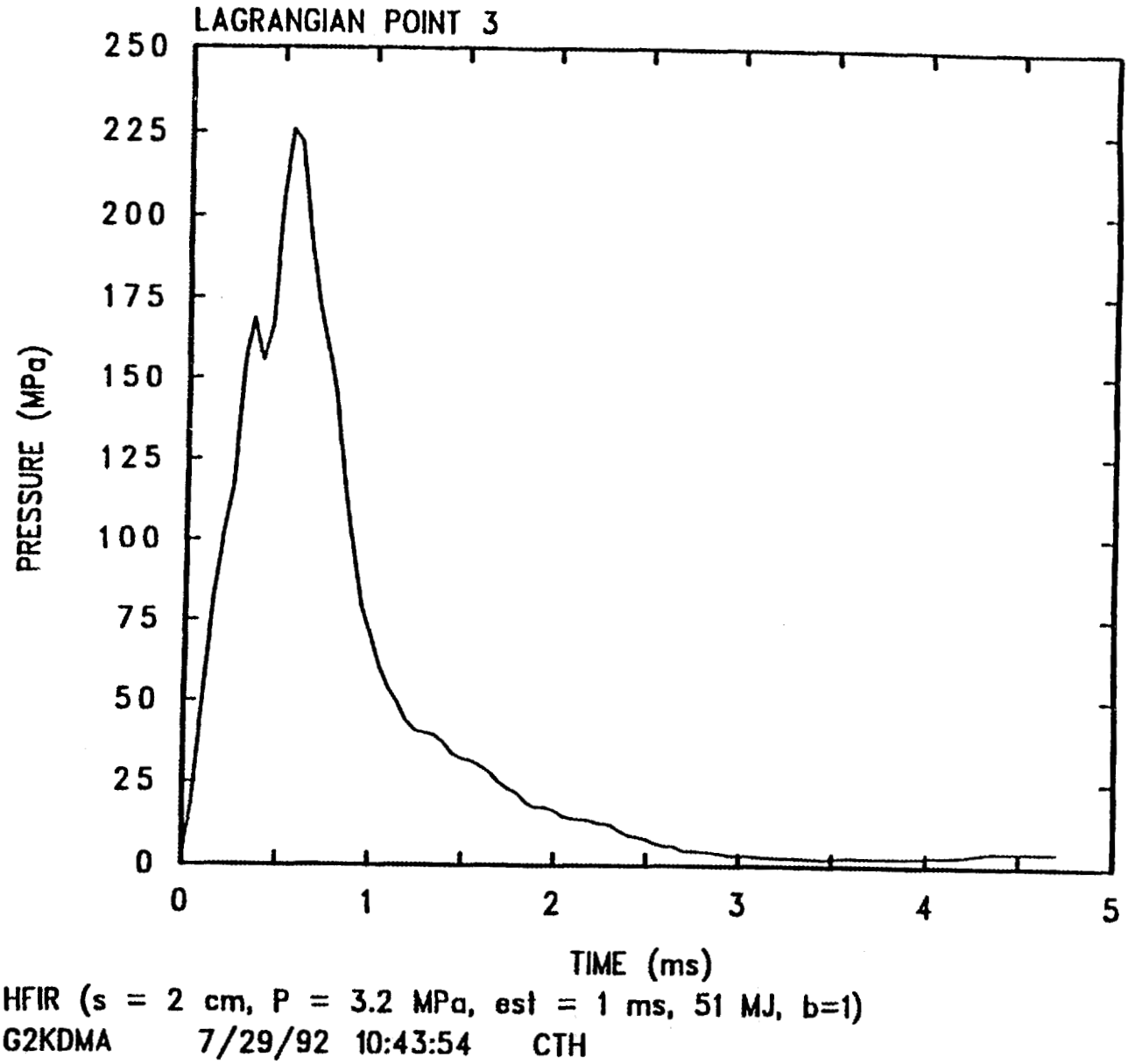

Fig. 3.19a Variation of Pressure vs Time for Model 3 (Lagrangian Point 3, 51 MJ Case)

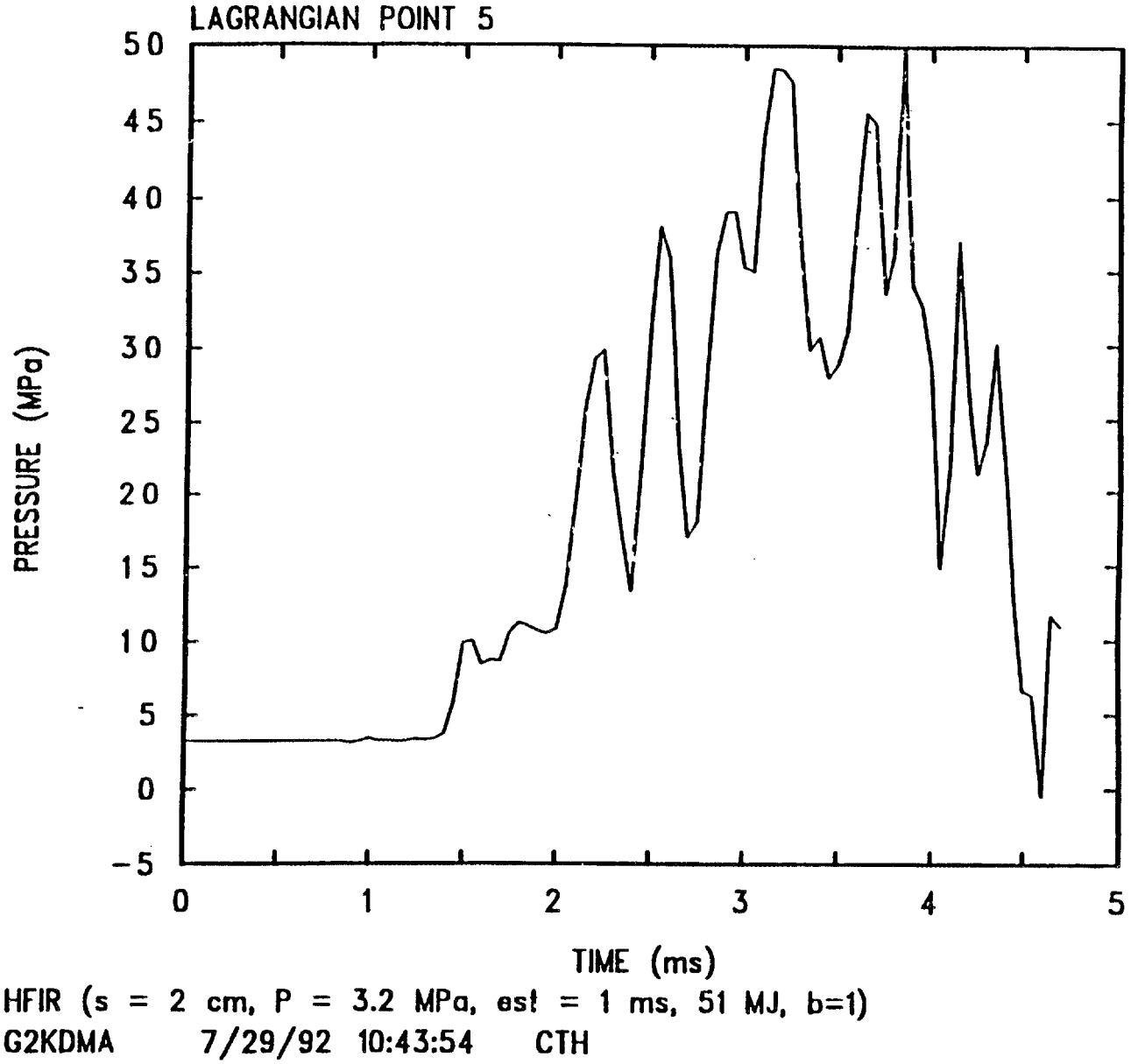

Fig. 3.19b Variation of Pressure vs Time for Model 3 (Lagrangian Point 3, 51 MJ Case)

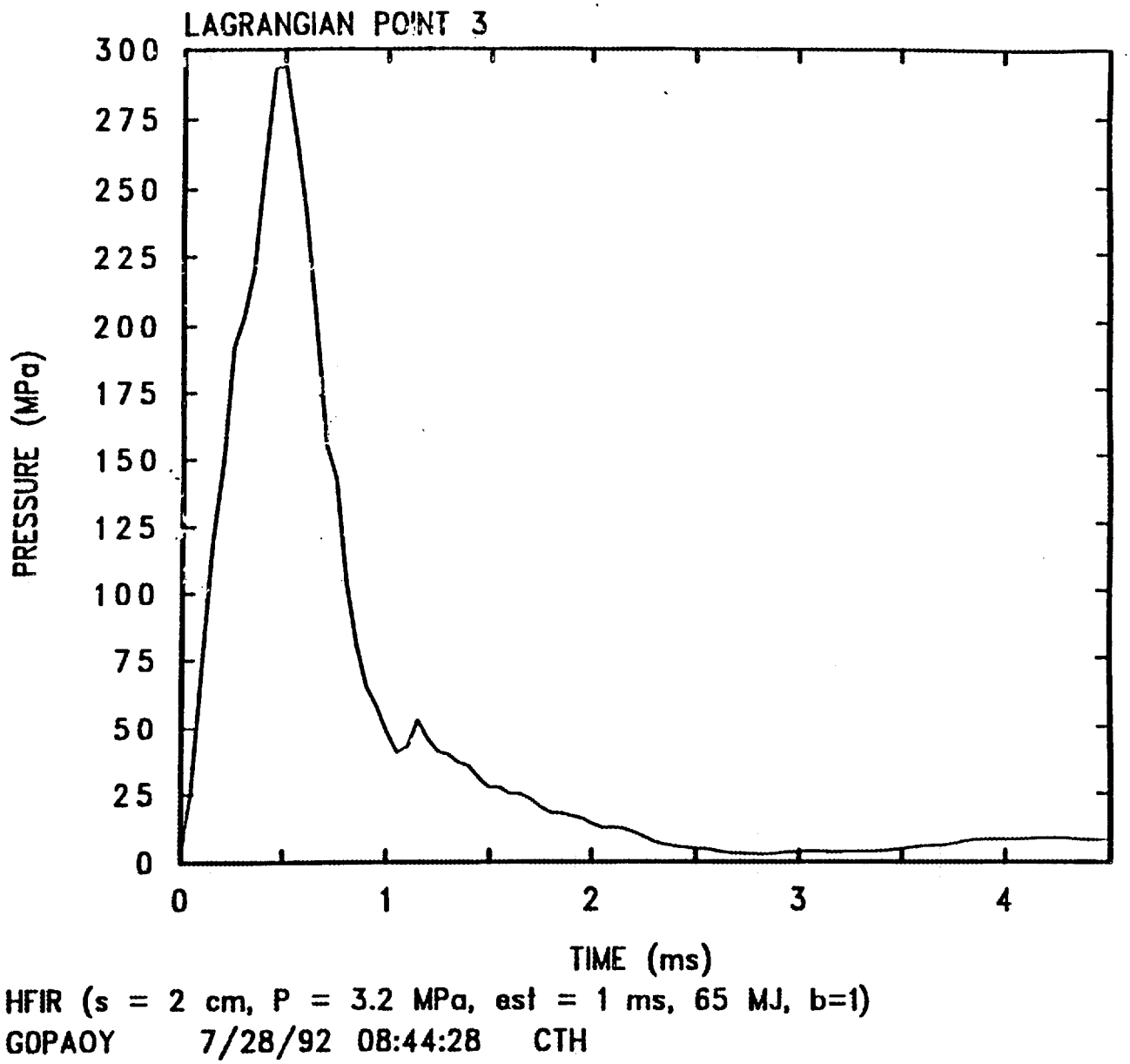

Fig. 3.20a Variation of Pressure vs Time for Model 3 (Lagrangian Point 3, 65 MJ Case)

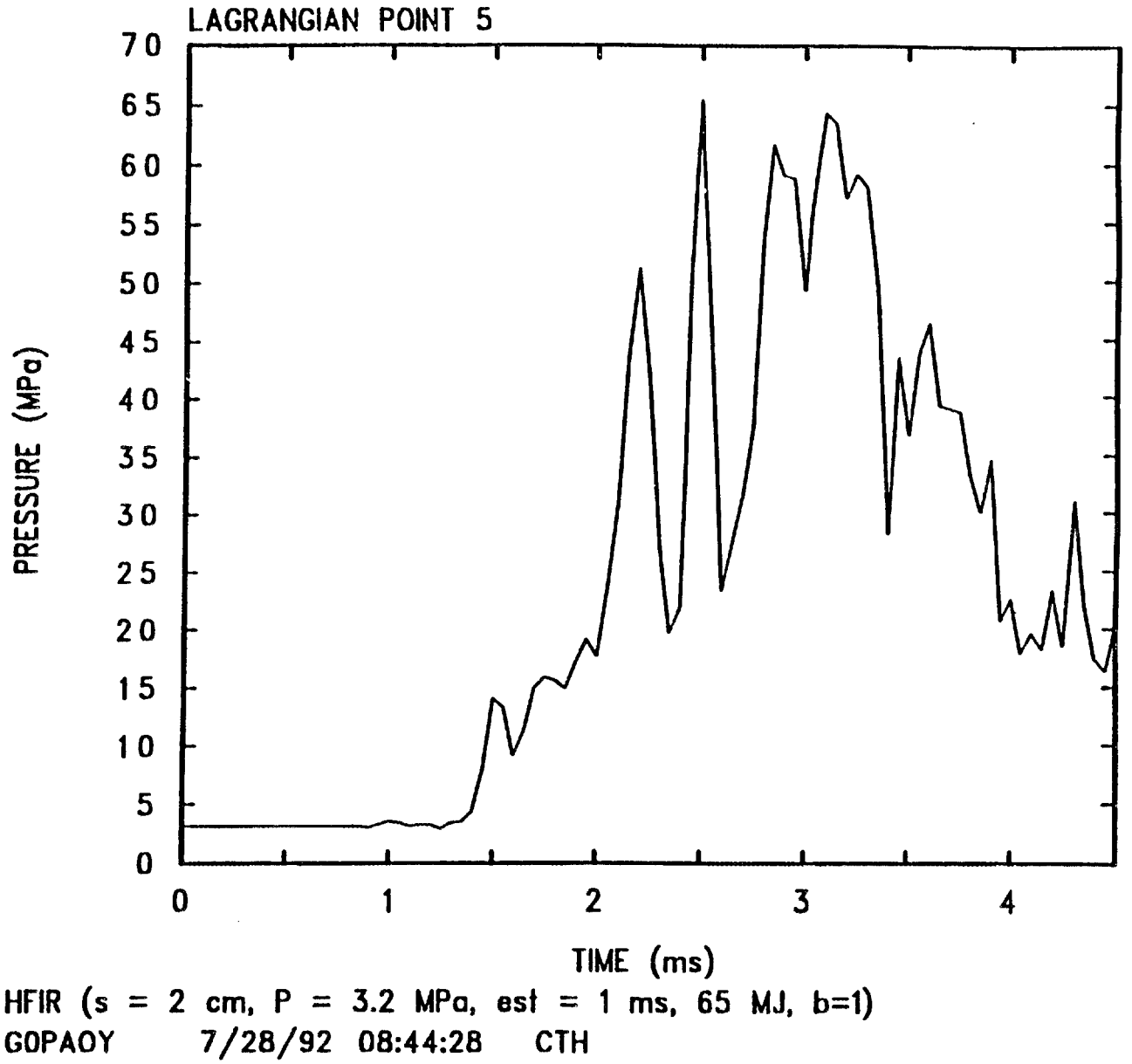

Fig. 3.20b Variation of Pressure vs Time for Model 3 (Lagrangian Point 3, 65 MJ Case)

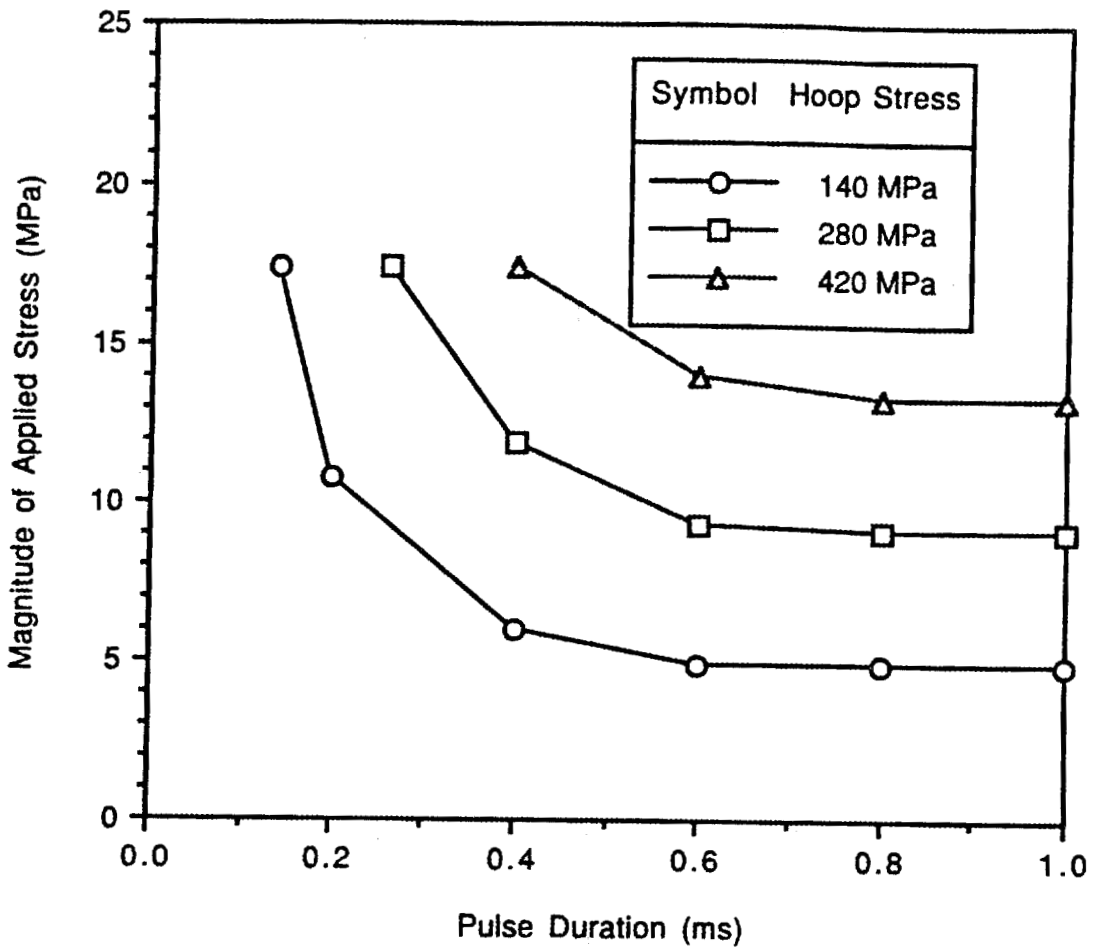

Fig. 3.21 HFIR Vessel Midplane Failure Envelopes

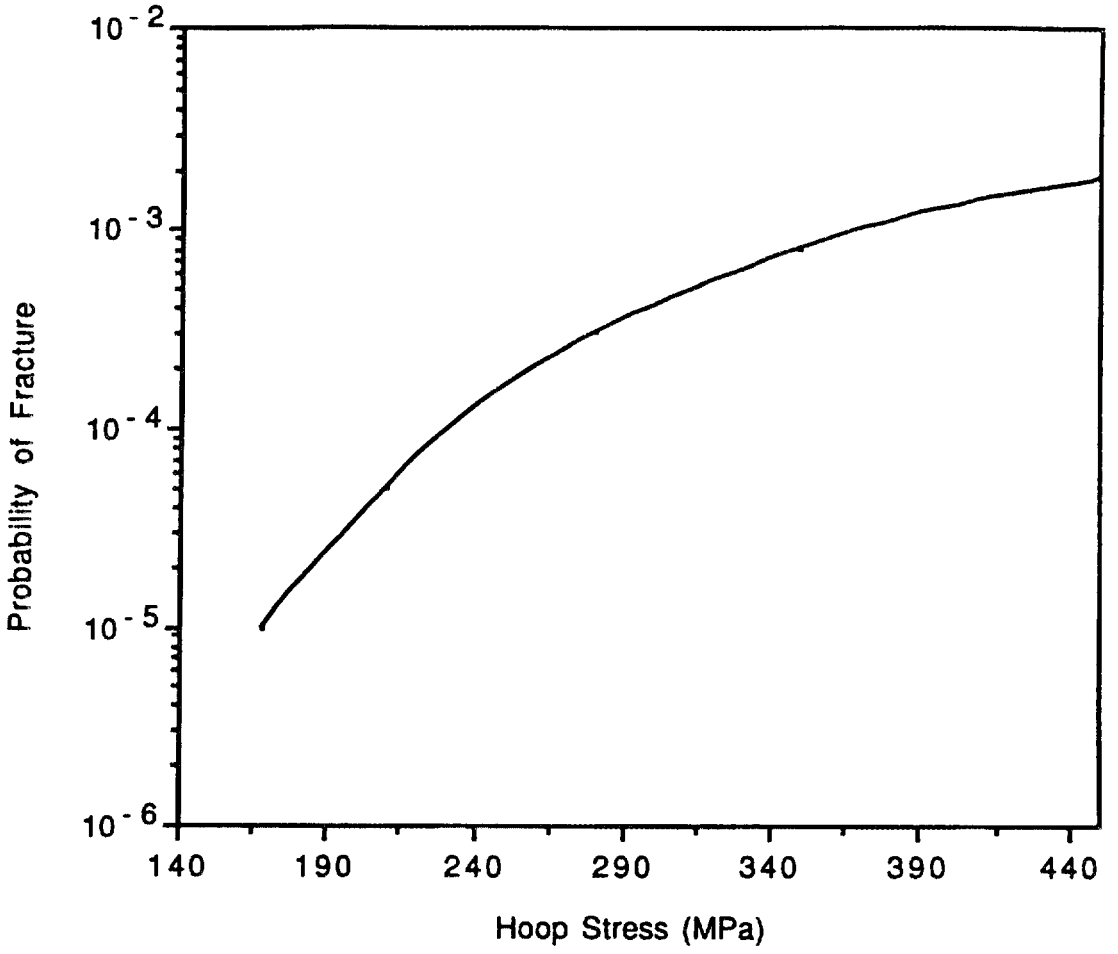

Fig. 3.22 Variation of HFIR Vessel Failure Probability vs Hoop Stress (.007 cracks/ft-2)

4. FURTHER WORK FOR BEST-ESTIMATE HFIR FCI ANALYSIS

Upon reading Sects. 2 and 3 and the various appendices, it is clear that several key assumptions had to be made to allow modeling and analysis to proceed. Some assumptions are clearly conservative, whereas others are unverified or best-guess estimates, and were made for modeling purposes. This chapter describes additional work that remains to be done to remove uncertainties, confirm assumptions, and conduct best-estimate HFIR FCI analysis. Several areas could benefit considerably from additional work are described sequentially.

4.1 STEAM EXPLOSION TRIGGERING

A key unverified assumption made in the analysis described in this report deals with the propensity for molten HFIR fuel to undergo steam explosions. It has been conservatively assumed that HFIR fuel upon melting will undergo a steam explosion event if the fuel-melt composition temperature is above the aluminum melting temperature (viz., 660°C). It is a well-known fact that U_3O_8 fuel interacts chemically with molten aluminum to form a "mushy" eutectic, which effectively increases the molten fuel viscosity. The propensity for molten aluminum to undergo steam explosions when in contact with water is also well-known. However, at the other end of the spectrum, it is self-evident that a material with infinitely large viscosity will not disperse or trigger. It may be that the "mushy" HFIR molten fuel characteristics would be such as to increase the apparent viscosity of the material mixture to effectively prevent a steam explosion occurrence, under conceivably available trigger mechanisms. This aspect is currently being studied both experimentally and analytically.

4.2 CORE MELT PROPAGATION

The FCI analysis to determine the quantity of core material that can melt and participate in a steam explosion was determined in a highly qualitative manner. Levels ranging from 10 to 24% were evaluated using various analytical techniques combined with unverified assumptions, for situations that did not consider propagation from localized explosions. For cases with localized explosions, a high-enough potential was determined to exist for damage propagation to occur without being able to determine the upper limit. Although it is felt that, based on engineering judgment, the upper limit would not exceed the threshold limit of 65% of the core mass, it would be highly desirable to quantify this limit. It is recognized that a detailed core melt progression capability may require very large resources. However, it is expected that a series of scoping analyses conducted in conjunction with related technology being developed elsewhere for other DOE reactors would provide valuable insights into this important phenomenon.

4.3 STEAM EXPLOSIONS IN THE SHIELD PLUG REGION

Because of time constraints, analyses for steam explosion energetics could not be conducted for possible steam explosions in the shield plug region. It is felt that the effects of resulting energetics for occurrences in this region may be less effective in causing confinement damage from missiles. This is due to the larger amounts of structural mass that may need to be accelerated upward through the reactor pool, compared to the case reported in this report where we only considered the top head as a possible missile.

4.4 PRESSURE PULSE AND CONVERSION RATIO EVALUATIONS FOR A CLOSED SYSTEM

As has been described earlier, the model of the FCIMOD code was developed for evaluating steam explosions in power reactors where a large void space is postulated to exist above the explosion zone. However, for the HFIR where steam explosions may occur because of flow blockages or reactivity insertion events, the RCS may be full of water. Under such circumstances, the feedback characteristics of the elastic system boundaries need to be accounted for. Such feedback effects were artificially accounted for with the present version of FCIMOD by varying the inertial constraint (i.e., slug mass). To incorporate a simple modification to the FCIMOD.ORNL code to include the effect of structural boundaries for instances where we analyze steam explosions with the RCS full of water would be highly desirable.

Improvements are also needed in the modeling of fuel fragmentation. Currently, only thermal effects have been incorporated in the FCIMOD code. Hydrodynamic effects that become predominant when pressure buildup occurs have not been included. This modeling is necessary for best-estimate evaluation of the actual amount of fuel thermal energy that is transferred to the coolant on an explosive time-scale. Such information would then be used to perform better estimates for multidimensional energetics calculations using CTH.

4.5 IGNITION OF ALUMINUM DURING STEAM EXPLOSIONS

For the purposes of the HFIR SAR we have assumed that aluminum-water reactions do not occur during steam explosions caused during melting from flow blockages. There is some precedent for making such an assumption. Flow-blockage-induced fuel melting in the Westinghouse Test Reactor (WTR) and also in the Oak Ridge Research Reactor (ORR) did not lead to energetic aluminum-water reactions. However,

the fuel-plate material and power density of these reactors was different from that of the HFIR. The key to determining whether aluminum ignition is relevant to the current situation is not just whether it will occur, but whether it will occur to a sufficient degree on an explosive time scale. It is expected that due to the postulated low propensity for HFIR fuel to disperse (because of higher apparent viscosity), the propensity for explosive aluminum ignition will also be negligible. This aspect is currently under study in conjunction with experimental and analytical work for determining triggering potential. This work is expected to demonstrate the appropriateness of this important assumption made relating to the absence of explosive aluminum-water reactions for HFIR fuel.

4.6 EFFECT OF FUEL IRRADIATION AND FISSION PRODUCT INVENTORY BUILDUP

One of the features that can suppress an explosive FCI from occurring is the presence of a gas layer that acts as a buffer between molten fuel and water. Such an effect has been shown experimentally. For the HFIR situation, we know that during irradiation, fission gases are going build up. During postulated meltdown conditions, these fission gases may act as a buffer that provides a suppressing effect for explosive FCI occurrence (with and without aluminum ignition). This effect has not been accounted for in the present study. It would prove highly beneficial to account for this effect both analytically and via small-scale experiments using dissolved simulants.

REFERENCES

1. "Final Report of SL-1 Recovery Operation," May 1961-July 1962, IDO-19311, July 1962.
2. J. R. Dietrich, "Experimental Investigation of the Self-Limitation of Power During Reactivity Transients in a Subcooled, Water-Moderated Reactor," BORAX-I Experiments, ANL-5323, Argonne National Laboratory, March 1957.
3. R. W. Miller et al., "Report of SPERT-I Destructive Test Program on an Aluminum, Plate-Type, Water-Moderated Reactor," IDO-16883, June 1964.
4. "Reactor Safety Study," WASH-1400, NUREG/75-0114, 1975.
5. R. P. Taleyarkhan, *Steam-Explosion Safety Considerations for the Advanced Neutron Source Reactor at Oak Ridge National Laboratory*, ORNL/TM-11324, February 1990.
6. "Automatic Dynamic Incremental Nonlinear Analysis," Users Manual, ADINA R&D, Inc., December 1987.
7. R. M. Summers et al., *MELCOR 1.8.0: A Computer Code for Nuclear Reactor Severe Accident Source Term and Risk Assessment Analyses*, NUREG/CR-5531, Sandia National Laboratories, 1991.
8. J. M. McGlaun et al., "CTH User's Manual and Input Instructions, Ver. 1.02," Sandia National Laboratories Report SAND88-0523, 1988.
9. R. O. Ivins et al., "Studies of the Aluminum-Water Reaction in TREAT," Chemical Engineering Division Summary Report, October through December, 1962, ANL-6648, p. 201 (1963).
10. K. E. Carlson et al., *RELAP5/MOD3 Code Manual, Code Structure, System Models, and Solution Methods*, Idaho National Engineering Laboratory, NUREG/CR-5535 (EGG-2596), June 1990.

11. S. Kaspirazak et al., "A Method of Analysis of Two Dimensional Melting and/or Freezing in Two-Material Structures," pp. 27-33 in *Proceedings of the 24th National Heat Transfer Conference and Exhibition, Pittsburgh, Pennsylvania, August 1987.*
12. PHOENICS
13. E. P. Hicks and D. P. Menzies, "Theoretical Studies on Fast Reactor Maximum Accidents," Argonne National Laboratory Report ANL-7120, 1965.
14. A. N. Hall, "Outline of a New Thermodynamic Model of Energetic Fuel-Coolant-Interactions," *Nuclear Science and Engineering*, Vol. 109, 1988.
15. S. J. Board and R. W. Hall, "Propagation of Thermal Explosions Part 2: A Theoretical Model," Central Electricity Generating Board Report RD/B/N3249, 1974.
16. K. H. Bang and M. L. Corradini, "Thermodynamic Analysis of Vapor Explosions: Comparison of Models," Technical Note (personal communication), 1991.
17. K. H. Bang and M. L. Corradini, "UWHM Code User's Manual," 1991.
18. K. H. Bang and M. L. Corradini, "UWHUGO Code User's Manual," 1991.
19. L. Haar et al., "NBS/NRC Steam Tables," Hemisphere Publishing Corp., New York, 1984.
20. M. D. Oh and M. L. Corradini, "A Propagation/Expansion Model for Large-Scale Vapor Explosions," *Nucl. Sci. and Eng.* 95, 225-240 (1987).
21. M. Ledinegg, "Instability of Flow During Natural and Forced Circulation," Die Warme, 61, 8 (1938).
22. J. Freels, "Estimate of HFIR Core Damage Following a Core Blockage Based on RELAP5/Mod2.5/v3t with HFIR CHF Extensions," C-HFIR-92-023, June 23, 1992.
23. R. C. Gwaltney, "Scoping Calculations to Estimate the Energy Release from a Steam Explosion Between HFIR Plates," STEAMING.ONE and STEAMING.TWO, May 1992.

24. Claire R. Luttrell, "Analysis of a Fuel Plate with the Side Walls Under Pressure Pulse Loading Applied to a Rectangular Area in the Middle of the Plate with Cyclic Boundary Conditions," UNXCZL3 through UNXCZL55, November, 1991

25. Claire R. Luttrell, "Analysis of a Fuel Plate with the Side Walls Under Pressure Pulse Loading Applied to a Strip in the Middle of the Plate with Cyclic Boundary Conditions," UNXCZL3 through UNXCZL55, November, 1991.

26. Claire R. Luttrell, "Analysis of 2-D Fuel Plates with their Fluid Coolant Channels and Cyclic Boundary Conditions Under Pressure Pulse Loadings," UNXCZL01, UNXCZL03 and UNXCZL04, November 18, 1991.

27. Claire R. Luttrell, "Analysis of Three 2-D Fuel Plates with Fluid Coolant Channels Under Pressure Pulse Loading," UNXCZL20 through UNXCZL22, October 25, 1991.

28. Claire R. Luttrell, "Analysis of Two 2-D Fuel Plates with Fluid Coolant Channels Under Pressure Pulse Loading," UNXCZL31 through UNXCZL34, October 25, 1991.

29. Claire R. Luttrell, "Analysis of One 2-D Fuel Plate Under Pressure Pulse Loading," UNXCZL58, UNXCZL59, UNXCZL61 through UNXCZL65, November 1, 1991.

30. Claire R. Luttrell, "Buckling of an Outer Fuel Plate Under Thermal Load," UNXCZL46, November 1, 1991.

31. Claire R. Luttrell, "Buckling of an Outer Fuel Plate Under Thermal Load," UNXCZL44 and UNXCZL45, November 1, 1991.

32. R. C. Gwaltney and C. Luttrell, "Critical Flow Velocity for Involute Parallel Plate Assemblies," *Transactions of the American Nuclear Society*, Vol. 57, 1988.

33. J. R. Kirkpatrick, "Estimate of Propagation of Melting in HFIR Fuel Plates Initiated by Blockage of Two Adjacent Channels," HFIR-CTD-91-JRK-15-2, May 15, 1991.

34. S. J. Chang, "Failure Envelopes of Simplified HFIR Vessel for Yield and Fracture," ORNL RRD Internal Report, May 9, 1991.

35. S. J. Chang, "Fracture Strength of HFIR Vessel with the Effects of Radiation Embrittlement and Fluid-Solid Interaction," Symposium on Fluid-Structure Interaction, ASME Pressure Vessel and Piping Conference, New Orleans, Louisiana, June 21-25, 1992.

36. R. D. Cheverton et al., *Evaluation of HFIR Pressure Vessel Integrity Considering Radiation Embrittlement,* ORNL/TM-10444, 1988, Oak Ridge National Laboratory, Oak Ridge, TN.

37. C. W. Nestor, "Checkout and Implementation of the FCIMOD Computer Program," C-HFIR-91-032, January 9, 1992.

38. C. W. Nestor, "Quality Assurance and Implementation of the CTH Package," C-HFIR-91-033, January 9, 1992.

39. C. W. Nestor, "Checkout and Implementation of the UWHUGO and UWHM Computer Programs," C-HFIR-91-034, January 9, 1992.

40. R. P. Taleyarkhan, "HFIR Debris Coolability Calculations for Fuel-Coolant-Interaction (FCI) Analysis in the Shield Plug Region," C-HFIR-91-035, January 9, 1992.

41. R. P. Taleyarkhan, "Analysis of HFIR FCI Energetics with UWHUGO and UWHM," C-HFIR-91-036, January 9, 1992.

42. R. P. Taleyarkhan, "FCIMOD Calculations for 1-D Energetics for HFIR FCI Analysis," C-HFIR-91-037, January 9, 1992.

43. C. W. Nestor, "Analysis of HFIR FCI Energetics with CTH," C-HFIR-91-038, January 9, 1992.

44. R. P. Taleyarkhan, "HFIR Debris Coolability Calculations for Fuel-Coolant-Interaction (FCI) Analysis in the Shield Plug Region," C-HFIR-91-035 (Rev. 1), August, 1992.

45. V. Georgevich, "Changes performed to the FCIMOD Code," C-HFIR-92-015, August 1992.

46. V. Georgevich, "Best-Estimate Model CTH Code Calculations for HFIR," C-HFIR-92-018, August, 1992.

47. R. P. Taleyarkhan, "Estimates of HFIR Vessel Wall and Top Head Bolt Failure Pressure Loads During Steam Explosion Events," C-HCIR-92-014, August, 1992.

48. V. Georgevich, "Thermodynamic and Mechanistic Energetics Calculations for HFIR," August, 1992.

49. C. W. Nestor, "Effect of Mesh Size on CTH Results," C-HFIR-92-017, August 1992.

50. C. W. Nestor, "HFIR Top Head Launch," C-HFIR-92-021, August 1992.

51. R.W.Cox and A.T. MacDonald, "Introduction to Fluid Mechanics (2nd Ed.)," John Wiley and Sons, New York, 1978, p. 427.

52. M. L. Corradini, "Comparison of a Vapor Explosion Model to Metal-Water FCI Tests," *Transactions of the American Nuclear Society*, Vol. 65, Boston, June, 1992.

53. F. T. Binford et al., *The High Flux Isotope Reactor: A Functional Description, Vol. 1A, Text and Vol. 1B, Illustrations*, ORNL-3572 (Rev. 2), Martin Marietta Energy Systems, Inc., Oak Ridge National Laboratory, June 1968.

54. T. E. Cole et al., *The High Flux Isotope Reactor Accident Analysis*, ORNL-3573, Union Carbide Corporation, Nuclear Division, Oak Ridge National Laboratory, April 1967.

55. J. Snelgrove, "A Review of the U_3O_8-Aluminum Reaction as a Potential Heat Source in Research and Test Reactor Accidents," *Proceedings of the 1992 National Heat Transfer Conference, San Diego, California, August 1992.*

56. D. R. Miller, "Critical Flow Velocities for Collapse of Reactor Parallel-Plate Fuel Assemblies," *Transactions of the ASME, Journal of Engineering for Power*, April 1960, pages 83-95.

APPENDIX A

Review of Fuel-Coolant-Interaction Analysis Reported in ORNL-3573 (Ref. 54)

A review was conducted of past work done to characterize fuel-coolant-interaction-(FCI)-related phenomena in the High Flux Isotope Reactor (HFIR) as documented in ORNL-3573 (Accident Analysis Report). Because of time constraints, efforts were concentrated on reviewing material related to FCIs initiated from a core flow blockage accident only.

A.1 GENERAL COMMENTS

In general, it can be said that the authors of ORNL-3573 conducted a fairly thorough treatment of the subject of FCI based on the information and insights available to them. However, several individuals contributed toward this analysis in a somewhat piecemeal fashion. As a result, the treatment of FCI and the resulting structural response is scattered throughout the report. In several areas, key unverified assumptions were made that were based solely on a perspective that the individual author(s) had on what might actually transpire. Some of these assumptions seem definitely conservative, whereas others are questionable and cannot be supported on the basis of what we know today.

A.2 SPECIFIC TECHNICAL COMMENTS

To provide uniform review comments, ORNL-3573 is taken as a focal point, and review comments are provided on individual chapters and appendices where FCI phenomena are treated. Therafter, a summary is provided on relevant findings and on areas that need to be investigated further to build upon what has been already done and to

provide a reasonably comprehensive analysis for the HFIR Safety Analysis Report (SAR). These comments are given below.

A.2.1 Comments on Sect. 4.1 (Sources and Magnitudes of Energy Releases)

The authors state that the maximum amount of energy that can be released from complete U_3O_8-Al mixture exothermic reactions is about 22.4 MJ. This energy release is initiated after the mixture temperature exceeds 650°C. These assertions are based on experimental evidence and are therefore irrefutable. The only uncertainty in this process lies in the rate of reaction, which is known qualitatively to be slow (i.e., requiring several minutes), but one that picks up as the mixture temperature rises. No firm experimental evidence exists to support rate-dependence evaluations.[55] Hence, estimates of energy-release potential from this reaction would need to be made carefully.

The authors have also acknowledged another potentially large energy source which comes from the Al-H_2O chemical reaction. Based on the 88 kg of aluminum in the HFIR core, about 1550 MJ of energy can be released. The authors correctly state that to achieve this quantity of energy release, the aluminum would need to be highly fragmented and sufficient water would also need to be available. They then state that these two factors are highly unlikely in the event of core melting resulting from flow blockages. The authors predicate these assertions on the assumption that the fuel plates would remain intact and would not leave the core region. If this is indeed the case for core melt progression, then these assertions are supportable because significant localized steaming would tend to restrict water availability.

For other cases where the FCI process involves a steam explosion, such assumptions cannot be supported, on the basis of what we currently know of steam explosion-related phenomena. Steam explosions cause considerable transient fragmentation and dispersion during the mixing and propagation stages. For such

instances, water availability and particle size constraints would not exist. Hence, this portion of the analysis does not seem defensible and needs upgrading.

A.2.2 Comments on ORNL-3573, Appendix D: Maximum Energy Release From Core Flow Blockage in the HFIR

In Appendix D the authors evaluate a maximum credible energy release from core flow blockage events. Once again, they defensibly evaluate the maximum quantity of energy release from U_3O_8-Al reactions. The amount of fission heat required for attaining the onset of significant Al-H_2O reactions at and beyond 1170°C also seems reasonable. However, the assumptions concerning the amount of aluminum that can react with water are questionable. The authors state that on the average only 40% of the available aluminum can react, due to further nonavailability of coolant. No supporting calculations are provided for this assertion, which gives about 1.04 MJ of chemical energy per plate or a total of 567 MJ, instead of about 2.87 MJ per plate that can be released if all the aluminum in the plate were to react. Clearly, the real answer will be lower than 2.87 MJ per plate because at least some of the aluminum would have been consumed from U_3O_8-Al reactions. However, the U_3O_8-Al reaction may proceed slowly as explained previously. Hence, for upper-bound estimates the amount of energy released per plate would amount to 2.87 MJ (Al-H_2O) + 0.25 MJ (fission energy) = 3.12 MJ.

The evaluation of the number of fuel plates, or fraction of the core that would be involved in overheating at full power, definitely seems conservative and presents the greatest potential for reducing the FCI energy source. This is true for the analysis of small and large flow blockages. However, it was not clear why the change in criticality for the coolant is evaluated differently for the small and large blockage cases. Table I.D.2 in ORNL-3573 uses a variable coolant temperature reactivity coefficient compared with a fixed value used for large flow blockages in Table I.D.3. If we are consistently conservative and use a fixed value for the coolant coefficient, the change in criticality is

evaluated as being 5.3% for the small flow blockage instead of 2.9%. If so, then the fraction of core involved at nominal core power (i.e., before scram) for the small flow blockage event would turn out to be = 0.7/(2.0 + 2.9) = 0.14, or 77 fuel plates. Thus, the maximum possible energy source for small and large flow blockages should be 240 and 406 MJ, respectively. This is in contrast to 78 MJ and 140 MJ evaluated by the authors under assumptions of nonavailability of sufficient water for complete Al-H_2O reaction. All said and done, this is clearly an area where it may be possible to obtain significant reductions in the amount of plate melting and energy liberated.

In their efforts to evaluate the maximum possible core fraction involvement and associated energy releases the authors have overlooked the possibility of damage propagation under decay heat conditions. For the core region, this scenario may give rise to multiple explosions sequentially as damage propagates throughout the core. The associated energy release rate sequence and amounts need to be analyzed and evaluated using conservative assumptions. Another aspect that has not been dealt with concerns a scenario where the core melt progression involves a considerable fraction of the core without a damaging steam explosion (caused by the stochastic nature of the process). In this case, melt progression under decay heat and low flows would likely lead to the eventual formation of a puddle on the shield plug. If the debris bed is in a noncoolable state, a steam explosion in this configuration cannot be discounted.

Additional energy sources that can be postulated deal with transients where the scram function is inoperable, or under certain melt progression conditions that may lead to recriticality conditions.

Finally, the authors correctly state that the time scale of events for steam explosions with simultaneous Al-H_2O reactions is considerably larger than seen for TNT explosions.

An effort to evaluate pertinent core debris heatup and melt progression aspects (conservatively, if necessary) is needed to address the perceived shortcomings mentioned in the previous paragraph.

A.2.3 Comments on Appendix I (Energy Releases From Al-H_2O Reactions in HFIR)

The authors go through a fairly lengthy discussion of possible energy release amounts and rates under various severe accident conditions. As an upper bound they consider ignition of aluminum, assuming the entire core coalesces into one large molten sphere. The rate of ignition progresses in a mass transfer limited process that is directly proportional to the surface area of the remaining molten sphere. This rate decreases monotonically until the aluminum sphere diameter reaches a diameter of 3.36 mm, after which no ignition is deemed to occur. As a consequence of this modeling process, the rate of energy release gets larger with decreasing initial diameters and then abruptly drops to zero when the particle size reaches a diameter of 3.36 mm. Experiments conducted at Argonne National Laboratory and elsewhere are used as supporting evidence.

Upon review of the experimental evidence, it was noted that the ANL experimenters had not evaluated molten droplet ignition characteristics for sizes below 5.3 mm. The ORNL-3573 authors came up with the lower limit of 3.36 mm by extrapolating the linear relationship between initial particle sizes and consumption time to that initial droplet diameter at which the consumption time would be zero. A seemingly reasonable argument is given that as the particle size lessens, radiation heat losses from the surface (or ignition front) increase enough to prevent high enough metal temperatures for combustion to continue. This assumption needs to be evaluated further. However, based on initial scrutiny, it seems to be highly nonconservative. It is well-known that fine aluminum powder is highly pyrophoric, which indicates that particle diameters much less than 3.36 mm can undergo ignition, at least in air. Therefore, another way of interpreting the linear extrapolation of zero consumption time for particle sizes at and below 3.36 mm

is that the rate of ignition is actually infinite, rather than zero as construed by the authors. An infinite rate is nonphysical; nevertheless, it does appear that the rate may actually be quite high.

Alternately, it is proposed as a start that no such limit on particle size diameter be used for evaluating ignition characteristics. Until we know more a similar rate of reaction evaluation should be used for particle sizes below 3.36 mm. That is, irregardless of the particle size the initial mass rate of consumption should be evaluated using modified forms of Eq. (8) (page 220 in ORNL-3573) and Eq. (6) (page 217 in ORNL-3573) given as,

$$Do = 0.45\ tc\ \text{-- (mm)} \tag{A.1}$$

and

$$-dm/dt = A \times 2.68\ \text{-- (g/min)} \tag{A.2}$$

After initial combustion, and for particle sizes less than 3.36 mm, the rate of energy production may thus be evaluated from [cf. Eq. (6), page 214 of ORNL-3573]:

$$P(t) = (82/Do) \times (0.45\ t/Do)^2\ \text{-- (Mw)} \tag{A.3}$$

An alternate formulation for Eq. (A.1) which uses an exponential formulation to connect consumption times from zero to 12 s may be more suitable. However, we do not have a physical basis for this assertion. The rate of energy release from use of the above-mentioned formulations should be compared with releases predicted from Arrhenius-type correlations for noncombustion chemical reactions. Such correlations predict large

energy releases as the particle sizes decrease. Simultaneous cooling evaluations (however rudimentary) should also be conducted.

Again, it should be noted that the equation (p. 212 of ORNL-3573) the authors use for evaluating aluminum oxidation without ignition is only applicable when fresh molten aluminum surface is not available and the process is essentially diffusion controlled. For situations where fresh molten aluminum is continuously available the rate of reaction increases by a factor of 16. Such instances can arise during steam explosions where molten particles get progressively fragmented into smaller size particles.

Finally, the authors have provided a simple but very insightful analysis of TREAT data taken with HFIR fuel samples that showed an apparent dependence on ambient pressure. The TREAT tests gave results that indicated the temperature for onset of aluminum ignition decreased with increasing ambient pressure. The authors conducted simple heat transfer calculations to show that the effect was caused by the ambient coolant temperatures being different between tests. Upon allowing for this effect and plotting the observed amounts of aluminum reacted with fuel temperature rather than energy input, the apparent pressure effect disappears. Based on this analysis it was surmised that for instances where rapid energy deposition occurs in HFIR fuel plates, substantial aluminum combustion can occur only above a fuel temperature of 1450°C. It should be recognized, however, that very recent (1989) tests conducted at Sandia National Laboratories significant aluminum ignition was observed at temperatures of 850°C. This precise temperature is still somewhat controversial. It is generally accepted that this is a scale dependent process wherein the ignition threshold temperature drops with increasing aluminum mass.

A.2.4 Comments on Appendix B and Appendix J (HFIR Vessel Containment Potential) - ORNL-3573

A review was conducted to evaluate past analyses conducted for evaluating maximum energy releases from a FCI that could then be contained by the HFIR vessel

and reactor coolant system (RCS). This review was somewhat limited, since checkout of structural response analysis and TNT-equivalence analysis were not conducted. However, a few general comments are given below.

The analysis of Appendix B provides estimates of containment potential for a variety of boundary conditions. Results for a case where the HFIR core region is devoid of water serve no practical purpose whatsoever, because a steam explosion cannot result without the presence of water. The most relevant case where the vessel is surrounded by water gave estimates of maximum energy sources that can be tolerated of about 220 and 660 MJ, respectively, depending on whether one-third or complete ultimate vessel strain levels were used for evaluation of failure. If we now combine these results with the evaluated maximum strain energy to rupture for the HFIR vessel evaluated in Appendix J of 200 MJ, the strain energy (i.e., mechanical energy released from the FCI) imparted to the vessel from a 660-MJ energy burst amounts to about 30%.

On the other hand, the evaluations for strain energy conducted using a steady-state thermodynamic method (page 233 in ORNL-3573) provide energy conversion ratios (i.e., ratio of strain energy to energy release from explosion) varying from about 5 to 12%. These evaluations conclude that steam explosions are inherently inefficient in producing damage when compared to TNT explosions. This was seemingly corroborated by validating the thermodynamic approach against an experiment for evaluating strain in a water-filled cylinder from a PETN explosion (pages 243 and 244 of ORNL-3573). However, it should be noted that this validation was conducted for evaluating strain energies resulting from high explosive charges and not for steam explosions. Transient effects such as pressure pulse generation, propagation, and dynamic interactions with the vessel structure were not evaluated.

Using various approaches developed for evaluating maximum mechanical energy conversion during steam explosions (such as the so-called Hicks-Menzies or the Board-Hall models), one can obtain conversion efficiencies close to 45% as demonstrated in

Sects. 2 and 3 of this report. The conversion efficiency depends very much on several parameters, some of the important ones being the fuel-coolant mixture void fraction, the amount of mixing between fuel and coolant, and the fuel and coolant temperatures. A final point needs to be made regarding use of TNT explosion methods for judging the nature of damage that can be produced in the surrounding structure. It is true that for a given energy release TNT explosions will provide much greater pressures than FCI-pressure pulses but of much shorter durations. However, as long as a structure's yield point is reached, the longer pulse can inflict more damage. Based on these aspects, it is not clear whether TNT equivalence methods will consistently provide conservative and defensible estimates of damage potential.

A.3 CONCLUDING REMARKS

To summarize, the authors of ORNL-3573 conducted a fairly thorough analysis on the subject of FCI based on the information they had. However, several shortcomings were noted in the various assumptions made and methods used for evaluating the overall damage potential to the HFIR RCS. Salient aspects of this review can be summarized and concluded as:

(1) The various potential sources of energy release have been identified correctly. Estimates of energy release from U_3O_8-Al reactions and fission energy have been evaluated correctly. The rate of such energy release was not evaluated due to lack of pertinent experimental data. Aluminum-water reaction energy release amounts resulting from core flow blockage events seem to have been significantly underestimated.

(2) The treatment of energy releases from combustion of aluminum was covered fairly extensively. However, an assumption was made that combustion ceases when the particle size decreases to below 3.36 mm. Based on experimental evidence, this seems

unjustifiable. An extension of the ORNL-3573 approach has been identified and is recommended for use when particle sizes get smaller than 3.36 mm.

(3) The simple method used by ORNL-3573 authors to estimate the number of fuel plates involved in small and large flow blockage events based on reactivity considerations is conservative, but somewhat inconsistent. The evaluation of the number of fuel plates involved in the small flow blockage case used a variable value for the coolant reactivity coefficient. In contrast, a fixed value was used for the large flow-blockage case. A fixed value for the coefficient gives significantly higher core melt fractions. However, using a variable reactivity coefficient can also be justified on physical grounds. It should be mentioned that the aspects of melt progression under decay heat conditions have not been considered. Such aspects may lead to the accumulation of core debris on the shield plug region. If debris coolability cannot be maintained, the likelihood of a steam explosion cannot be overruled.

(4) HFIR RCS failure analysis was conducted using TNT-equivalence methods based upon strain energy levels that can be tolerated. Another method used static thermodynamic evaluations to evaluate strain energy levels. Upon close scrutiny, it was concluded that the methods used by the authors cannot be expected to consistently provide conservative estimates of thermal-to-mechanical energy conversion during steam explosions. Various physical aspects such as transient melt fragmentation, dispersion, mixing, and propagation were not accounted for. However, the TNT-equivalence methodology should be employed where possible (but not to the exclusion of current methods) to provide an alternate means for estimating RCS failure.

(5) The ORNL-3573 analysis does not discuss the potential for missile generation. This is a concern that may have been overlooked. Another area that has been omitted deals with the possible failure of vessel structural supports from loads generated during steam explosion events, coupled with levitation of the entire vessel. Finally, it is

mentioned that the aspects of reactor scram failure and recriticality have not been addressed in conjunction with potential energy releases from core flow blockage events.

APPENDIX B

Thermal-Hydraulic Conditions for Structural Response Calculations

The thermal-hydraulic conditions for various scenarios which may lead to core melt progression are described in this appendix. Further description of the various scenarios are given in Sect. 2 of this report.

B.1 THERMAL-HYDRAULIC CONDITIONS FOR SCENARIO 1

For scenario 1 where plates ablate, the thermal-hydraulic conditions used for conducting structural response calculations are given below:

B.1.1 Pressure Variations

- at inlet, pressures are the same as the system pressure — Ps = 3.29 MPa (470 psia);
- core outlet pressures (Po) = Ps - 0.7 MPa;
- axial pressure variation in the core is linear;
- as gaps get larger, radial pressure gradients and tend to get established; however, for scoping purposes radial pressure variations are assumed to be negligible and set to zero.

B.1.2 Coolant Temperatures

- at core inlet 49°C,
- at core outlet 76°C,
  - coolant temperatures vary linearly from core inlet to outlet.

B.1.3 Fuel Plate Temperatures

- The radial temperature variation from centerline to plate surface is usually less than 6°C and may thus be approximated as a linear variation for the current analyses.
- Fuel plate temperatures vary in the axial direction due to coolant heatup.
- The following expressions were used for evaluating plate temperature [Tp(i,j)],

where

i = axial location; j = radial location from surface to centerline of plate:

- Tp(i,1) = Tc(i) + 52 (i.e., for the plate surface node),
- Tp(i,centerline) = Tc(i) + 58 (i.e., for the plate centerline node),
- Tc(i) = coolant temperature at axial node i.

B.1.4 Gap Size, and Velocity Distribution

This information is provided in Table B.1.

B.2 THERMAL-HYDRAULIC CONDITIONS FOR SCENARIO 2

B.2.1 Pressures

- At channel entrance, pressures for blocked and unblocked channels = Ps.
- For unblocked flow channel, axial pressure variation in the core is linear and should be assumed to vary from Ps at inlet to Ps - 0.7 MPa at the channel exit.
- For the blocked flow channel (which voids out providing adiabatic-type conditions for heat transfer) the pressures throughout the channel were assumed to be equal to Ps.

- Thus, for bending evaluations, the maximum radial pressure gradient existing at the core exit = 0.7 MPa (100 psi).

B.2.2 Coolant Temperatures

For the unblocked flow channel:

- At core inlet 49°C,
- At core outlet 49 + 27*3/2 = 89°C,

Coolant temperatures vary linearly from core inlet to outlet.

For the blocked flow channel

- Assume no axial variation of coolant temperatures
- Ambient steam temperature = fuel plate temperature adjacent to steam region (see Sect. B.4).

B.2.3 Fuel Plate Temperatures

The radial variation of fuel plate temperature should be evaluated based upon the expression developed in Sect. B.4 [Eq. (B.8)].

B.3 THERMAL-HYDRAULIC CONDITIONS FOR SCENARIO 3

B.3.1 Pressures

- At channel entrance pressures for blocked and unblocked channels = Ps.
- For unblocked flow channel, axial pressure variation in the core is linear and should be assumed to vary from Ps at inlet to Ps - 0.7 MPa at the channel exit.
- For the blocked flow channel (which voids out, providing adiabatic-type conditions for heat transfer), the dynamic pressure pulses throughout the channel were assumed to be uniformly distributed and triangular in shape.

B.3.2 Coolant Temperatures

Fluid temperatures for the unblocked flow channel were set as follows:

- At core inlet 49°C,
- At core outlet 49 + 27*3/2 = 89°C,

Coolant temperatures vary linearly from core inlet to outlet.

For scoping evaluations, an averaged value of 70°C was used.

For the blocked flow channel, fluid temperatures were set as follows:

- It was assumed that axial variation of coolant temperatures do not exist.
- Ambient steam temperature = 0.5 * (1000 + 232) = 616°C.

It was assumed that the steam explosion is going to cause plate melt superheat to 1000°C, and the steam produced before the explosion is going to be at the saturation temperature corresponding to the core-averaged pressure of about 425 psia (whereby saturation temperature of steam is 232°C).

B.3.3 Fuel Plate Temperatures

For scoping calculations of plate deformation and possible failure from high pressures produced during steam explosions, it was assumed that the plate temperatures would be equal to 155°C axially and radially at the onset of being subjected to a pressure pulse from one side. The temperature of 155°C was evaluated using Eq. (B.8) of Sect. B.4 and taking the average of nodal temperatures (from cold and hot sides) at core outlet coolant temperature of 89°C.

B.4 EVALUATION OF TEMPERATURE DISTRIBUTION ACROSS PLATE FOR SCENARIO 2

Several assumptions made for the evaluation of temperature distribution across the plate:

1. Axial effects are negligible.
2. Uniform internal energy generation exists in the fuel plate.
3. One plate side is insulated.
4. Average coolant properties for the unblocked flow channel are:[53]

$$\left(T_{coolant} = \frac{120 + 170}{2} = 145^{\circ}F\right)$$

$$h_{film} = 15000 * 5.67 \frac{W}{m^2 K}$$

The one-dimensional heat conduction equation can be written as:

$$\frac{d^2T}{dx^2} + \frac{q'''}{K} = 0 \quad . \tag{B.1}$$

Integrating Eq. (B.1) gives

$$\frac{dT}{dx} + \frac{q'''}{K} x = C_1 \quad , \tag{B.2}$$

and

$$T + \frac{q'''}{K} \frac{x^2}{2} = C_1 x + C_2 \quad , \tag{B.3}$$

which are to be solved subject to the following boundary conditions:

$$\text{at } x = \delta, \frac{dT}{dx} = 0 \quad , \tag{B.4}$$

and

$$\text{at } x = 0,\ T = T_w = \frac{q'''V_h}{A_{surf}h_{film}} + T_c \quad . \tag{B.5}$$

Using Eqs. (B.2) through (B.5) gives

$$C_1 = \frac{q'''\delta}{K},\ C_2 = T_w \quad , \tag{B.6}$$

so that the temperature distribution can be approximated by

$$T(x) = \frac{q'''\delta}{K}x + \frac{q'''V_h}{A_{surf}\ h_{film}} + T_c - \frac{q'''x^2}{2K} \tag{B.7}$$

or

$$T(x) = q'''\left[\frac{\delta x}{K} + \frac{V_h}{A_{surf}\ h_{film}} - \frac{x^2}{2K}\right] + T_c \quad . \tag{B.8}$$

At a power level of 85 MW(t):

$$q''' = \frac{85(10^6)}{V_h},\ \text{where } V_h = \frac{25}{1000}\,m^3$$

or

$$q''' = 3.4(10^9)\,WE/m^3,$$

A_{surf} for core = 40 m^2, but with one side insulated,

A_{surf} for core = 20 m^2,

h_{film} = 15000 Btu hr•ft^2•°F = 15000*5.67 W/m^2•K

so that

$$\frac{V_h}{A_{surf}\, h_{film}} = 1.47\ (10^{-8})$$

Under averaged nominal conditions only, $T_c = 63°C$, so that, from Eq. (B.8) we obtain

$$T(x) = 3.4\ (10^{9})\ [7.57\ (10^{-6})\ x + 1.47\ (10^{-8}) - 2.98\ (10^{-3})\ x^2] + T_c,$$

where T has units of degrees Celsius and x has units of meters. At x = 0, T = 113°C, versus 102°C under nominal conditions, and with δ = 0.00127 m, $T(\delta)$ = 129°C.

Table B.1. HFIR melt propagation input (Scenario 1)

Nom. Flow Vel. [Vo - (cm/s)] = 127.00
Nom. Flow Area (sq. cm) = 1.93
Nom. Wetted Per. (cm) = 30.65
Nom. Hyd. Diam [Do - (cm)] = 0.25

Number of channels ablated	New gap width (cm)	New flow area (sq. cm)	New hyd. Dia. (Dn) (cm)	Dn/Do	Vn/Vo (Kin[a] = 0)	Vn/Vo (Kin[a] = 0.385)
1	0.38	5.79	0.74	2.07	1.72	1.59
2	0.64	9.65	1.22	4.88	2.21	1.91
3	0.89	13.51	1.68	6.72	2.59	2.11
4	1.14	17.37	2.13	8.50	2.92	2.26
5	1.40	21.23	2.56	10.24	3.20	2.38
6	1.65	25.10	2.98	11.91	3.45	2.47
7	1.91	28.96	3.39	13.54	3.68	2.54
8	2.16	32.82	3.78	15.12	3.89	2.60
9	2.31	36.68	4.16	16.66	4.08	2.65
10	2.67	40.54	4.54	18.15	4.26	2.69
11	2.92	44.40	4.90	19.60	4.43	2.73
12	3.18	48.26	5.25	21.01	4.58	2.76
13	3.43	52.12	5.60	22.38	4.73	2.79
14	3.68	55.98	5.93	23.72	1.87	2.81
15	3.94	59.84	6.25	25.02	5.00	2.84
16	4.19	63.70	6.57	26.28	5.13	7.86
17	4.45	67.56	6.88	27.51	5.25	2.88
18	4.70	71.42	7.18	28.71	5.36	2.89
19	4.95	75.29	7.47	29.89	5.47	2.91
20	5.21	79.15	7.76	31.03	5.37	2.92
21	5.46	83.01	8.04	32.14	5.67	2.93
22	5.72	86.117	8.31	33.13	5.76	2.95

[a]Kin - Channel Inlet Loss Coefficient.

APPENDIX C

Core Melt Initiation and Propagation Calculations

To provide some degree of quantification of core melt initiation and propagation, separate calculations were conducted to determine the quantity of core fuel plates that might melt from flow blockage events. This appendix summarizes results of hand calculations and insights developed from use of the RELAP5 code. Various calculations conducted are summarized below.

C.1 CONSERVATIVE CORE MELT PROPAGATION CALCULATIONS

A simplified analysis was conducted to evaluate aspects dealing with the general subject of fuel plate melting and propagation from flow blockage accidents in HFIR. Modeling and analysis details are given in Ref. 22. Briefly, a scoping calculation was first conducted to determine if a plate melting incident could occur if a single coolant channel were to be completely blocked. Simple heat balance calculations reveal that even if one face of a heat-generating fuel plate were treated as being blanketed with steam such that adiabatic conditions were to be imposed, the resulting plate temperature would still be far less than that required for the onset of melting.

Next, it was shown (as expected) that complete blockage of both coolant channels around a fuel plate results in rapid melting of the fuel plate.

A postulated model was developed to evaluate the degree of melt propagation before arrest via scram. It was assumed that a fuel plate that melts collapses uniformly on its neighboring channel, such that those plates now start to heat up and melt. Thereafter, melting propagation occurs in a domino fashion until the scram function is completed. This type of calculation is similar to the one done by earlier researchers as described in

Appendix A and in Ref. 33. Overall, this approach predicts that up to 77 plates (or 14% of the core fuel plates) could melt and participate in a steam explosion.

In addition to this approach, another method (referred to as Model A) was devised[22] to evaluate another important parameter related to fuel melting during flow blockage events. The parameter of interest relates to the minimum overall area of flow that needs to be blocked before plate melting can begin. In this method, a postulate is made that the critical blockage size would be related to a certain critical mass flow rate. This critical mass flow rate would be that which would lead to complete vaporization of all liquid that normally would flow through a coolant gap. The corresponding critical steam velocity is simply,

$$V_C = m_C/(\rho A) \ , \qquad (C.1)$$

where, m_C is the critical mass flow rate, r is the steam density, and A is the coolant channel flow area. For HFIR conditions, Vc is evaluated to be 46.6 m/s (153.4 ft/s). This V_C is used to evaluate a corresponding pressure drop accross the length of the core which amounts to a value of 0.11 MPa (15.9 psid). The critical blockage size is then evaluated as that size blockage which causes a certain increase in local hydraulic loss coefficient at channel inlet. This increased inlet loss coefficient would then cause a sufficient drop in pressure such that the core overall pressure drop is the same as that for unblocked channels [viz., 0.75 MPa (107.14 psid)]. Based on this analogy, it was evaluated that a blocked flow area of about 74% or greater would be sufficient to lead to fuel plate melting.

C.2 RELAP5 CALCULATIONS FOR ESTIMATION OF CRITICAL BLOCKAGE AREA

To confirm the hypothesis and postulate associated with Model A (outlined in the previous section), a more detailed 10-channel model (referred to as Model B) was set up utilizing the RELAP5 code. The RELAP5 model is shown in Fig. C.1. As seen from this figure, the base model (viz., Model B) represents ten different coolant flow channels. These coolant channels are referred to as pipe volumes using RELAP5 jargon, and are connected between two plena (tdv-001 and tdv-002) at the inlet and outlet of the HFIR core, respectively. In this model, heat structures representing core structures on an averaged basis are also represented and are referred to as hs-001 to hs-999 in Fig. C.1. The overall nomenclature used in Fig. C.1 follows standard RELAP5 component-naming convention and is shown below:

Nomenclature	RELAP5 Component
tdv	time-dependent volume
valve	valve junction
hs	heat structure
pipe	pipe volume
sj	single junction
bv	branch volume
tdj	time-dependent junction

Time-dependent volume 001 represents the fluid volume directly above the core (upper plenum), with fixed fluid thermodynamic state specified via pressure and temperature (subcooled liquid). Valve junctions 102 through 902 inclusive are nine flow paths (HFIR flow channels) of time-varying area representing possible flow blockages. Single junction 004 represents the remainder of the nonblocked flow channel (viz., a bypass flow path). Further details of the naming convention and model development are given in Ref. 22.

Model B was not set up to examine the effects of core flow blockage from a best-estimate standpoint. As a result, details such as specifying axial power profiles, hot spots and hot streaks, and corrosion layer buildup on the fuel plate surface are not modeled.

The primary purpose of this model is to provide a good estimate of overall thermal-hydraulic behavior in blocked flow channels and to determine what level of flow blockage area at the entrance would lead to onset to fuel plate melting. It is also recognized that Model B provides one-dimensional thermal-hydraulic response characteristics only. However, it represents a major improvement over simplistic hand calculations, and does include modeling and resolution of axially varying spatial effects in the flow channels. Important conservatisms built into the model include absence of heat dissipation in fuel plates (axially and radially) from conduction heat transfer, and the absence of possible power reduction in the core region from void-reactivity feedback. Further, important phenomena such as flow and temperature excursions are indeed accounted for.

Transient calculations were conducted in a specified manner. A steady state calculation is performed from 0.0 to 0.25 s. Thereafter, a transient is initiated by changing valve junctions 102 through 902 inclusive from fully open to partially closed over an arbitrarily chosen time period of 0.1 s. The time of 0.1 s rather than 0.0 s was chosen to avoid numerical oscillations and to allow for a stable simulation of the event. After several simulations were performed the results were found to be best summarized by looking at two blockage area cases. The first case, 91% flow blockage, does not cause any melting to occur, whereas melting does occur for the 92% case. Details of pressure, velocity, void fraction, and temperature traces are given in Ref. 22. Here we only show the relevant results for coolant void fraction and heat structure surface temperatures in Figs. C.2 and C.3. As an aside, it should be mentioned that for the 91% case CHF was not observed. CHF was observed for the 92% blockage case ~1.0 s into the simulation. In addition, the coolant velocity in both cases drops to about 2.14 m/s (7 ft/s) from 15.5 m/s (51 ft/s). As seen in Fig. C.2 for the 91% case, the liquid void fraction reduces from 1.0 to a new steady state value of 0.97. However, for the 92% case [Fig. C.2(b)], the liquid void fraction drops to 0.4 (i.e., 60% vapor fraction) at the inception of CHF before

rising again (due to decreased heat transfer to the coolant). Radically different results are also seen for the plate surface temperatures at the core exit section for the two cases. As seen in Fig. C.3, the plate surface temperature for the 91% case remains bounded and well below the melting temperature of aluminum (viz., 660°C), whereas for the 92% case, the fuel plate surface temperature rises to about 660°C about 1.0 s after completion of the flow blockage at the entrance. A simple hand calculation indicates that the rate of temperature rise upon inception of CHF is close to the rise rate under adiabatic conditions. Temperature responses for the right and left faces of the fuel plates in blocked channels are essentially the same for both cases.

Interestingly, the base model (viz., Model B) also allows one to evaluate the effects of flow blockage at the core entrance to varying degrees. To evaluate the effects of complete flow blockage of one flow channel, or to evaluate the effects of completely blocking two flow channels adjacent to a fuel plate, the valve openings at the core entrance were set to zero. The base model with this entrance specification is referred to as Model C. Therefore, Model C is very similar to and is a special case of Model B. The transient calculation using Model C was conducted in the same manner as that for Model B. Two situations were analyzed using Model C. The first situation represents complete blockage of a single channel (via closure of valve in junction 502), whereas, the second situation is a full blockage of three flow channels (via closure of valves in junctions 402, 502, and 602). It was found that a single channel full flow blockage will not lead to fuel melting, because the heat sink available from the adjacent flow channels is sufficient to cool the fuel plates bounding the blocked channel. As may be expected, complete flow blockage of multiple channels did lead to fuel plate melting. This is in relative agreement with results presented earlier with Model B which stated that partial flow blockages of multiple channels of >91% would lead to fuel melting in the affected channels.

C.3 RELAP5 AND OTHER CALCULATIONS FOR ESTIMATION OF DAMAGE PROPAGATION

To evaluate the propensity for core damage propagation, another RELAP5 model (viz., Model D) was set up. This model endeavors to shed some light on the issue of whether a series of melted plates could lead to additional melting of (previously unmelted) adjacent plates. Model D was designed such that a core symmetry plane is created around the "melted box" consisting of a set number of plates that have melted and fused together. A conservative assumption is made such that the heat flux from the melted box to the flow channel adjacent to the next unmelted fuel plate is a multiple of the nominal heat flux. This multiple essentially corresponds to the number of melted plates contained in the "melted box." This calculation will determine at what multiple does the heat transfer condition in the fluid channel adjacent to the next unaffected plates deteriorate enough to cause melting to begin. It is clear that this calculational scheme would tend to provide conservative estimates for damage propagation since no credit is taken for possible steam cooling of melted plates and also for the possibility of melted plates relocating away from the core region. Essentially, the RELAP5 Model D was obtained by expanding Models B and C described earlier. Some of the important modeling changes are given below:

- The heat transfer boundary condition on the left surface of heat structure 001 was changed from convection to/from fluid volume 999 to a user-specified heat flux boundary condition.
- The pipe volume and heat structure 999 are replaced with a tenth pipe volume and heat structure identical to those with ten axial nodes per channel.
- Additional heat structure/pipe volume pairs were appended to the model to facilitate an adiabatic boundary condition on the right side. As mentioned previously, a core symmetry plane is created about the melted box. For the inner fuel element, the

symmetry plane is at 85.5 plates, whereas for the outer element it is at 184.5 plates. Therefore, the number of heat structure/pipe volumes appended to the Model D to ensure an adiabatic boundary about the melted box is 85 and 184 for the inner and outer fuel elements, respectively. In so doing, the actual number of appended heat structure/pipe volume pairs is reduced by the number of melted fuel plates imposed via heat flux on the left-most boundary.

- The heat transfer surface area of each fuel plate is changed to represent the inner or outer element fuel plate surface areas as needed.

Further details of the RELAP5 modeling for Model D are reported in Ref. 22.

A preliminary estimate for the likelihood for damage propagation was made using the "melted box" model (viz., Model D). Note that Model D uses conservative assumptions relating to heat transfer from the so-called "melted box" to the neighboring unmelted fuel plates. Results of the analysis using Model D revealed that up to 9 or 7 fuel plates in the inner or outer fuel element regions, respectively, can melt without causing the neighboring fuel plates to heat up to melting conditions. For any number of plates less than 9 or 7 in the inner and outer fuel elements, sufficient heat transfer is possible around the unmelted plates to prevent temperature rise (all the way to melting conditions). In other words, if a flow blockage occurs that causes melting of ~5 or 2% of the fuel plates in the inner or outer fuel elements, then damage propagation is likely to continue. It is recognized that Model D estimates do not account for several severe accident phenomenological aspects such as onset of fuel blistering, state of the fuel after aluminum melting occurs, eutectic formations, and fluid-structure interactions. Nevertheless, the model does provide an indication of the relative degree of flow blockage area necessary for damage propagation to begin.

Model D using the RELAP5 code would tend to provide an estimate for the approximate amount of initial plate melting necessary in the core regions (i.e., inner or

outer fuel elements). However, these calculations do not provide an estimate of how many plates would melt once propagation does occur, under full-power conditions. For developing insights into this aspect, we go to the simple but conservative model described earlier in this appendix. This model postulates that any plate once melted would slump onto its neighbor. Thereafter, the fused plates would heat up together until the reactor is scrammed. The time limit available for this domino-effect to keep propagating is set as 3 s, based on the transit time for a fluid particle to reach regions where high levels of radiation can be detected, which then initiates a scram signal. This is a highly conservative method for evaluating the degree of melt propagation. The size of a flow blockage will determine how many plates melt simultaneously before propagation occurs. However, in the absence of apriori knowledge of this parameter, it is assumed that, at first, one fuel plate will melt and slump onto its neighbor. Additional details are given in Ref. 33. The analysis of this reference led to the conclusion that only up to 14% or 77 fuel plates would melt in this domino fashion before core-power-level reduction would occur due to scram.

Overall, the extent of damage propagation is difficult to state with confidence, essentially due to the absence of a properly validated and integrated melt progression modeling capability. However, based on the HFIR control system design and previous conservative analyses conducted and reported in ORNL-3573, an upper bound may be set at 24%. That is, up to 24% of the core material may be conservatively assumed to melt and participate in a steam explosion event during core flow blockage accidents in HFIR. Further review comments on the previous HFIR analyses for core melt levels following a flow blockage are provided in Appendix A.

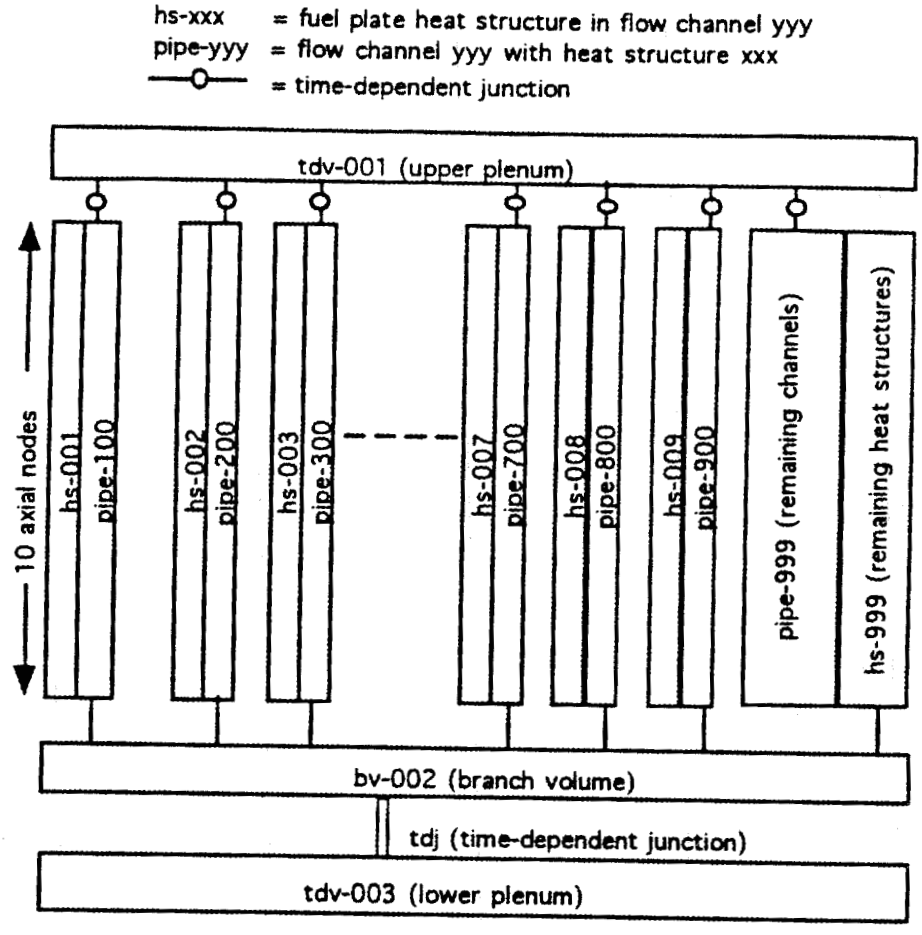

Fig. C.1 Node Map of the HFIR FCI Flow Blockage RELAP5 Model B

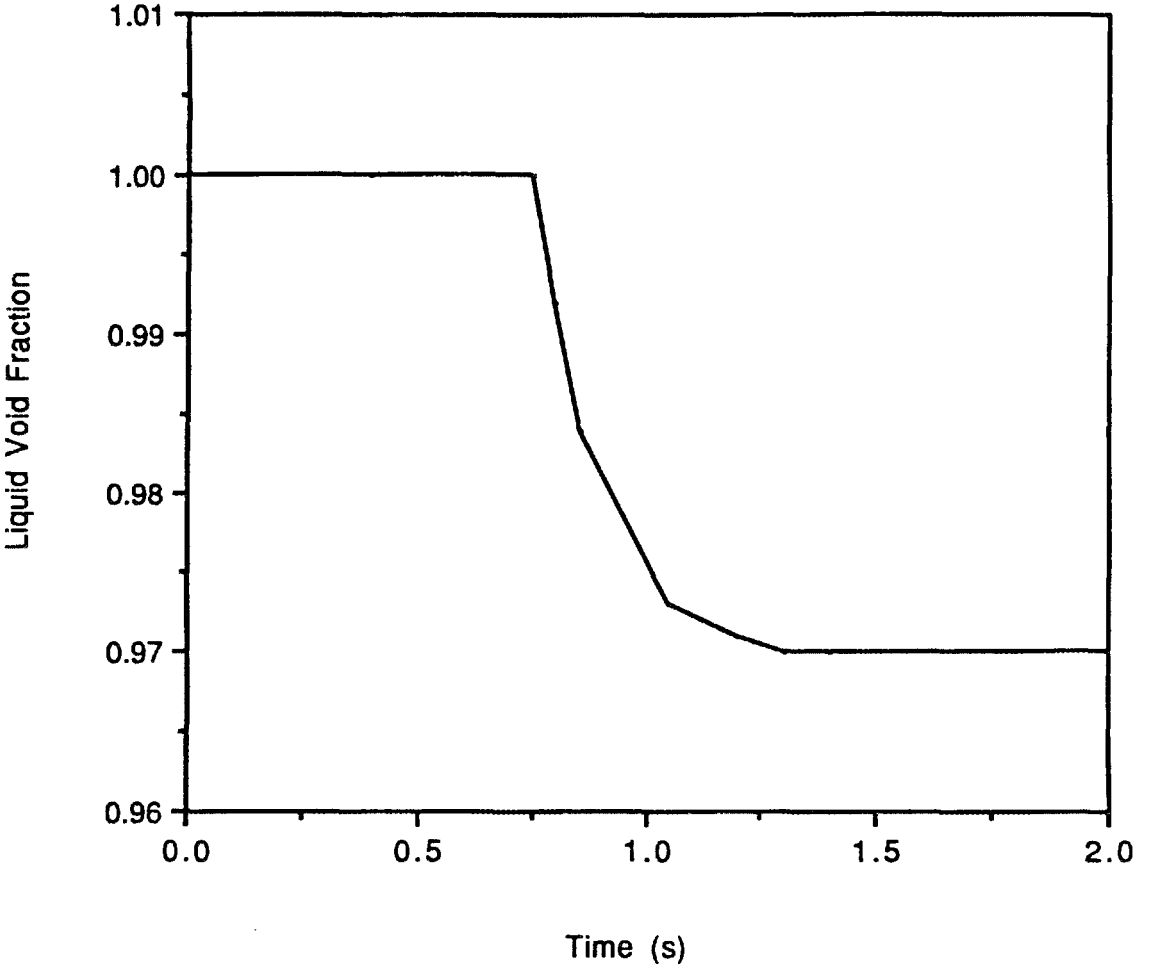

Fig. C.2 Liquid Void Fraction at the Bottom of a Representative Blocked Channel for a 91% Flow Blockage

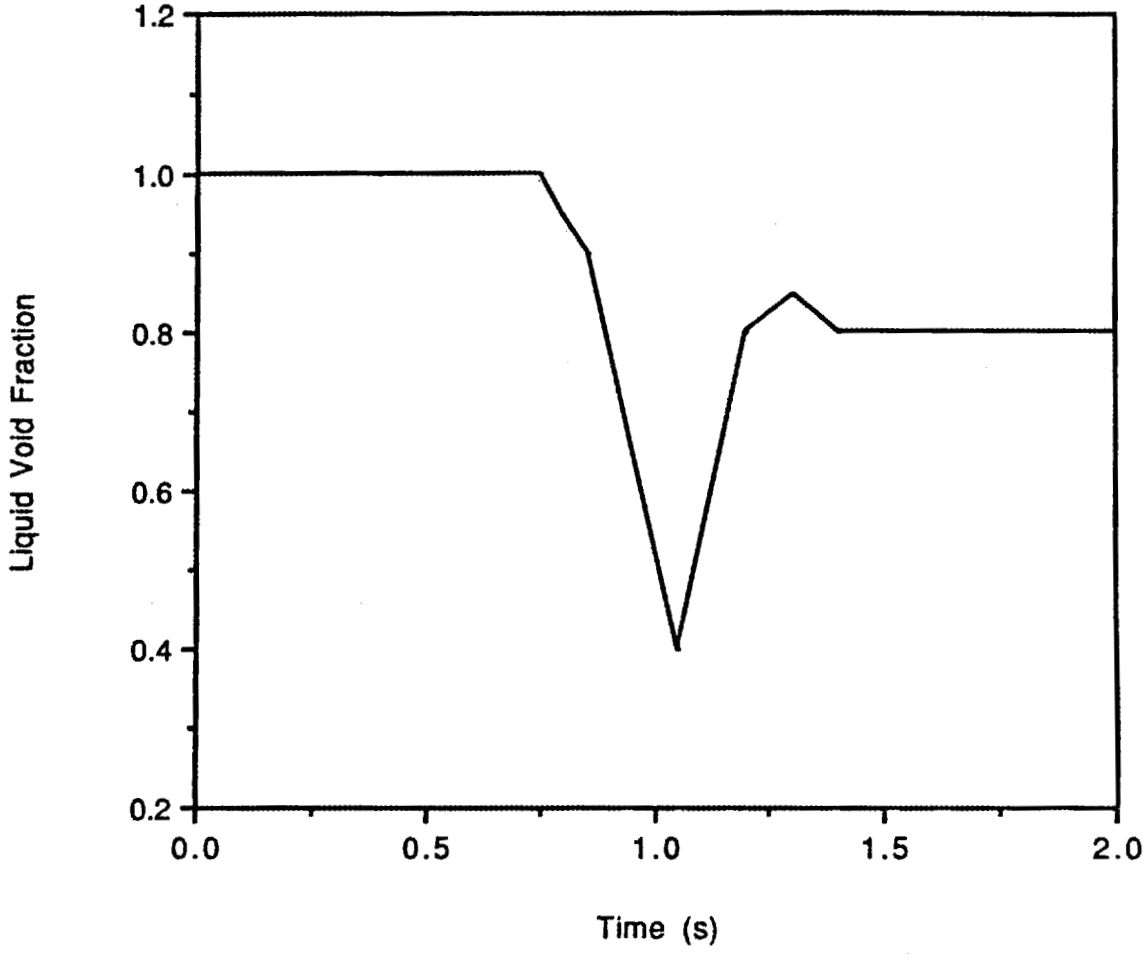

Fig. C.3 Liquid Void Fraction at the Bottom of a Representative Blocked Channel for a 92% Flow Blockage

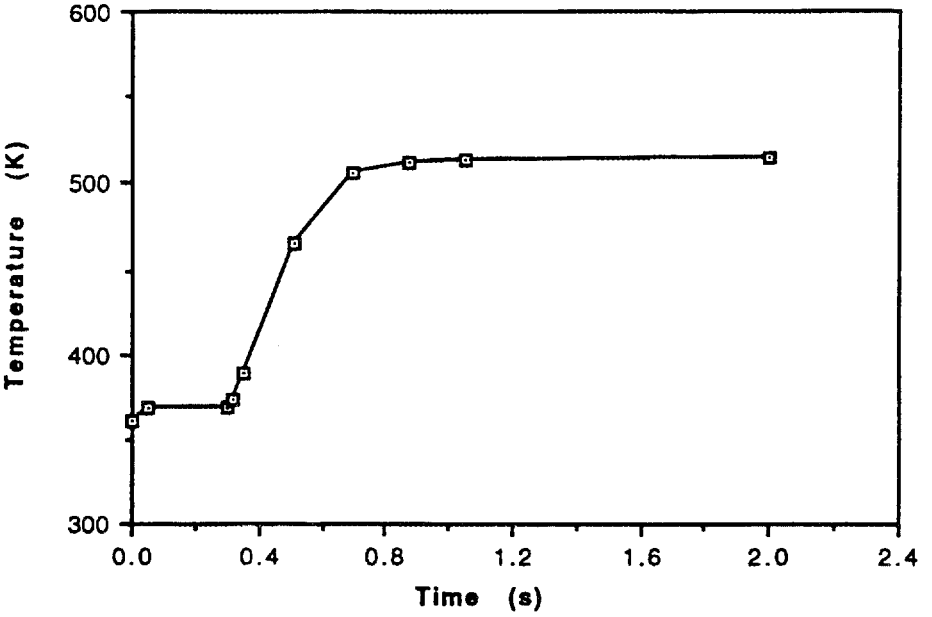

Fig. C.4 Fuel Plate Surface Temperature to the Left and Bottom of a Representative Blocked Channel for a 91% Flow Blockage

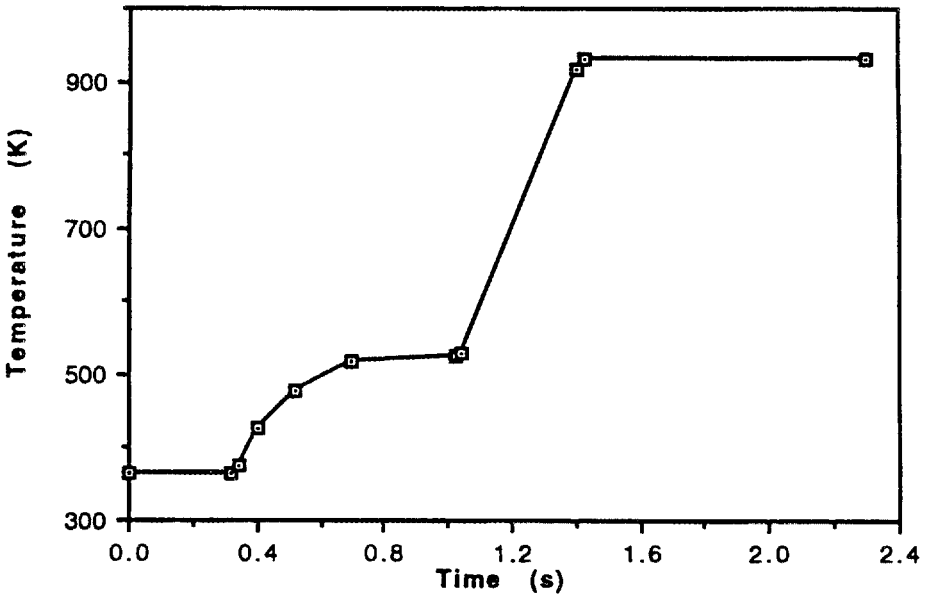

Fig. C.5 Fuel Plate Surface Temperature to the Left and Bottom of a Representative Blocked Channel for a 92% Flow Blockage

APPENDIX D

Modeling and Analysis for Fluid-Structure Interactions in the HFIR Core Region

The work performed to model and analyze fluid-structure interactions in the HFIR core region during postulated steam explosion events generated from flow blockages is summarized in this appendix. Several aspects of the in-core fluid-structure interaction phenomena were studied. Salient aspects are described below:

D.1 PLATE BUCKLING CAUSED BY LARGE COOLANT VELOCITY

As shown in Appendix A, for flow blockage events, it may be possible that the fluid velocity in the rest of the flow channels would increase due to flow starvation in blocked channels. It is well known that beyond a certain so-called "critical velocity (Vc)" the fuel plates are liable to buckle and collapse. A closed-form solution for Vc was derived[32] and is given by the following equation:

$$Vc^2 = (hg/4\alpha)(b/\int yds), \qquad (D.1)$$

where,

y = deflection of the plate relative to the supports,

s = width (i.e., chord) of the plate,

h = initial flow channel thickness (i.e., channel gap),

b = width (i.e., chord) of the involute plate,

g = gravitational acceleration,

α = weight density of the coolant.

To evaluate the integral in Eq. (D.1) the deflection curve for the fuel plate must be obtained. The ADINA code was used for this purpose. Results for critical velocity, using the so-called Miller Analogy[56] in conjunction with the ADINA code results, are shown in Table D.1. Also shown are results of critical velocity obtained by Chapman, which are seen to be larger than the calculated velocities using the Miller Analogy. As noted, the critical buckling velocity is much larger than postulated velocities that can occur as given in Appendix B.

Table D.1 Critical flow velocities for HFIR

Method/method	Element	Critical velocity (m/s)
Miller analogy	Inner	49.8
Miller analogy	Outer	47.1
Chapman*	Inner	77.7
Chapman*	Outer	71.6

D.2 PLATE DEFORMATION FROM STATIC PRESSURE AND TEMPERATURE DIFFERENTIAL LOADS

As mentioned in Sect. 2, the maximum pressure difference across a plate during flow blockage events would amount to about 0.7 MPa (100 psia). Beyond a certain threshold pressure difference, the plates may buckle. A series of buckling analyses were conducted[30] to estimate the buckling loads that will cause collapse of the outer HFIR fuel plates. The loads considered to be most likely to cause the plate to become unstable are a

*Calculations were done and documented in an internal letter from T. G. Chapman to J. R. McWherther, "Critical Velocity for HFIR Fuel Plates," April 24, 1962.

sustained pressure difference loading applied across the complete concave surface of the plates combined with overheating of the plates. First, the estimation of the pressure difference buckling loads was made by using 2-D analysis of a fuel plate without constraint of the side plates, and 3-D shell analysis of the fuel plate without the constraint of the side plates.

These analyses were done by modeling the plates with the ABAQUS and ADINA codes. A 2-D analysis using ADINA gave a buckling pressure difference of 1.6 MPa (235 psia). The 3-D shell analysis was conducted using both codes, which gave buckling loads for the first three buckling modes as,

- Mode 1 buckling pressure = 1.23 MPa (176 psia),
- Mode 2 buckling pressure = 1.24 MPa (177 psia), and
- Mode 2 buckling pressure = 1.28 (183 psia).

As seen from the above results, all of the calculated sustained pressure buckling loads are well above the assumed 0.7 MPa (100 psia) static pressure difference which would occur as a maximum across the plates due to abnormal or blocked flow. The actual pressure difference will vary from 0 to about 0.7 MPa (100 psia). Therefore, based on the critical buckling pressure differences calculated above, it is clear that plate buckling from static pressure differences cannot occur. This rules out another mode for damage propagation.

Thermal buckling loads needed to cause fuel plate collapse were also evaluated. For all three buckling modes, it was evaluated that if the temperature difference from centerline to surface exceeded about 2.9 times the temperature difference during normal operating conditions, fuel plate buckling would be initiated.

D.3 FAILURE ENVELOPES FOR FUEL PLATES

Structural failure envelopes were evaluated for a variety of different boundary conditions and geometrical setups to evaluate the response of fuel plates to dynamic loads. Such dynamic loads may be caused by localized steam explosions or, to a lesser degree, water-hammer loads. Failure envelopes were developed for the fuel plate subjected to triangular pulses caused by steam explosions on the entire surface using a 2-D model, or selectively as a pressure strip or a patch using a 3-D model. From a conservative standpoint, the outer fuel plate was chosen because this plate is more flexible than the inner fuel plate. The increased flexibility results from the longer span between the side plates for the outer fuel plates.

The analysis to develop the failure envelope was based on an elastic-plastic dynamic solution of a 2-D model of the outer HFIR fuel element. The fuel plate was assumed to be an elastic perfectly plastic aluminum material operating at 165°C. Four 2-D analyses were done for different conditions as follows:

1. single plate with no determination of accounting for fluid inertia or inertia of side plates;
2. two plates with a coolant gap in between, with no accounting for inertia of side plates;
3. three plates with the coolant gaps between them, with no accounting for inertia of side plates; and
4. two plates, three coolant gaps, and side walls to model the complete outer fuel core plates.

Failure envelopes for the four cases mentioned above were obtained using ADINA and are shown in Figs. D.1 and D.2. In each case the pressure pulse acted on the concave face of the fuel element. Adding plates and coolant causes inertia to increase the

maximum pressure at which the fuel plate fails by becomes plastic throughout its thickness (Fig. D.2) and fails. Figure D.2 also shows that by increasing inertia in the response system analysis the required pressure pulse increases quite dramatically if the pulse width is small enough.

Another 2-D confirmatory analysis was done with more elements in the span direction to check for convergence. In addition to the 2-D analyses discussed above, two 3-D analyses were also conducted to ensure that the 2-D analyses were giving reasonable failure envelopes. These were:

1. 3-D model of an outer fuel plate where the pulse was applied to a strip that covered the span of the plate and was 68 mm (2.67 in.) wide in the axial direction, and
2. 3-D model of an outer fuel plate where the pulse was applied to a patch which had dimensions of 25.4 mm (1.0 in.) in the span direction and 68 mm (2.67 in.) in the axial direction.

Results of the additional 2-D analyses and the two 3-D analyses are shown in Fig. D.3. As seen from Fig. D.3, the results show that the single plate, the single plate with more elements, and the 3-D plate with a pressure strip across the span give essentially the same results. Only the 3-D plate model with a pressure patch in the center of the plate gives a somewhat higher failure envelope.

All in all, dynamic structural analyses indicate that for steam explosions with pressure pulses in the millisecond duration range, plate failure will occur if the steam explosion pressure magnitude is above about 1.75 MPa (250 psi).

Further details on the modeling and analyses covered in this appendix are reported in Refs. 23 through 32.

Table D.1 Critical flow velocities for HFIR

Method/method	Element	Critical velocity (m/s)
Miller analogy	Inner	49.8
Miller analogy	Outer	47.1
Chapman*	Inner	77.7
Chapman*	Outer	71.6

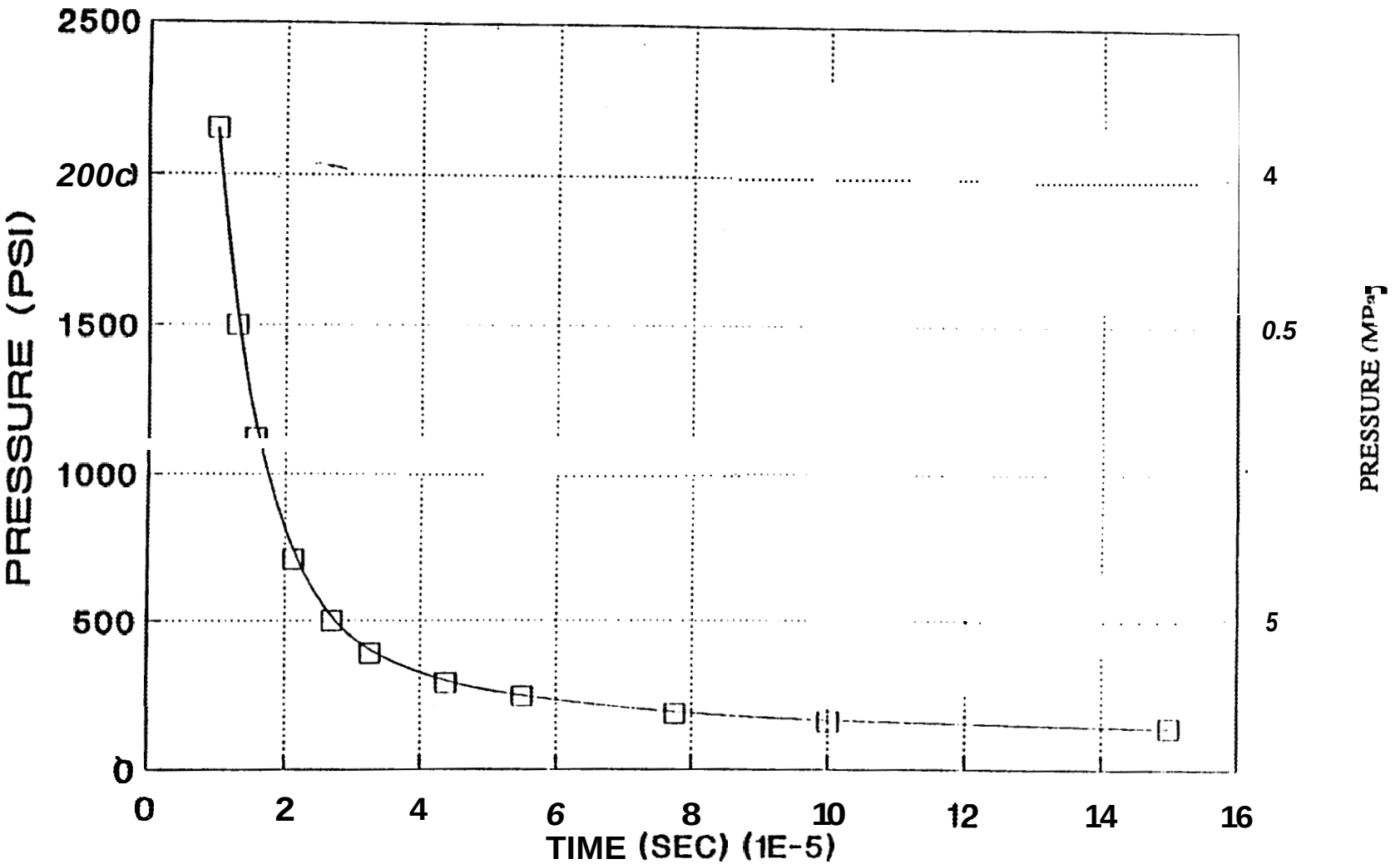

Fig. D.1 Failure Envelope for a Single Outer HFIR Fuel Plate (2D Model Results)

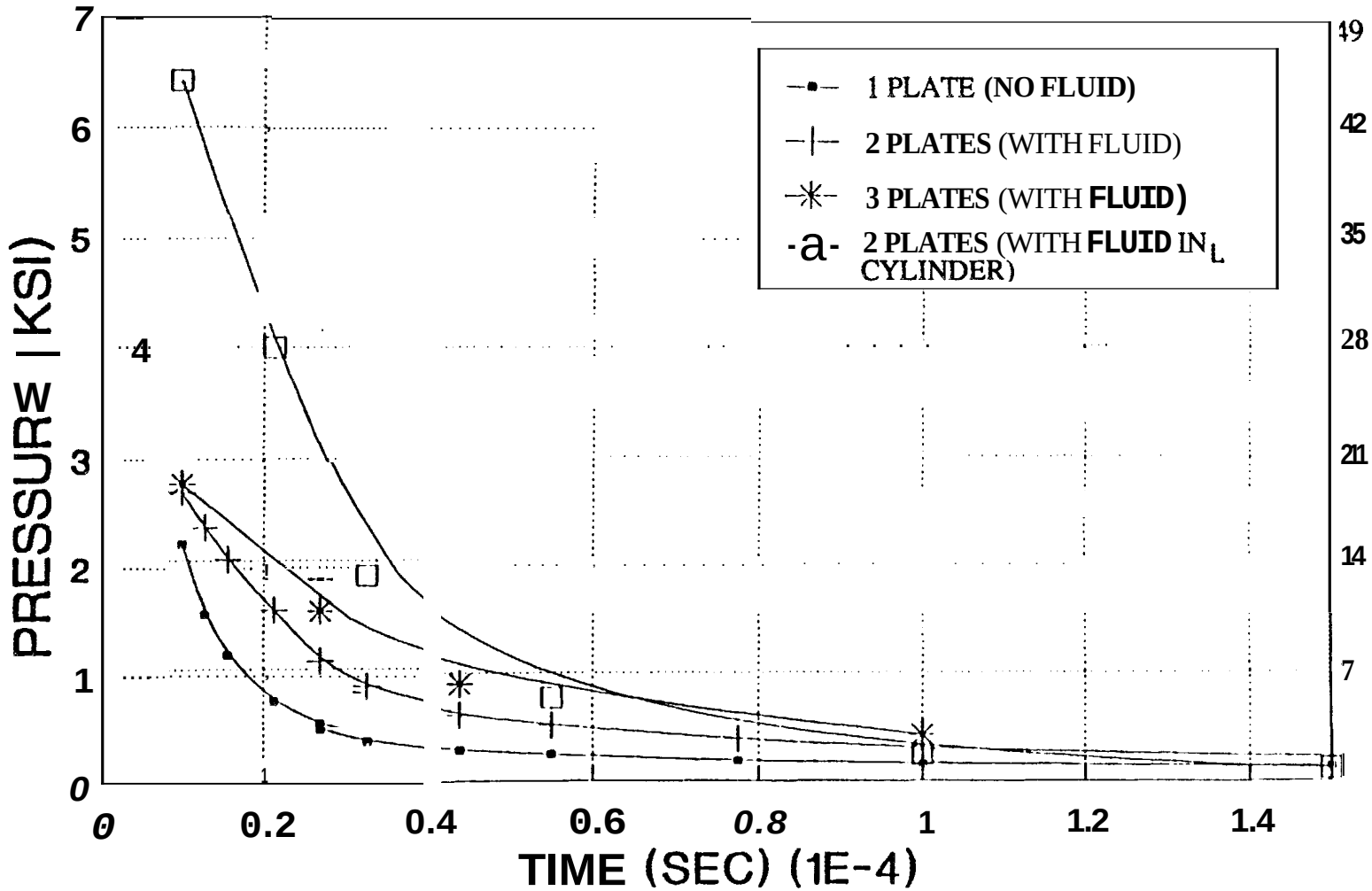

Fig. D.2 Failure Envelopes for Single and Multiple HFIR Fuel Plates (28 Model Results)

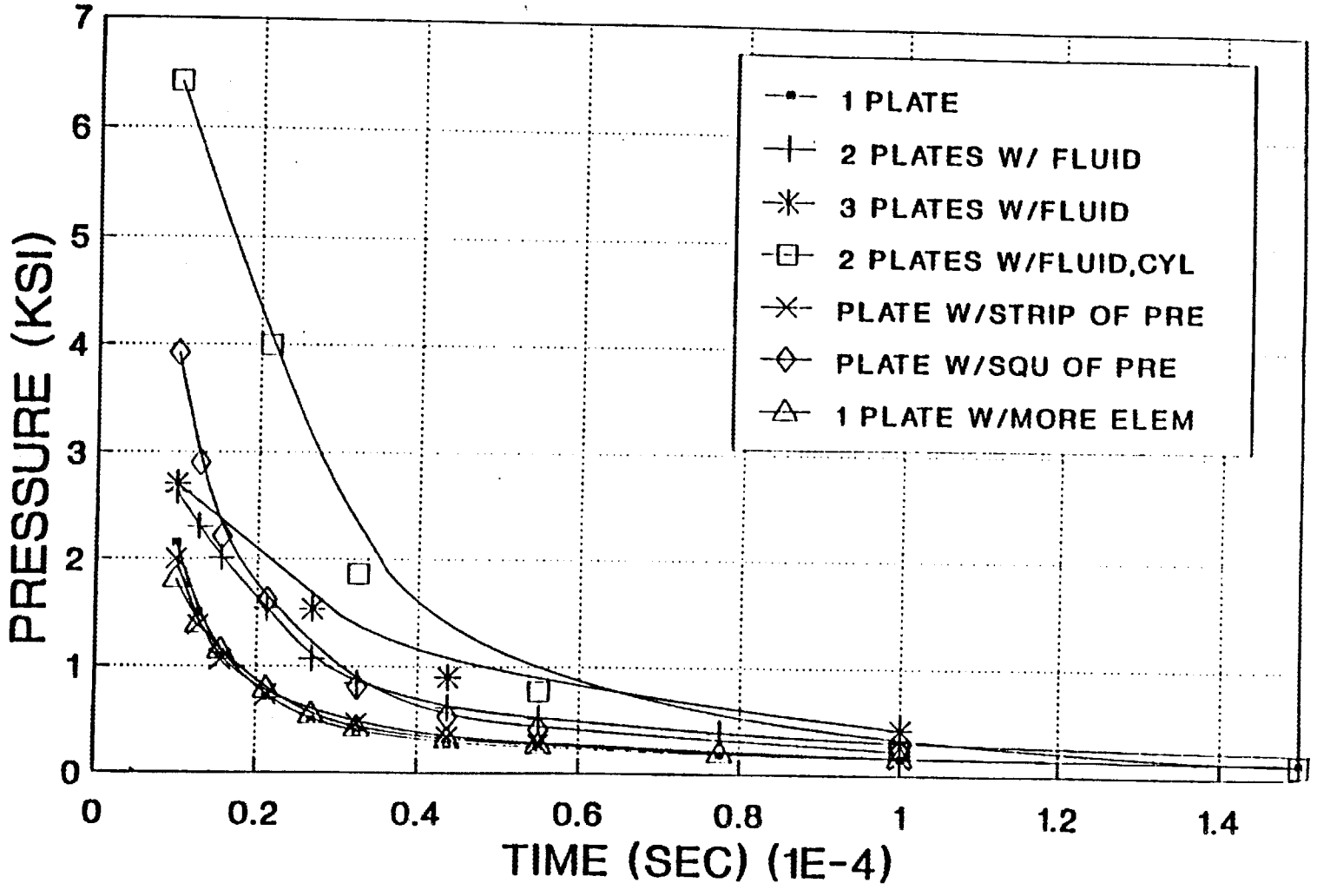

Fig. D.3 Failure Envelopes for Single and Multiple HFIR Fuel Plates (2D & 3D Model Results)

APPENDIX E

HFIR Debris Coolability Calculations for FCI Analysis in the Shield Plug Region

Occurrence of steam explosions in the core region is considered to be somewhat stochastic in nature (albeit primarily due to a lack of sufficient understanding of the physics involved). Under some circumstances, the HFIR core material may melt and then relocate onto the steel shield plug in the HFIR pressure vessel. The core debris could then heat up, melt, and undergo a steam explosion. It is thus important to evaluate the possibility of debris coolability and the extent of melt superheat that is possible. These characteristics would then feed directly into calculations for fuel-coolant-interaction (FCI) energetics. This appendix summarizes the work performed to model and analyze HFIR debris coolability if the core material relocates onto the lower shield plug region.

The principal tool used for determining debris coolability characteristics was the 2DKO computer code,[11] in conjunction with some ancillary analysis using MELCOR.[7] The 2DKO computer code is a program for analysis of two-dimensional (2-D) melting and/or freezing in two-material structures. The model used in 2DKO accounts for 2-D phenomena related to simultaneous heat transfer and phase change (melting/freezing) between hot liquids and relatively cold solids. Various applications of the mathematical model include the melting of a solid structure when in contact with a continuously delivered liquid, melting of a solid plate subjected to an impinging jet of hot liquid, and melting of a vertical wall in contact with a liquid pool. The physical boundary volume problem solved for by 2DKO is depicted in Fig. E.1 (in cartesian coordinates). As shown therein, the user can specify boundary conditions on all four sides for conducting a 2-D calculation.

The 2DKO model has been validated against experimental data and showed good agreement. This code was considered useful for the current analysis since it allows transient deposition of hot corium onto the upper shield plug. Note that the model also

allows for analyzing the case where the debris bed on the shield plug is fixed. Aspects dealing with porting of the code and quality assurance have been documented[40] and are not repeated here. Other aspects dealing with problem formulation, etc., are described subsequently.

E.1 PROBLEM FORMULATION FOR FCI ANALYSIS ON UPPER SHIELD PLUG REGION

As mentioned previously, fuel melting in the core region may not result in steam explosions. The core debris would then most likely relocate onto the lower regions of the HFIR pressure vessel. Without a mechanistic model for evaluating core melt progression to evaluate effects of dispersion and candling, it is assumed that the core debris would relocate coherently (in various amounts) onto the upper shield plug and spread uniformly over the entire cross-sectional area. This relocation in reality would have to occur over a period of time. But once again, without a mechanistic modeling capability, evaluation of debris coolability was divided into two modes. In the first mode, the HFIR core debris of a specified amount is supposed to form a debris bed on the shield plug of a fixed height instantly. For the second mode of calculations, we assume that the core debris would relocate onto the shield plug over a time of 10 s (which constitutes an unverified assumption). Further, the calculations are conducted with varying amounts of decay power generation in the debris to simulate the result of volatile fission product release from the heated fuel mixture.

E.2 MODELING AND ASSUMPTIONS

The 2DKO code model was also compared against the results of a 1-D heat transfer model developed using the CVH and HS modules of the MELCOR code. A MELCOR model was also developed to evaluate appropriately reasonable values for the

fuel

debris-to-reactor pool water, and shield plug-to-water convective heat transfer coefficients. MELCOR's HS module was employed to simulate the two-slab geometry, and the specific heat capacities of the debris and shield plug materials were modified to account for the effects of melting and freezing. That is, the specific heat capacity of each slab material is increased by an amount equal to the latent heat of fusion divided by a temperature range equal to 5 K centered around the material melting temperature. The range of 5 K was chosen as a reasonable range for MELCOR calculations. This was necessary because MELCOR heat structures are not allowed to melt or ablate. The MELCOR system representation included the aspects dealing with pressure relief from the reactor vessel to the reactor pool. That is, if the reactor vessel pressure exceeds 5.35 MPa (778 psi) a relief valve is assumed to open up (instantly) and allow pressure relief to the large reactor pool. The overall model is shown in Fig. E.3. Additional details are given in Ref. 44.

The nodalization process and the respective models are shown in Figs. E.2 and E.3. As seen in Fig. E.2, the surface control volumes modeled the HFIR reactor vessel volume and the water cavity below the shield plug region. For MELCOR calculations, the additional (i.e., lower) shield plug below the shield plug in contact with the core debris was included (to take into account possible radiative losses if the shield plug temperature becomes high enough). For the MELCOR model, the water in the two adjacent control volumes receive heat via convection and radiation. For the 2DKO model, the surface heat transfer is governed by a user-specified overall heat transfer coefficient and the ambient temperature (which is also to be user-specified). The MELCOR model provided a basis for setting up these input requirements for 2DKO calculations.

The basic assumptions for debris-plug interaction analyses are as follows:

- Multidimensional thermal-hydraulic effects are negligible.
- Core debris spreads uniformly and instantaneously over the upper shield plug.
- Transient variations in fission product or aerosol release are negligible, and the debris power level is governed only by the user-specified decay power variation as a function of time.
- Eutectic formations and their effects on melting/freezing are negligible.
- Upper shield plug structural integrity is not compromised such that the plug collapses or opens a pathway by which the fuel debris can escape.
- Aluminum in the core debris does not undergo oxidation or ignition. That is, no violent churning or additional energy source is available, and the debris thermal characteristics are driven from decay of fission products alone (as simulated via user-specified decay energy source vs time).
- The core debris mass is constituted of 100 kg of aluminum into which decay heat is generated and distributed uniformly. That is, no fuel material stratification will occur.

As a practical note, it should be recognized that all of the above assumptions were made to allow for the development of a reasonable modeling framework in the absence of a mechanistic core melt progression capability, and to obtain order of magnitude or "ball-park" estimates of debris temperatures. Some of the above assumptions are clearly unrealistic. For example, at temperatures above 660°C we know that volatile fission products will get released over a period of time. But to capture such releases in an integrated fashion is not possible in a relatively crude study such as this. The same can be said for the assumptions relating to eutectic formation and for aluminum oxidation/ignition (at high temperatures) which can generate very high sources of energy.

The effect of assuming no transient fission product release with increasing temperatures is clearly to predict higher temperatures. But the effect can be bounded by conducting calculations that assume all of the volatile fission products are released and by

specifying that the thermal energy levels in the debris are a certain fraction of the full value. This aspect is considered during the development of an appropriate test matrix. The impact of neglecting eutectic formation is not clear, except to note that such effects can cause a loss in structural integrity. The impact of neglecting aluminum ignition is clearly to vastly underestimate temperatures. But ignition can begin provided the aluminum temperature reaches high levels (viz., >1100K). The effect of neglecting the U_3O_8 fuel and assuming that all of the debris is aluminum can be expected to be small because the overall volume fraction of the fuel is quite small (<5%) in the total core. The results displayed later should be viewed in light of all of these assumptions, some of which can lead to conservative predictions for debris temperature and others that would tend to result in nonconservative predictions. However, where temperatures in excess of about 1100°K are indicated, the possibility of aluminum ignition cannot be overlooked.

E.3 TEST MATRIX DEVELOPMENT

The test matrix of runs made with MELCOR and 2DKO is shown in Table E.1. Input parameters used in setting up the MELCOR and 2DKO models, their values, and sources of information are given in Table E.2. Case 1 was a rudimentary effort to compare results from MELCOR and 2DKO codes. This comparison exercise was deemed useful to judge the overall response behavior predicted from use of the two codes, and to make sure that no gross variations are displayed (which would then seem to indicate significant modeling error). Boundary conditions are set up as being adiabatic for this sample comparison calculation which simulates the thermal response of molten superheated aluminum debris (with no decay power generation) on a cold HFIR shield plug. In Table E.1, the debris height of 0.073 m corresponds to the height of the debris bed equivalent to the whole core (100 kg of aluminum) relocating to the shield plug with no

porosity. Thereafter, variations in this height essentially constitute evaluations for different amounts of the core material relocation.

The debris decay power level was also parametrically varied to account for reduced core material inventory relocating to the shield plug (e.g., Case 3) and for situations where debris power reduction occurs because of loss of volatile fission products (e.g., Case 6).

Specification of the debris surface-to-pool water heat transfer coefficient for the base case (i.e., Case 2) was estimated as being close to 3000 W/m^2-K based on MELCOR predictions of Fig. E.6. From the same MELCOR run, the shield plug-to-water (in the shield plug cavity) convective heat transfer coefficient was estimated in the vicinity of 250 W/m^2-K. The value of 3000 W/m^2-K for the debris surface does not include the effect of the radiative heat transfer component, which can be estimated as being equal to several hundred W/m^2-K based on the temperature differences observed between the debris surface and the pool water. Hence, parametric 2DKO evaluations were made with this value increased to 4000 W/m^2-K (i.e., Cases 4 and 5). Additionally, runs are also made with 2DKO with the assumption (unverified) that the core debris relocating onto the shield plug would do so over a period of 10 s (i.e., Cases 8, 9, and 10).

E.4 COMPARISON OF MELCOR VERSUS 2DKO PREDICTIONS FOR CASE 1

Results of comparisons between MELCOR and 2DKO temperature predictions are shown graphically in Fig. E.4. As can be seen in Fig. E.4, the two models give results that are in reasonable agreement with one another after the first minute of transient time. It should be recognized that in 2DKO the material property values, such as density and heat capacity, are held constant over the entire temperature range whereas in MELCOR they are variable. Again, as mentioned previously, in MELCOR the process of melting is simulated by artificially increasing the specific heat capacity over a small temperature range, whereas melting is specifically accounted for in 2DKO. Considering these basic differences, it can be seen that good overall agreement is obtained.

E.5 RESULTS OF MELCOR AND 2DKO EVALUATIONS FOR VARIOUS CASES IN TEST MATRIX

The results of MELCOR calculations for control volume pressures, node temperatures and heat transfer coefficients are displayed in Figs. E.5 and E.6 for Case 2. As seen from Fig. E.5, reactor vessel pressure rises sharply during the initial stages of heatup of water (from radiative and convective heat transfer). Vessel pressure relief is rapid, once the pressure level reaches and exceeds 5.35 MPa. Thereafter, liquid mass flow to the large reactor pool occurs and pressures in the various control volumes stabilize.

Figure E.5 indicates that debris temperature (at various locations) rises sharply due to the large decay power density. As shown in Fig. E.6, the debris-to-pool convective heat transfer coefficient is close to 3000 W/m^2-K. The shield plug-to-water convective heat transfer coefficient is quite a bit lower at about 250 W/m^2-K.

Results of 2DKO calculations for Cases 2 through 10 are displayed in Figs. E.7 through E.15. In addition to temperature variation, we also show the variation in debris freezing and plug material melting.

Debris-to-pool heat transfer under severe accident conditions is a complex thermal-hydraulic phenomenon. We have modeled the heat transfer process as being one of direct metal-to-water convective heat transfer. In reality, fission product release will also occur simultaneously in the form of aerosols, noncondensible gases, and vapors. Such a process may lead to a lowering of the heat transfer coefficient between the debris and pool water. For this reason, and for completeness, 2DKO calculations were also completed with the debris-to-pool heat transfer coefficient at a reduced level of 2000 W/m^2-K. Selected results of these calculations showing temperature and melting/freezing histories as a function of time are included in Figs. E.7 through E.15. Note that these cases are identified in the figure captions where the debris-to-pool heat

transfer coefficient (hd) value is stated. As can be seen from the plots generated with hd = 2000 W/m^2-K, significant variations can be obtained in the amount of temperature excursion, as well as for the amounts of debris mass frozen or plug mass that has melted, when compared to corresponding results obtained with hd = 3000 W/m^2-K. For the sake of conservatism, it is recommended that we use results obtained with hd = 2000 W/m^2-K.

Results of runs for Cases 2 to 10 are also summarized in Table E.3. As seen in Table E.3, the maximum debris temperature for Case 2 can get close to 1660°C, or even 2065°C depending on the surface heat transfer conditions. However, this is true only in the extreme case where all of the core debris has relocated instantly and none of the volatile fission products leave the debris bed. Under similar conditions with the exception that only half of the core relocates down to the shield plug region, the maximum debris temperature reached is significantly lower (by about 45%) as seen for Case 3. If the surface heat transfer coefficient is higher than thought (i.e., 4000 W/m^2-K instead of 3000 or 2000 W/m^2-K), the corresponding maximum debris temperatures are lowered to 1452 and 794°C, respectively, as seen for Cases 3 and 4. Cases 3 and 4 are the same as Cases 2 and 3, with the exception of the debris-to-reactor pool heat transfer coefficient.

Starting with Case 2 again, if we now look for the effect of debris power reduction from complete loss of volatile fission products, we see from Case 6 that the reduction in maximum temperature is similar to that for Case 3 (where only half the core debris had relocated). If only half of the core debris relocates and all of the volatile fission products are released to the reactor pool, no debris heatup is obtained as seen for Case 7. That is, enough heat transfer capacity is available to prevent debris bed superheating beyond melting. Cases 8 through 10 are the same as Cases 2, 3, and 6, with the exception that the core debris is allowed to relocate onto the upper shield plug over 10 s instead of instantly. The results for maximum temperature rise indicate that the increased time span over which debris relocation occurs does have a beneficial effect.

That is, the maximum temperature rise is lower for the case where the debris relocates over a given time period instead of relocating instantly. The amount of temperature lowering is small for the situations being analyzed. Because of the absence of a core melt progression capability, it is difficult to state with confidence what level of temperature lowering one might see in reality. Therefore, for evaluating FCI loads, it is recommended that the results obtained, assuming instant relocation onto the upper shield plug, be used.

Further details involving time histories of the key variables (viz., temperatures and melting/freezing fractions) are given in Refs. 40 and 44.

Table E.1 Test Matrix of Debris Heatup / Coolability Calculations

Case	Code	Debris Ht. (m)	Initial Debris Power Level (Mw and %)	Debris-Pool Ht. Transf. Coeff. (W/m2-K)	Plug-Air Ht. Transf.Coeff. (W/m2-K)	Comments
1	MELCOR/2DKO	0.073	0.0 / 0.0	0	0	Benchmark Calculations
2	MELCOR/2DKO	0.073	85 / 100	2000	2	All Core Debris Relocated on Shield Plug; No Fission Product Escape - Nominal Case
3	2DKO	0.037	42.5 / 100	2000	2	Same as Case 2 but only half of core debris on Shield Plug
4	2DKO	0.073	85 / 100	4000	2	Same as Case 2 but with enhanced heat transfer
5	2DKO	0.037	42.5 / 100	4000	2	Same as Case 3 but with enhanced heat transfer
6	2DKO	0.073	42.5 / 50	2000	2	Same as Case 2 but with 50% of decay power (simulates volatile fission product escape)
7	2DKO	0.037	21.25 / 50	2000	2	Same as Case 3 but with 50% of decay power (simulates volatile fission product escape)
8	2DKO	0.073	85 / 100	2000	2	Same as case 2 but assuming a falling core debris over 10 s.
9	2DKO	0.037	42.5 / 100	2000	2	Same as Case 3 but assuming a falling core debris over 10 s.
10	2DKO	0.073	42.5 / 50	2000	2	Same as Case 6 but assuming a falling core debris over 10 s.

Table E.2. Key values for geometry and boundary conditions

Parameter	Value	Source/reasoning
HFIR vessel volume (m^3)	20.00	Approximate value from ORNL-3572[a]
Initial pressure in HFIR Vessel (MPa)	3.30	Nominal HFIR operating pressure
Coolant temperature (K)	343.00	Core average coolant temperature from ORNL-3572
Shield plug length (m)	0.48	Estimated from ORNL-3572
Shield plug diameter (m)	0.8	Estimated from ORNL-3572
Shield plug area (m^2)	0.49	3.14*0.8*0.8/4
Whole core debris height on shield plug (m)	0.07	core mass/Al density/shield plug area
Initial debris temp. (K)	933.00	Aluminum melting temperature
Initial plug temp. (K)	303.00	Set at coolant ambient temperature
Shield plug cavity volume (m^3)	0.50	Estimated from ORNL-3572

[a]Include Ref. 53 here.

Table E.3 Results of Debris Heatup / Coolability Calculatio

Case	Debris Ht. (m)	Initial Debris Power Level (Mw and %)	Debris-Pool Ht. Transf. Coeff. (W/m2-K)	Maximum Debris Temperature (K)	Plug Mass Melted (%)	Comments
2	0.073	85 / 100	3000	1660	2.10	Maximum temperature reached in 500 s; No debris freezing.
			2000	2065	10.30	Maximum temperature reached in 500 s; No debris freezing.
3	0.037	42.5 / 100	3000	912	0	Maximum debris temperature reached in 100 s; Complete debris freezing in 1000 s.
			2000	1080	0	Maximum debris temperature reached in 100 s; Complete debris freezing in 4670 s.
4	0.073	85 / 100	4000	1452	2.10	Maximum debris temperature reached in 100 s; No debris freezing
5	0.037	42.5 / 100	4000	794	0 0	Maximum debris temperature reached in 100 s; Complete debris freezing in 622 s.
6	0.073	42.5 / 50	3000	890	0	Maximum debris temperature reached in 100 s; Complete debris freezing in 2772 s.
			2000	1085	0	Maximum debris temperature reached in 500 s; 32% of debris freezes in 5000 s.
7	0.037	21.25 / 50	3000	660	0	Debris freezes continuously; Complete debris freezing within 100 s.
			2000	660	0	Debris freezes continuously; Complete debris freezing within 297 s.
8	0.073	85 / 100	3000	1638	2.10	Characteristics similar as for Case 2.
			2000	2050	9.80	Characteristics similar as for Case 2.
9	0.037	42.5 / 100	3000	733	0	Characteristics similar as for Case 3.
			2000	1042	0	Characteristics similar as for Case 3.
10	0.073	42.5 / 50	3000	861	0	Characteristics similar as for Case 4.
			2000	1077	0	Characteristics similar as for Case 4.

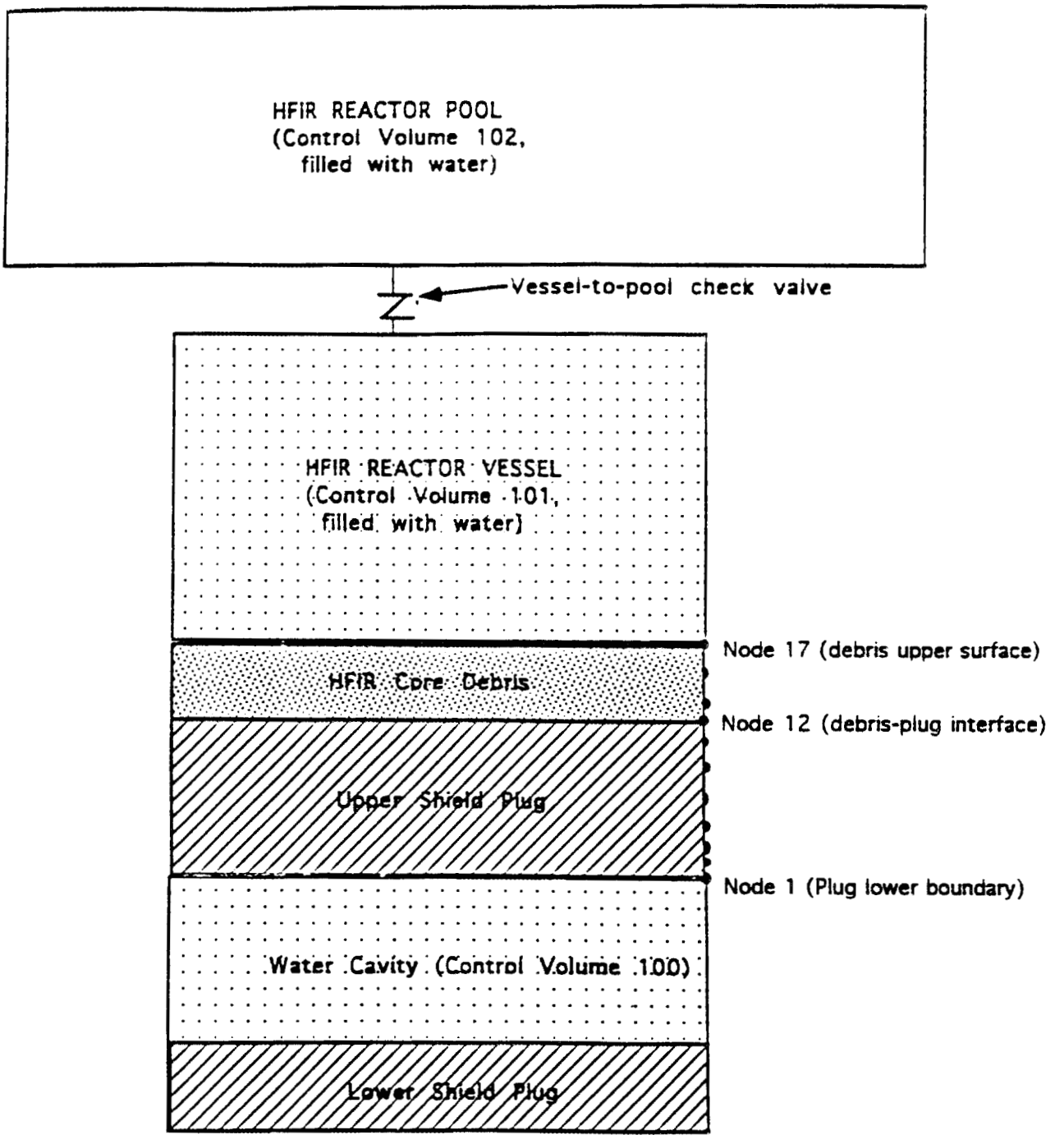

Notes:
1) At debris and shield plug interfaces with adjacent atmospheres, heat transfer is due to convection and radiation

Fig E.1 MELCOR Model for Debris-Shield Plug Interaction Verification Calculations

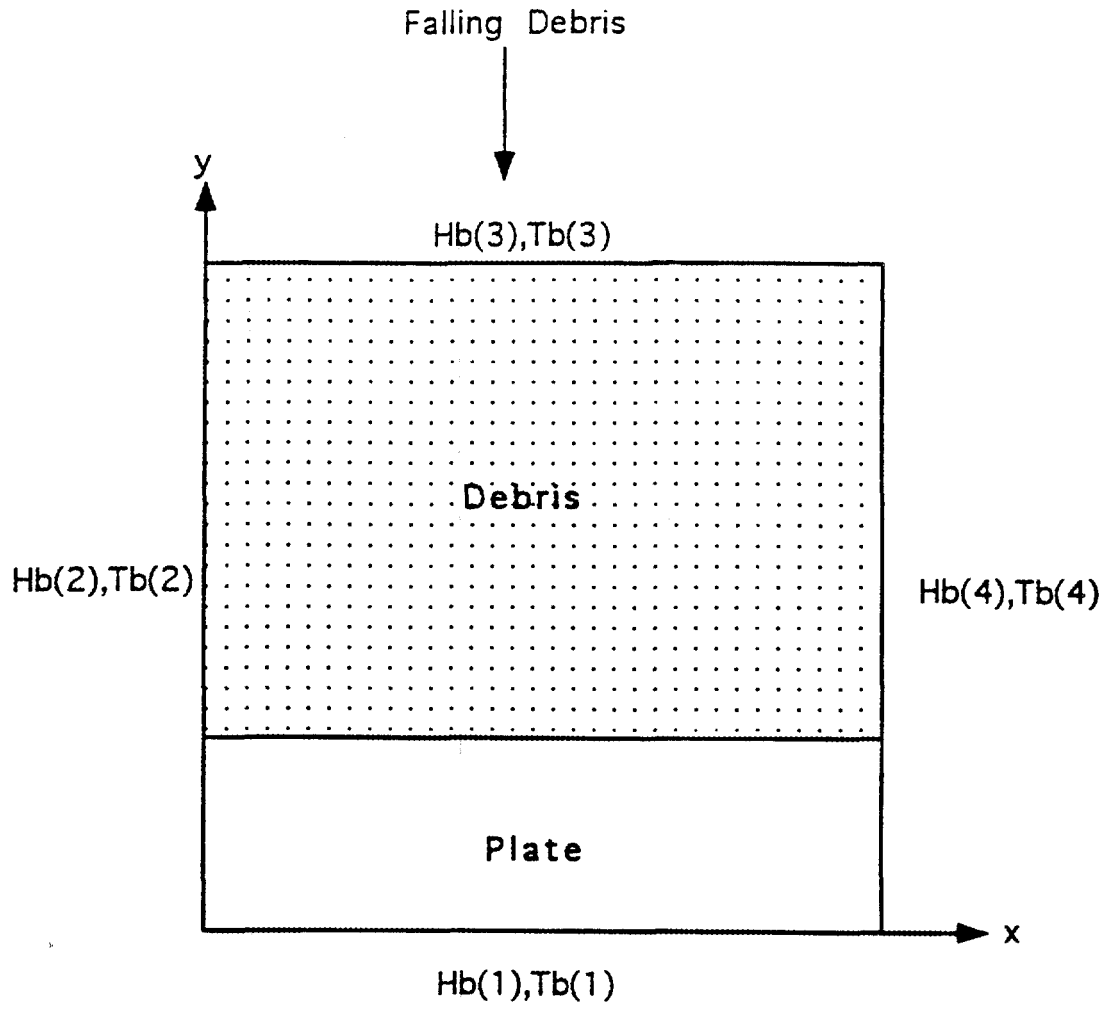

Notes:

1) Hb(i), Tb(i) - Surface Heat Transfer Coefficient & Temperature at Boundary i
2) Ta(i) - Ambient Temperature around Boundary i

Fig. E.2 2DKO Model for Debris-Plate Interaction Analysis

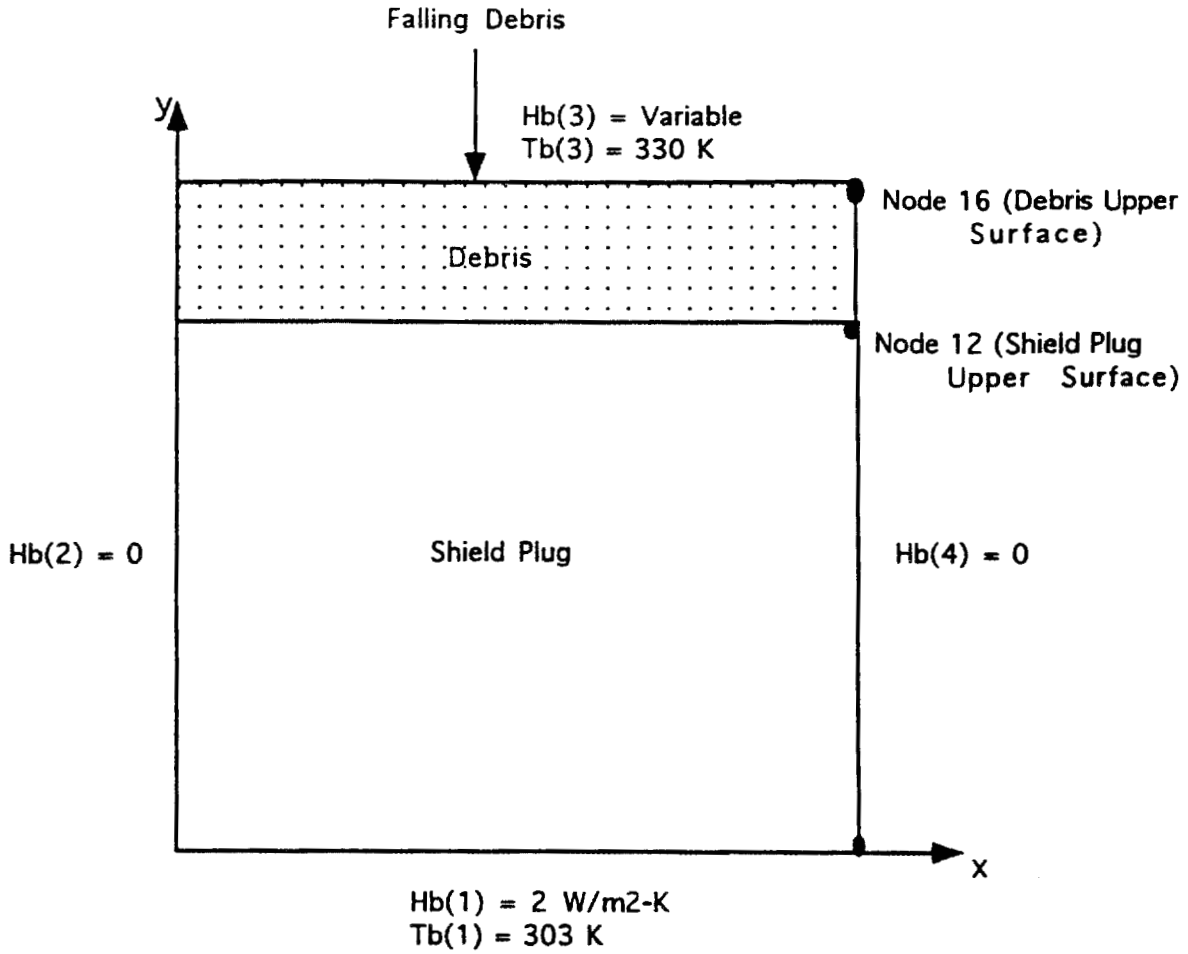

Notes:
1) Hb(i), Tb(i) - Surface Heat Transfer Coefficient & Temperature at Boundary i
2) Ta(i) - Ambient Temperature around Boundary i

Fig. E.3 2DKO Model for Debris-Plug Interaction Analysis

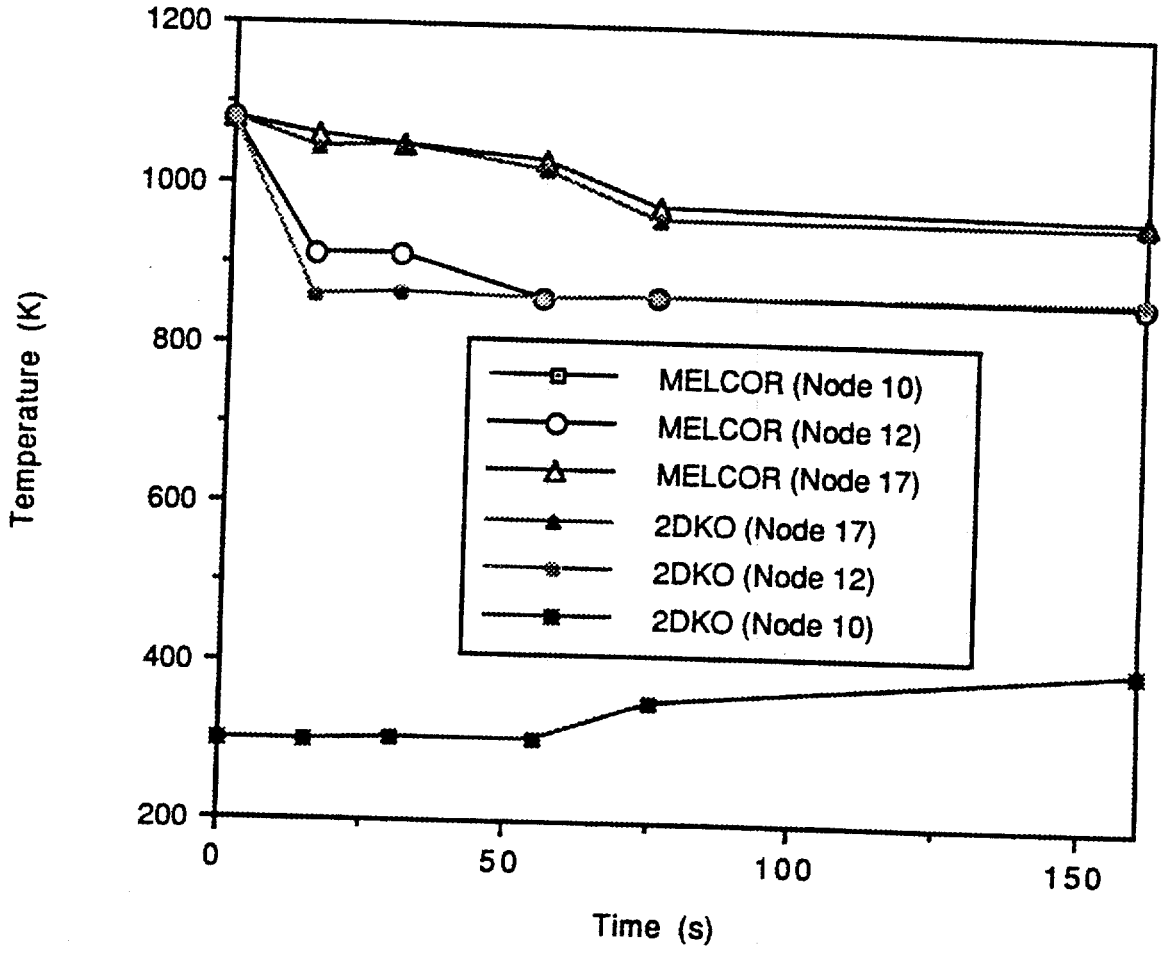

Fig. E.4 Comparison of Predictions by MELCOR and 2DKO

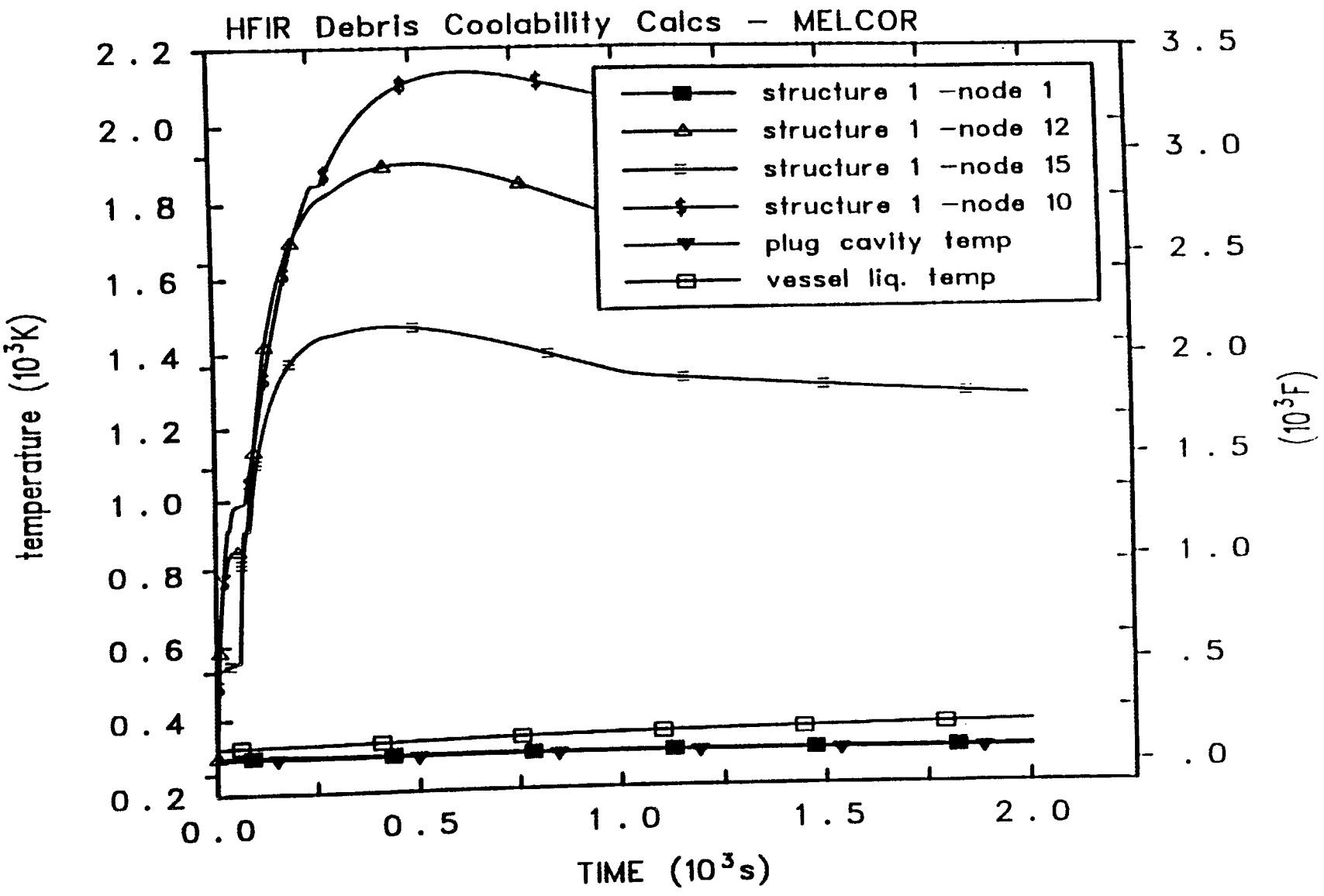

Fig. E.5 Variation of Debris and Plug Temperature vs Time (MELCOR Results for Case 2)

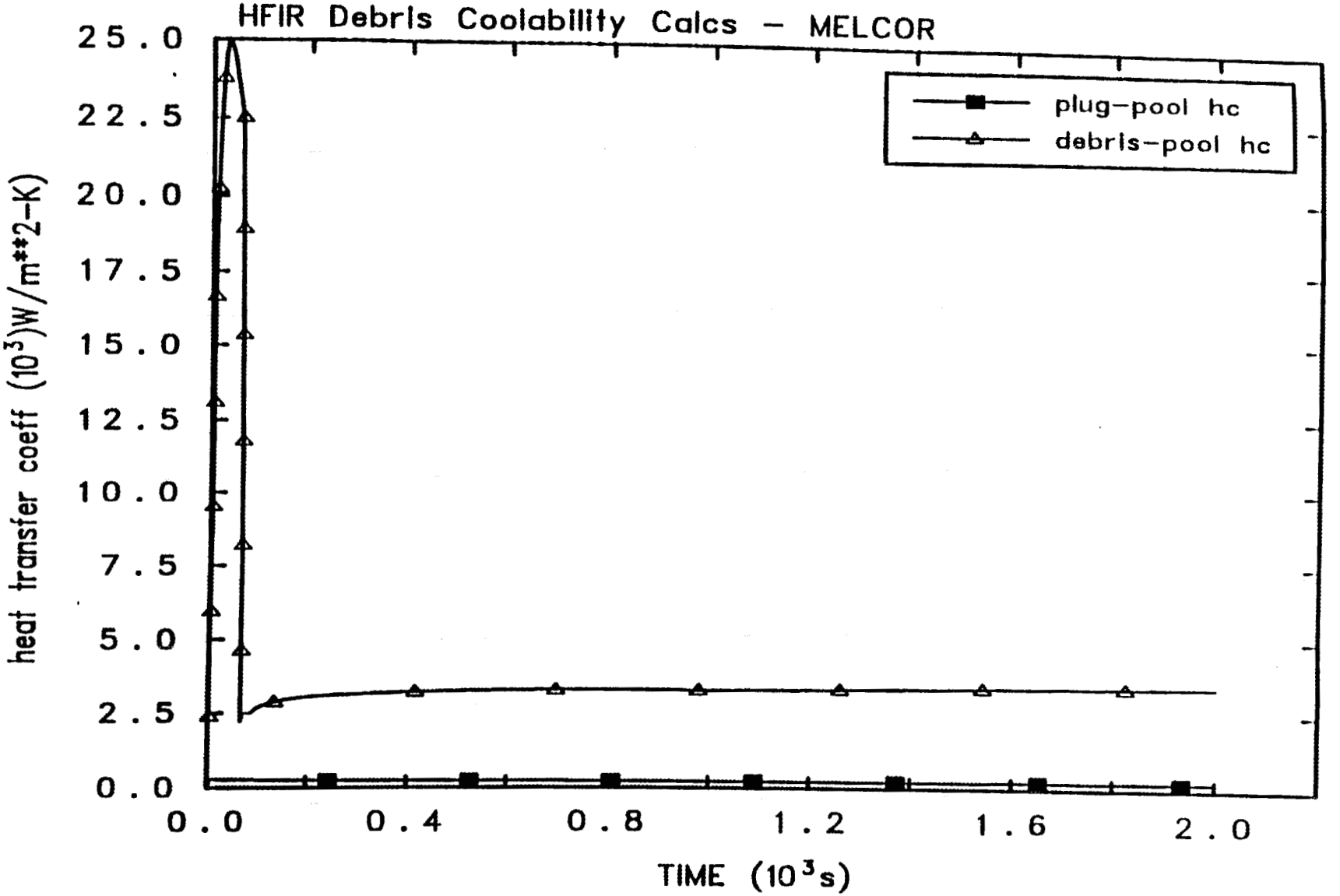

Fig. E.6 Variation of Debris-to-Pool and Plug-to-Pool Heat Transfer Coefficients vs Time (MELCOR Results for Case 2)

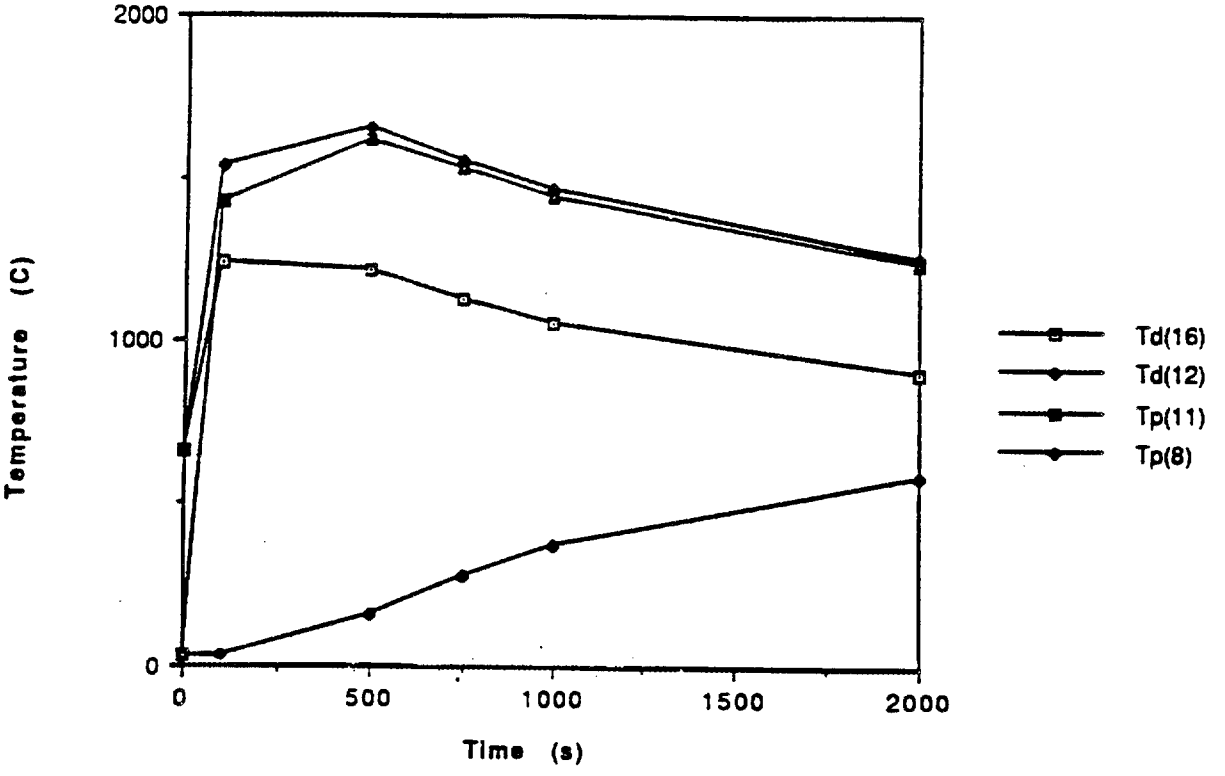

Fig. E.7a Fuel-Plug Transient Temperature Profile Predictions by 2DKO (Case 2)

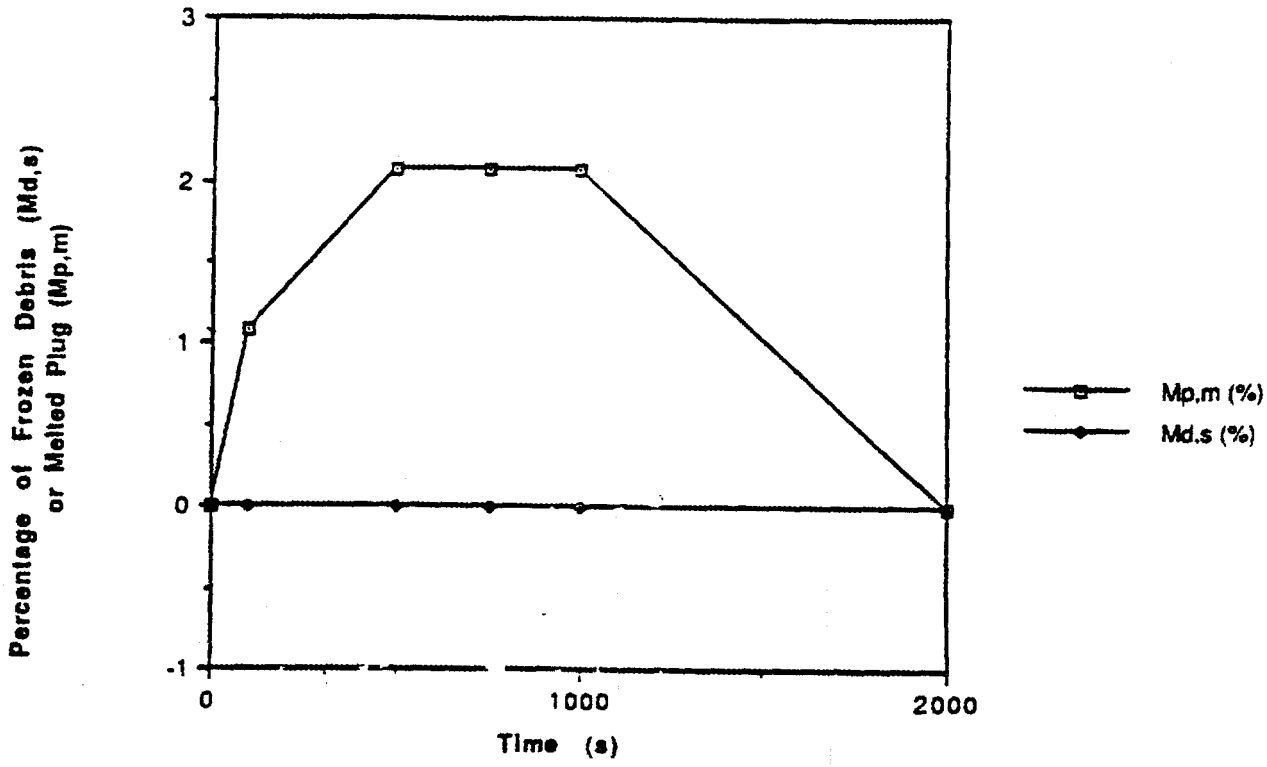

Fig. E.7b Fuel-Plug Transient Melting-Freezing Profile Predictions by 2DKO (Case 2)

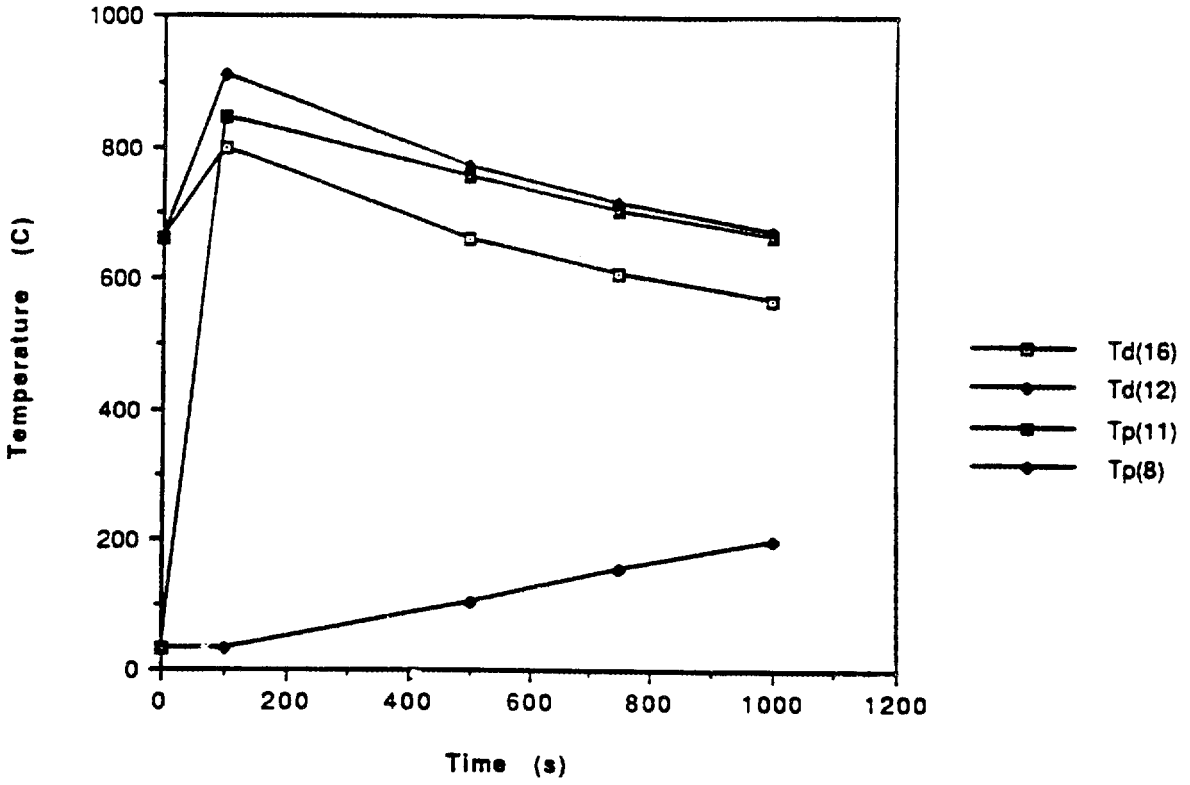

Fig. E.8a Fuel-Plug Transient Temperature Profile Predictions by 2DKO (Case 3)

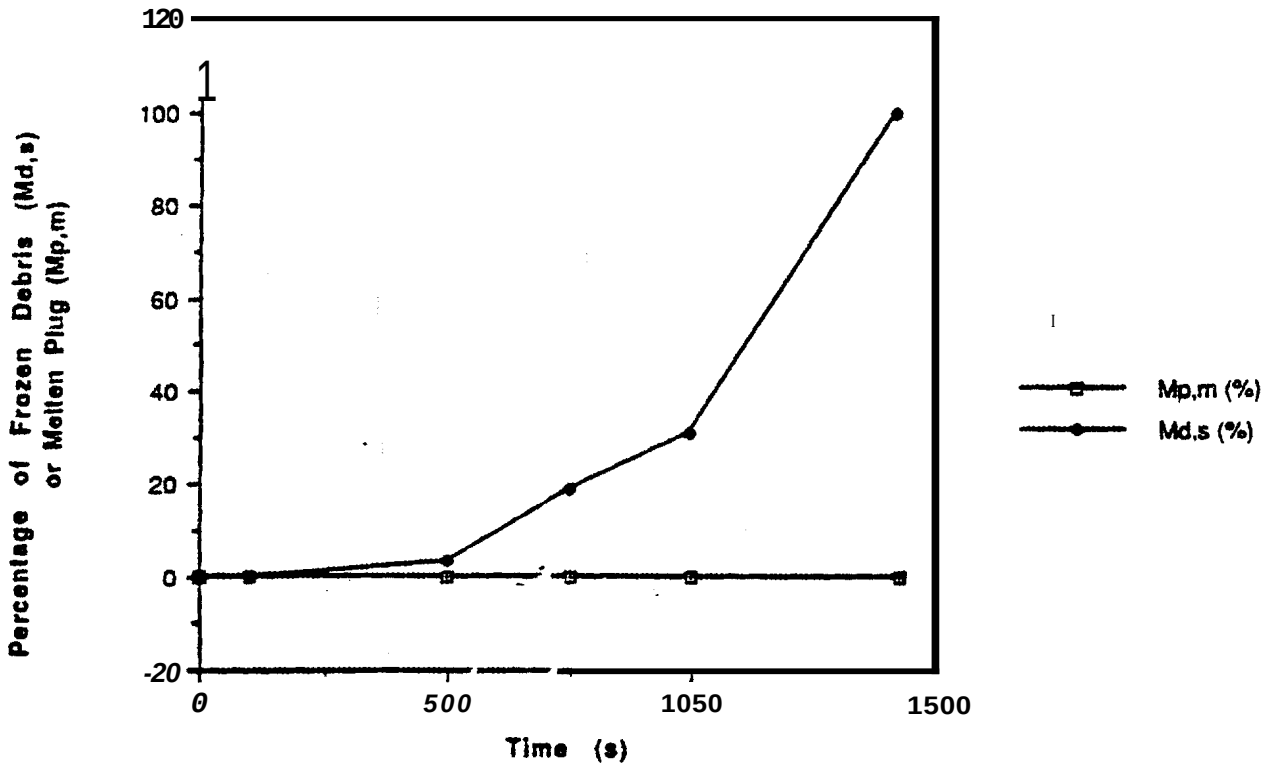

Fig. E.8b Fuel-Plug Transient Melting-Freezing Profiie Predictions by 2DK0 (Case 3)

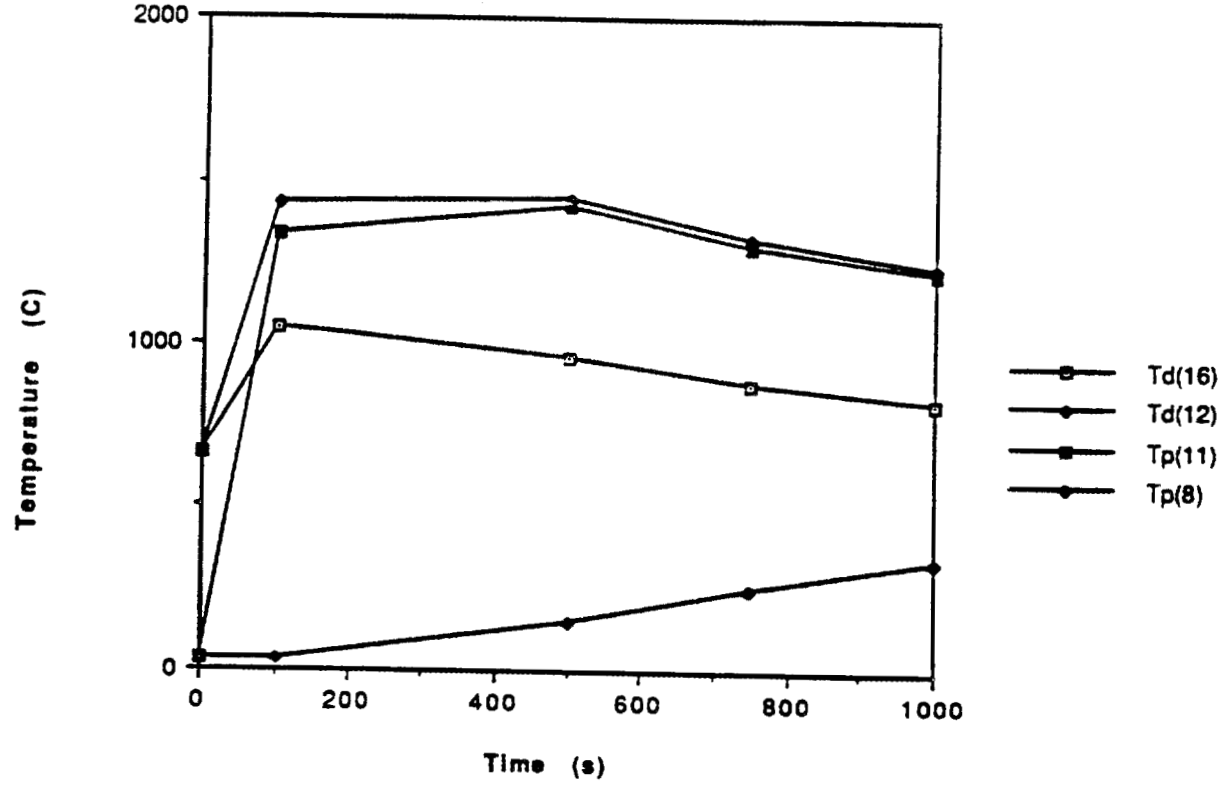

Fig. E.9a Fuel-Plug Transient Temperature Profile Predictions by 2DKO (Case 4)

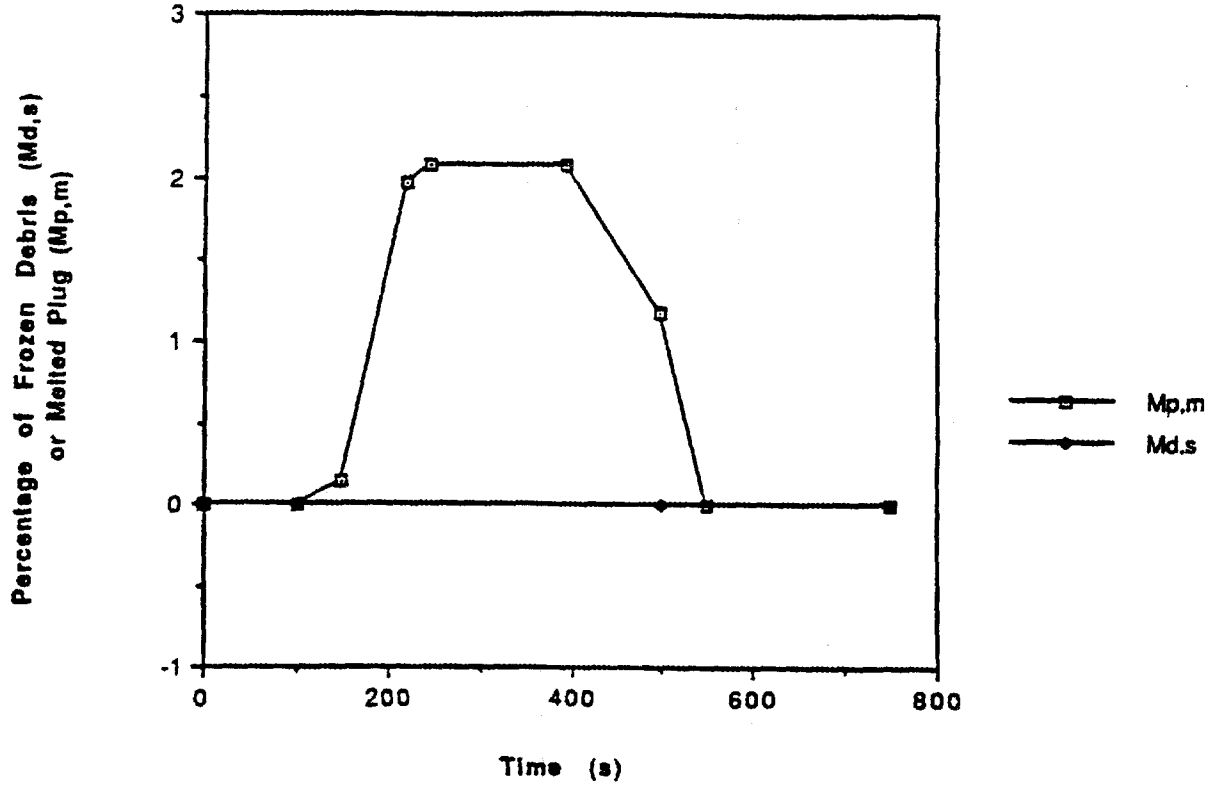

Fig. E.9b Fuel-Plug Transient Melting-Freezing Profile Predictions by 2DKO (Case 4)

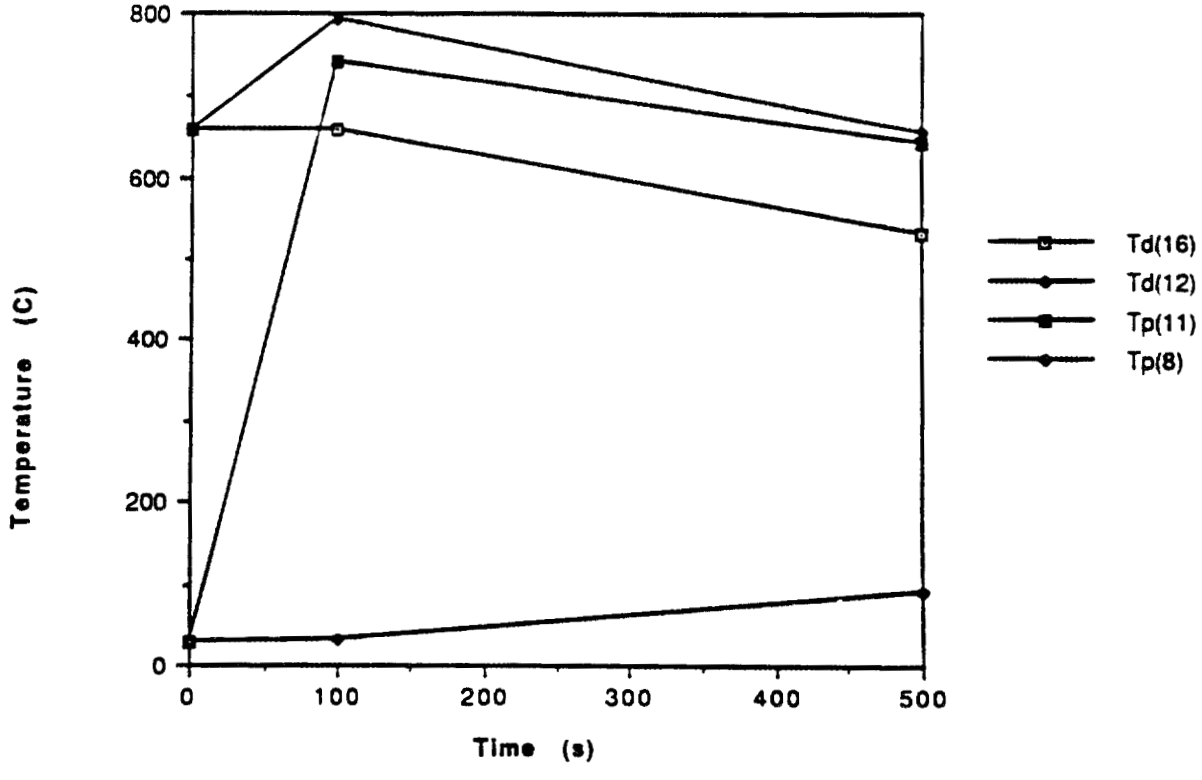

Fig. E.10a Fuel-Plug Transient Temperature Profile Predictions by 2DKO (Case 5)

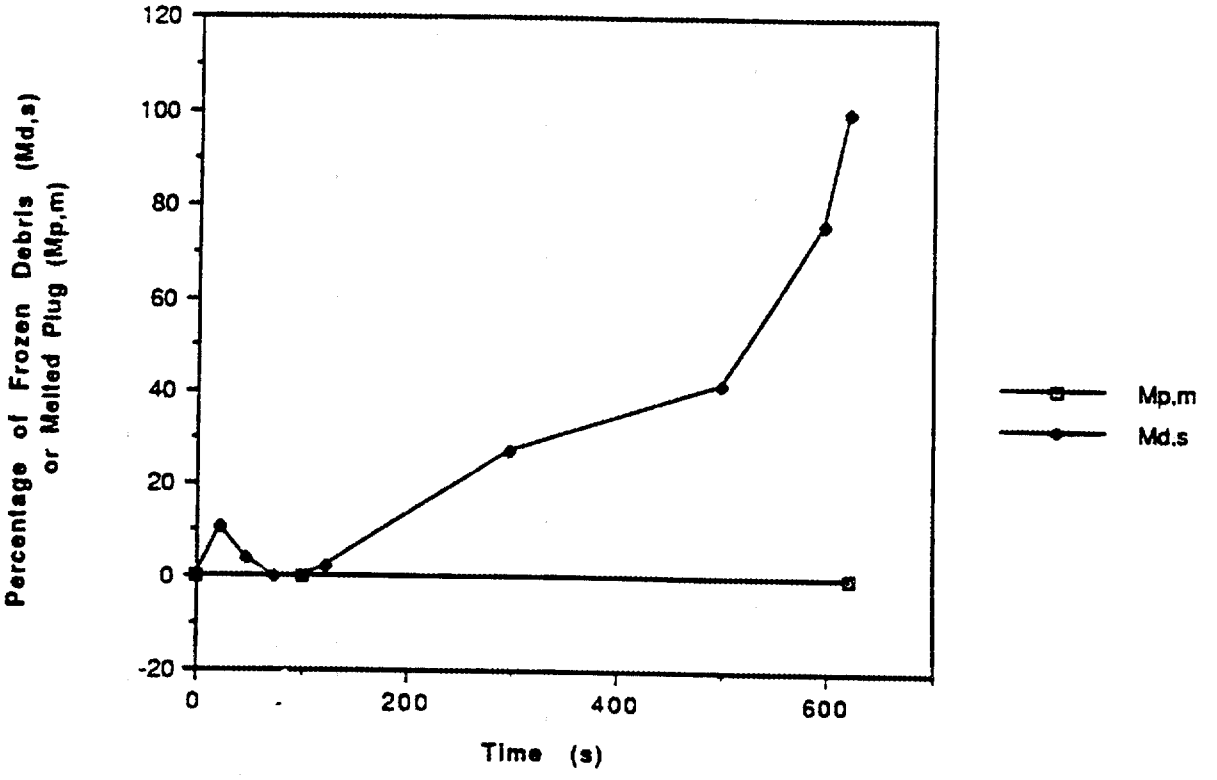

Fig. E.10b Fuel-Plug Transient Melting-Freezing Profile Predictions by 2DKO (Case 5)

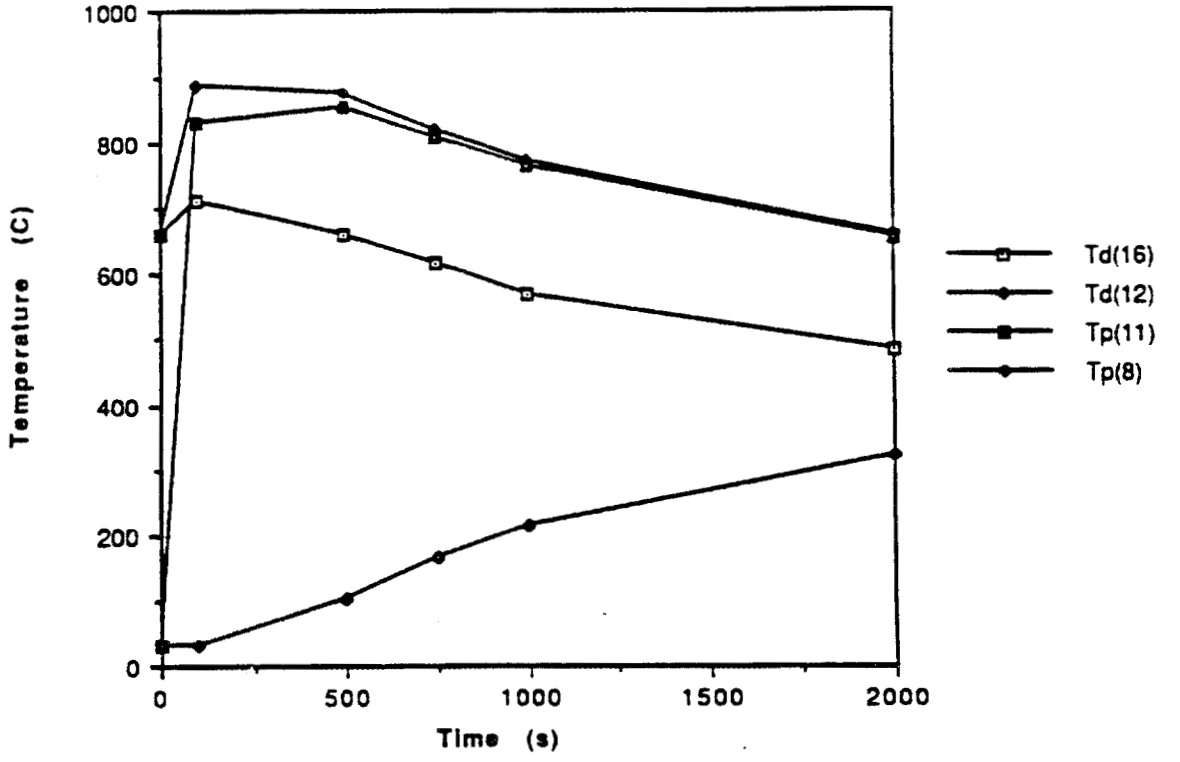

Fig. E.11a Fuel-Plug Transient Temperature Profile Predictions by MELCOR (Case 6)

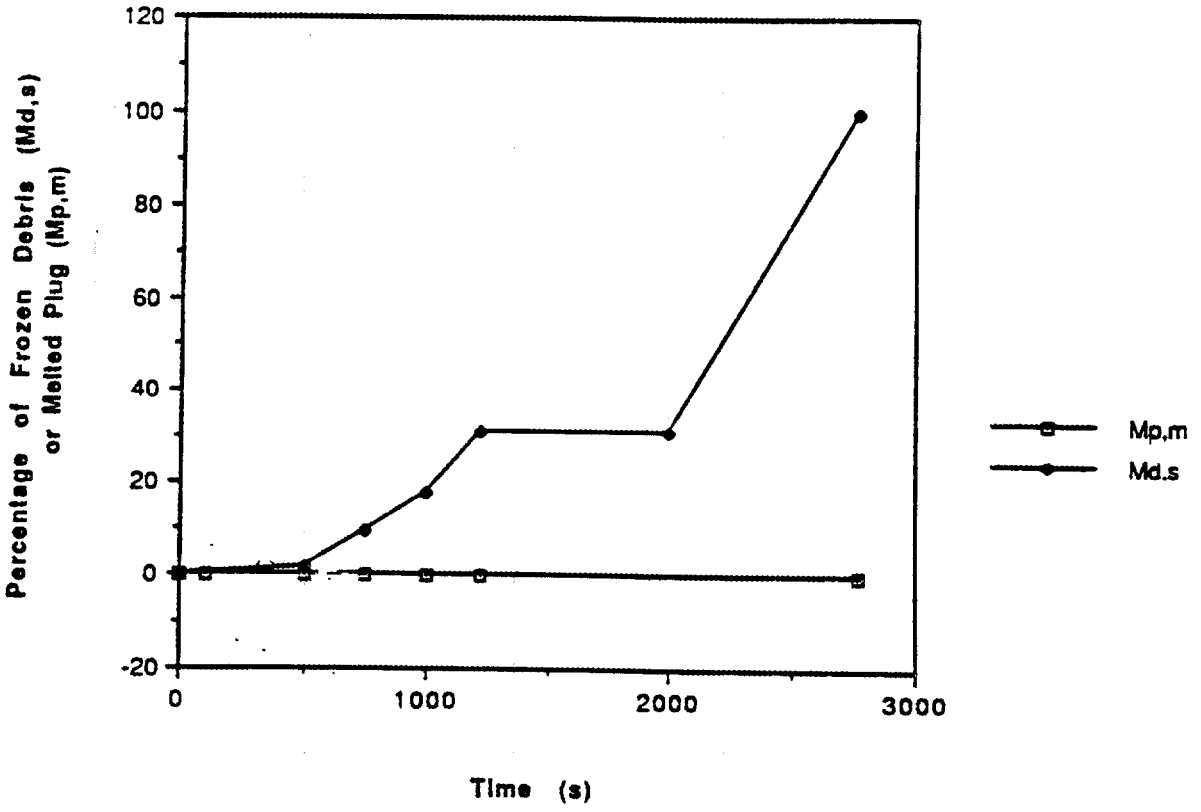

Fig. E.11b Transient Convective Heat Transfer Coefficient Profiles by MELCOR (Case 6)

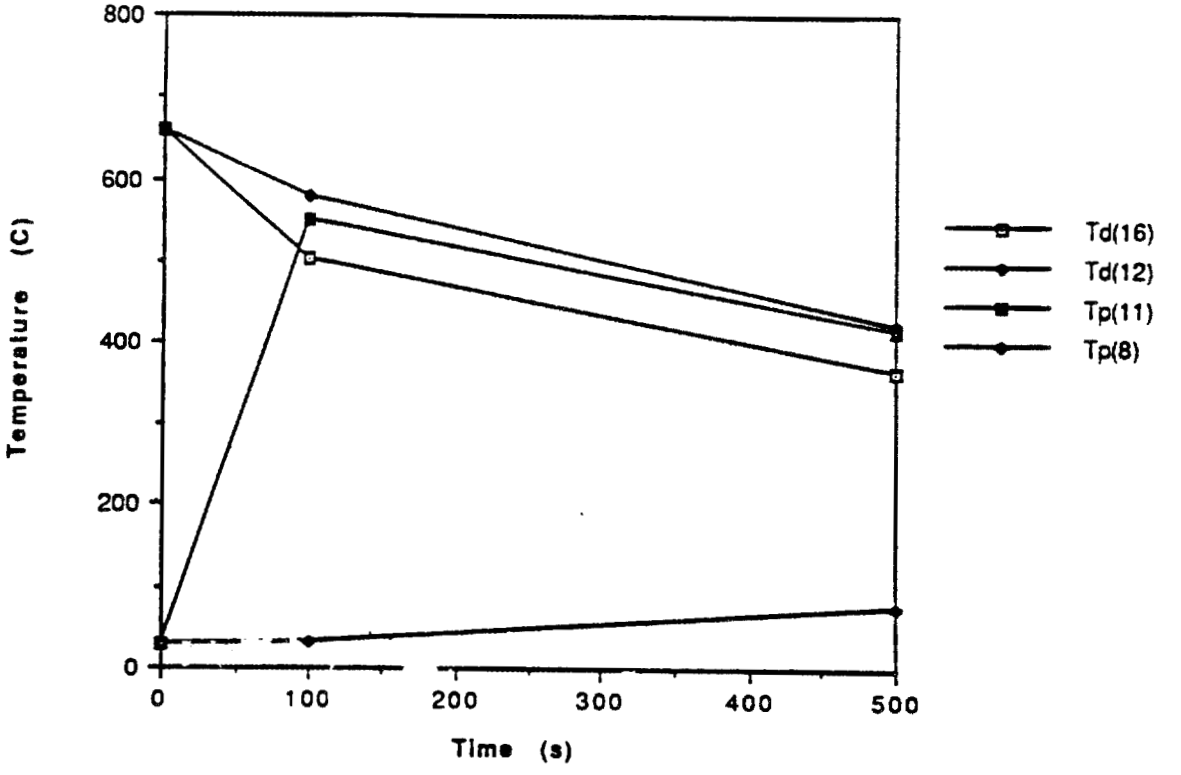

Fig E.12a Fuel-Plug Transient Temperature Profile Predictions by 2DKO (Case 7)

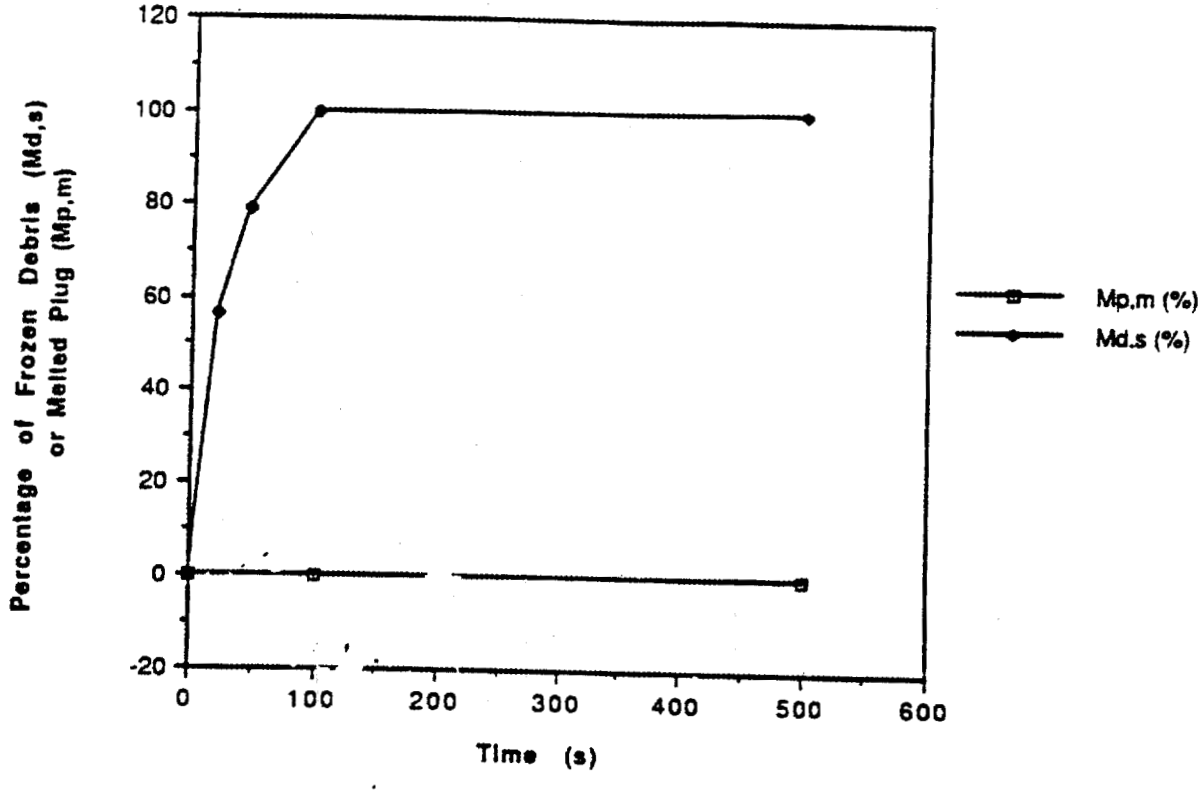

Fig. E.12b Fuel-Plug Transient Melting-Freezing Profile Predictions by 2DKO (Case 7)

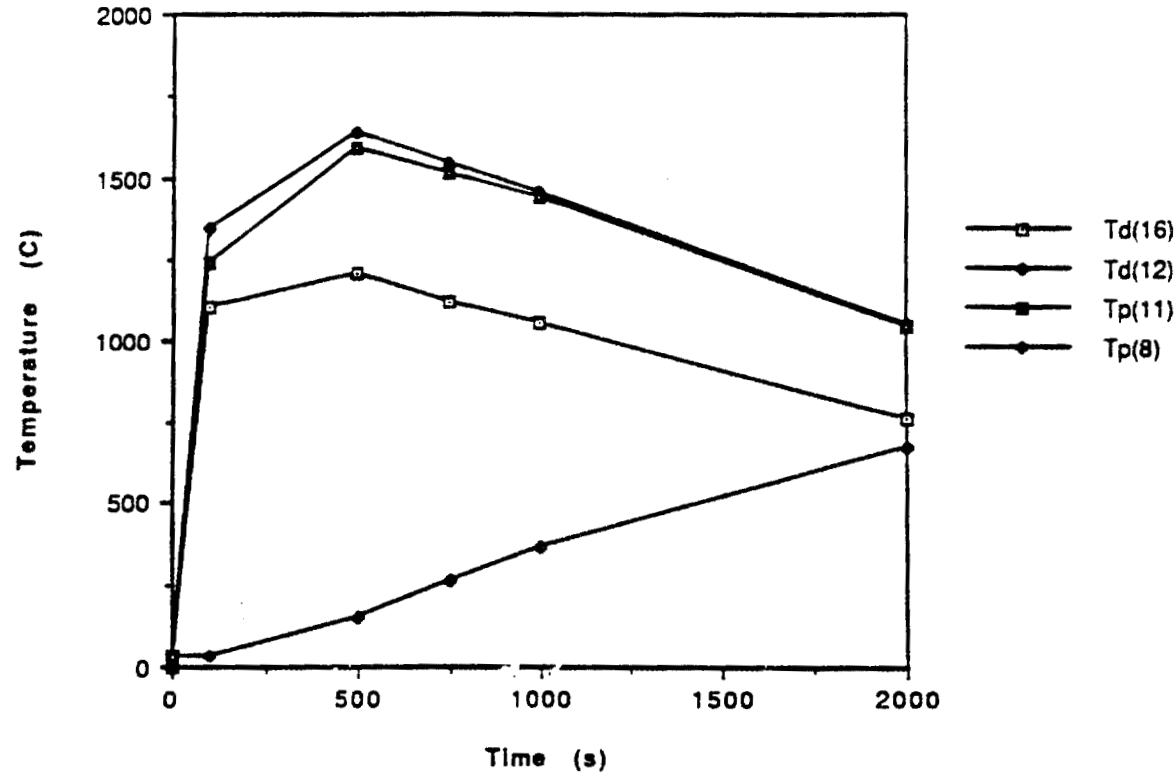

Fig. E.13a Fuel-Plug Transient Temperature Profile Predictions by 2DKO (Case 8)

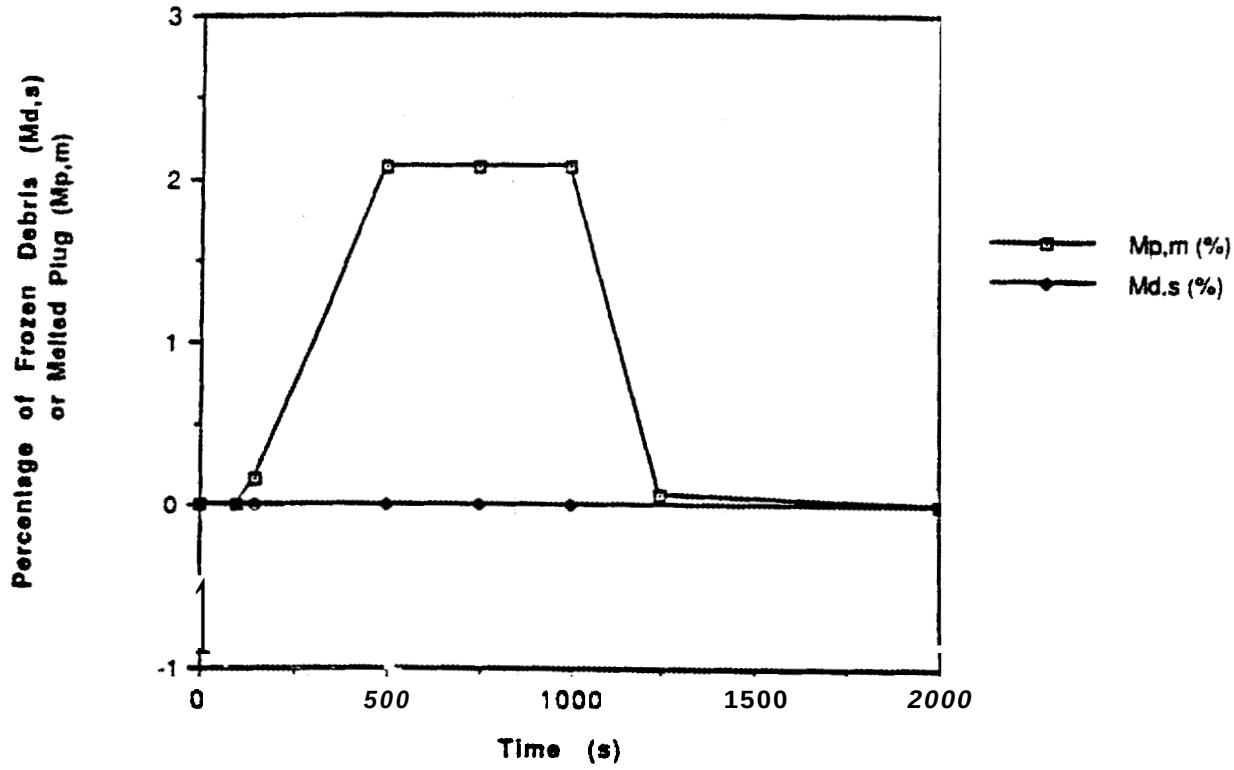

Fig. E.13b Fuel-Plug Transient Melting-Freezing Profile Predictions by 2DKO (Case 8)

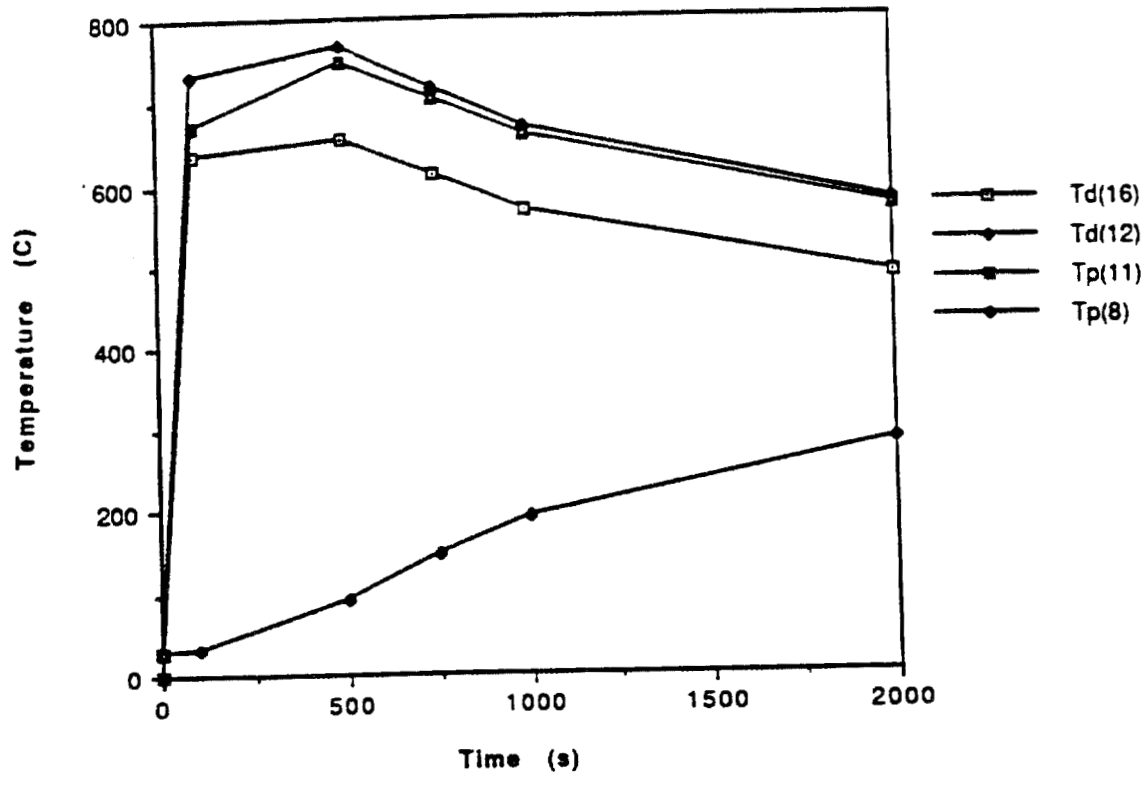

Fig. E.14a Fuel-Plug Transient Temperature Profile Predictions by 2DKO (Case 9)

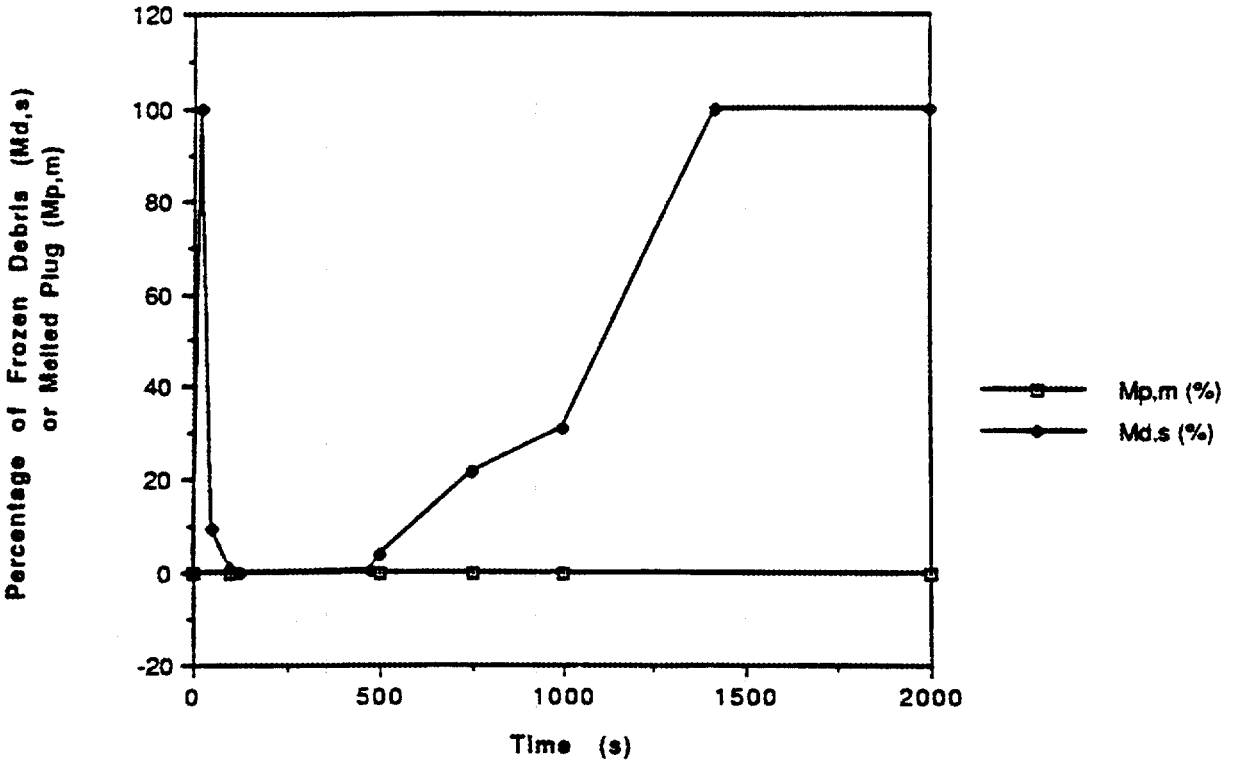

Fig. E.14b Fuel-Plug Transient Melting-Freezing Profile Predictions by 2DKO (Case 9)

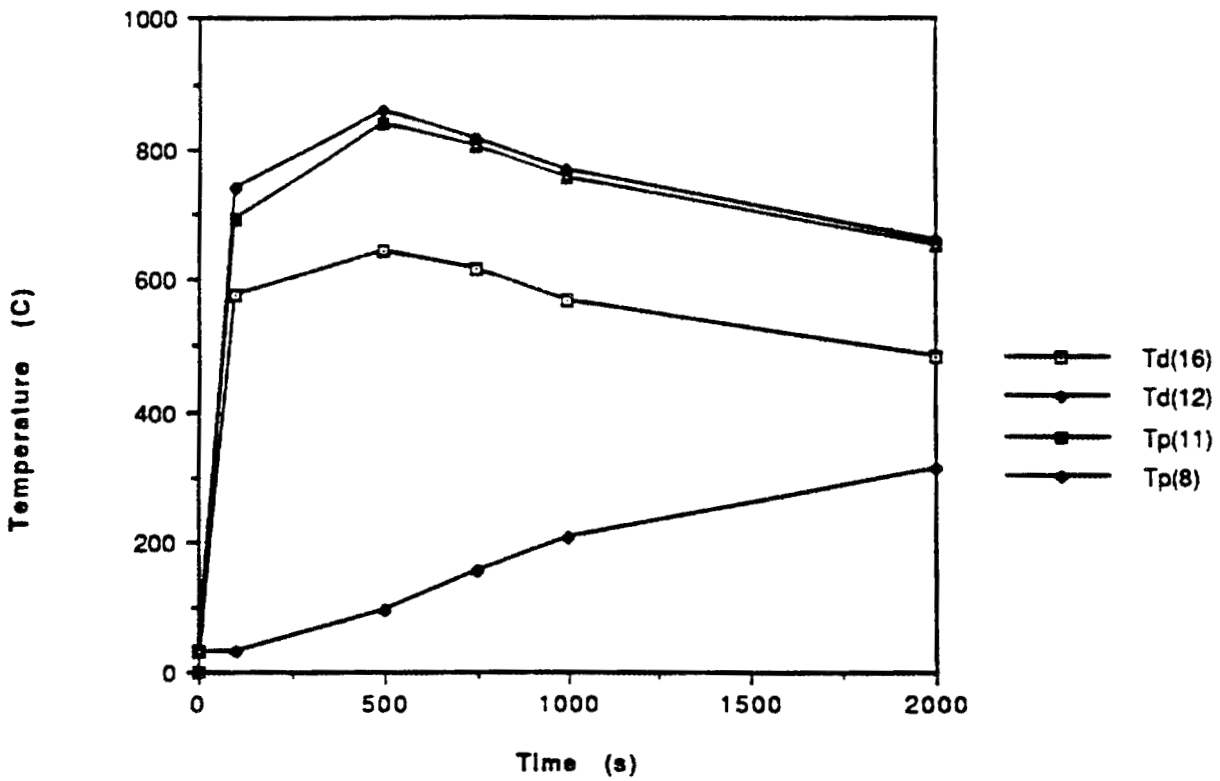

Fig. E.15a Fuel-Plug Transient Temperature Profile Predictions by 2DKO (Case 10)

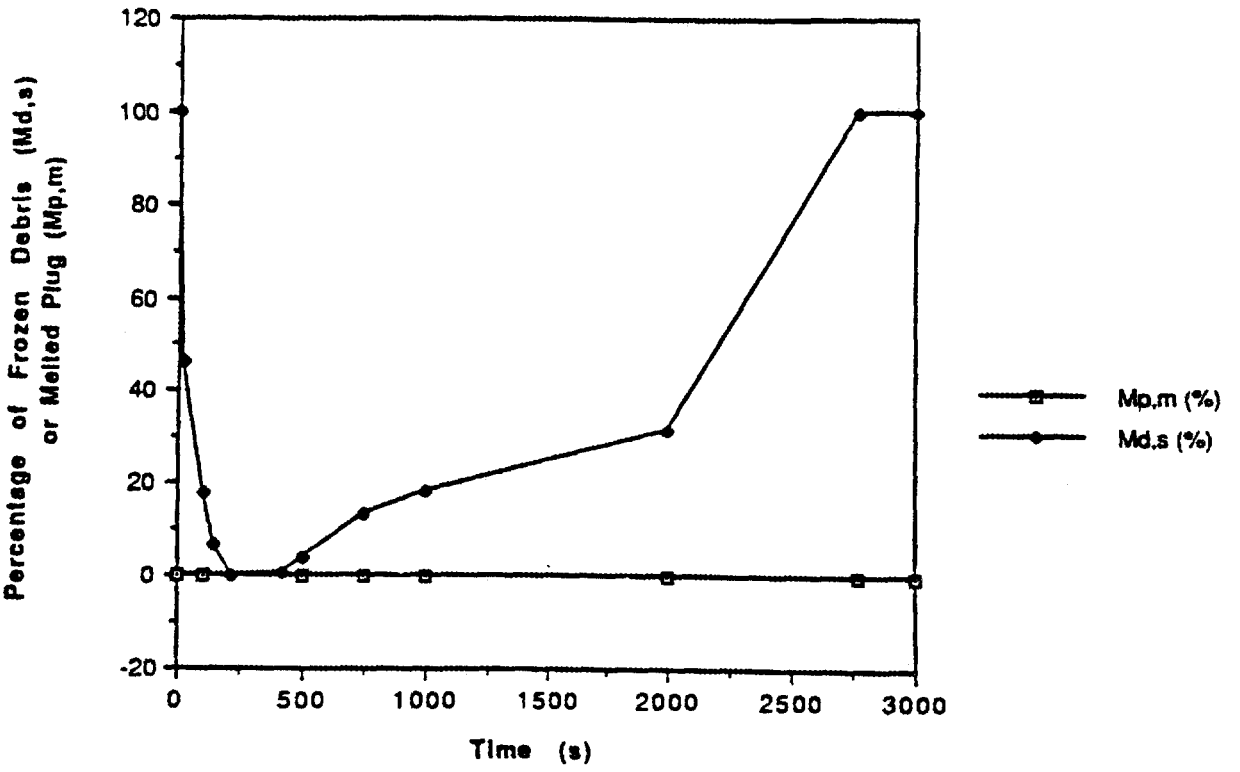

Fig. E.15b Fuel-Plug Transient Melting-Freezing Profile Predictions by 2DKO (Case 10)

APPENDIX F

Thermodynamic and One-Dimensional Mechanistic Calculations for HFIR Fuel-Coolant-Interaction Analyses

During loss-of-coolant or loss-of-pressure accident conditions in the HFIR core region, conditions may be produced that lead to melting of certain segments of the core fuel plates. As can be expected, the amount of melt formation depends on the sequence of events that follow. Different event sequences can produce different end results regarding the amount of melt formation. Steam explosion occurrences following such melting incidents in the presence of water can be expected to display different energetics. By performing energetics calculations for different combinations of core melt mass, coolant mass, ambient pressure, and different void fractions, important trends can be noted. Such calculations can be performed with tools of varying degrees of sophistication. The purpose of this appendix is to document the Fuel-Coolant-Interaction (FCI) energetics calculations performed using thermodynamic models and a mechanistic one-dimensional (1-D) model of the FCIMOD.ORNL code.[45] Details of the calculations are not presented here, but can be found Refs. 41, 42, and 48.

F.1 EVALUATION OF FCI ENERGETICS WITH THERMODYNAMIC MODELS

Steam explosions in the HFIR core region can result in the generation of significant pressure pulses and mechanical work. Estimates for pressurization and mechanical energy generation can be made using thermodynamic modeling approaches as well as best-estimate techniques. It should be kept in mind that thermodynamic modeling approaches provide *bounding* estimates. Such estimates are useful for providing guidance and checks (for best-estimate calculations) and to provide a structured approach for evaluating upper-bound values of pressure buildup or mechanical work. Evidently, if one can show that the system under consideration can withstand thermodynamically

evaluated maximum loads, then a very strong case can be made for closure of issues related to steam explosions.

F.1.1 Introduction to Thermodynamic Maximum Energetics Evaluations

As mentioned earlier, thermodynamic models for FCI energetics evaluations provide estimates for upper bounds of pressurization and mechanical work. A thermodynamic model describes the mixing and explosion expansion phases of steam explosions connecting the three points that describe (1) the initial coarse mixture, (2) the equilibrium high-pressure state, and (3) the final expanded state. Because work done during the expansion is a path-dependent quantity, the path of constant entropy can provide the maximum work output - as proposed by Hicks and Menzies.[5] The thermodynamic path in their model assumes that equilibrium mixing occurs between the fuel and coolant adiabatically without volume change, followed by isentropic expansion to a specified end state. Another model that provides an estimate for the maximum work output was proposed by Board and Hall[6] by using an analogy to chemical detonations. UWHUGO and UWHM are computer codes that implement the thermodynamic models for FCI energetics developed by Board and Hall and by Hicks and Menzies, respectively. We have ported the UWHUGO and UWHM computer codes developed at the University of Wisconsin, Madison under Professor Corradini to our IBM RISC/6000 workstation (Ref. 39).

F.2 EVALUATION OF ENERGETICS WITH FCIMOD.ORNL

Steam explosions in the HFIR core region can result in the generation of significant pressure pulses and mechanical work. As mentioned previously, bounding estimates can be made using thermodynamic models (3) for evaluating the degree of pressurization and energy conversion. However, bounding estimates for pressures and

mechanical energies are usually intolerable. To obtain best-estimate results of pressure pulse and energy conversion evolution with time in a one-dimensional (1-D) geometry, the FCIMOD.ORNL code is used. Specific results of these FCIMOD calculations are also to be used for evaluating energy sourcing rates for more sophisticated two-dimensional calculations using the CTH code described in Appendix G.

The FCIMOD computer code models a one-dimensional FCI in the geometry shown schematically in Fig. F.1. It is assumed that there is a mixing zone at the bottom of the system under consideration where molten fuel is fragmented into small particles and mixed with liquid coolant. The shaded area depicts an enlarged view of a molten fuel particle, surrounded by a vapor blanket. Above the mixing zone, there is a region called the slug zone, filled with coolant which will be accelerated upward by the expanding vapor generated in the mixing zone. The slug is free to travel upward into the expansion zone. We have shown a planar mixing zone-slug interface. Although the code can treat the case of a hemispherical slug, the planar slug usually leads to higher peak pressures. The entire assembly is a right circular cylinder. Most of the essential physics for evaluating steam explosion energetics has been included in FCIMOD. To summarize, the model is a lumped-parameter formulation that treats the whole fuel-coolant mixture as one control volume, with another control volume modeling the inertial constraint of an overlying slug. The expansion dynamics is treated in a one-dimensional fashion, either in a planar or hemispherical geometry with possible entrainment of the liquid slug into the mixture due to Rayleigh-Taylor instabilities with associated slug breakup. The fuel fragmentation process is postulated to be controlled by coolant jet penetration of the fuel droplet surface during film collapse.

F.2.1 Problem Formulation for Steam Explosion Energetics Evaluation

As mentioned above, FCIMOD models a 1-D FCI in the geometry shown in Fig. F.1. A mixing zone exists at the slug-mixture interface. For our situation, the

interface was deemed to be best represented by a planar interface. The inertial constraint is another key parameter that needs to be used. For a power reactor scenario, this is essentially the mass of slug over the mixing zone. However, for a solid system, such as the HFIR during a core flow-blockage accident condition, the proper choice of an inertial constraint is not that clear. Hence, as a first step, a test matrix of runs has been developed that considers various values for the inertial constraint. This is described later in this appendix.

The assumptions made in FCIMOD calculations are consistent with the mathematical model of FCIMOD for 1-D energetics evaluations. Details are given in Ref. 42.

F.3 CALCULATIONAL TEST MATRIX AND ANALYSIS RESULTS

A test matrix was developed for evaluating pressurization and conversion ratios using thermodynamic models and the 1-D model in FCIMOD. The same matrix is used for both evaluation schemes. Such an approach provides for a direct comparison of results from models predicting bounding estimates for energetics versus the more sophisticated mechanistic model of FCIMOD. As mentioned previously, FCIMOD models FCI as a 1-D process wherein a mixing zone exists at the slug-mixture interface. The inertial constraint is another key parameter that needs to be used. For a power reactor scenario, this is essentially the mass of slug over the mixing zone. However, for a solid system, such as the HFIR during a core flow-blockage accident condition, the proper choice of an inertial constraint is not that clear. Hence, as a first step, a test matrix of runs has been developed that considers various values for the inertial constraint.

The desired test matrix of runs is given in Table F.1. As seen, 34 cases have been identified. The test matrix considers variations in key input parameters. These are:

- mass of molten fuel
- mass of coolant in explosion zone with which the molten fuel mixes
- fuel temperature
- coolant void fraction in explosion zone
- inertial constraint (i.e., slug mass)
- ambient pressure before explosion

F.4 RESULTS OF ENERGETICS CALCULATIONS WITH THERMODYNAMIC MODELS AND FCIMOD

In this section, results for FCI energetics are presented using thermodynamic and best-estimate models. Results are first provided from the thermodynamic models and then for the more realistic cases (predicted using FCIMOD.ORNL).

Table F.2 provides results from use of thermodynamic models for selected cases (viz., Cases 2, 5, and 7). As can be seen, the thermodynamic model estimates for pressurization and energy conversion are quite high relative to what one might expect for steam explosion events (as will be demonstrated later from mechanistic evaluations). As an example, for Case 2 the Board-Hall model[15] calculated a peak pressurization value of 1427 MPa compared to a value (shown later) of about 78 MPa calculated by FCIMOD for the same operating parameters. Again, the thermal-to-mechanical energy conversion ratio is seen to be much higher as predicted by the model of Hicks and Menzies[13] (i.e., a value of 23% vs ~8.2% from FCIMOD calculations). The degree of conservatism inherent in thermodynamic model estimates should be evident from these rudimentary evaluations. Similar results are obtained for Cases 5 and 7.

An important characteristic to note concerns the values of peak pressurization predicted by UWHUGO and UWHM. Recall that UWHUGO implements the model of Board and Hall which draws similarities to chemical detonations. This is the primary

reason for the pressurization values predicted by UWHUGO being significantly larger than corresponding pressures predicted by UWHM. However, both codes predict the same value for overall thermal-to-mechanical energy conversion. Another aspect of note concerns the effect of the ratio of mass of coolant to mass of fuel that participates in the explosion. As can be seen from the three cases in Table F.2, work output peaks when the mass of coolant-to-mass of fuel is about 0.3. This is an important effect and underscores the need for proper modeling of the premixing process.

The variation of pressurization and conversion ratio with initial mixture void-fraction (i.e., before an explosion) is also important to ascertain. Thermodynamic models such as in UWHUGO and UWHM provide quick estimates on the sensitivity of pressurization and mechanical work to this important but difficult to estimate parameter. For this exercise, it was assumed that 10 kg of fuel at 1300 K would interact with 10 kg of water at 330 K (i.e., variations of Case 7) with different values of initial mixture void fractions. Results of these evaluations with UWHUGO and UWHM are shown graphically in Figs. F.2 through F.5. As can be noted from results of both codes, the energy conversion parameter is a strong function of initial mixture void fraction only at either low (i.e., 0 to 25%) or high (i.e., 80 to 100%) values (i.e., of void fraction). Interestingly, the peak pressurization is strongly dependent on initial void fraction only for low values (i.e., of mixture void fraction). Such trends have several implications the most important of which deals with steam explosions under highly voided conditions. *For highly voided conditions, the threat from large degrees of overpressurization, and consequently from the imparted mechanical work, can be an order of magnitude lower than under conditions of low values of mixture void fraction.* Such evaluations also provide an indication of the importance of knowing with reasonable certainty the mixture void fraction. Finally, it should be kept in mind that the variational trend shown in Figs. F.2 through F.5 will be different for different operating conditions, but should remain independent of the thermodynamic model chosen.

We now present results for all the 34 cases of Table F.1 using the mechanistic model of FCIMOD.ORNL. Results for peak pressures, pulse duration, and thermal-to-mechanical energy conversion are summarized in Table F.1 (where the test matrix conditions are also given). Note that for Case 26, a slug breakup condition was encountered wherein FCIMOD.ORNL code aborted the calculation. The slug breakup occurs when vapor "bubbles out" of the water rather than pushes the slug as a missile. A study of the transient plots of pressure and conversion ratio for the 34 cases provided the following insights:

- An increase in the fuel temperature increases the peak pressure pulse magnitude. This is to be expected, since higher fuel temperatures contribute to increased energy transfer to the coolant. Figure F.6 displays the peak pressure variation by test case and also fuel temperature.
- As seen from Fig. F.7, an increase in the vapor volume in the explosion zone generally decreased the peak pressure pulse magnitude. The size of the pressure shock depends on the vapor generation rate and both are also governed by resistances to energy transfer. Some of the resistances are: resistance of the fuel, resistance of the vapor region, and resistance of the liquid. Of these, the vapor layer contributes the greatest resistance because of its relatively low thermal conductivity.
- An increase of coolant mass in the explosion zone reduces the peak pressure magnitude. This is caused by increased energy requirements for heating up the liquid instead of production of vapor. Clearly, a tradeoff exists because, as we have stated earlier, increased vapor production beyond a certain value also decreases pressure pulse generation capability.
- An increase in the ambient pressure does not significantly affect the pressure pulse magnitude; however, the conversion ratio decreases as seen from Table F.1.

- An increase of the slug mass (i.e., inertial constraint) increases the peak pressure pulse magnitude, but also tends to reduce the overall thermal-to-mechanical energy conversion ratio.

Selected results of the pressure pulse and conversion ratio versus time for Cases 1 through 4 are shown in Figs. F.8 through F.11. Further details are presented in C-HFIR-92-016, which also provides further details of comparisons between thermodynamic estimates and FCIMOD.ORNL predictions for all 34 cases. Specifically, for Case 2 a direct comparison can be made with values obtained from thermodynamic calculations. FCIMOD predictions indicate a pressure rise and conversion ratio of 78 MPa and 8.5%, respectively. These can be seen to be a lot lower than the corresponding HM calculated values of about 571 MPa and 23%. The degree of conservatism is reduced by not using thermodynamic maximum values.

A few further observations are in order. Note that the rapid oscillations in the pressure in the neighborhood of the critical point (22.055 MPa) for Case 4 are a symptom of difficulty with the NWSTEAM subroutine package in FCIMOD. We plan to replace this with a different package based on relatively new data and fits (National Bureau of Standards). As a result of this problem, the conversion ratio has a maximum value of about 5.4% at about 45 ms and then begins to decrease. The break in the liquid coolant temperature curve at just past 1 ms indicates the beginning of transfer of more cool liquid into the mixing zone from the slug.

F.4 EFFECT OF FCI ON REACTOR VESSEL

Previous FCI work done for HFIR[54] had estimated that the pressure required to burst the HFIR vessel would be 35.7 MPa. FCI energetics calculations reported in this appendix using FCIMOD.ORNL have shown that such a pressure level can certainly be

reached and exceeded in the explosion zone (but for short durations only). However, the strain energy required to rupture the vessel was calculated at 200 MJ, which represents the work performed by pressurized fluid expanding in a given volume. It should be noted that the peak pressure predicted by FCIMOD.ORNL is not a static pressure rise. Based on the predictions of thermal-to-mechanical energy conversion during steam explosions for

Cases 1 through 34, it was found that the mechanical work performed (see Table F.1) is not sufficient to cause gross rupture of the vessel. It is recognized that FCIMOD results are one-dimensional in nature, whereas the results of Ref. 54 are for the overall vessel. Therefore, any interpretation should be made carefully. For applying FCIMOD results to HFIR vessel failure one would need to use the FCIMOD calculated energetics focus on a section of the overall surface. At this stage, it should be mentioned that vessel failure characteristics have been studied with more sophisticated tools for the current work and are reported in Appendix H.

F.5 DYNAMIC PRESSURE PULSES FROM LOCALIZED FUEL MELTING IN THE HFIR CORE

In the event of fuel melting of certain fuel plates, it was postulated in Chapter 2 that a localized FCI may produce a large enough pressure pulse to cause damage propagation. In Appendix D, failure envelopes were developed for the fuel plates in the HFIR core. These failure envelopes indicated that pressure pulses of magnitude greater than 1.75 MPa (250 psi) and lasting for a milisecond or more would cause plate failure.

To evaluate pressure pulses likely in the explosion zone, FCIMOD.ORNL calculations were performed. Two selected cases given below show that the pressures reached during an energetic FCI under likely thermal-hydraulic conditions can be at least

as high as 25 MPa regardless of whether one or two fuel plates have initially melted. The following two cases were analyzed:

Case 1: One molten fuel plate and water from two coolant channels mix before an explosion, and

Case 2: Two molten fuel plates and water from three coolant channels mix before an explosion.

Input parameters for FCIMOD.ORNL calculations are the mass of fuel, coolant, and slug, and the void fraction in the explosion zone. For both cases, a column of water 1.2 m in height (representing water above the core) was used to estimate the slug mass (viz., inertial constraint). The cross-sectional area of the reaction zone is the sum of the cross-sectional areas of the fuel plate(s) and the cross-sectional area of the coolant flow channels. Two different void fractions were evaluated, [viz., 25% (i.e., CVOID = 0.33)] and 75% (i.e., CVOID = 3.0), respectively.

Results obtained for the two cases are shown in Figs. F.12 and F.13. As seen from these figures, for low void fraction (CVOID = 0.33) the pressure pulse generated by the melting of a single plate does not differ significantly from the pressure pulse generated from the two-plate melting case. For both cases, with a CVOID = 0.33 peak, pressure pulses reached are 23 MPa and 26 MPa, respectively. For the high void fraction situation (i.e., CVOID = 3.0), the respective pressure levels are 6 and 9 MPa. In all instances, the pressure pulse width is several miliseconds long and much greater than the required 1.75 MPa pressure level for adjacent plate failure.

Table F.1 Test matrix with results of steam explosion energetics calculations

Case	Mfuel (kg)	Mc (kg)	Tfuel (K)	CVOID	mc/mf	Mtot (kg)	Pinc (kPa)	Conv. rat. %	Peak Press (Mpa)	Pulse width (msec)	Work energy KJ	Case
1	10	1	1100	0.33	0.1	500	101	8	65	0.8	911.4	1
2	10	1	1300	0.33	0.1	500	101	8.2	78	0.8	1081.8	2
3	10	1	1600	0.33	0.1	500	101	8.3	140	0.7	715.2	3
4	10	1	1300	3	0.1	500	101	7	23	8	923.5	4
5	10	3	1300	0.33	0.3	500	101	6	30	2	791.6	5
6	10	3	1300	3	0.3	500	101	3.5	8.5	20	461.7	6
7	10	10	1300	0.33	1	500	101	7	25	20	923.5	7
8	10	3	1300	3	0.3	5000	101	4	17	30	527	8
9	10	10	1300	0.33	1	5000	101	4.5	30	40	593.6	9
10	10	3	1300	0.33	0.3	500	3300	2.5	30	10	329 8	10
11	10	3	1300	3	0.3	500	3300	1.2	11	20	158.3	11
12	10	10	1300	0.33	1	500	3300	2.5	21	15	329.8	12
13	10	10	1300	3	1	500	3300	0.9	6.6	30	118.7	13
14	10	3	1300	0.33	0.3	5000	3300	1.6	40	15	211	14
15	10	10	1300	0.33	1	5000	3300	1.5	30	15	197 ti	15
16	10	3	1300	3	0.3	5000	3300	4	20	60	527.7	16
17	10	3	1300	3	0.3	5000	3300	4.5	25	70	715.2	17
18	50	5	1100	0.33	0.1	500	101	7	100	5	3987.5	18
19	50	5	1300	0.33	0.1	500	101	8	110	10	5277.2	19
20	50	5	1600	0.33	0.1	500	101	8.5	160	10	5607	20
21	50	5	1300	3	0.1	500	101	7	37	50	4617.5	21
22	50	15	1300	0.33	0.3	500	101	3	27	50	1978.9	22
23	50	15	1300	3	0.3	500	101	3.5	12	50	2308	23
24	50	50	1300	0.33	1	500	101	4.5	23	50	2968.4	24
25	50	15	1300	3	0.3	500	101	2.5	22	50	1649.1	25
26	50	50	1300	0.33	1	5000	101	<<<<<Slug breakup>>>>>				26
27	50	15	1300	0.33	0.3	5000	3300	1.5	25	50	989.5	27
28	50	15	1300	3	0.3	500	3300	2.1	14	60	1385.3	28
29	50	50	1300	0.33	1	500	3300	2	23	60	1119.3	29
30	50	50	1300	3	1	500	3300	1.2	8	70	791.6	30
31	50	15	1300	0.33	0.3	500	3300	1.1	80	8	725.6	31
32	50	50	1300	0.33	1	5000	3300	0.7	23	40	461.7	32
33	50	15	1300	3	0.3	5000	3300	1.7	23	40	1121.4	33
34	50	15	160	3	0.3	5000	3300	1.7	27	30	1121.4	34

Legend:
Mfuel - Mass of Fuel
Mc - Mass of coolant
Tfuel - Initial Fuel Temperature
Pinc - Initial system pressure

Conv.rat. - conversion ratio
CVOID - Ratio of volume of vapor to volume of liquid
Mtot - Total mass of the fuel coolant and the overlying slug
mc/mf - mass of coolant to mass of fuel ratio

Table F.2 Results of specific thermodynamic calculations for steam explosion energetics

Case	Fuel mass (kg)	Fuel temperature (K)	Water mass (kg)	Water temperature (K)	Hickes-Menzies		Board-Hall	
					Pressure rise (MPa)	Conversion ratio	Pressure rise (MPa)	Conversion ratio
2	10.00	1300.00	1.00	330.00	571.82	0.23	1427.40	0.27
5	10.00	1300.00	3.00	330.00	427.57	0.41	869.80	0.46
7	10.00	1300.00	10.00	330.00	57.53	0.23	164.30	0.25

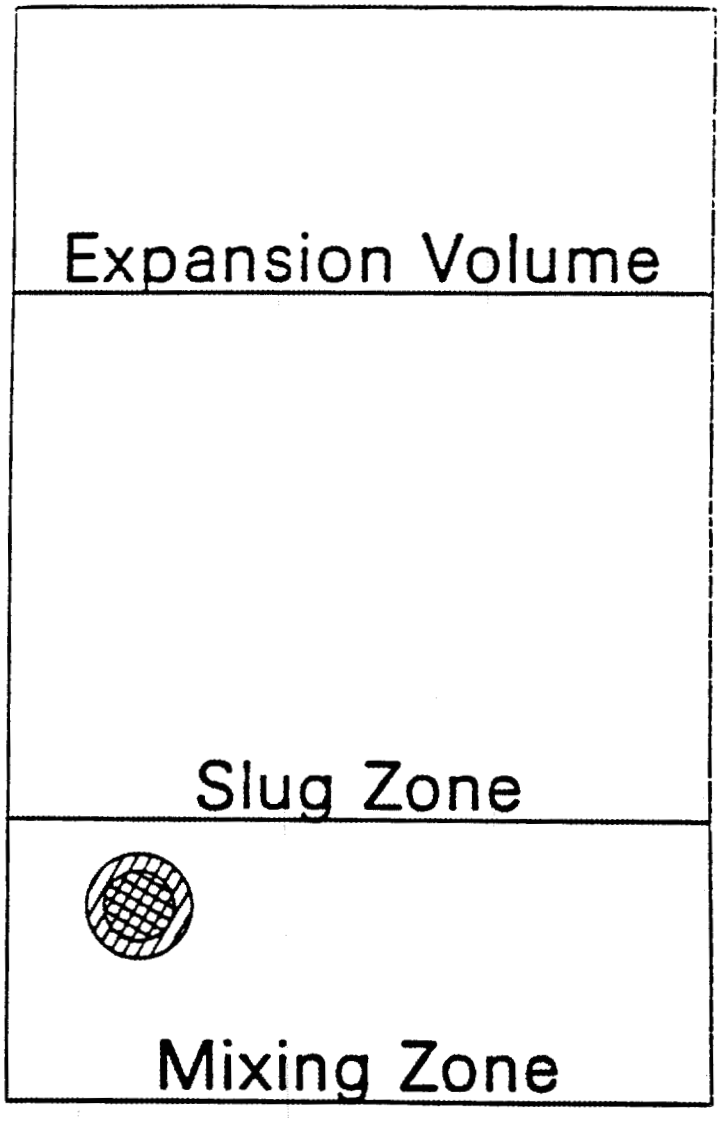

Schematic Vapor Explosion Geometry

Fig. F.1 Schematic Vapor Explosion Geometry Modeled by FCIMOD

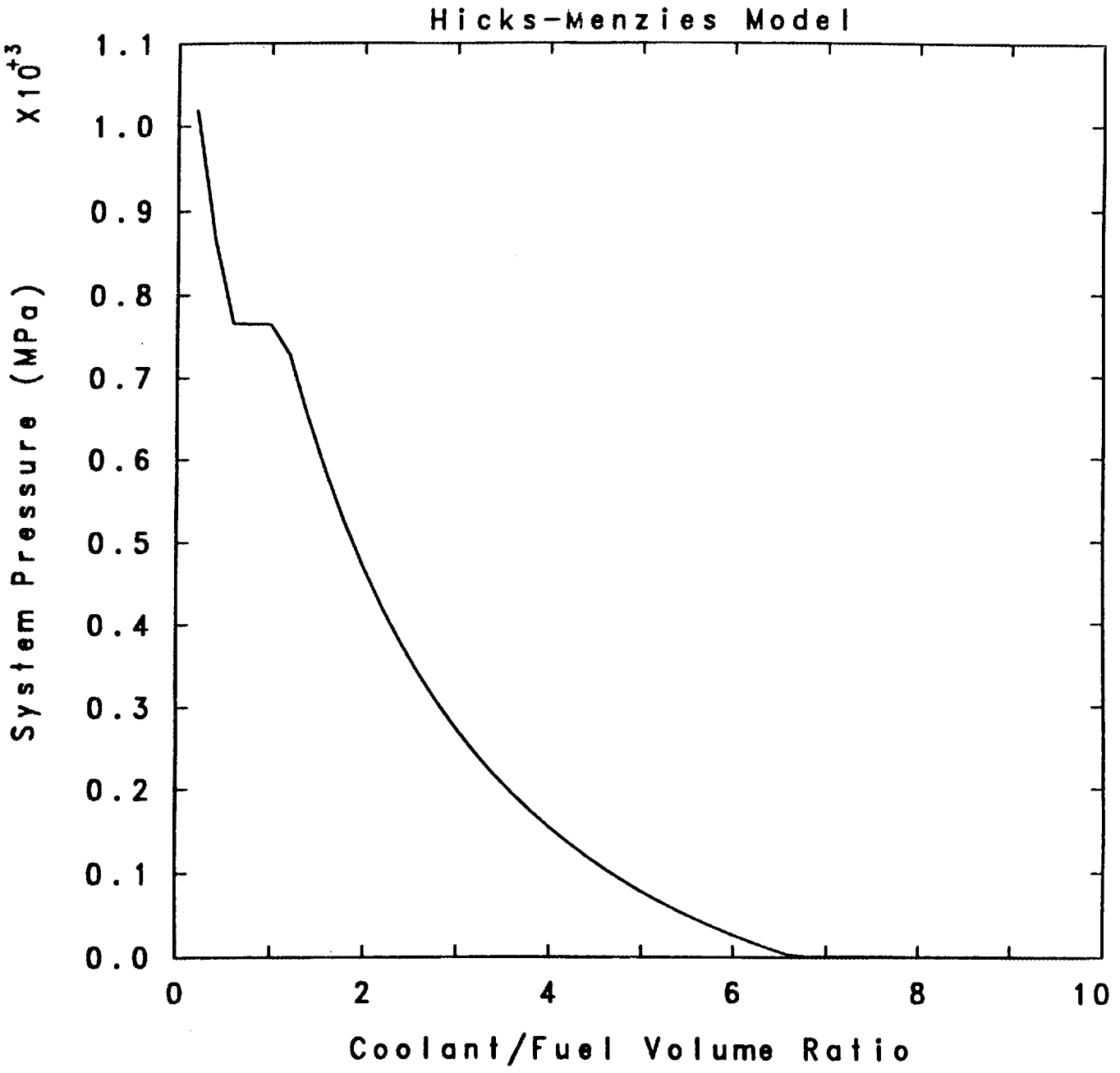

Fig. F.2 Pressurization versus Coolant-to-Fuel Volume Ratio Predictions (Hicks-Menzies Model)

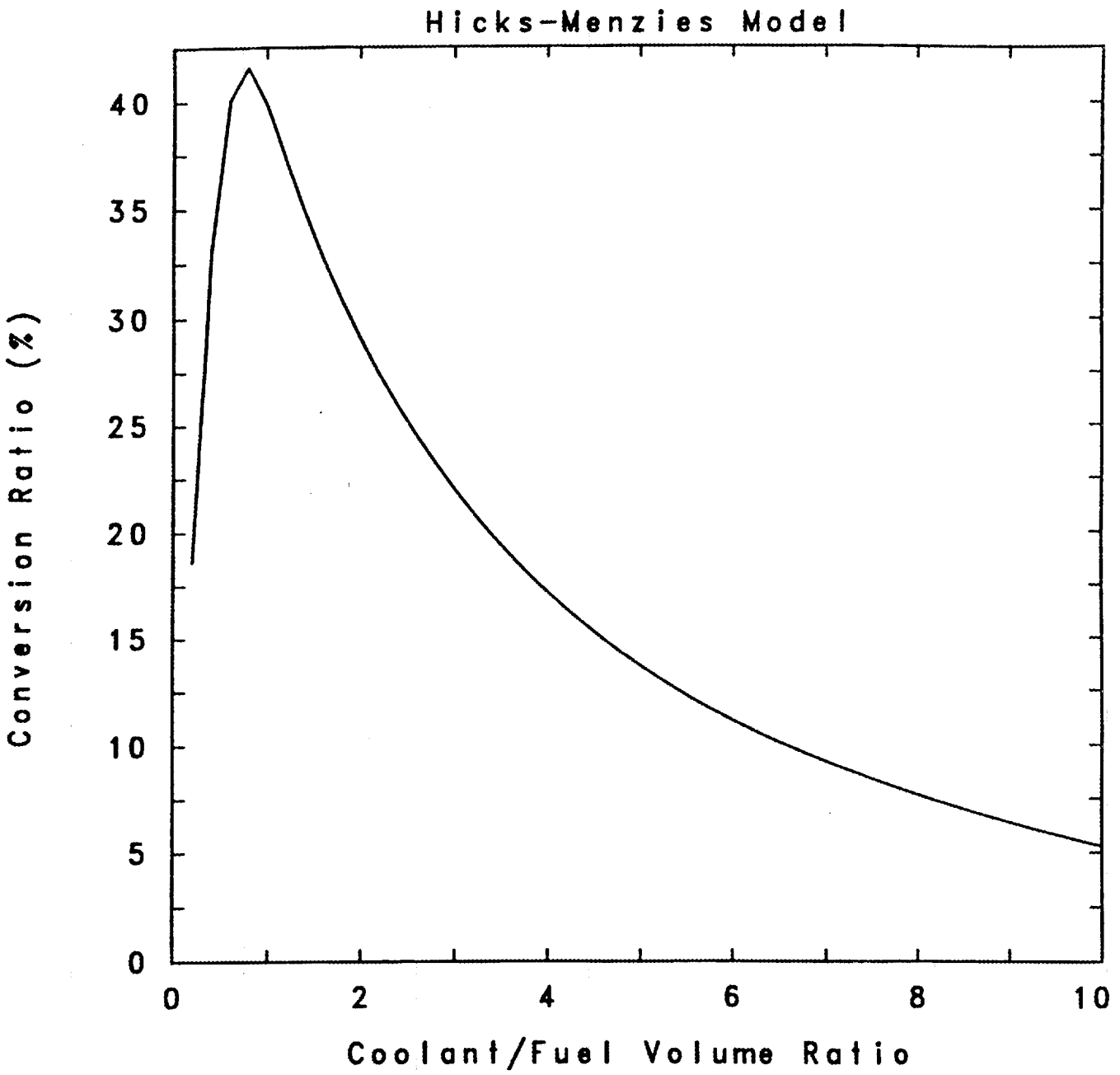

Fig. F.3 Conversion Ratio versus Coolant-to-Fuel Volume Ratio (Hicks-Menzies Model)

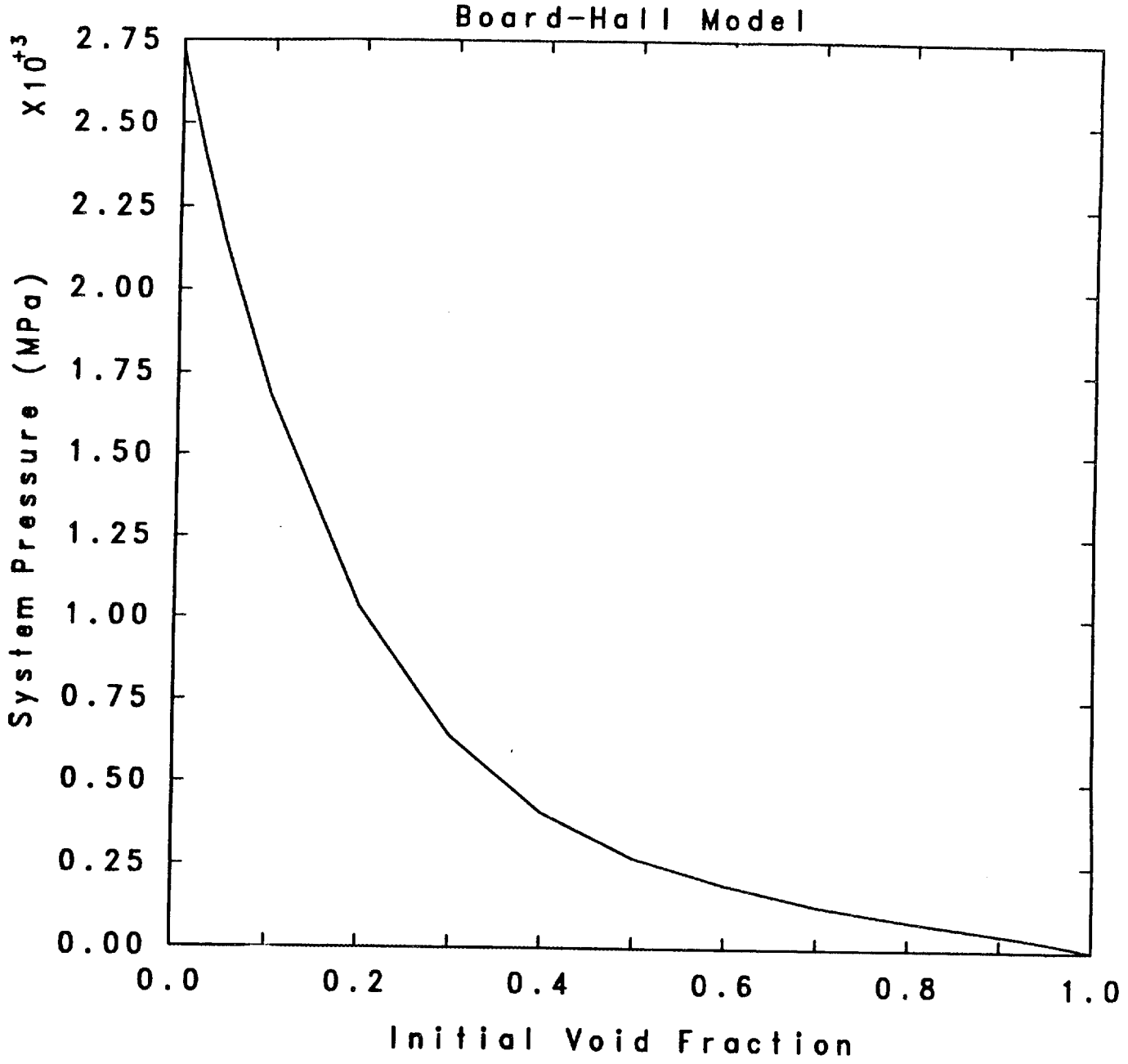

Fig. F.4 Pressurization versus Initial Void Fraction (Board-Hall Model)

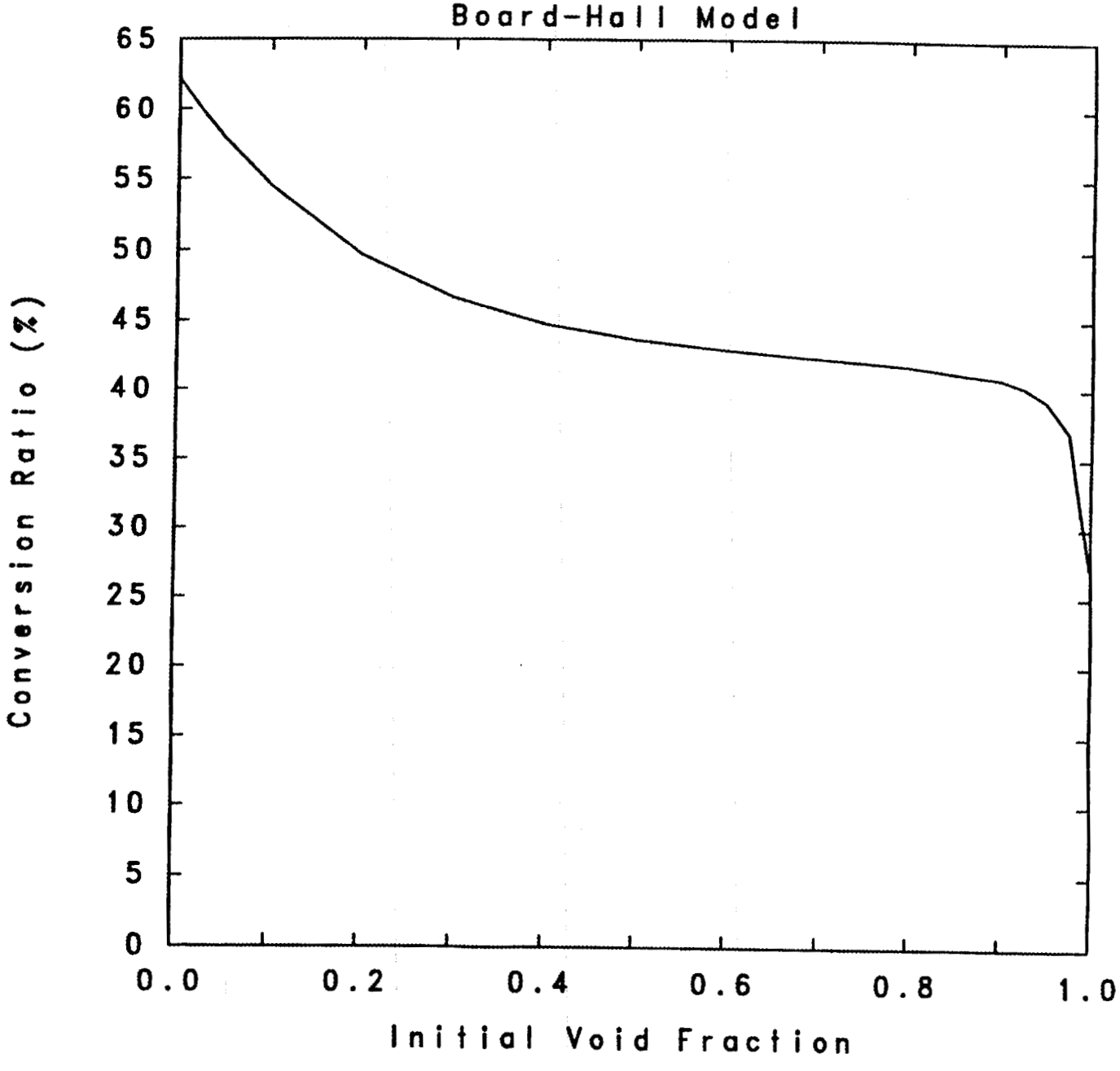

Fig. F.5 Conversion Ratio versus Initial Void Fraction Predictions (Board-Hall Model)

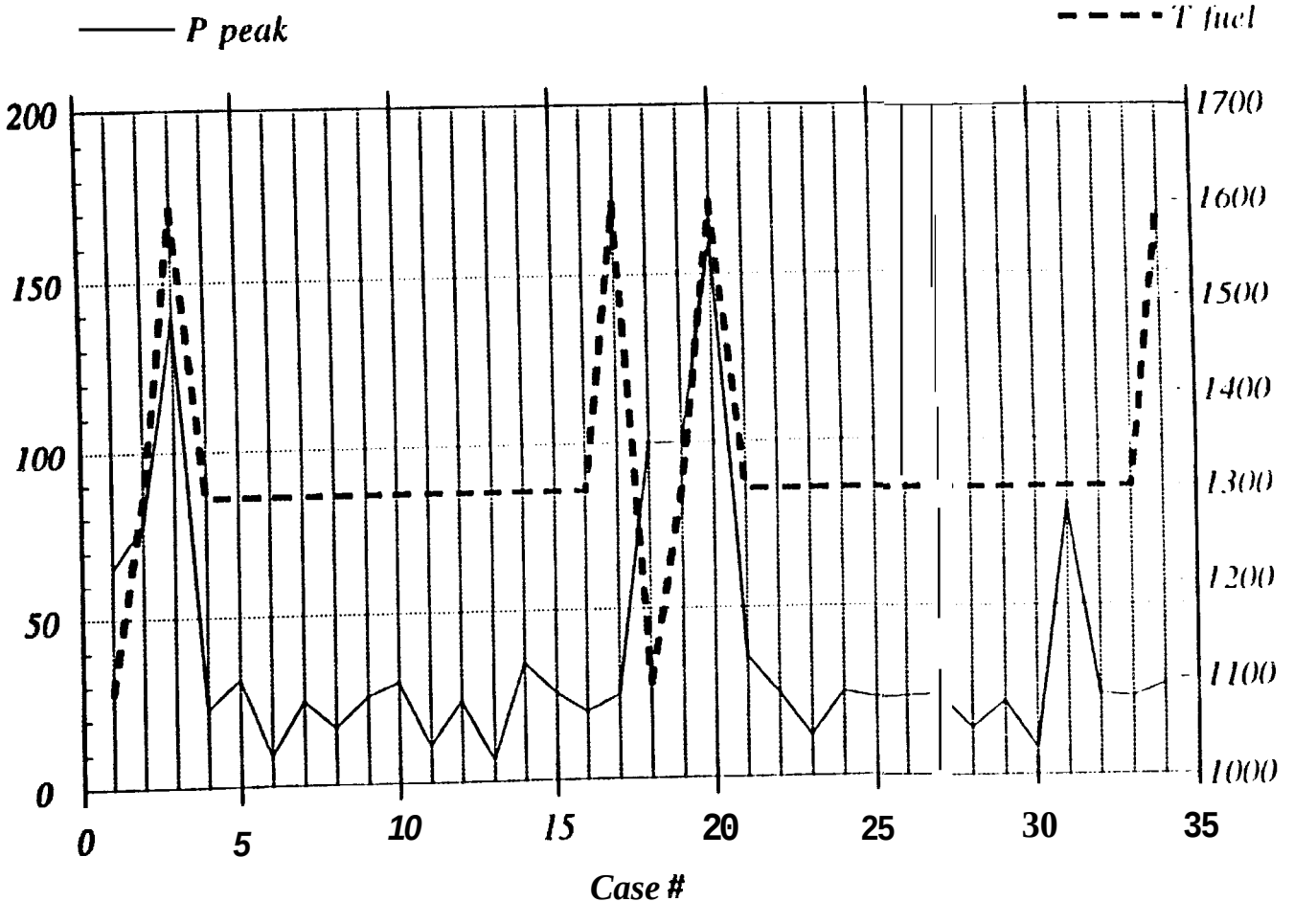

Fig. F.6 Effect of Fuel Temperalure on Peak Pressure Magnitude for Cases 1 to 35

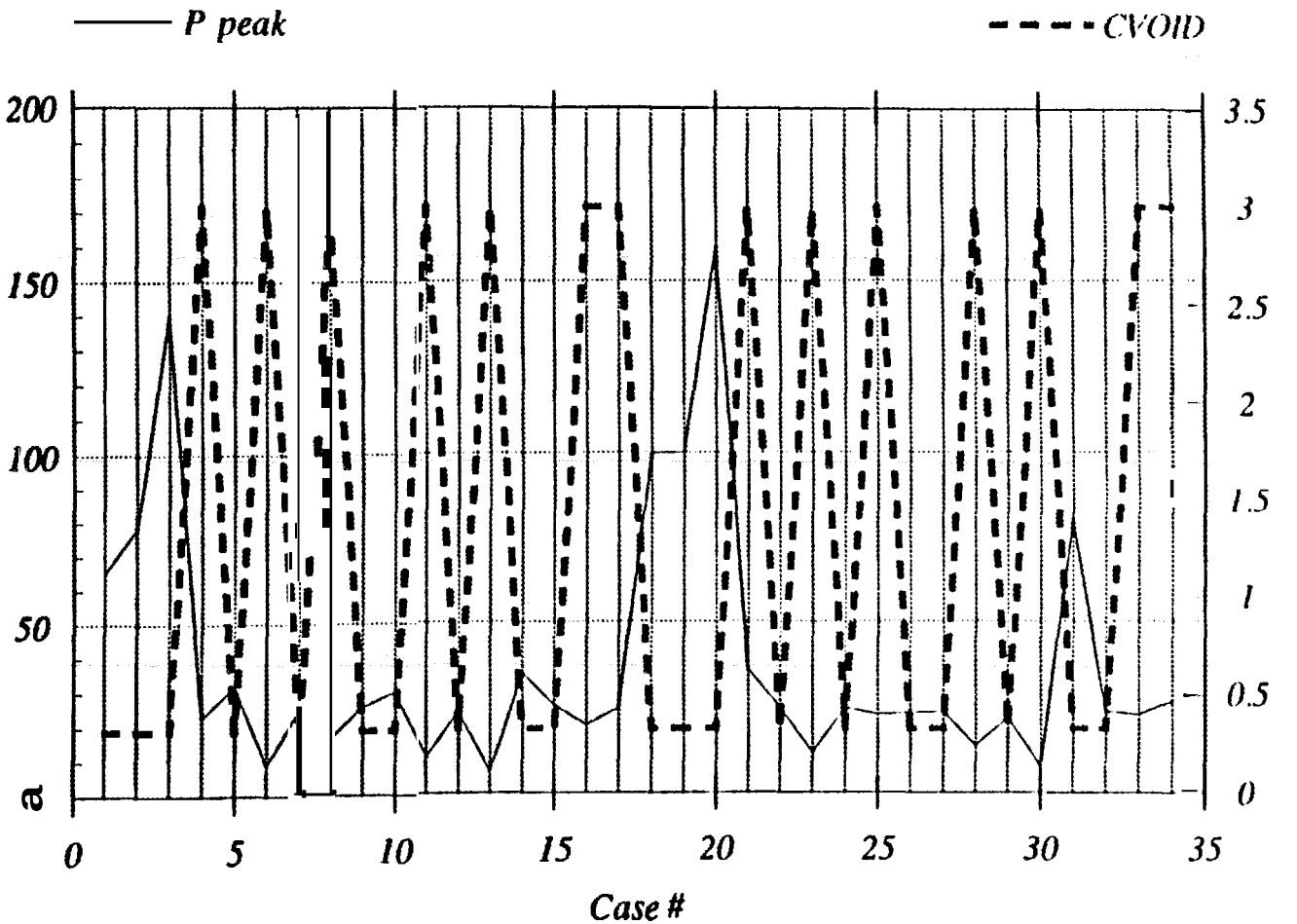

Fig. F.7 Variation of CVOID and Peak Pressure Magnitude for Cases 1 to 35

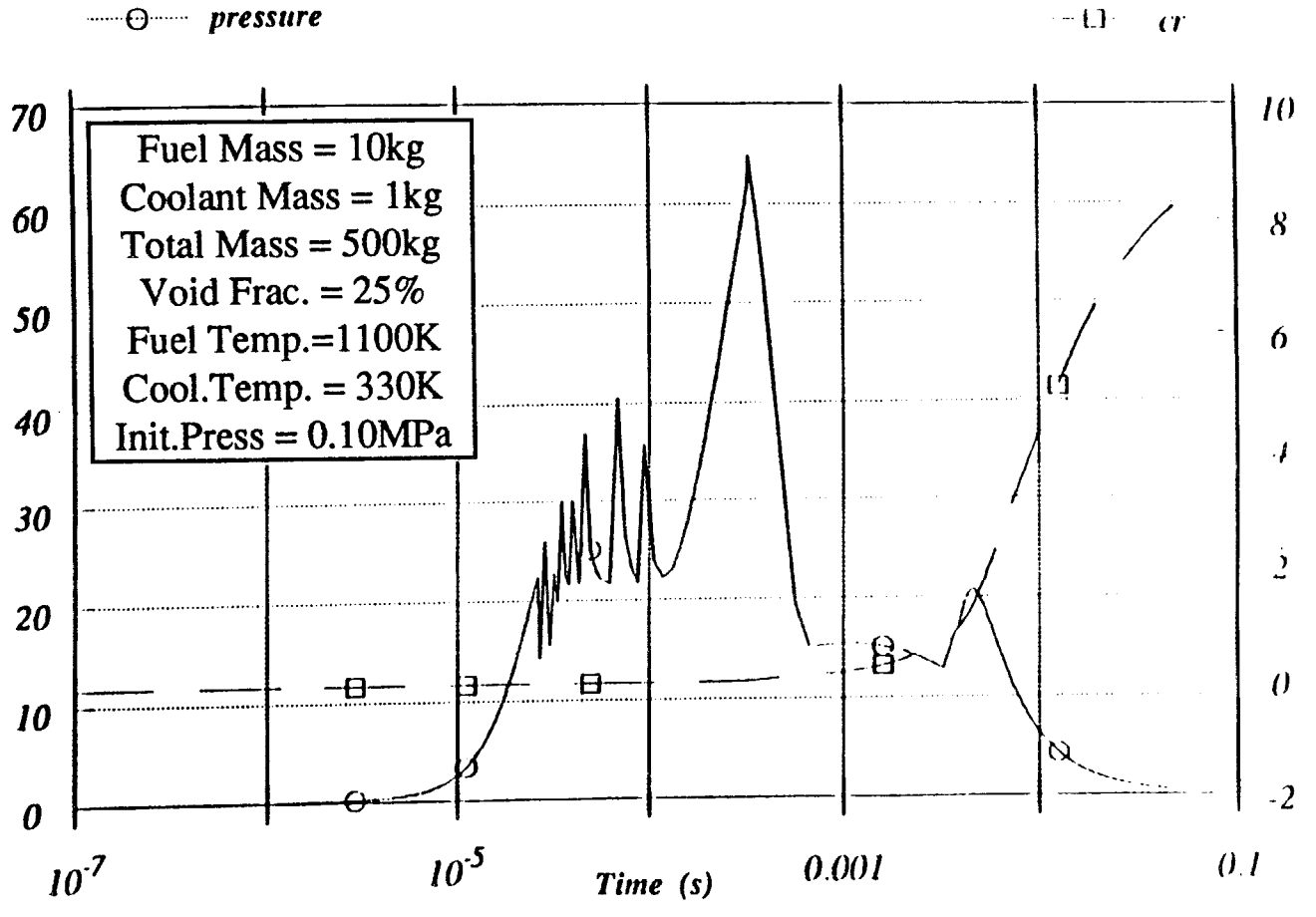

Fig. F.8 Variation of Peak Pressure and Conversion Ratio vs Time for Case 1

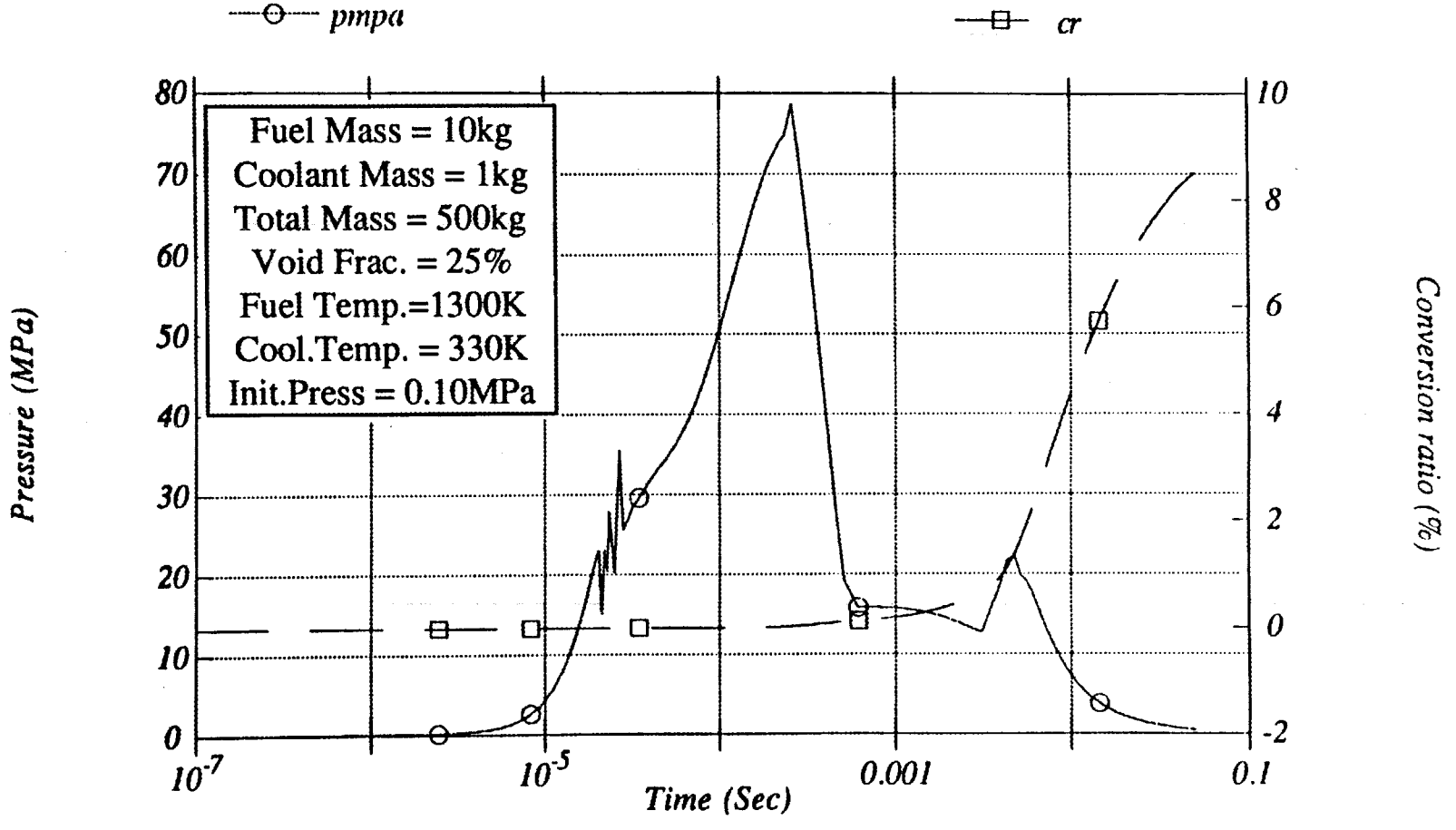

Fig. F.9 Variation of Peak Pressure and Conversion Ratio vs Time for Case 2

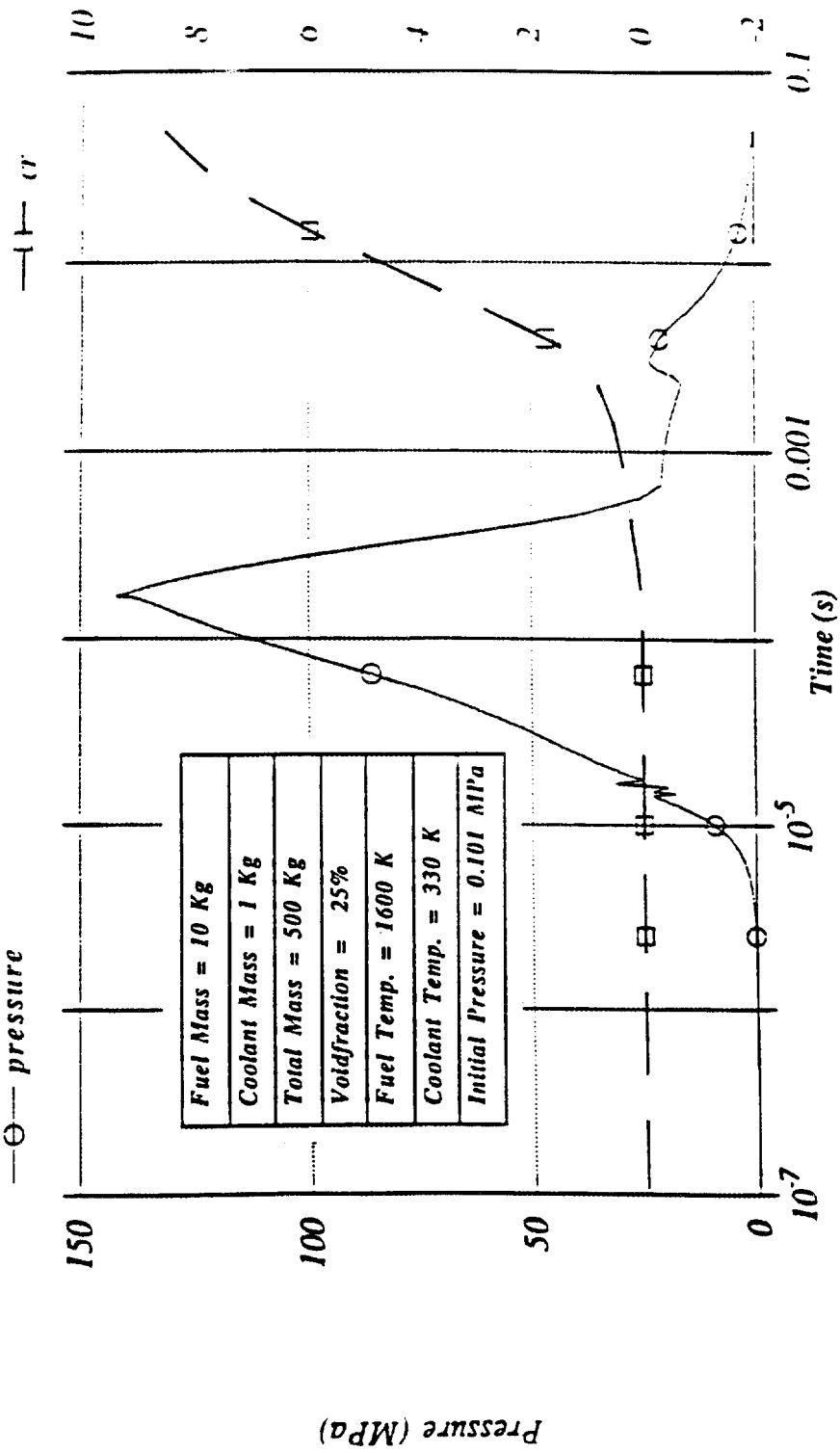

Fig. F.10 Variation of Peak Pressure and Conversion Ratio vs Time for Case 3

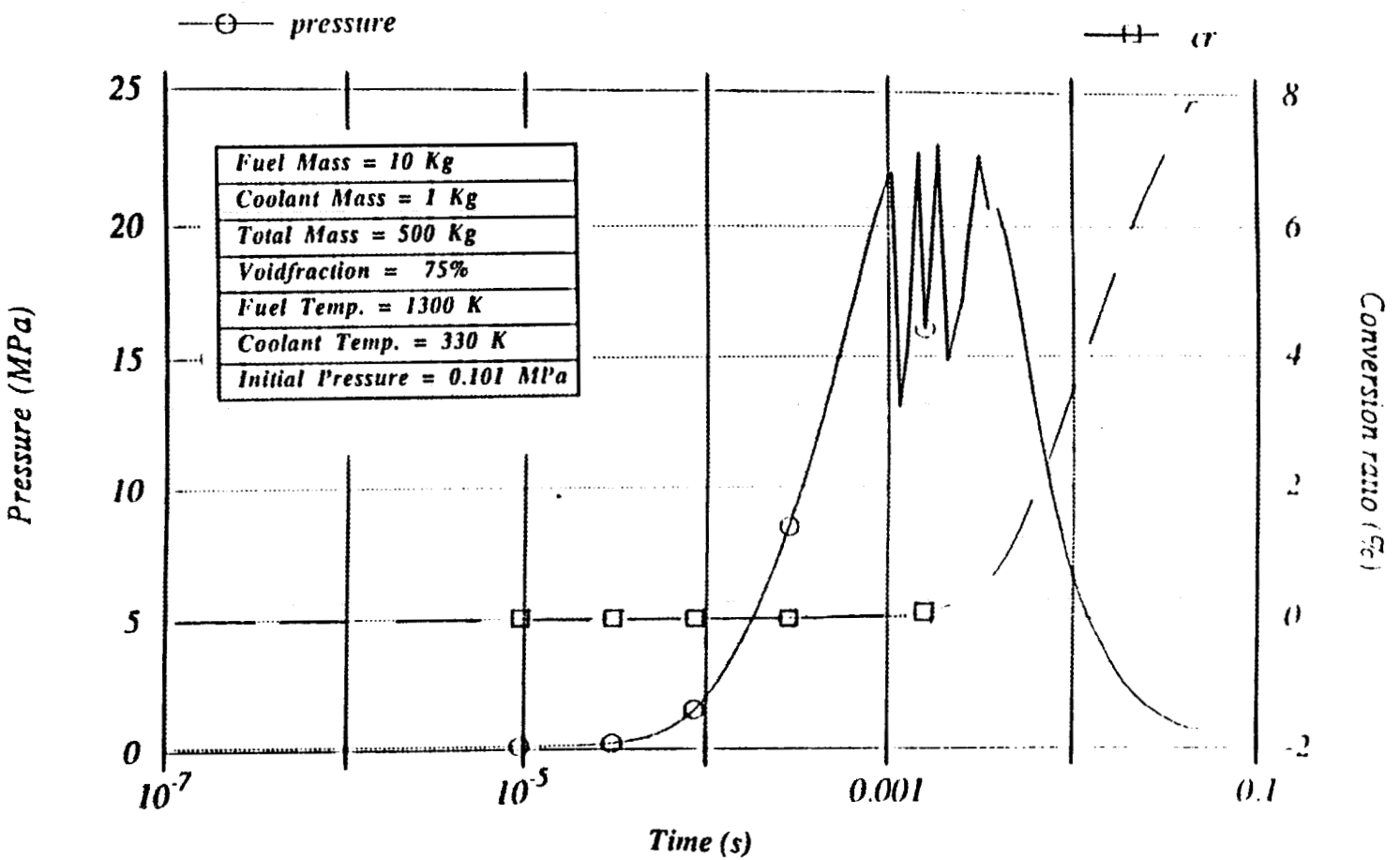

Fig. F.11 Variation of Peak Pressure and Conversion Ratio vs Time for Case 4

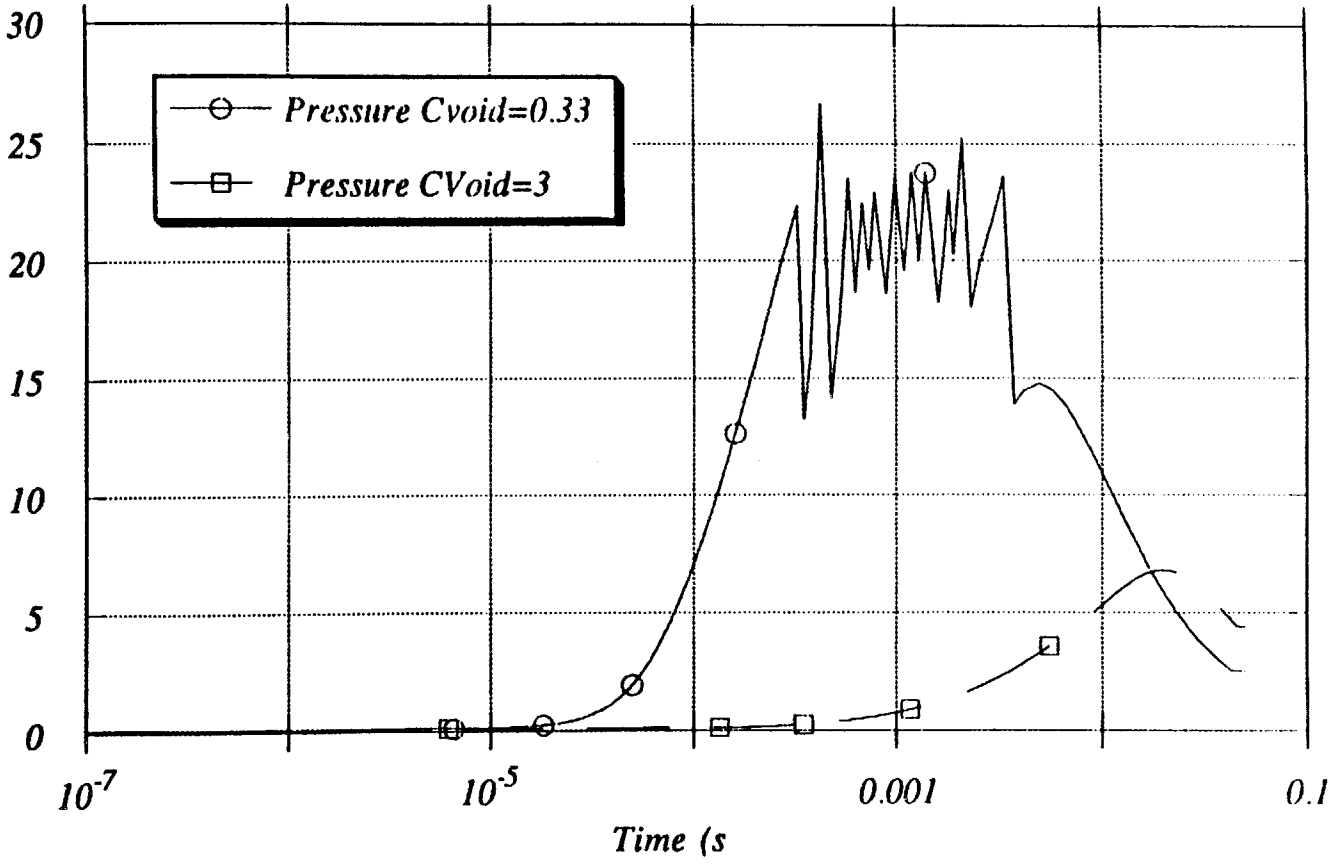

Fig. *F.12: FCI pressure caused by a single plate melt interacting with two channels of water.*

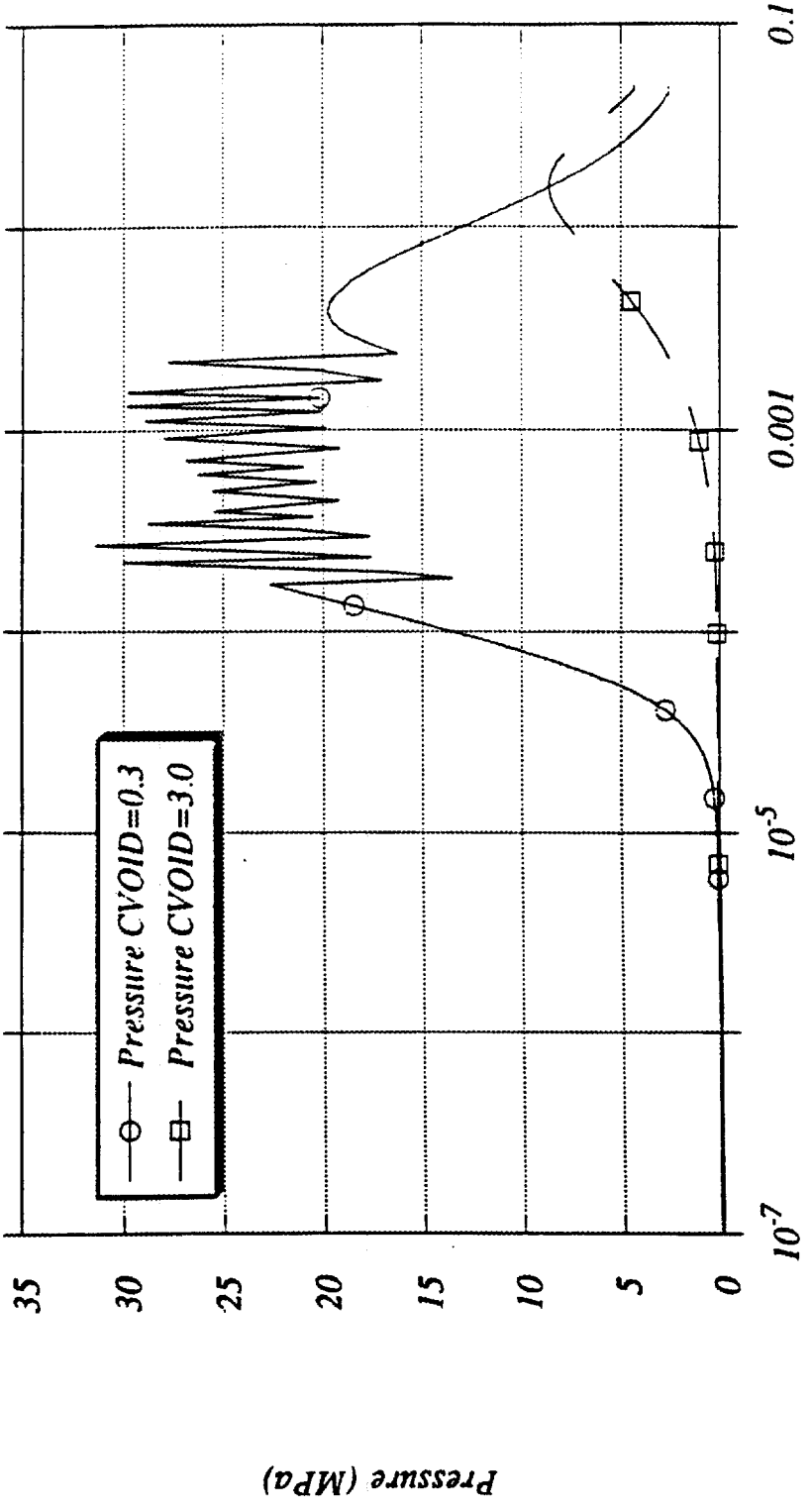

Fig. *F.13: FCI pressure caused by two plate melt interacting with three channels of water.*

APPENDIX G

Two-Dimensional Energetics and Fluid-Structure Interaction Modeling and Analysis With CTH

This appendix provides a summary of the modeling and analysis work performed for evaluating shock-wave physics, phase transformation, multimaterial motion, and fluid-structure interactions during the energetics phase of in-core steam explosions in the HFIR.

G.1 MODELING THE HFIR

The CTH computer program package[8] was used to analyze several postulated fuel-coolant-interaction (FCI) events with models of increasing levels in sophistication. Detailed modeling of the internals of the HFIR would require complex, three-dimensional (3-D) calculations that would be extremely time-consuming. Therefore, it was decided that a two-dimensional (2-D) representation of the HFIR vessel and internals should be attempted first to obtain relevant information and to conduct parametrics before embarking on a 3-D study.

The first model (Model 1) consisted of a tank of water, roughly the size of the HFIR pressure vessel but simplified to a right circular cylinder, containing a cylindrical annulus of beryllium to represent the reflector. In the second model (Model 2), we added an aluminum pipe inside the reflector, extending from the bottom of the tank to about 1.5 m above the reactor midplane to simulate the control plate supports below the core, the tank and some of the structure of the outer fuel annulus within the core, and the target tower supports and associated structures above the core. In the third model (viz., Model 3 - best-estimate representation), a cylindrical steel shell was added with a hemispherical lower section and a thick top plate to represent the pressure vessel and the top head. The three models are shown schematically in Fig. G.1(a-c). The points labelled L1, L2, and

so on, are locations where the pressure, temperature, density, and other variables are recorded at selected times during the calculation. A constant mesh spacing of 20 mm was used for all calculations. This assumption was checked with a smaller mesh spacing and found to be good enough in terms of providing an adequate degree of resolution.

Calculations were performed with CTH for the first two models with initial pressures of 3.2 MPa (normal operating pressure) and 0.1 MPa (atmospheric pressure), a uniform initial temperature of 330 K, and two choices of boundary conditions (viz., reflecting and absorbing), simulating the first 4 ms of an FCI event. To ensure that late time-reflected peak pressures have not been neglected, a calculation was done simulating the first 12 ms with the best-estimate model.

Since CTH calculations require significant computational resources, steam explosion energetics were studied for selected thermal energy deposition levels only. These levels were 7, 15, 31, 51, and 65 MJ to approximately represent HFIR core melt fractions participating in steam explosion events of about 7, 15, 31, 51, and 65%, respectively. The simpler models (viz., Model 1 and Model 2) were exercized with an energy deposition level of 15 MJ. For these cases, it was assumed that the explosion zone in the core region extends in radius from 80 mm to 180 mm, and in height from 80 mm below to 80 mm above the core midplane to represent an explosion zone comprising about 30% of the core volume. However, the best-estimate model (viz., Model 3) was exercized with energy levels of 7, 31, 51, and 65 MJ, for which the height of the explosion zone was increased to range from -120 mm to 120 mm in the axial direction (i.e., about 50% of the core volume) to account for larger core mass participation. The reason for using the same core volume for the explosion energy deposition with Model 3 was to allow for direct comparison of the relative effects of energy deposition levels. Based on thermal-to-mechanical energy conversion ratio variation, with time profiles predicted using the FCIMOD.ORNL code, a simple representation for the specific power, r(t), as a function of time was developed as

$$r(t) = 4\, r_o\, (t/t_o)\, (1 - t/t_o)\,, \qquad (G.1)$$

where t_o is the duration of the energy source and r_o is the peak specific power. Integrating this expression over the duration of the pulse and setting the result equal to the desired energy density allowed evaluation of the peak specific power r_o and to construct a table of specific power values at selected times, as required by CTH. Due to the particular nuance associated with the interpolation scheme utilized in CTH, combined with coolant flashing in the explosion zone, the actual energy input is somewhat different from the desired energy input (but not by much), as shown for a typical case in Fig. G.2.

Finally, as mentioned previously, two different boundary conditions were tested, viz., reflecting and absorbing. It was assumed that one can obtain upper-bound estimates of pressure by letting all boundaries be reflecting, and lower-bound estimates by letting the outer boundaries be absorbing (i.e., by permitting mass and energy transfer out of boundary).

Further details relating to modeling aspects and setting up of input parameters are given in Refs. 43 and 46.

G.2 SUMMARY OF RESULTS

Enormous quantities of information were generated from these evaluations for which details exist in calculational notes and in Refs. 43 and 46. Only selected results are presented here.

Selected results for pressurization using Model 1 (i.e., simple model without aluminum tube), with an initial pressure of 3.2 MPa and an energy source of 15 MJ, are shown in Figs. G.3(a-c) and G.4(a-c) for the reflecting and absorbing boundary conditions, respectively. As seen from these figures, even though the pressure buildup in

the explosion zone is similar for the two boundary conditions, the pressure buildup at the top head lower surface is considerably lower for the case with an absorbing boundary condition. It clearly underscores the importance of appropriate modeling of boundary conditions.

Selected results for pressurization using Model 2 (i.e., simple model with aluminum tube), with an initial pressure of 3.2 MPa and an energy source of 15 MJ, are shown in Figs. G.5(a-c) and G.6(a-c) for the reflecting and absorbing boundary conditions, respectively. The effect of absorbing versus reflecting boundary conditions is similar to that seen earlier with Model 1. In addition, we see that the effect of the aluminum tube is to increase the pressure buildup in the explosion zone, but to reduce the pressure buildup at the top head lower surface. This is attributed to greater resistance to energy dissipation from the explosion zone, which causes a higher pressure buildup there. However, the aluminum tube material also acts as an energy absorbing medium that assists in reducing the shock wave energy levels at the various vessel surfaces.

Calculations were also performed with the various models using the initial system pressure as 0.1 MPa (i.e., atmospheric pressure). However, it was found that both initial system pressures produce about the same pressure rise from initial conditions.

Additional scoping calculations were performed to evaluate the impact of lengthening the time span over which the energy deposition occurs in the explosion zone (from 1 to 2 ms). No discernible differences were observed.

Upon completion of scoping calculations with the simplified models (i.e., Models 1 and 2), the best-estimate model, viz., Model 3 was exercised. Because of the significantly increased machine time requirements for analyzing Model 3, scoping calculations were not performed with different boundary conditions. It was judged that for best-estimate calculations the absorbing boundary condition should be used. As mentioned previously, runs were made with energy deposition levels of 7, 31, 51, and 65 MJ. The cases with 7 and 31 MJ of thermal energy inserted in the explosion zone over 1

ms did not result in sustained pressure levels in excess of failure levels for the vessel or top head (viz., about 21 MPa on the average for greater than 0.6 ms for the reactor vessel, and more than 26 MPa required for failure of top head bolts, as described in Appendixes I and J). The case with 31 MJ of energy deposition does give pressure pulses > 26 MPa in the centerline region right under the top head. However, these are peak pulse magnitudes and do not last for more than about 0.5 ms. In addition, the pulse magnitude decreases significantly from the centerline to the vessel wall interface region, with the result that vessel failure pressure level (of 21 MPa lasting for more than 0.6 ms) is not reached. These attributes are clearly seen in Figs. G.7 through G.10 for the two cases under consideration. An important aspect of the situation for these two cases relates to the fact that the mechanical integrity of the aluminum shroud tube is not affected. This accounts to a large measure for the significant variation in pressure pulse magnitudes from the top head centerline to the vessel wall-top head interface. For these instances, the shroud acts as a sort of gun barrel, directing pressure waves upwards, and thus limits the degree of dissipation in the radial direction. It also serves to act as a kind of organ pipe giving rise to significant ringing effects as seen in the high frequency pressure waves being built up as the transient progresses and reflected waves tend to overlap.

The two additional cases with 51 and 65 MJ energy insertion did cause the aluminum shroud to rupture from the FCI energetics. This is seen in Figs. G.11 and G.12 for these two cases. The rupture of the shroud allows for increased dissipation of explosion energy in the radial direction, and also leads to significant reduction or even elimination of the buildup of the above-mentioned "organ-pipe" effect. Salient pressure pulse histories for these two cases are shown in Figs. G.13 and G.14. Note from Figs. G.13 and G.14 that the pressure pulse magnitudes underneath the top head display much less variation in the radial direction than that seen for the earlier cases where the shroud had not ruptured. Note that for the 51- and 65-MJ cases, the average pressure

below the top head and in the vicinity of the reactor vessel is larger than the required 21 MPa pressure (lasting more than 0.6 ms) required for vessel rupture from fracture, and, thereafter, for generation of an energetic missile. These results would indicate that the energy level required to cause imminent vessel failure would amount to a value between 31 and 51 MJ. Engineering judgment indicates that this value is likely around the 40-MJ energy level. For the 51-MJ case, the average pressure over the top head under surface amounts to about 30 MPa lasting about 3 ms, whereas the corresponding values for the 65 MJ case are in the vicinity of about 35 MPa also lasting for around 3 ms. Further details are given in Ref. 46.

If we estimate that an average pressure (P_{av}) acts on the top head for a given time (τ) after the bolts are broken, the initial upward velocity of the top head is estimated as

$$Vo = \frac{P_{av} A \tau}{\rho_s A H}, \qquad \text{(G.2)}$$

where H, the thickness of the top head, is 0.36 m; ρ_S, the density of the steel is 8000 kg/m^3, and τ, the time over which the force acts (beyond the about 0.6 ms required for failing the vessel or bolts via fracture). For the two high energy cases, the initial velocity is then calculated as

Energy (MJ)	P_{av} (MPa)	τ (ms)	Vo (m/s)
51	30	3.0	31
51	30	2.4	25
65	35	3.0	37
65	35	2.4	30
65	40	2.4	35

Additional details of the calculational results relating to relative surface displacements, material motions, phase transformations, etc., are given in Ref. 46.

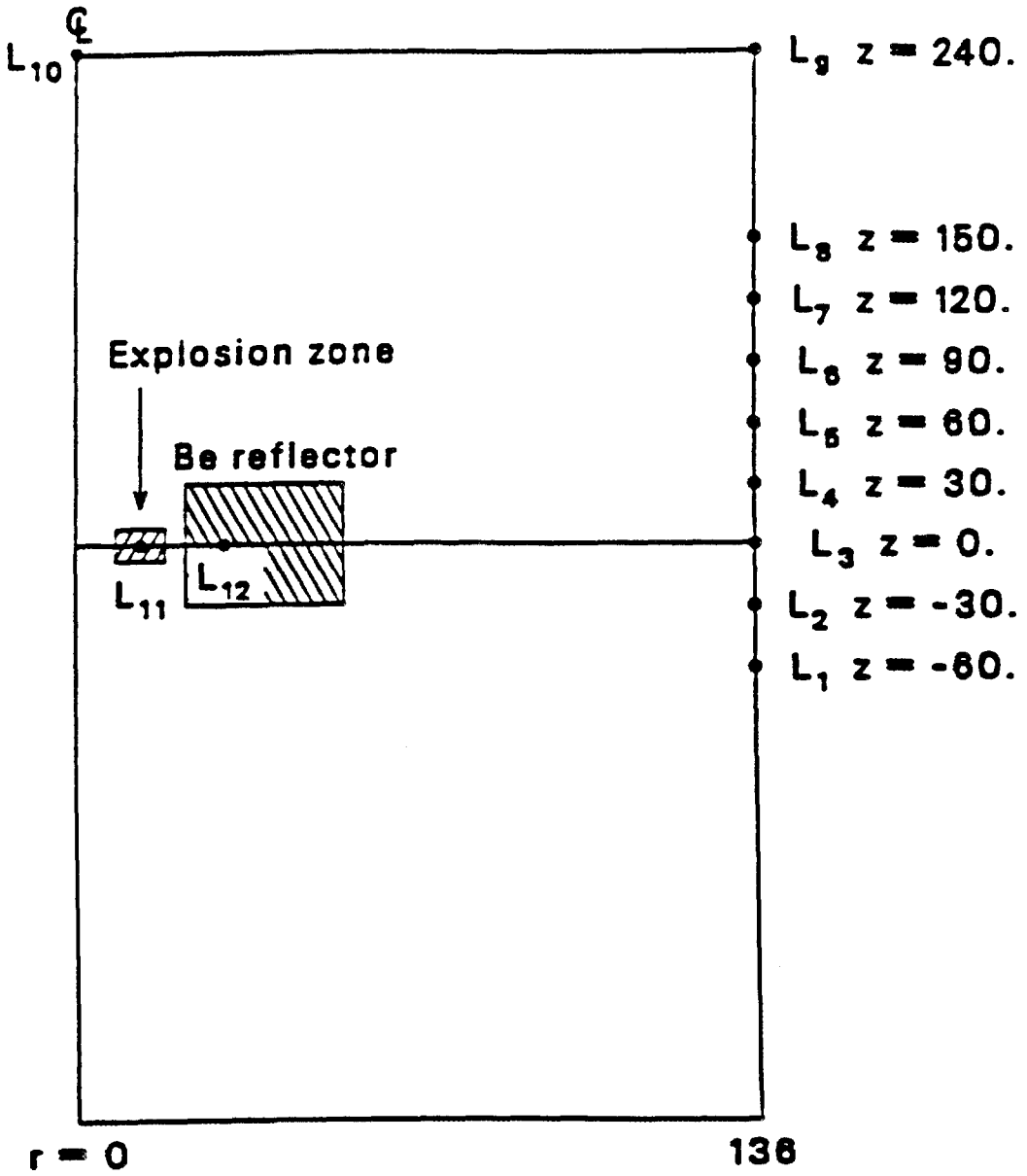

All dimensions in centimeters

Initial Temperature 330 K, Initial Pressure 3.2 MPa

Fig. G.1a Model 1 of HFIR for CTH Calculations

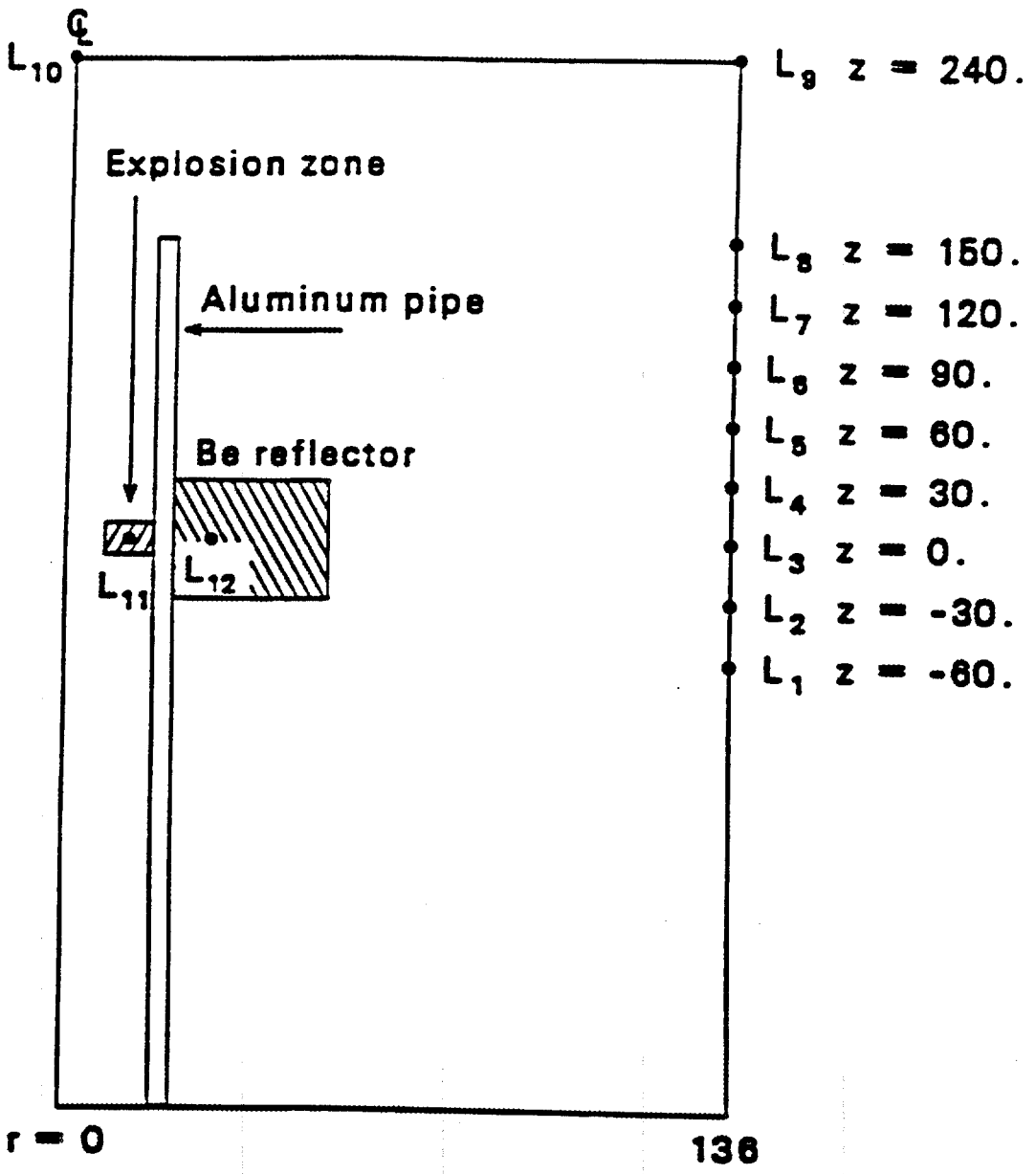

All dimensions in centimeters

Initial Temperature 330 K, Initial Pressure 3.2 MPa

Fig. G.1b Model 2 of HFIR for CTH Calculations

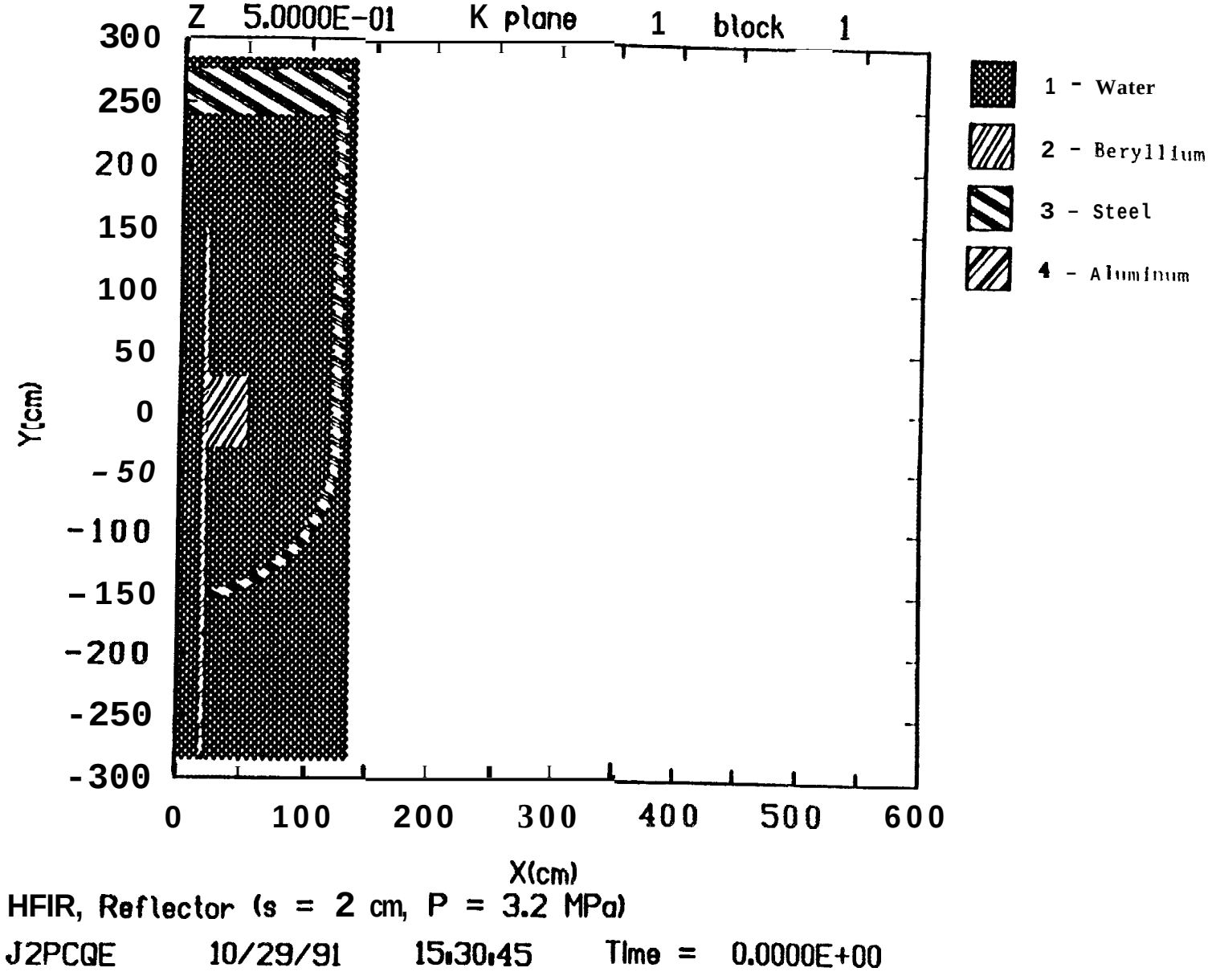

Fig. G.1c Model 3 of H for CTH Calculations

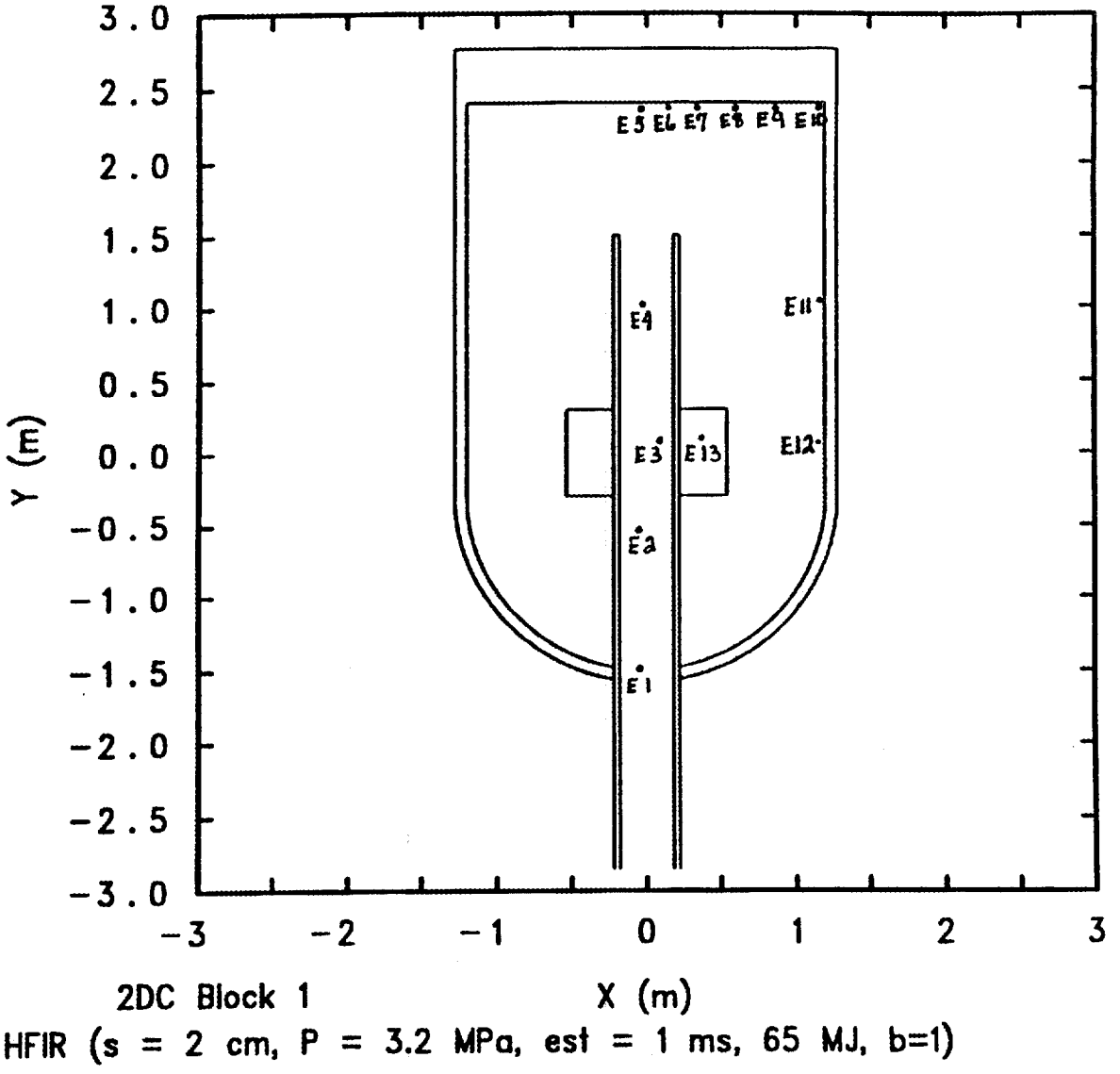

Fig. G.1d Model 3 of HFIR for CTH Calculations (Location of Lagrangian Points)

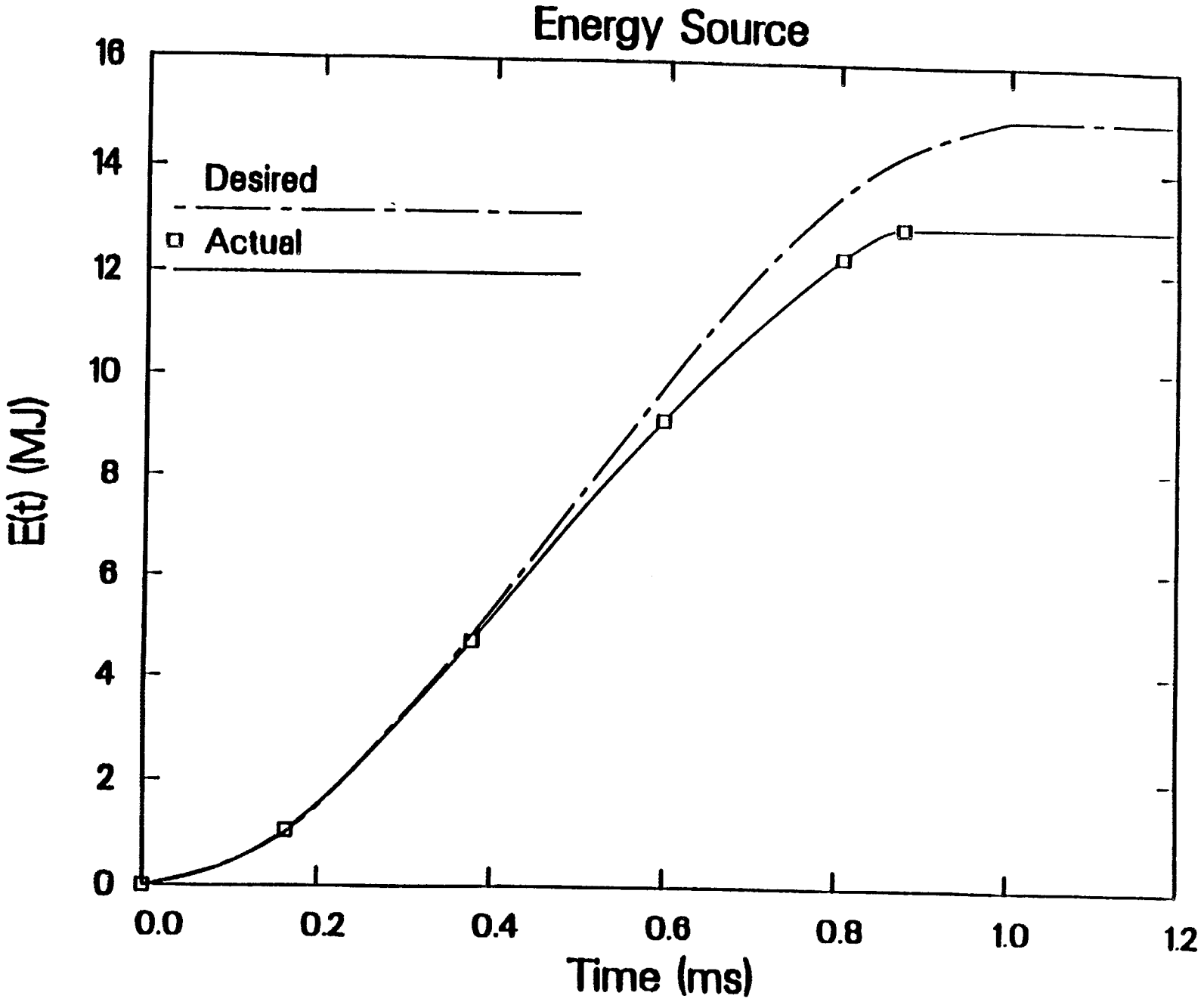

Fig. G.2 Computed and Desired Energy Source Variations vs Time for CTH Calculations

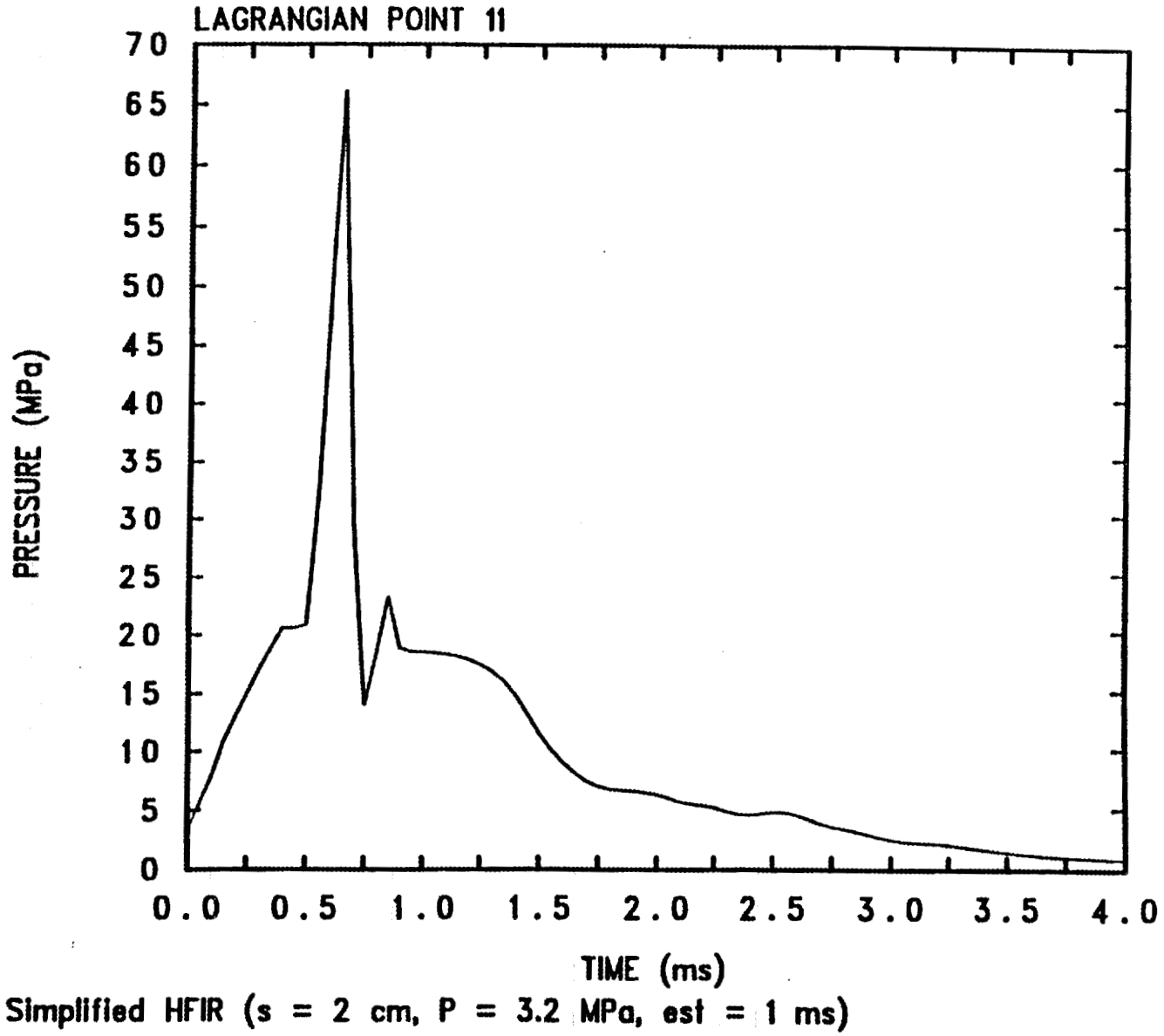

Fig. G.3a Variation of Pressure vs Time for Model 1 (Reflecting Boundary Condition, Explosion Zone)

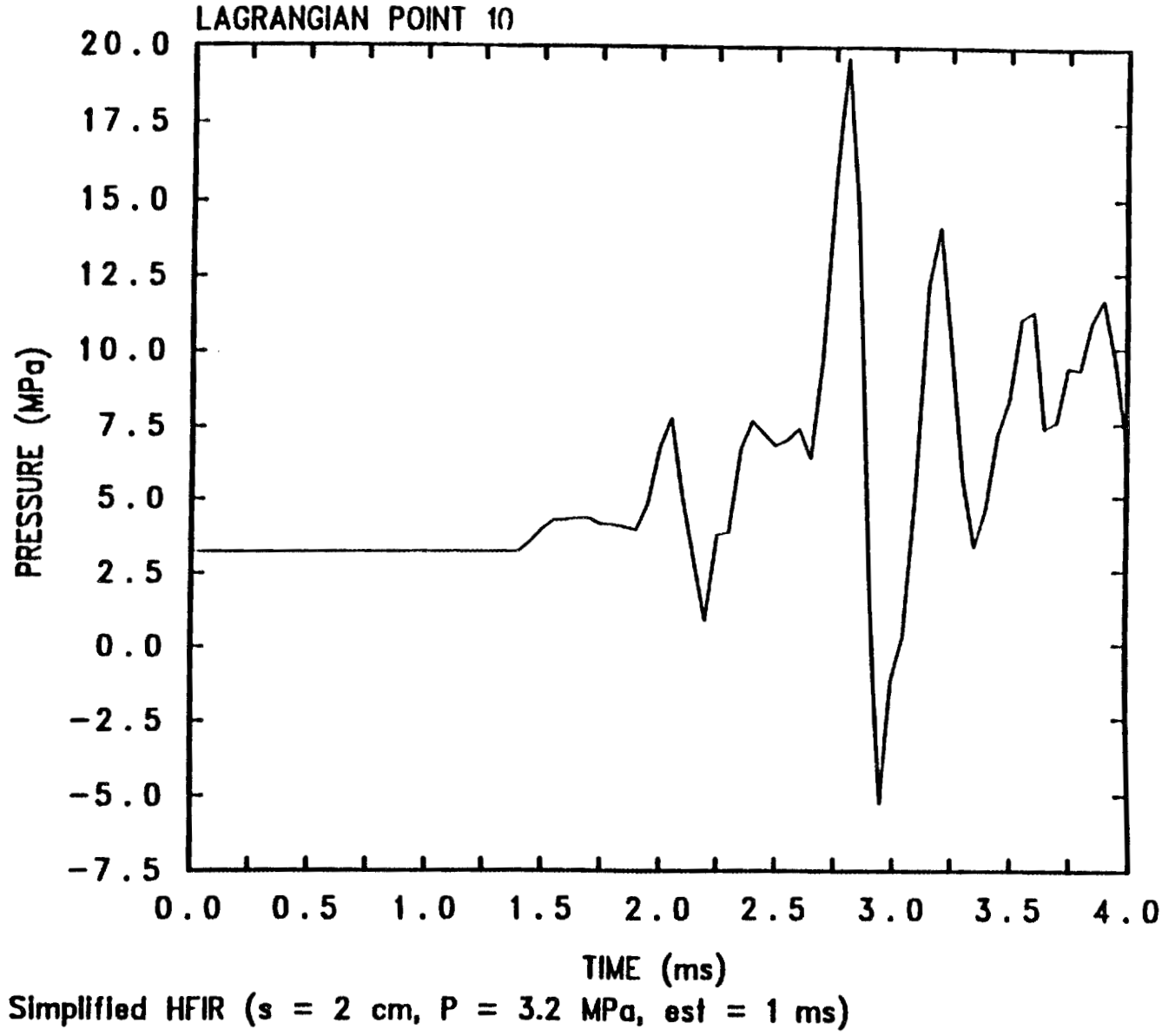

Fig. G.3b Variation of Pressure vs Time for Model 1 (Reflecting Boundary Condition, Top Head Lower Surface Reactor Centerline)

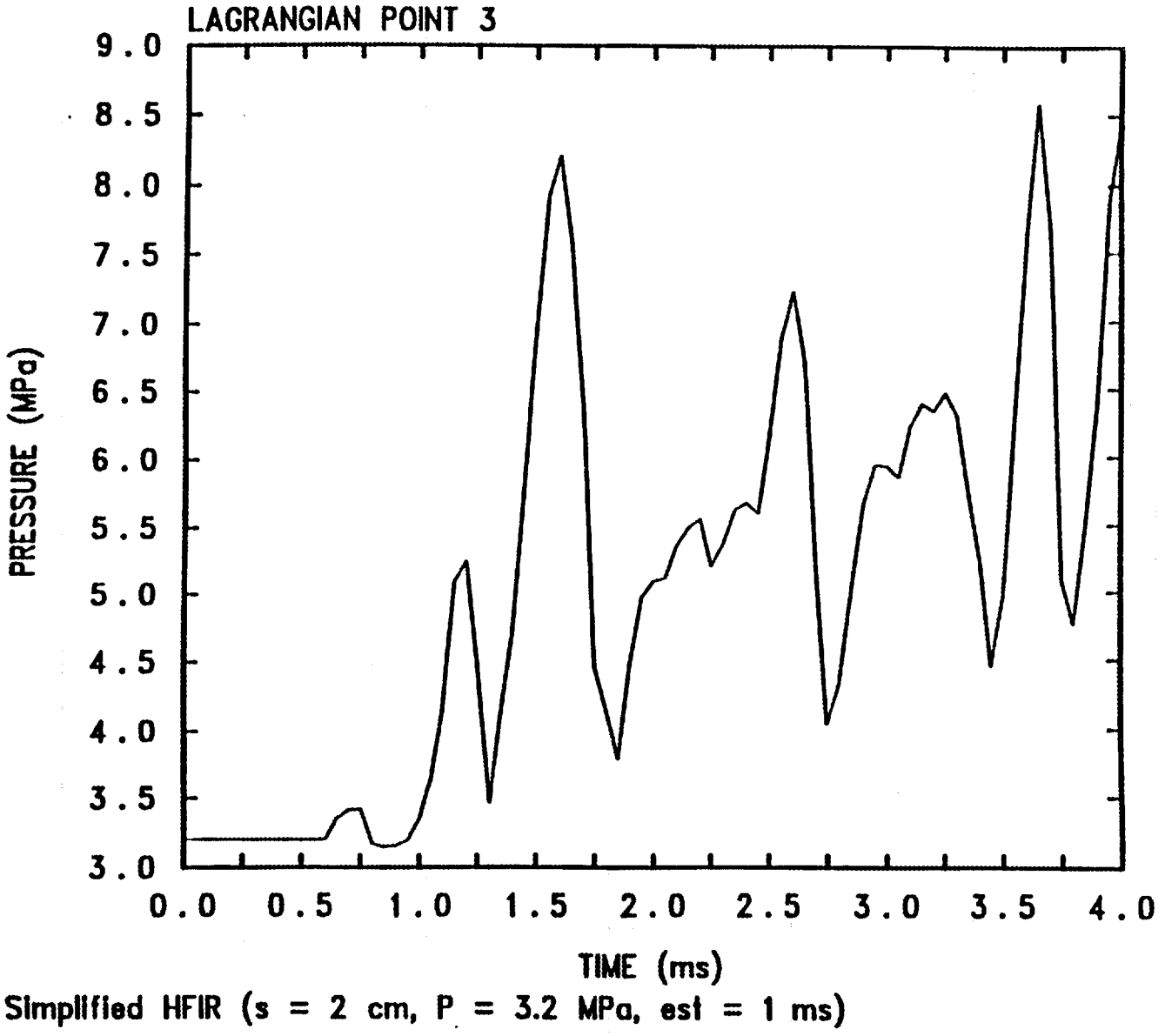

Fig. G.3c Variation of Pressure vs Time for Model 1 (Reflecting Boundary Condition, Reactor Midplane Pressure Vessel Inner Surface)

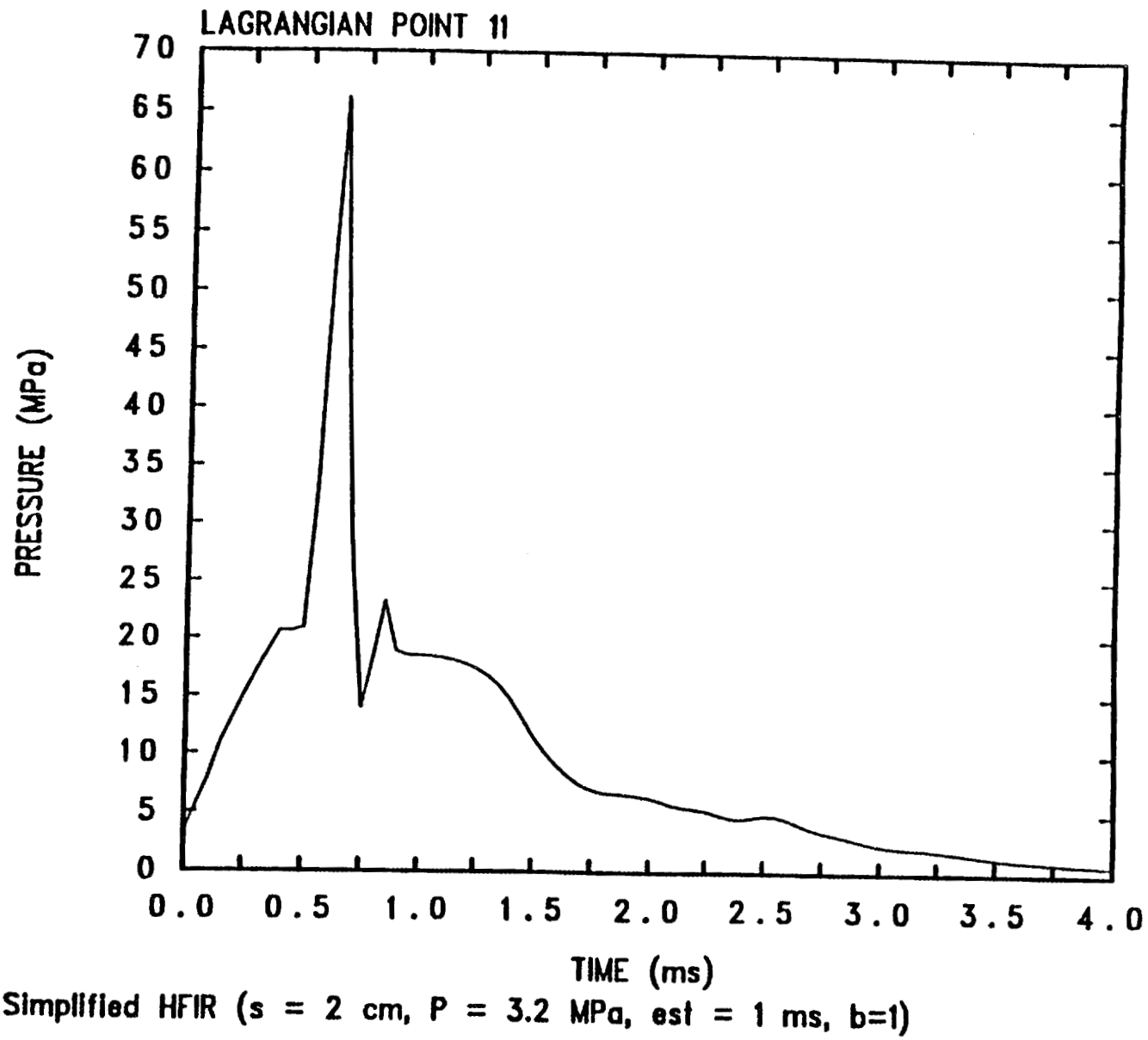

Fig. G.4a Variation of Pressure vs Time for Model 1 (Absorbing Boundary Condition, Explosion Zone)

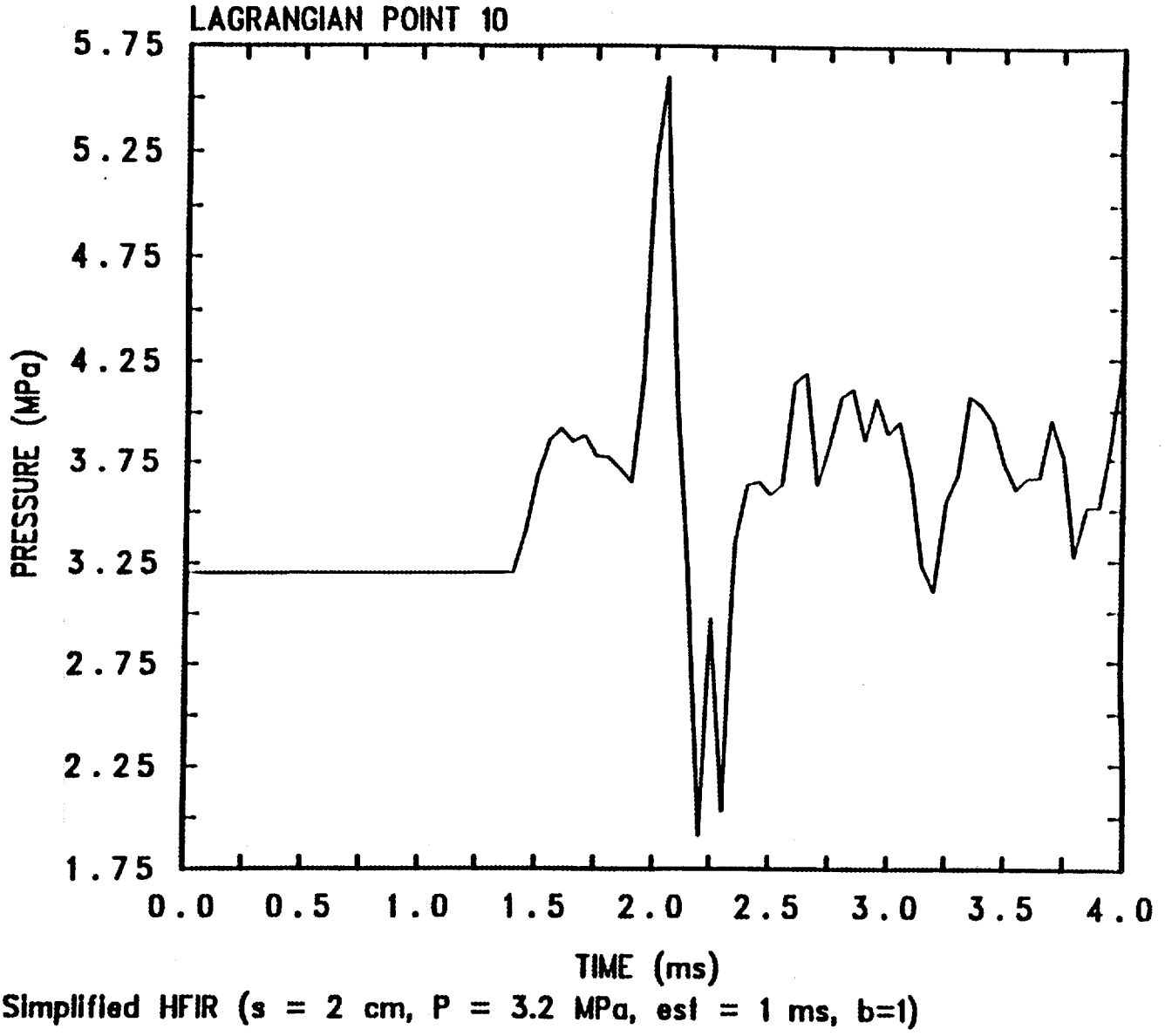

Fig. G.4b Variation of Pressure vs Time for Model 1 (Absorbing Boundary Condition, Top Head Lower Surface Reactor Centerline)

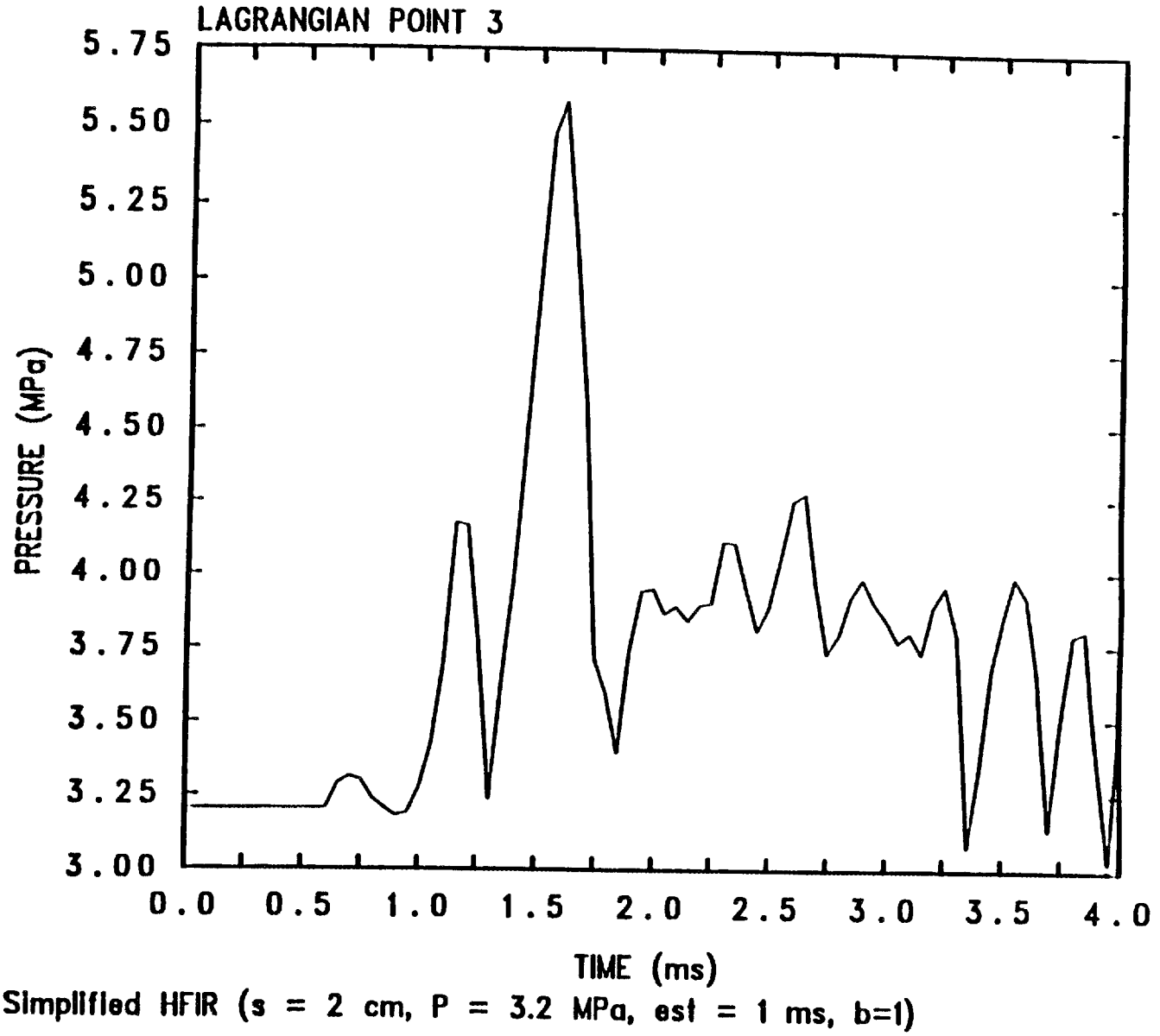

Fig. G.4c Variation of Pressure vs Time for Model 1 (Absorbing Boundary Condition, Reactor Midplane Pressure Vessel Inner Surface)

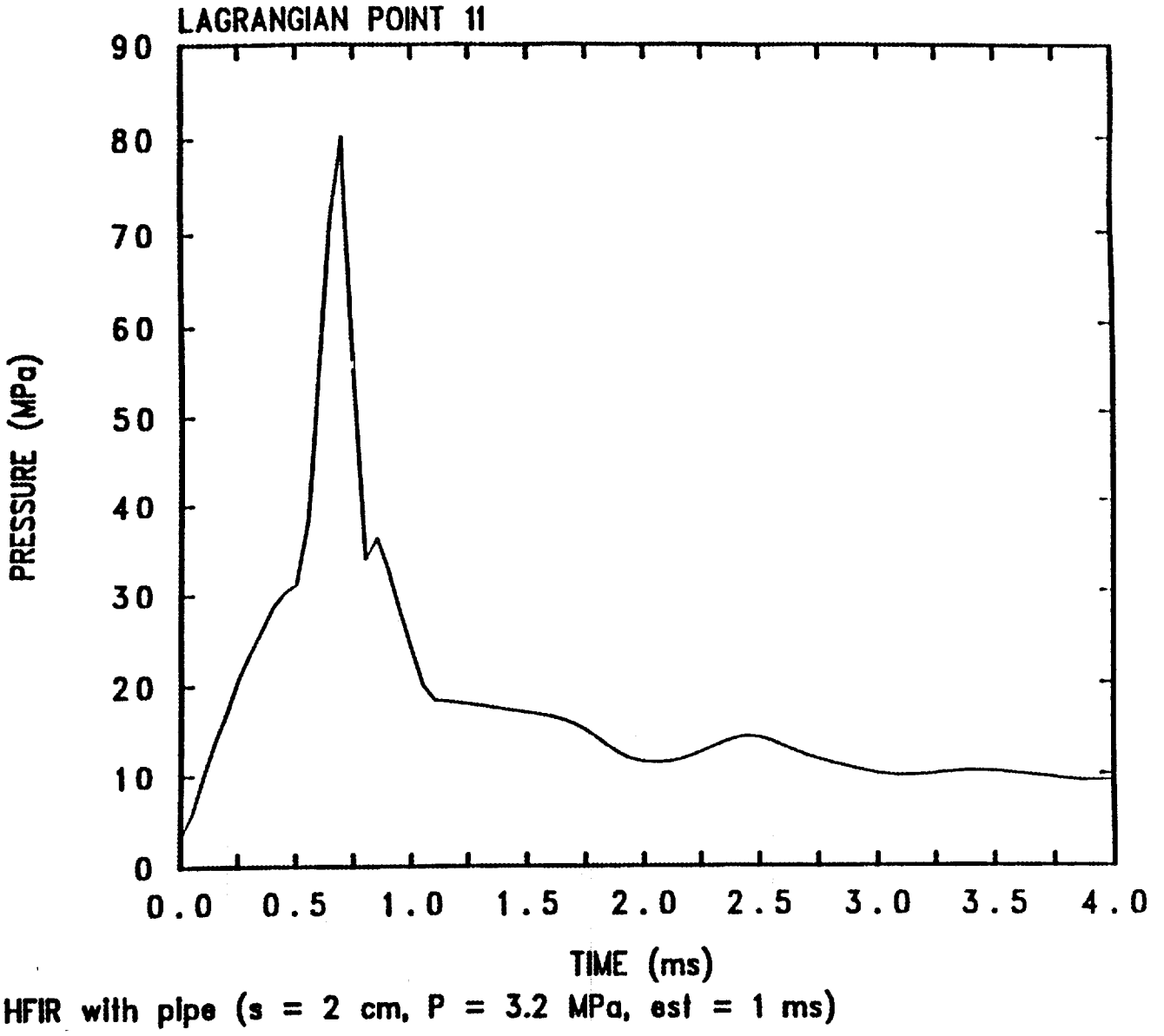

Fig. G.5a Variation of Pressure vs Time for Model 2 (Reflecting Boundary Condition, Explosion Zone)

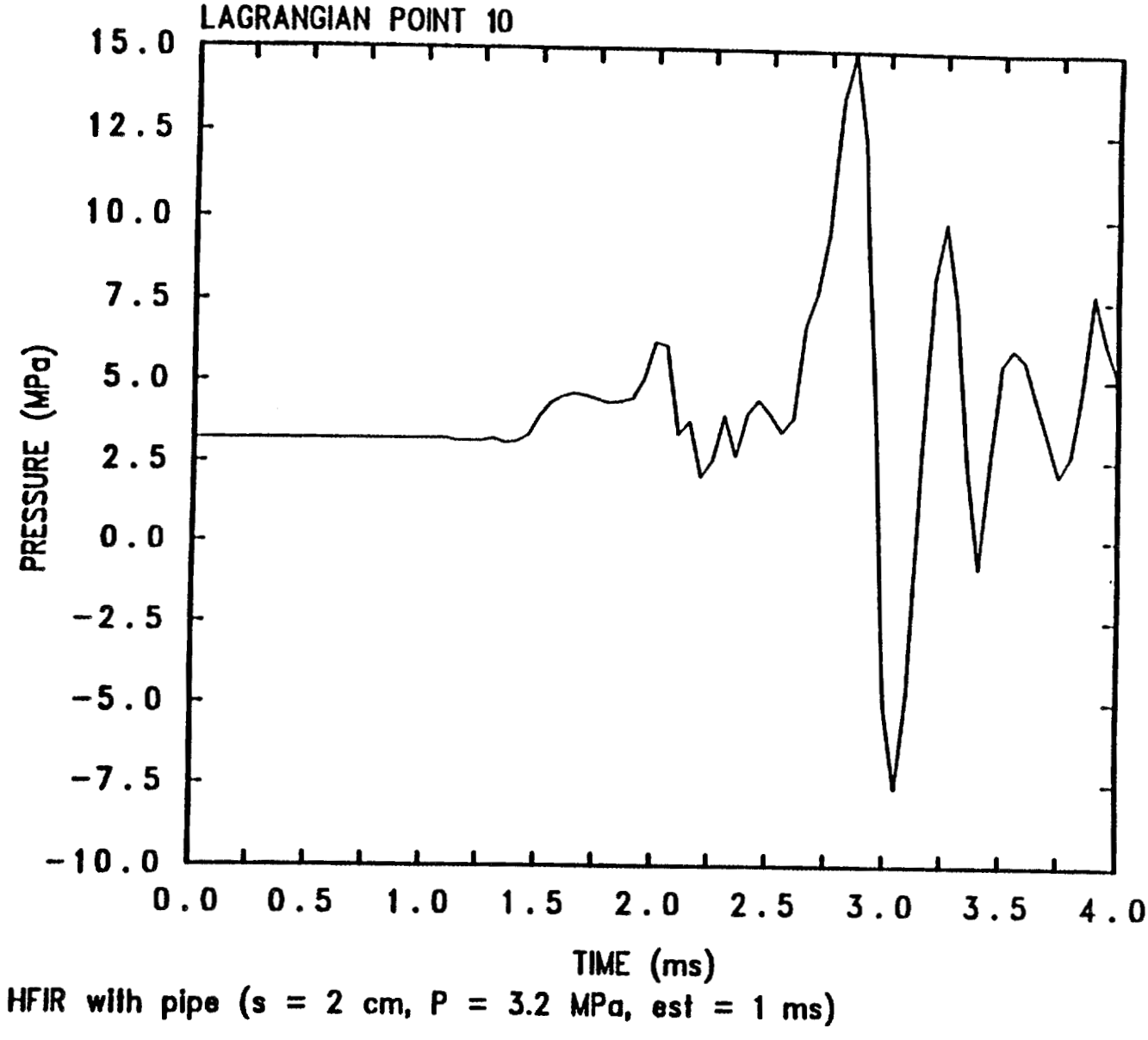

Fig. G.5b Variation of Pressure vs Time for Model 2 (Reflecting Boundary Condition, Top Head Lower Surface Reactor Centerline)

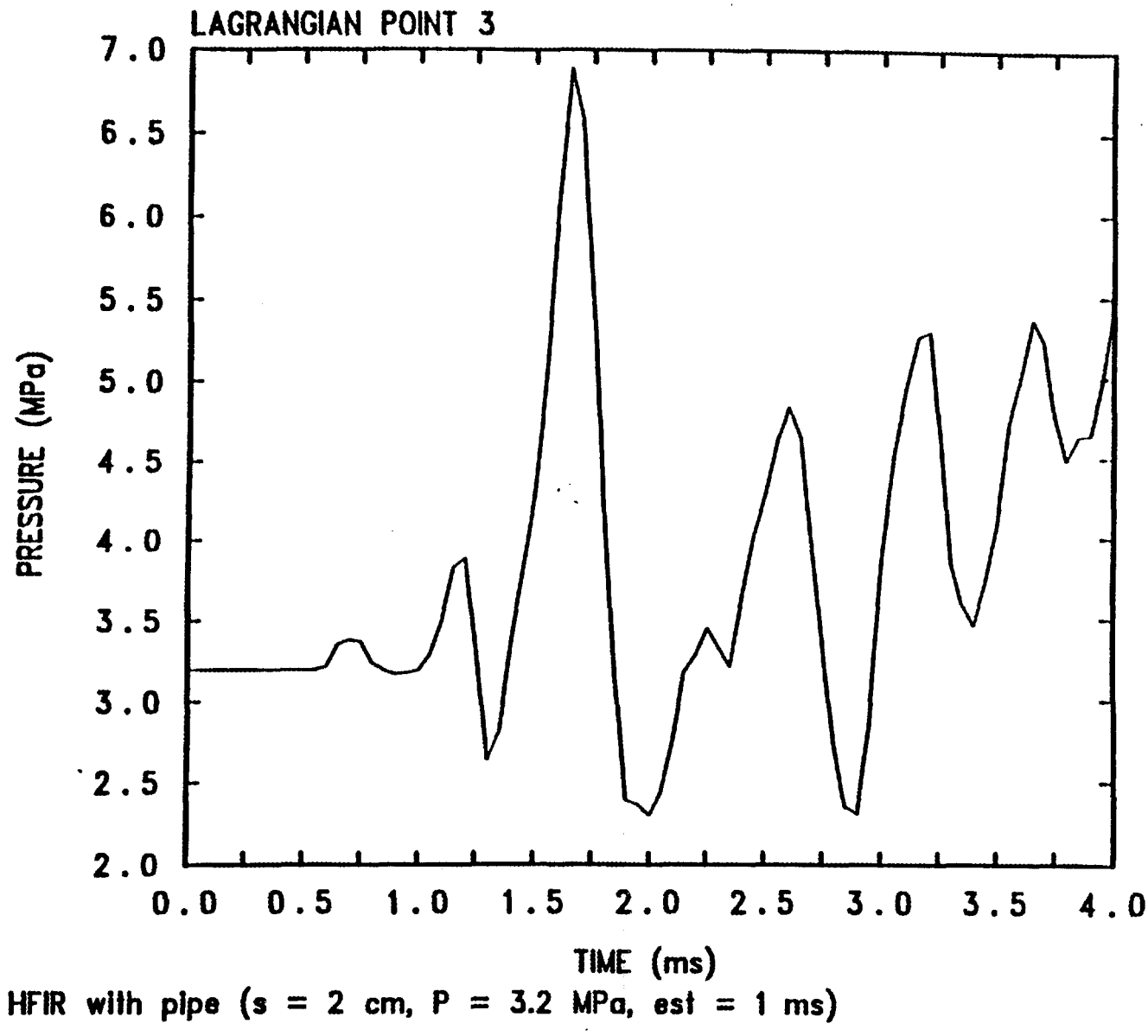

Fig. G.5c Variation of Pressure vs Time for Model 2 (Reflecting Boundary Condition, Reactor Midplane Pressure Vessel Inner Surface)

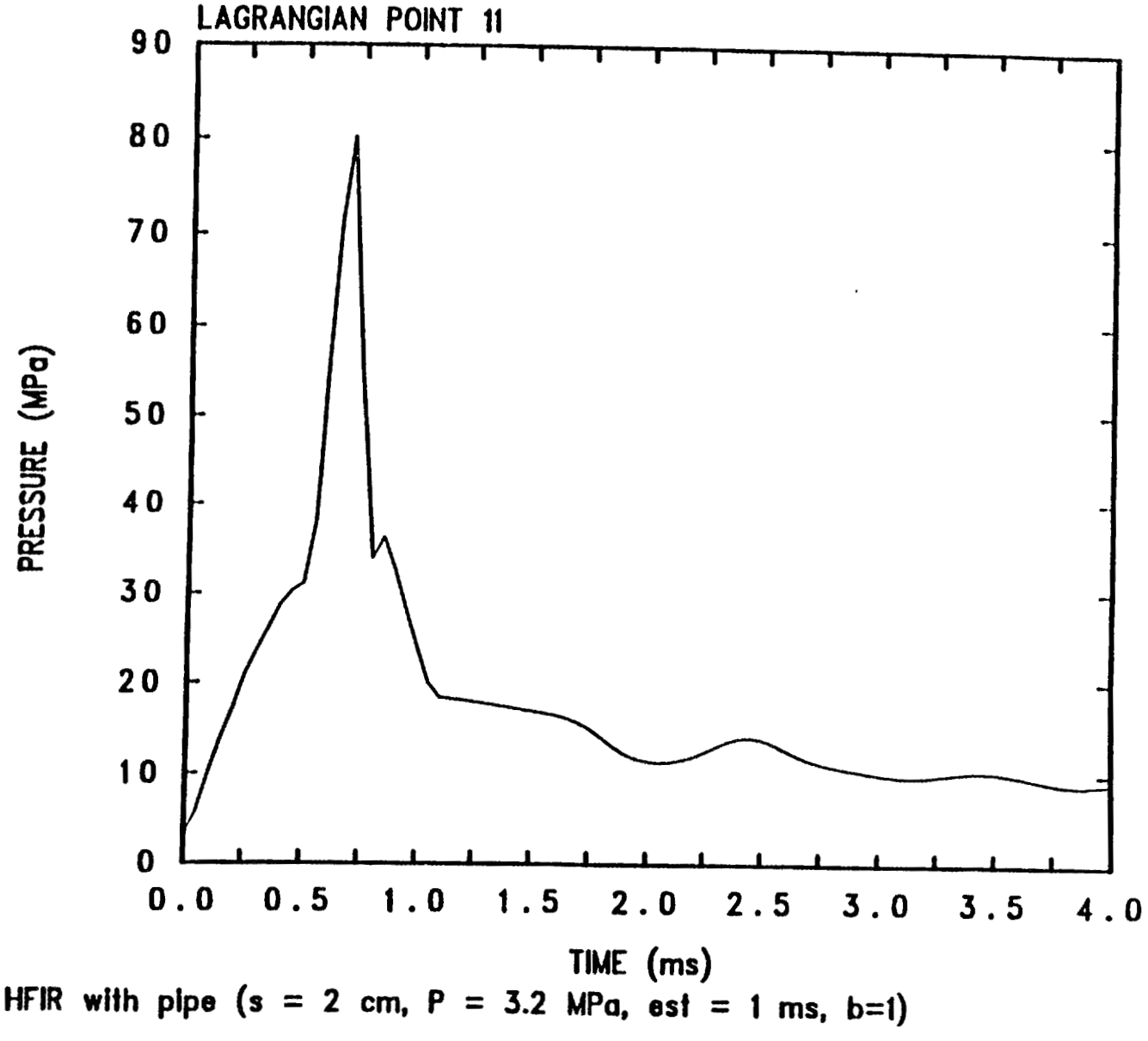

Fig. G.6a Variation of Pressure vs Time for Model 2 (Absorbing Boundary Condition, Explosion Zone)

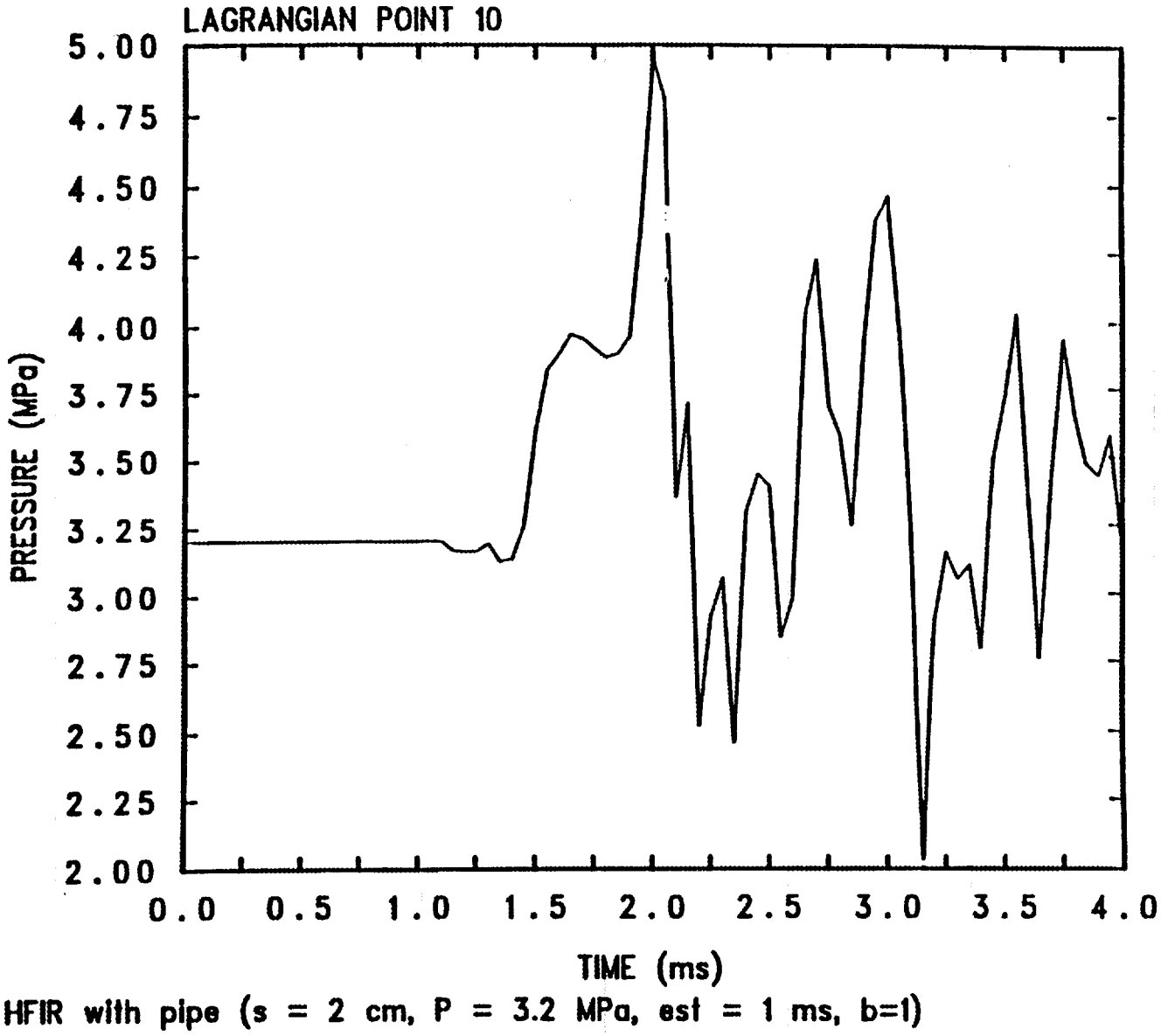

Fig. G.6b Variation of Pressure vs Time for Model 2 (Absorbing Boundary Condition, Top Head Lower Surface Reactor Centerline)

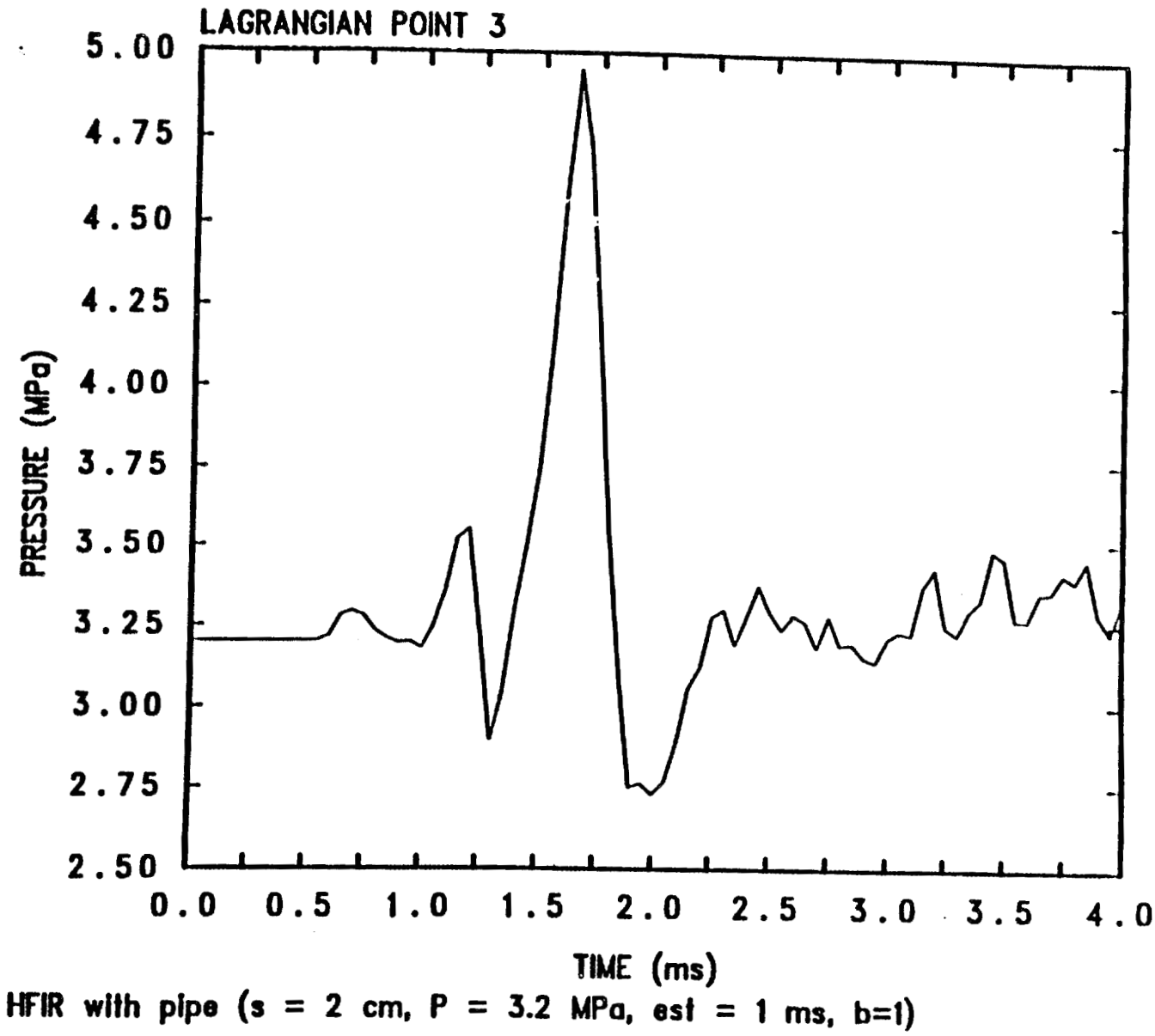

Fig. G.6c Variation of Pressure vs Time for Model 2 (Absorbing Boundary Condition, Reactor Midplane Pressure Vessel Inner Surface)

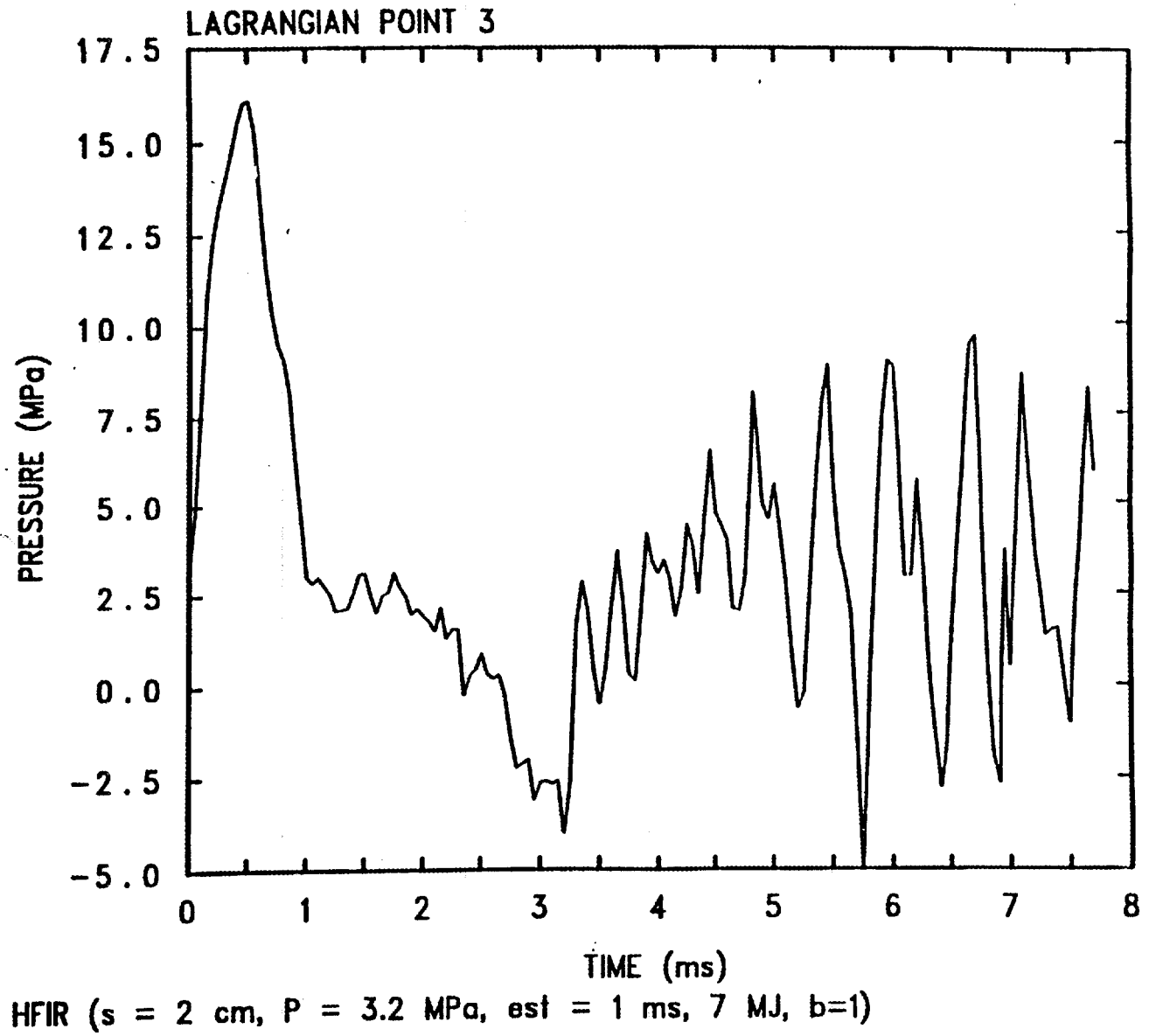

Fig. G.7 Variation of Pressure vs Time in Explosion Zone for Model 3 (Lagrangian Point 3, 7 MJ Case)

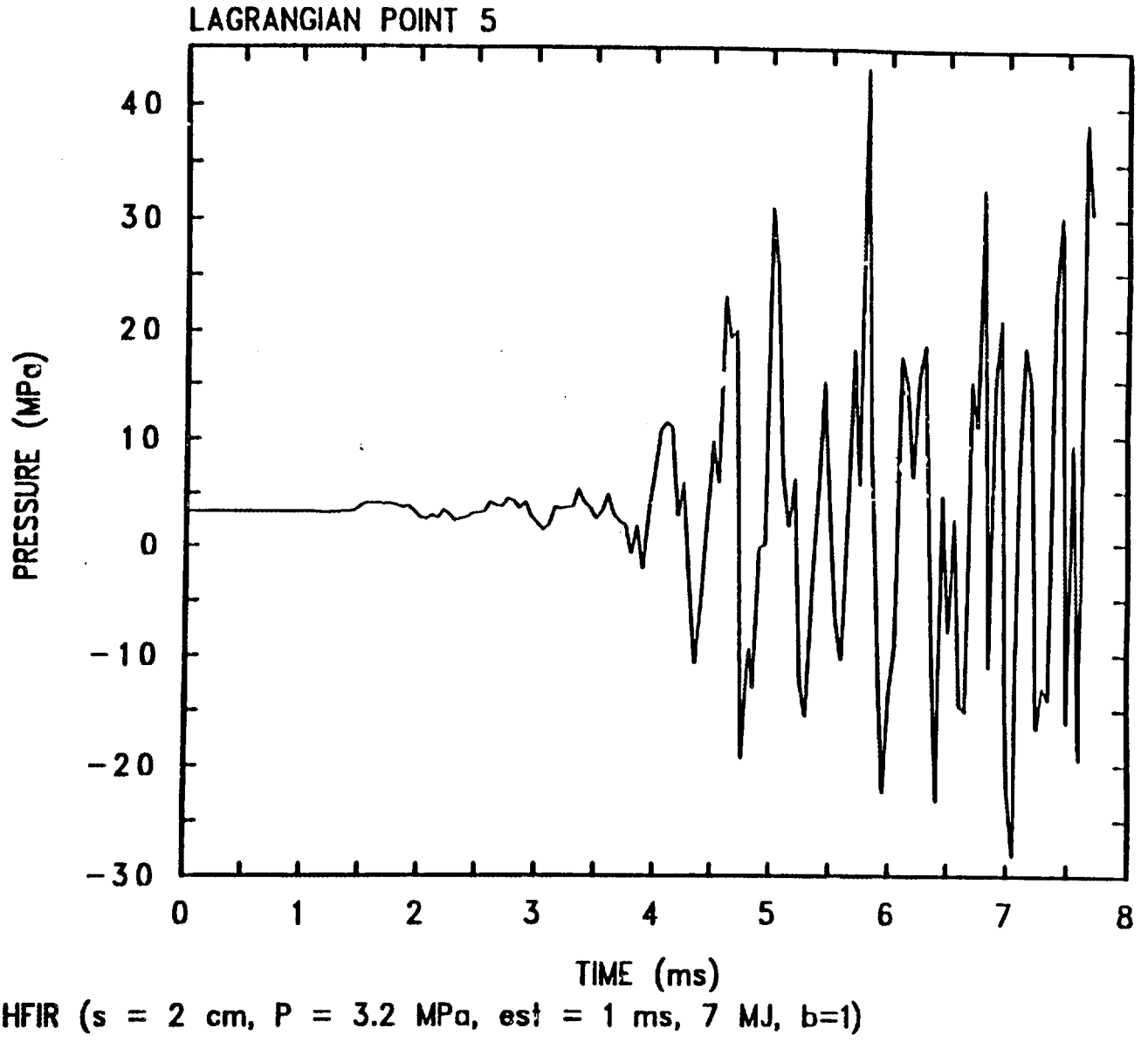

Fig. G.8a Variation of Pressure vs Time for Model 3 (Lagrangian Point 5, 7 MJ Case)

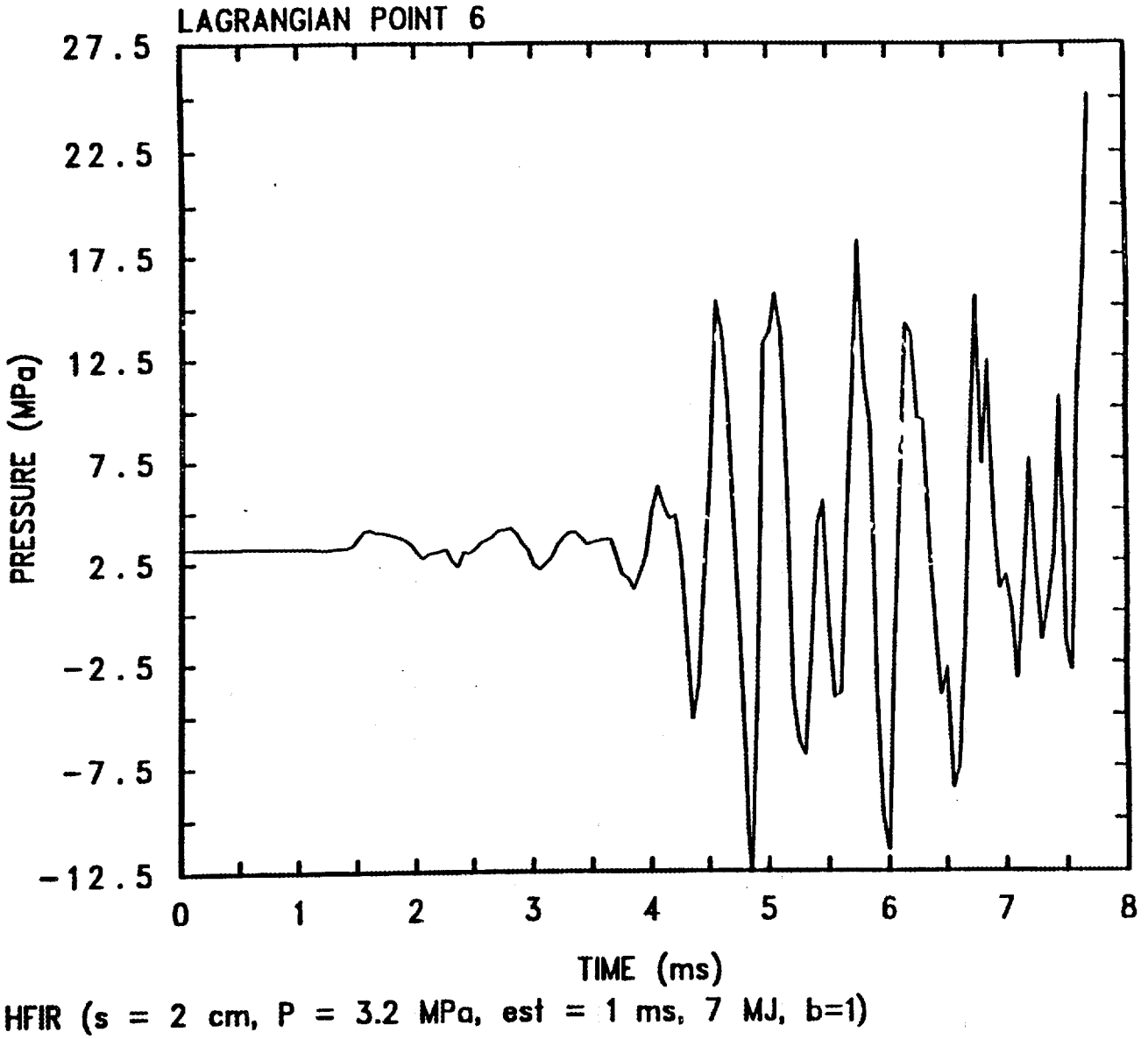

Fig. G.8b Variation of Pressure vs Time for Model 3 (Lagrangian Point 6, 7 MJ Case)

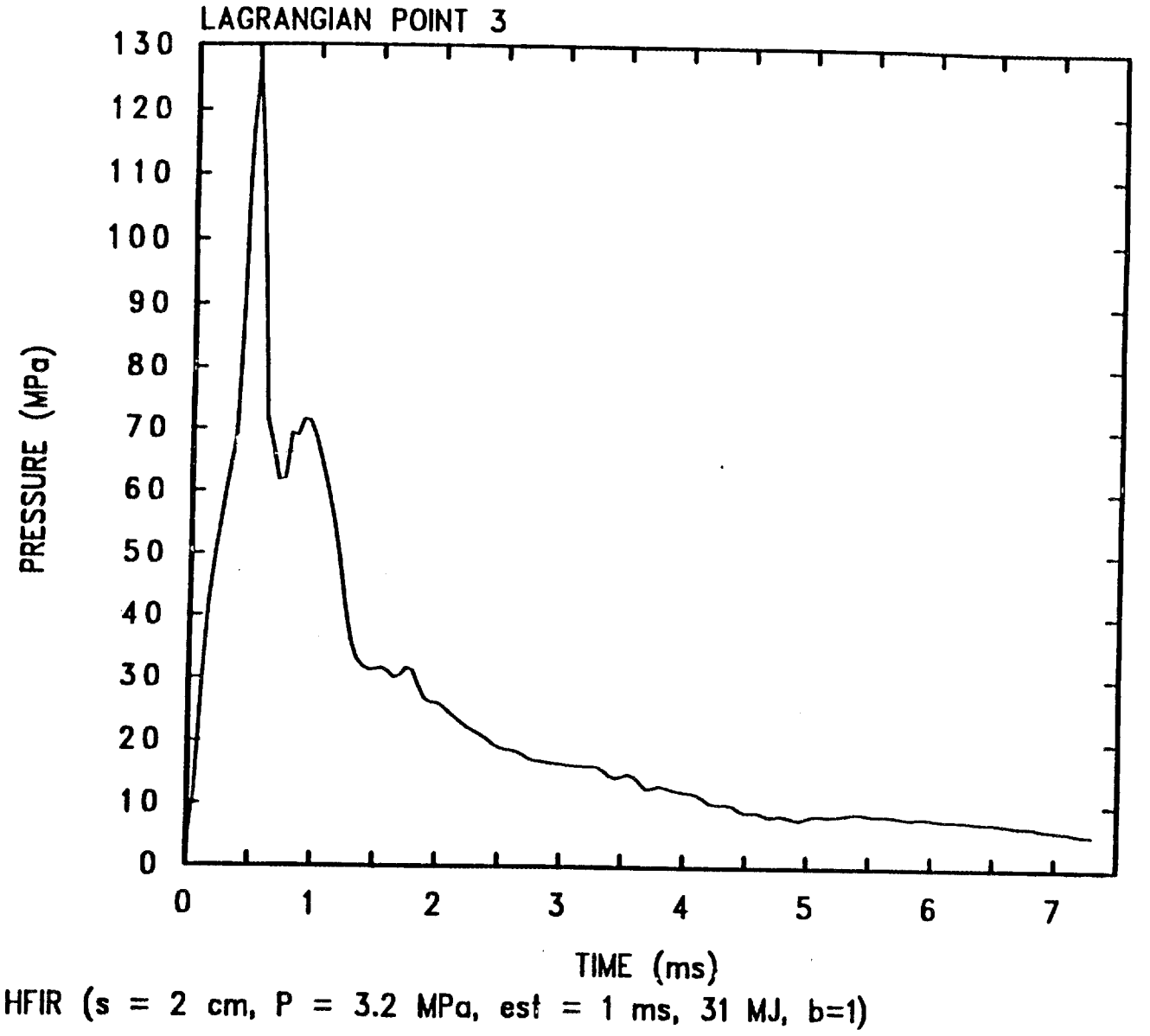

Fig. G.9 Variation of Pressure vs Time in Explosion Zone for Model 3 (Lagrangian Point 3, 31MJ Case)

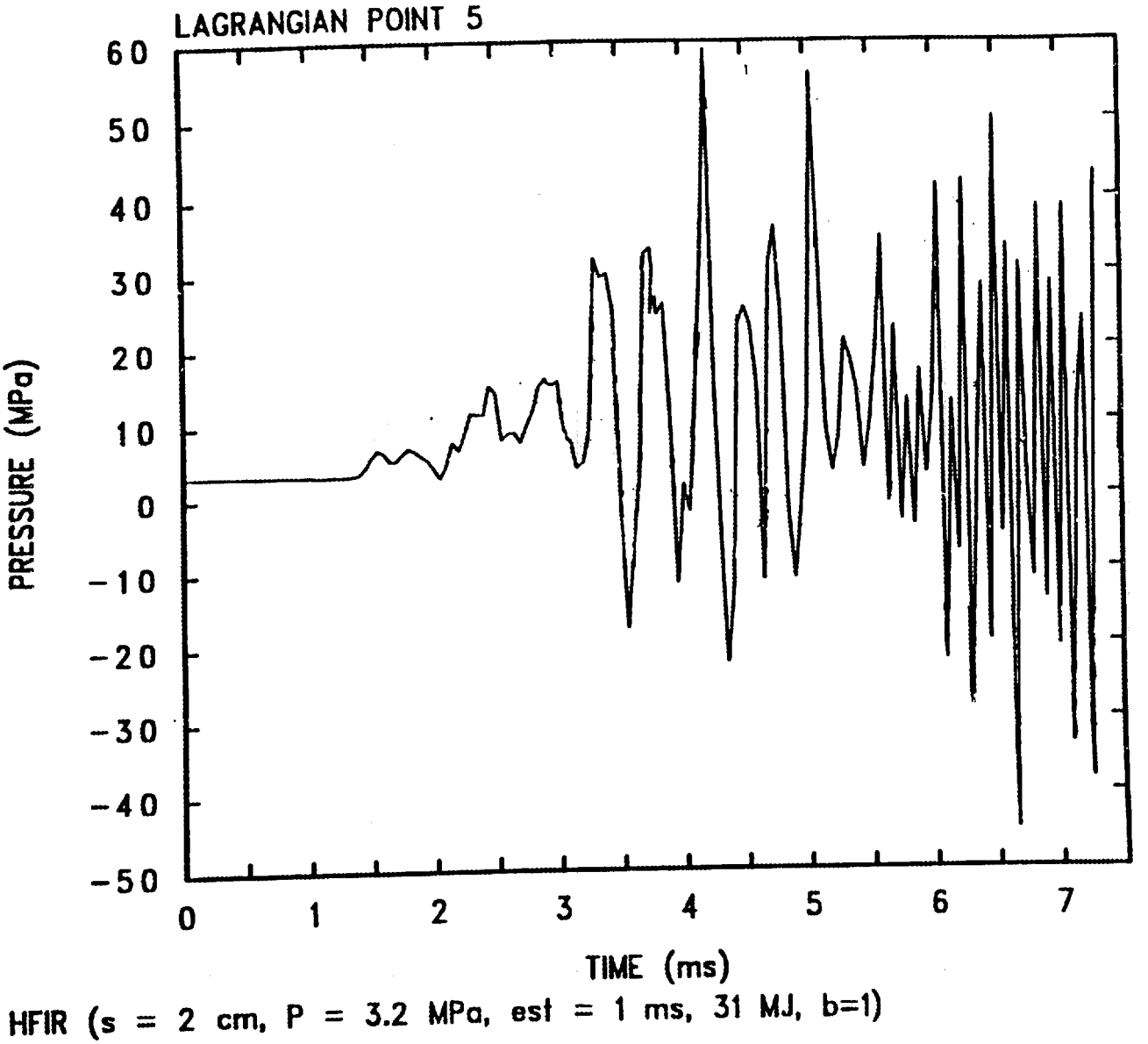

Fig. G.10a Variation of Pressure vs Time for Model 3 (Lagrangian Point 5, 31 MJ Case)

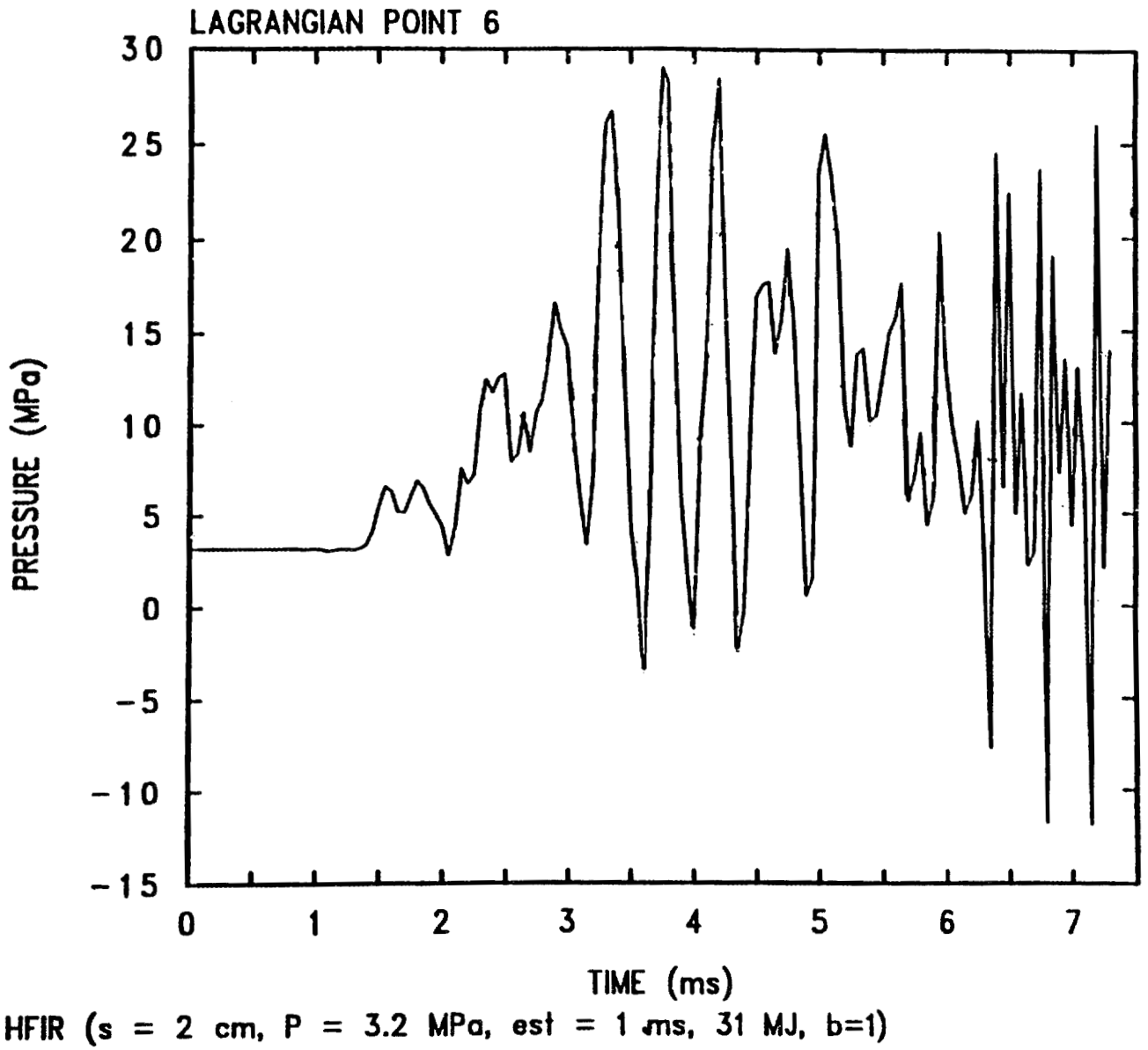

Fig. G.10b Variation of Pressure vs Time for Model 3 (Lagrangian Point 6, 31 MJ Case)

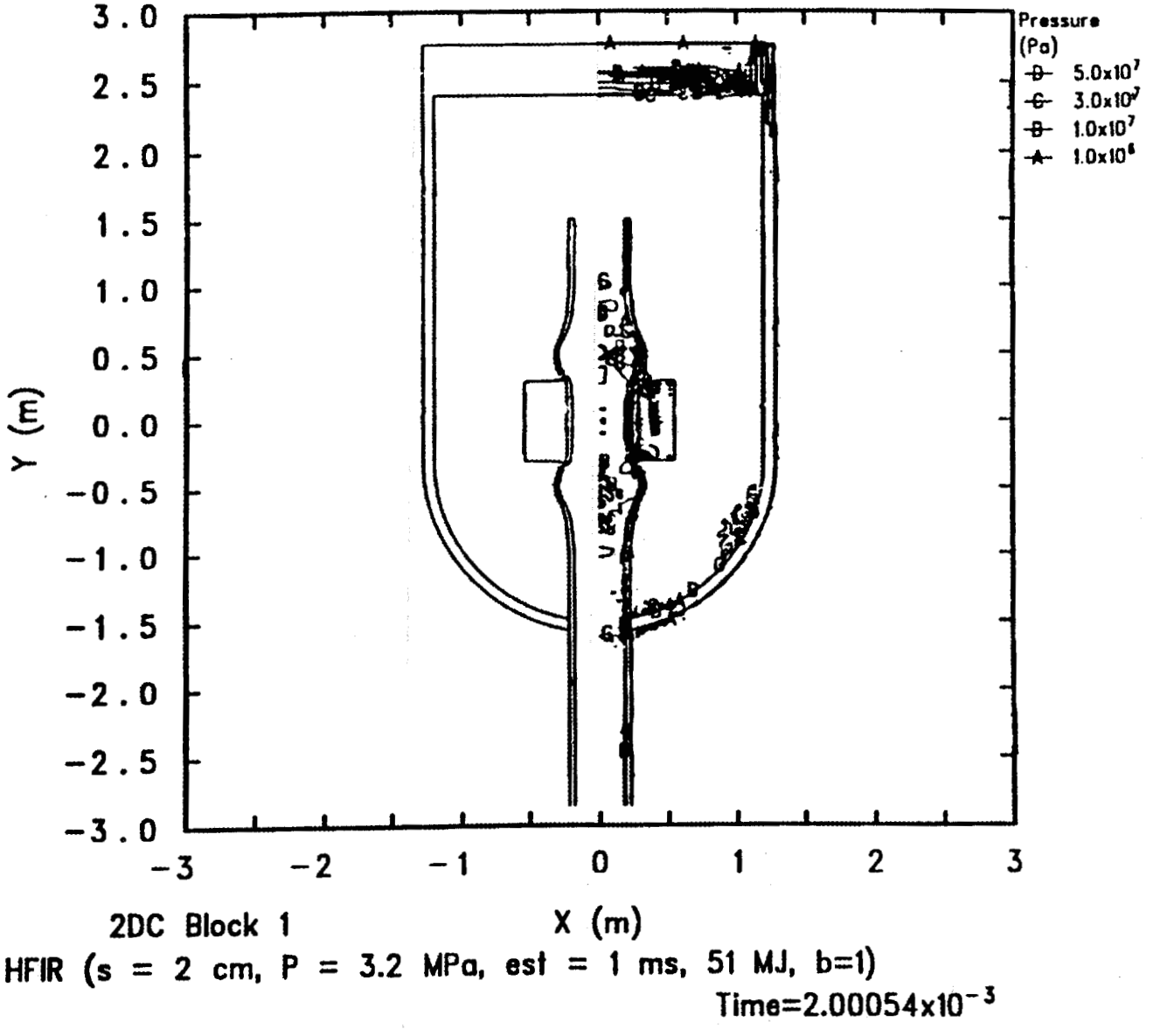

Fig. G.11a Structural Response and Pressure Contour Plots for Model 3 (51 MJ Case, t = 2 ms)

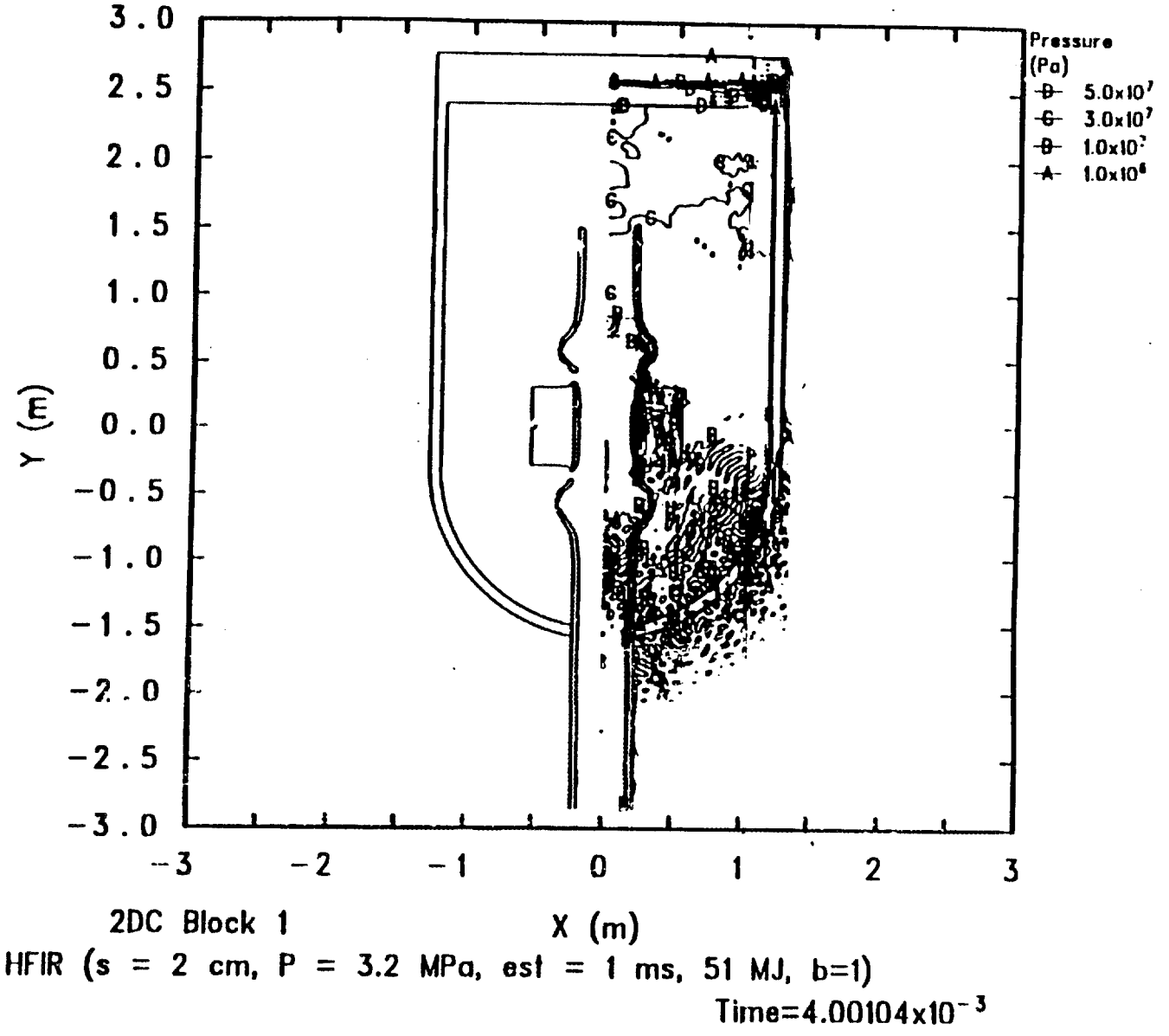

Fig. G.11b Structural Response and Pressure Contour Plots for Model 3 (51 MJ Case, t = 4 ms)

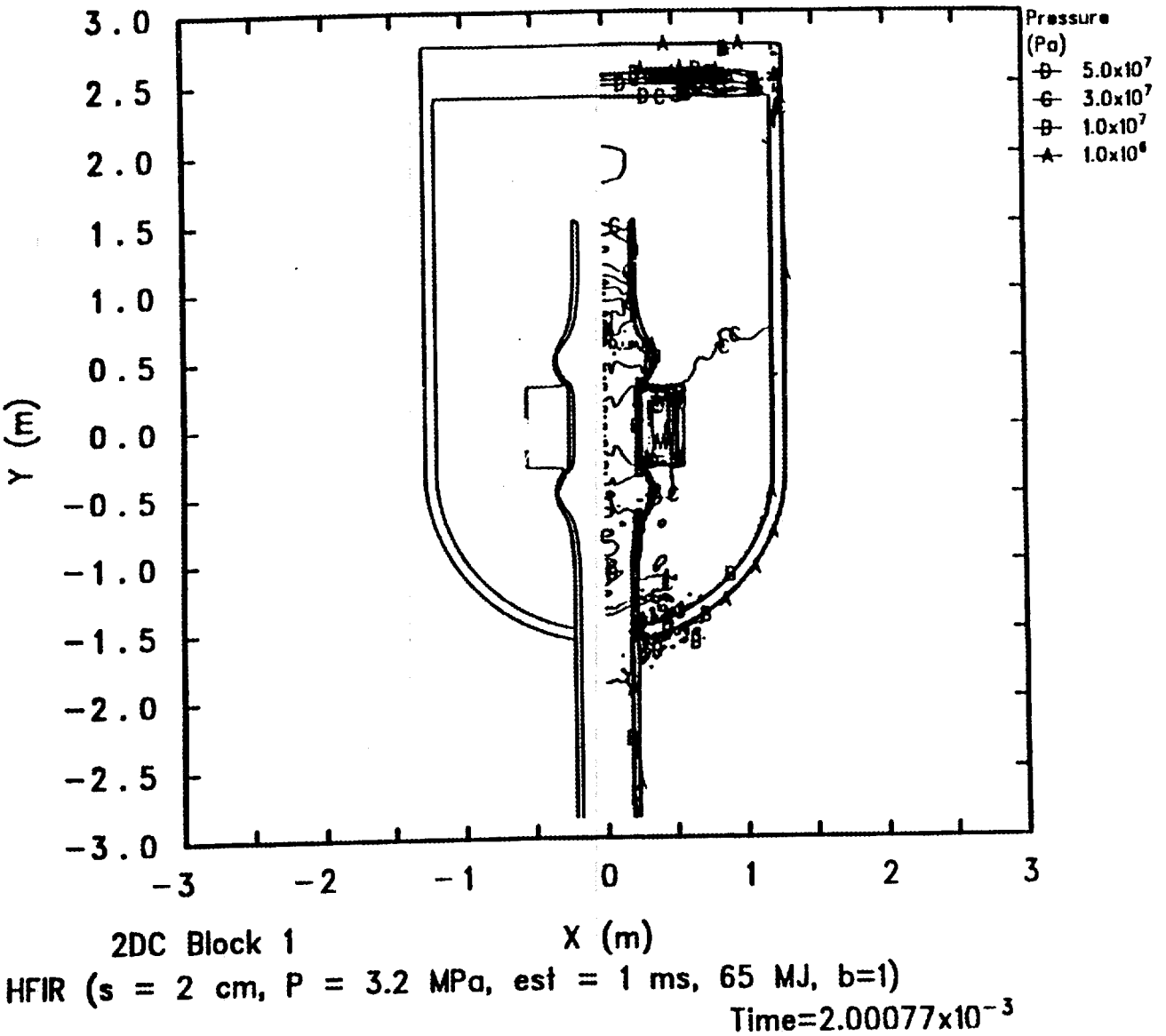

Fig. G.12a Structural Response and Pressure Contour Plots for Model 3 (65 MJ Case, t = 2 ms)

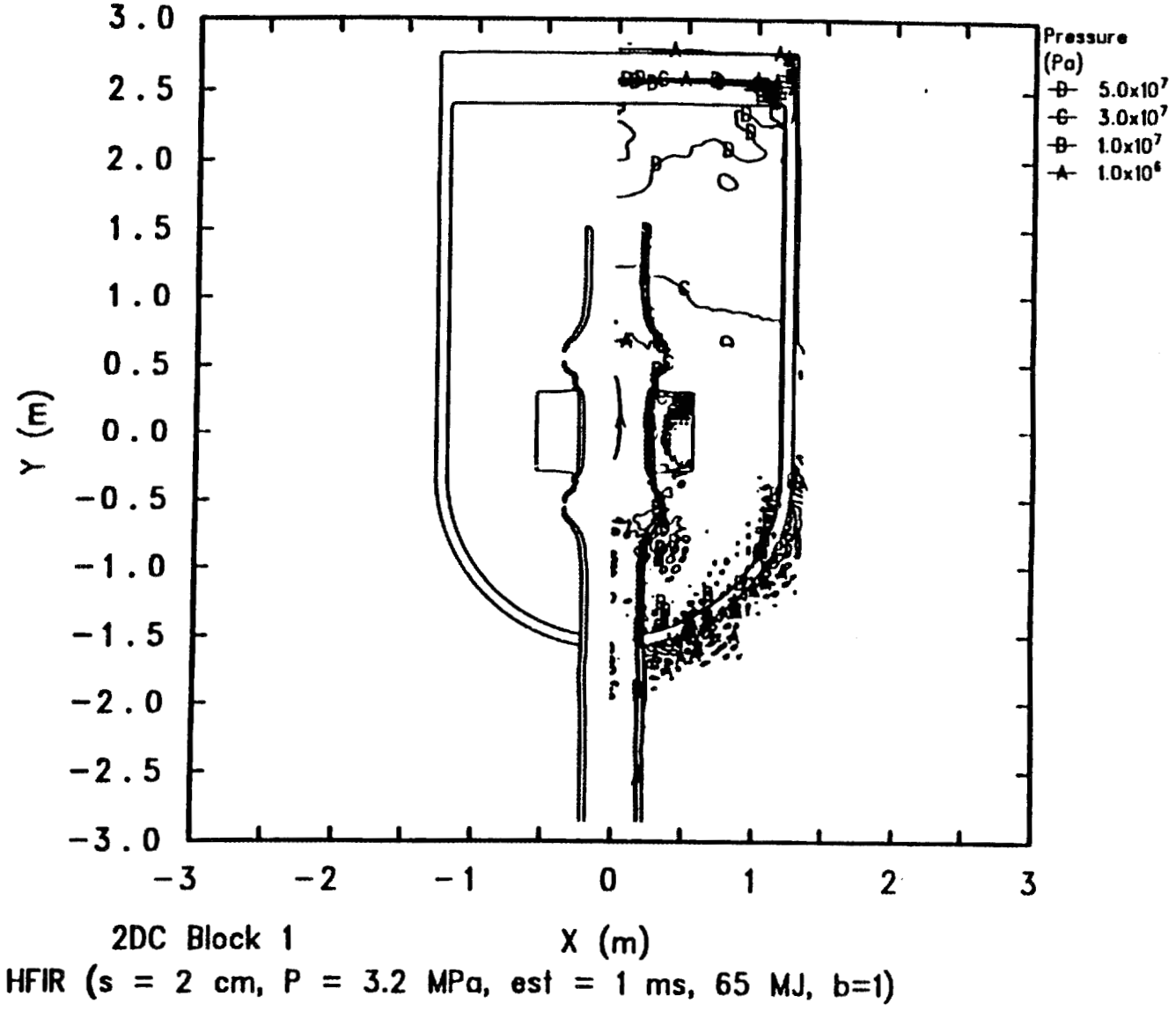

Fig. G.12b Structural Response and Pressure Contour Plots for Model 3 (65 MJ Case, t = 3 ms)

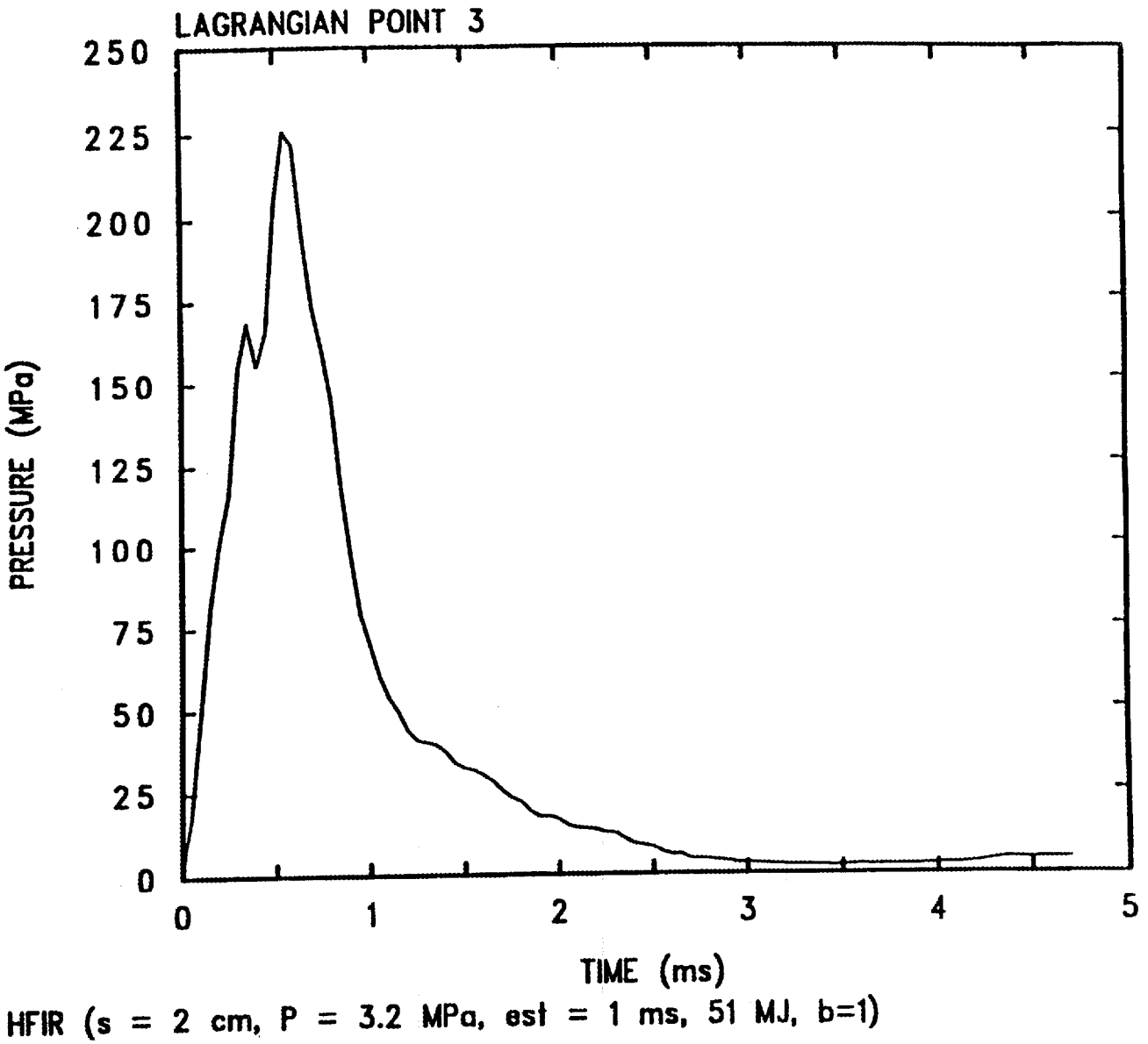

Fig. G.13a Variation of Pressure vs Time in Explosion Zone for Model 3 (Lagrangian Point 3, 51 MJ Case)

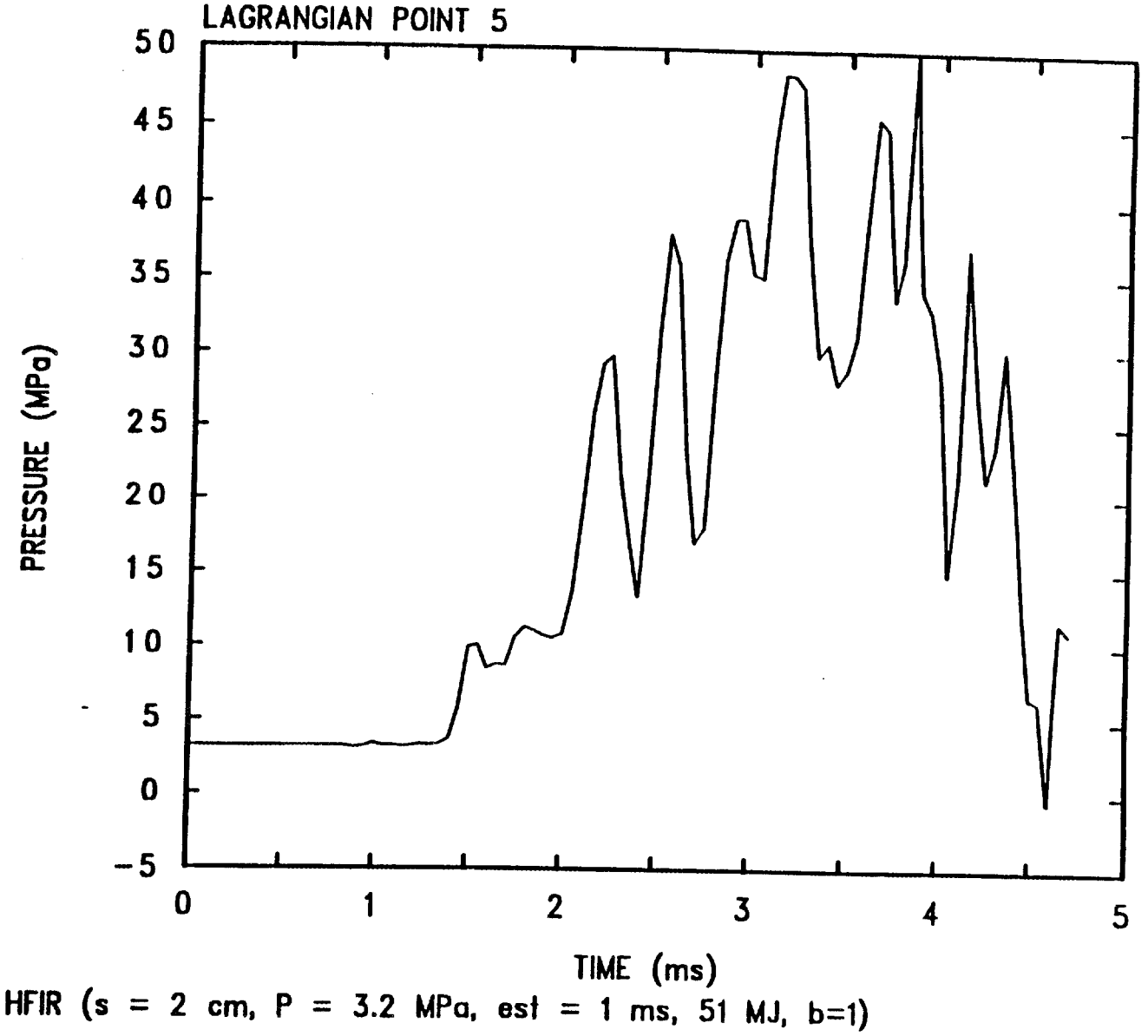

Fig. G.13b Variation of Pressure vs Time for Model 3 (Lagrangian Point 5, 51 MJ Case)

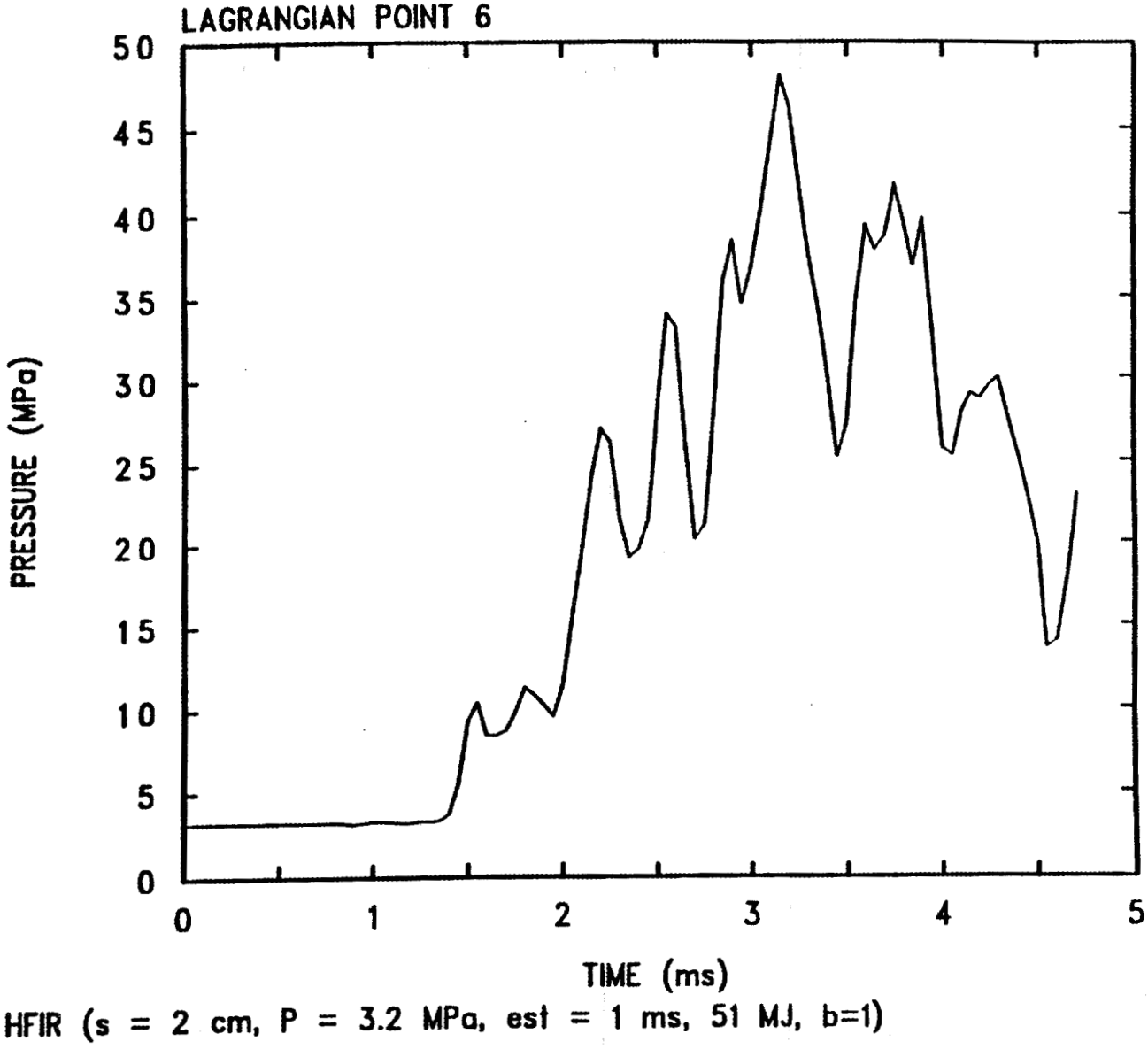

Fig. G.13c Variation of Pressure vs Time for Model 3 (Lagrangian Point 6, 51 MJ Case)

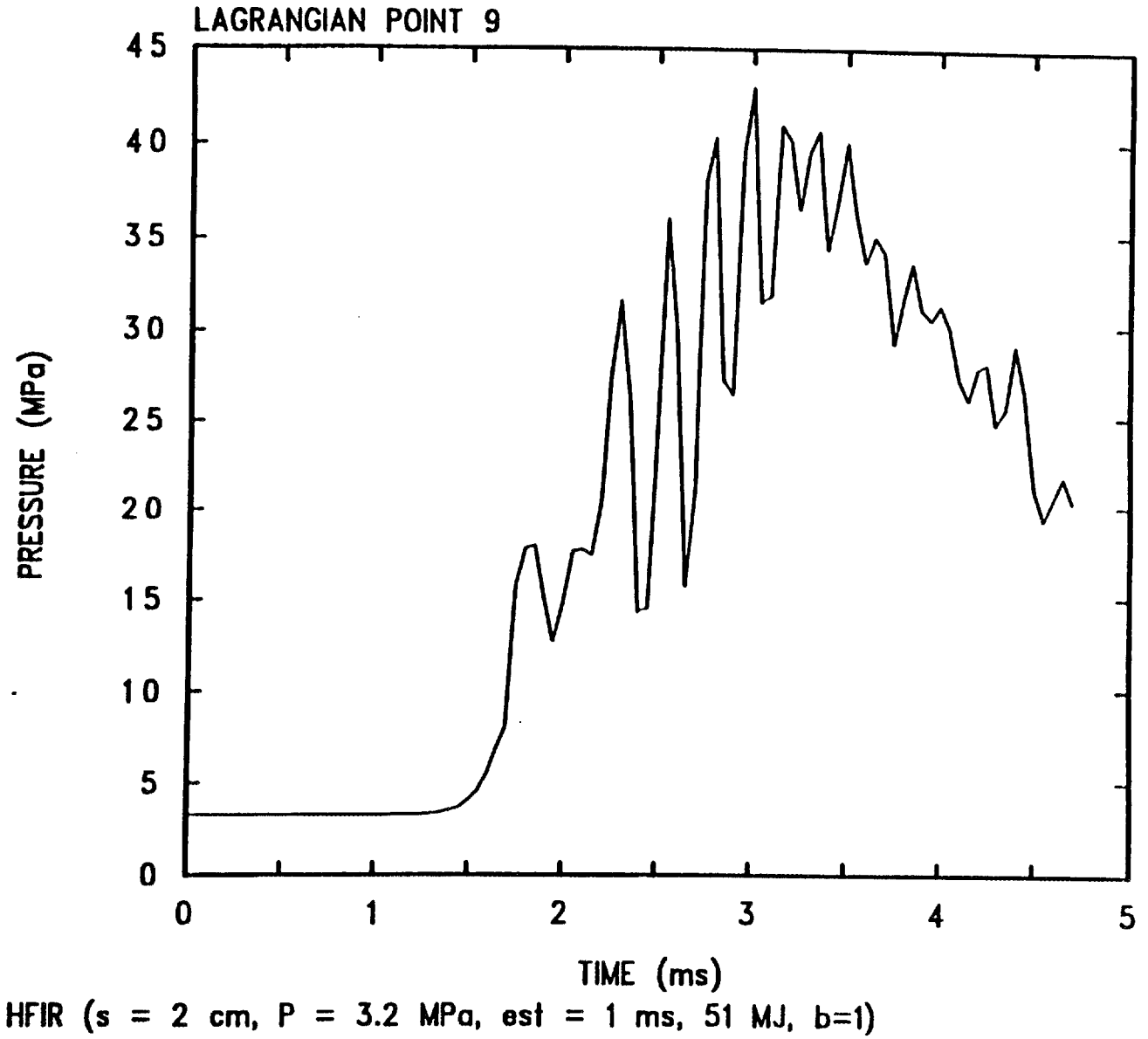

Fig. G.13d Variation of Pressure vs Time for Model 3 (Lagrangian Point 9, 51 MJ Case)

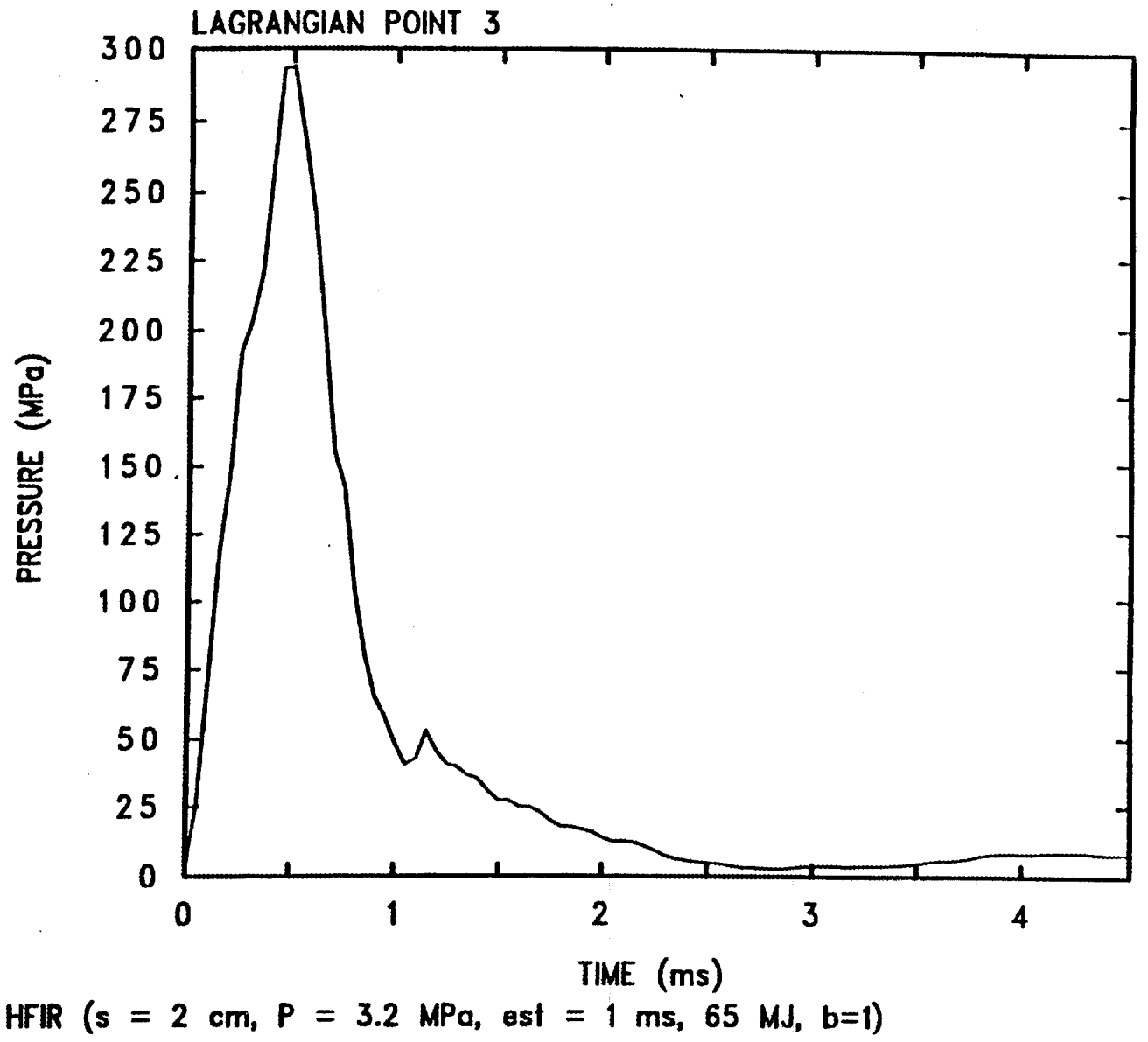

Fig. G.14a Variation of Pressure vs Time in Explosion Zone for Model 3 (Lagrangian Point 3, 65 MJ Case)

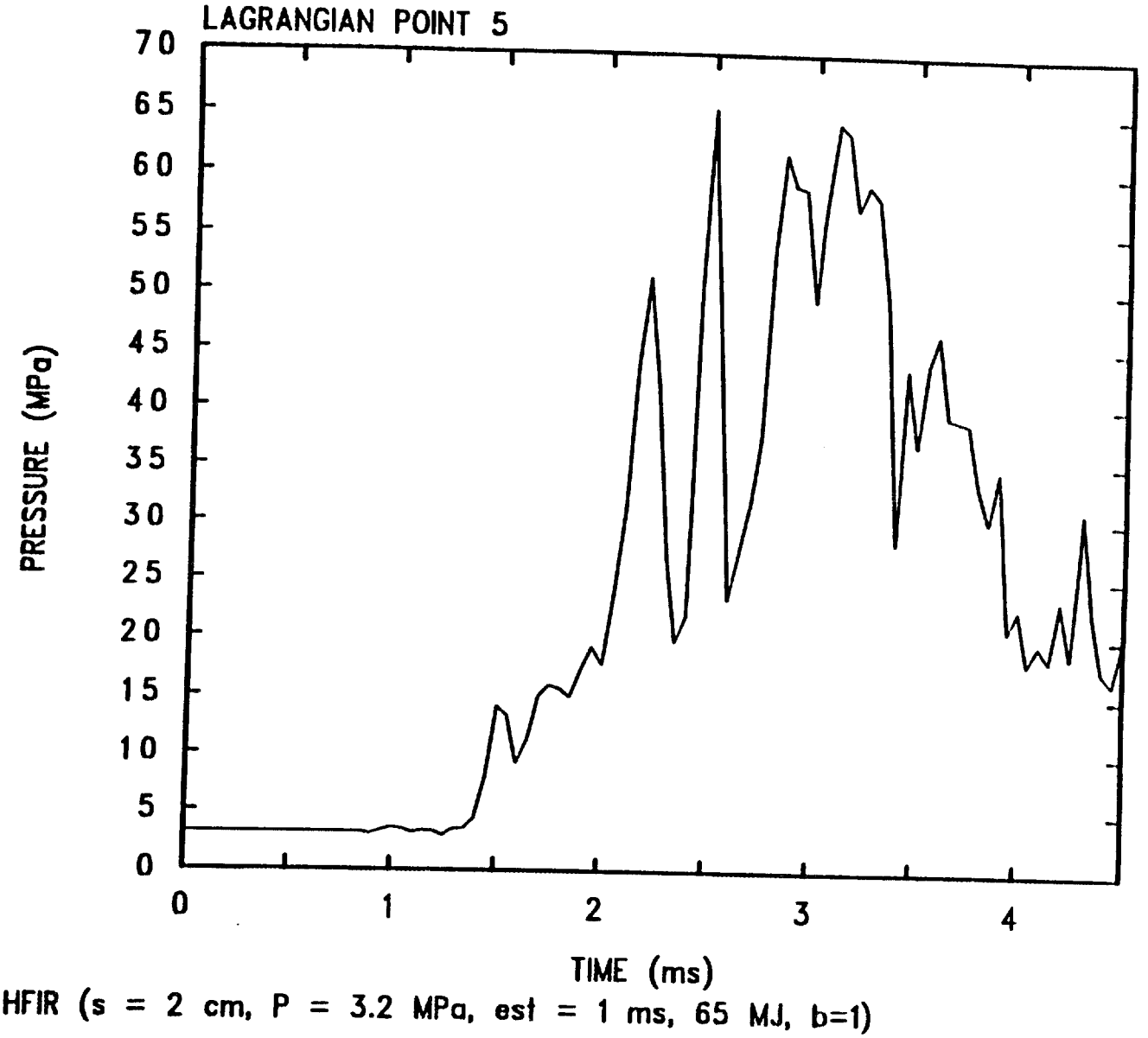

Fig. G.14b Variation of Pressure vs Time for Model 3 (Lagrangian Point 5, 65 MJ Case)

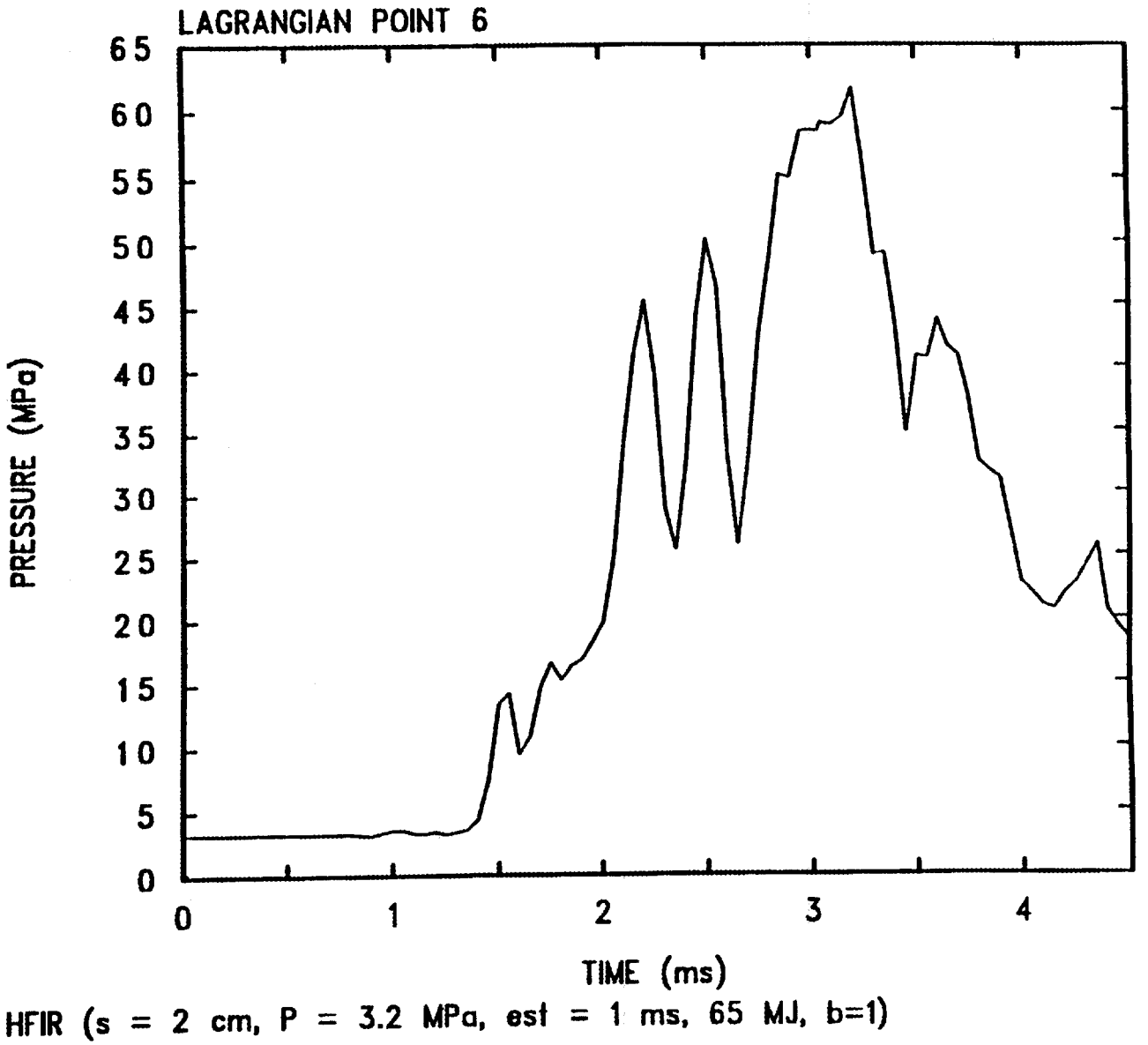

Fig. G.14c Variation of Pressure vs Time for Model 3 (Lagrangian Point 6, 65 MJ Case)

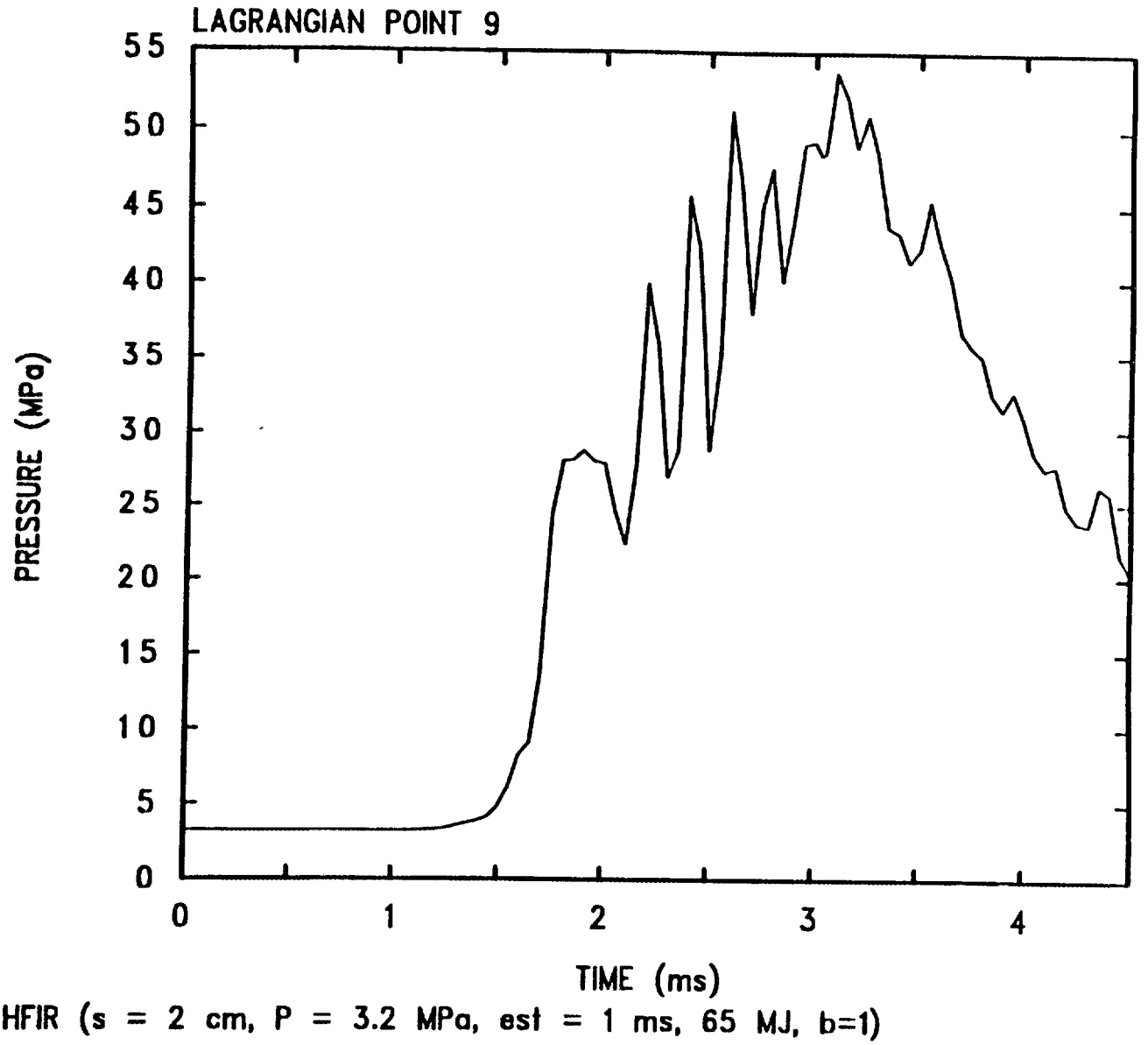

Fig. G.14d Variation of Pressure vs Time for Model 3 (Lagrangian Point 9, 65 MJ Case)

APPENDIX H

Evaluation of Failure Characteristics for HFIR Vessel and Top Head Bolts

During explosion events in the HFIR vessel, it is necessary to know what levels of loads are sufficient to cause vessel failure in order to gauge the potential for confinement damaging missile generation. To evaluate the failure characteristics of the HFIR vessel and top head cover, it was decided to evaluate the necessary loads correlated to steam explosion energetics. That is, for steam explosions occurring in the core region, we wish to evaluate the amount of thermal energy deposition that will lead to enough dynamic pressurization for causing vessel rupture and missile evolution. For this, we need to know failure characteristics of the HFIR vessel in various regions. However, for the sake of evaluating threats from missiles, the most interesting and vulnerable regions are the vessel wall in the vicinity of the top head cover and also the bolts holding down the top head cover onto the vessel. The problem formulation consists of evaluating the dynamic pressure fields in the fluid just below the top head cover all across the radial region. These pressures would then need to be compared to failure stresses in the above-mentioned two regions. This appendix summarizes the work done for evaluating HFIR vessel and top head bolts failure characteristics.

H.1 VESSEL FAILURE CHARACTERISTICS

A detailed study was conducted[35] to evaluate vessel failure characteristics, both from a conservative deterministic sense and from a probabilistic standpoint. Both approaches briefly summarized here utilized the principles of fracture mechanics.

As mentioned above, the dynamic strength of the HFIR vessel to resist hypothetical accidents was analyzed by using the methods of fracture mechanics. Vessel critical stresses were estimated by applying dynamic pressure pulses of a range of

magnitudes and pulse durations. The geometry of the HFIR vessel was modeled using the ADINA[6] code package, with 41 elements in a finite element formulation. Nozzles along the vessel surface were neglected to simplify modeling. A two-dimensional (2-D) formulation was developed as shown in Fig. H.1. Internal pressure is applied uniformly along the inner surface of the vessel, with a square pulse applied suddenly for a range of durations. Pressure pulse magnitude and duration ranges were 0.0 to 17.5 MPa, and 0.0 to 1.0 ms, respectively.

Elastic dynamic ADINA calculations were performed to obtain hoop stress magnitudes at the three locations shown in Fig. H.1. It was found that the effective stress values for the points "a" and "b" are essentially similar. However, for point "d" the effective stresses in the material were seen to be significantly higher. This is to be expected, since point "d" is at a location where significant stress concentrations can occur. Point "d" values are not considered here because in reality the top head is bolted to the vessel. Therefore, for evaluating vessel failure the failure envelopes for the midplane will be taken as being the representative ones. It was also noted that the hoop stress does not vary much across the vessel wall, which indicates the absence of significant bending moments to modify the hoop stress variation. So-called failure envelopes generated are shown in Fig. H.2. These are essentially plots of peak induced stresses in the vessel wall when subjected to an external pressure pulse (y-axis) of a given magnitude (x-axis).

Thereafter, a conservative deterministic estimate was made[34] to evaluate vessel failure loads. This conservative approach was based on ASME guidelines in which a 25.4-mm (1-in.) crack was assumed in conjunction with a factor of safety of 1.0 and an operating temperature of 367 K. This resulted in a failure hoop stress of about 245 MPa (35 ksi). The calculation was based on the evaluation of a fracture toughness of $78\,\mathrm{MPa}\bullet\sqrt{\mathrm{m}}\left(70\,\mathrm{ksi}\bullet\sqrt{\mathrm{in.}}\right)$ based on the original HFIR nill ductility temperature (NDT) of 192 K (-115°F), coupled with a geometric factor of 2.1 based on an analogy with

membrane tension. The allowable hoop stress is then simply a ratio of the fracture toughness to the geometric factor.

If we now look at Fig. H.2, and combine it with the knowledge of the allowable vessel effective/hoop stress of 245 MPa (35 ksi) lasting for more than a millisecond, we note that the largest pressure pulse that can be tolerated is no more than 1.5 ksi (i.e., 10 MPa).

The above-mentioned approach gives rise to conservative estimates for vessel failure loads. To evaluate best-estimate loads required, a probabilistic framework was also developed. The resulting calculation is probabilistic owing to the fact that the crack depths on the vessel surface have been assumed to follow a probability distribution.

A closed form expression to calculate the fracture probability of the vessel containing small fractional number of cracks is derived by applying the weakest link hypothesis for strength or Weibull's method of strength. Weibull's method was developed to estimate the strength of the material by assuming a large number of cracks in a material body. The method was extended to the present case to calculate the fracture probability for a structure under the condition that only a few cracks may exist in the steel vessel. The crack density is much smaller than one. The study of Ref. 35 used the steel embrittlement data obtained from studies made earlier by Cheverton et al.[36] to evaluate the HFIR vessel steel radiation embrittlement condition and the suitability of the reactor to stay in operation. However, it should be stressed that this data base was used in conjunction with dynamic rather than static stresses for the current study (for which the ADINA code was used). The main result of the work presented in Ref. 35 is the calculation of a probability curve which provides the probability of fracture versus the critical stresses generated in the vessel caused by the dynamic pressure pulses. Results are summarized in Fig. H.3. Results of the study showed that [assuming a crack density of 0.0753 cracks/m^2 (0.007 cracks/ft^2)] the probability of fracture is 7×10^{-6} after ten effective full-power years (EFPY) of embrittlement since 1986 for the stress level of 161

MPa (23 ksi). The probability increases to 5×10^{-3} as the stress increases to 518 MPa (74 ksi) which may occur under severe accident loading conditions. If the crack density were higher (viz., unit crack density) the probability for fracture at a given stress level increases proportionally as is clearly seen in Fig. H.3b.

Based on the probabilistic approach results outlined in Fig. H.3, it is seen that the 10-MPa failure pressure [corresponding to a hoop stress of 245 MPa (i.e., 35 ksi)] has a low fracture probability of 10^{-4}. However, for higher values of hoop stresses [viz., >500 MPa (or > 70 ksi)], the corresponding failure pressure rises to about 20 MPa with a much higher fracture probability approaching 10^{-2}.

Several mathematical model development aspects which have been left out can be found in Ref. 35.

H.2 TOP HEAD BOLT FAILURE CHARACTERISTICS

In this section, we describe some of the salient aspects of the relatively simple modeling and analysis aspects related to failure loads evaluation of the top head bolts.

H.2.1 Modeling, Assumptions, and Justifications

To conduct a preliminary analysis of the failure characteristics of the bolts, several key assumptions had to be made. Assumptions along with justifications are given below:

1. For evaluating top head bolt failure characteristics, the top head is represented as a circular disk with a radius of 2.504 m (49.5 in.) and a thickness of 0.356 m (14 in.). According to Ref. 54, the top head is a circular disk with an outside diameter of 2.62 m (103 in.) and a thickness of 0.368 m (14.5 in.). It has a central hole 0.76 m (30 in.) in diameter, in which the quick-opening-hatch cover is inserted. Details of the central

hole region, including the various structural components there, were omitted from the modeling process because of their adding undue complexity of representation. From the standpoint of evaluating failure stresses, we then evaluated the effective area over which the pressure acts. That is, the effective diameter of the top head is calculated as being = Sqrt (103^2 - 30^2) = 2.507 m (99 in.).

2. It is assumed that the 44 bolts that hold the top head in place uniformly absorb pressure loads. Each bolt has a diameter of 0.076 m (3 in.). The 44 bolts are spaced uniformly around the top head as mentioned in Ref. 53. Further, pressure waves generated in the core region are first channelled upward through the circular downcomer region (above the core) before encountering free space in the HFIR vessel. Such channelling would tend to spread the waves uniformly over the top head. The effect of the multitude of penetrations and tubes, etc., that traverse the HFIR vessel is too complex to account for in terms of their effects on travelling shock waves. They would certainly tend to absorb shock wave energies to a certain extent. To what level is difficult to say at this stage. Therefore, neglecting these structures would tend to provide a reasonably conservative basis for evaluating loads on the bolts.
3. Based upon modeling assumptions 2 and 3 mentioned above, the average stress σ_{av} on each bolt is calculated from

$$\sigma_{av} = P\, A_{head}/(N\, A_{bolt}) + \sigma_t, \qquad \text{(H.1)}$$

where P is the pressure, A_{head} is the area of the head, N is the number of bolts, A_{bolt} is the area of a bolt, and σ_t is the pre-existing tension stress in the bolts or studs holding down the top head to the reactor vessel. This pre-existing tension stress arises because of a torque applied to the studs before the top head is bolted in place. We assume that this value remains constant over the life cycle of the reactor. It is further assumed that the

pressure required to break the bolts is that pressure which gives rise to a value of σ_{av} which exceeds the yield stress (σ_y) of the steel bolts. That is, failure will occur if

$$\sigma_{av} > \sigma_y. \tag{H.2}$$

This assumption is based on well-known laws of material behavior which indicate that upon exceeding the yield stress, further loads can lead to plastic deformation. It is recognized that the bolts do not actually break until the ultimate tensile stress is exceeded. However, this assumption is made from the standpoint of conservatism and from taking into account the fact that the HFIR bolts even under normal conditions are under considerable tension, and there may be flaws existing in the materials that could cause stress concentrations.

An important feature of this assumption is related to the time duration of the pressure pulse. As is well-known, permissible material stress levels can increase quite sharply if the duration of the imposed pressure pulse gets smaller and smaller. Such an evaluation would require a dynamic structural analysis. In the absence of such an analysis, we use the results of Ref. 35 (shown as failure curves for the HFIR pressure vessel) to provide guidance on the time duration of pulses necessary after which the failure curve tends to flatten out. A summary of failure curves generated for the HFIR steel vessel is shown in Fig. H.2. As seen in the figure, the failure curves tend to flatten out after the pulse duration exceeds about 0.6 ms. Now, if we note the time duration of pressure pulses on the top head region (best-estimate energetics calculations of Appendix G), we note, for example, that the pulse duration from steam explosions is typically greater than 1.5 to 2 ms for the 51-MJ case. Hence, use of Eq. (H.2) to judge failure of bolts is justified assuming the material response characteristics of the bolts and vessel walls are similar. This aspect remains an unverified assumption, which, based on engineering judgment, should be valid.

H.2.2 Top Head Bolt Failure Loads

With the dimensions of the disk and bolts listed above, and using Eqs. (H.1) and (H.2), we obtain the ratio of effective stress in bolts to pressure

$$\frac{(\sigma a_v - \sigma_t)}{P} = 24.6 \ . \qquad \text{(H.3)}$$

If we take the yield strength and initial tension stress during bolting of the steel bolts from Ref. equal to 840 MPa, and 210 MPa respectively, the pressure required to break the bolts is then about 26 MPa.

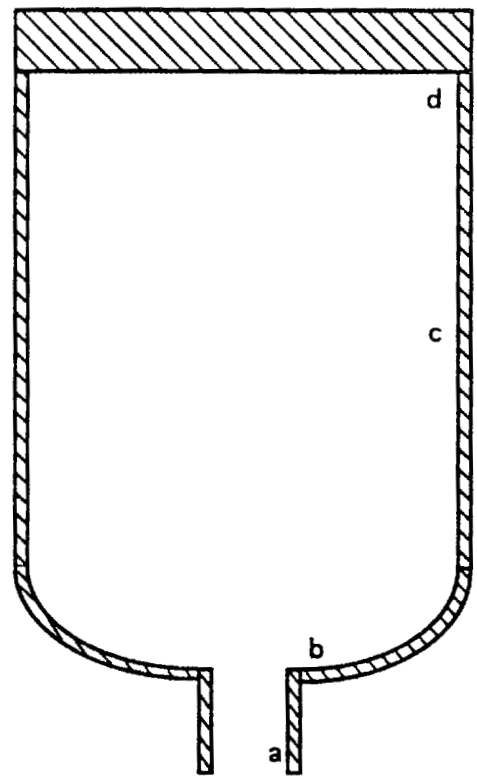

Fig. H.1 ADINA Model of HFIR Pressure Vessel for Dynamic Calculations

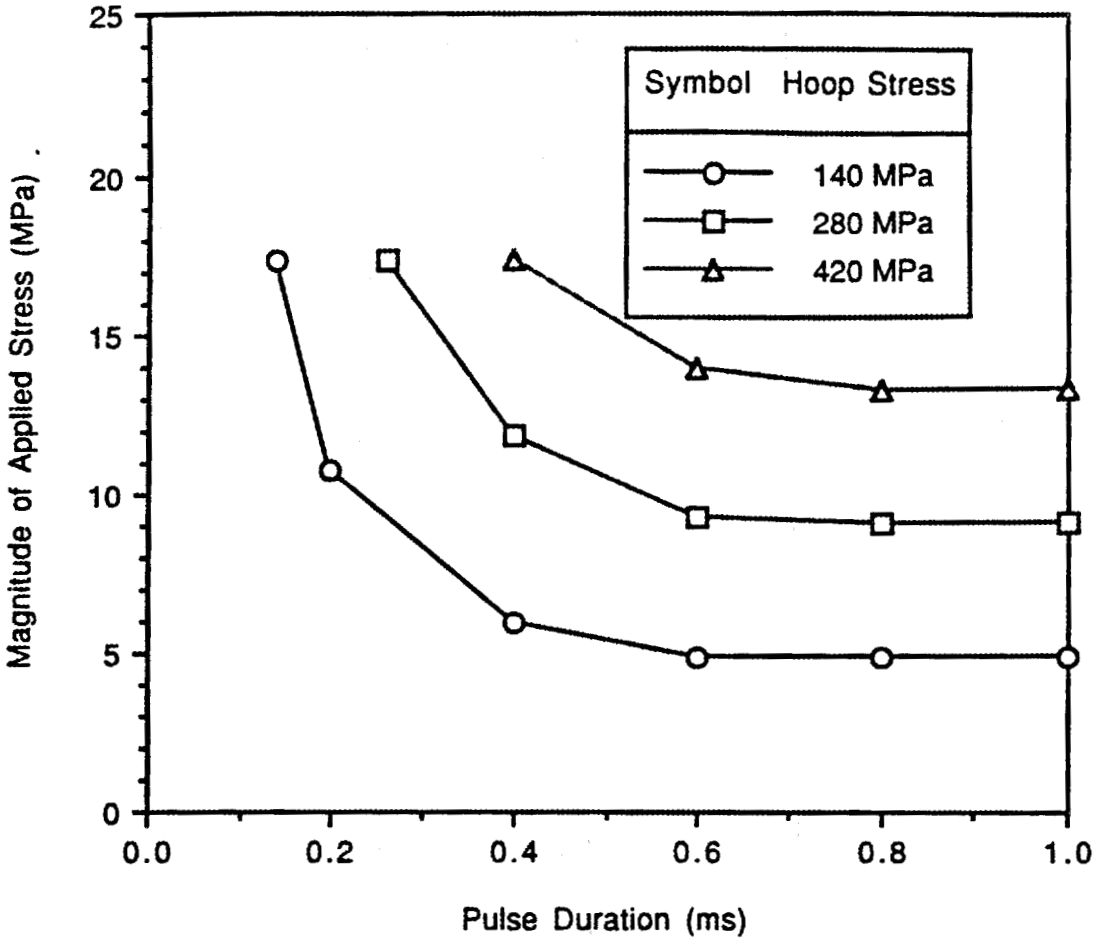

Fig. H.2 **HFIR Vessel Midplane Failure Envelopes**

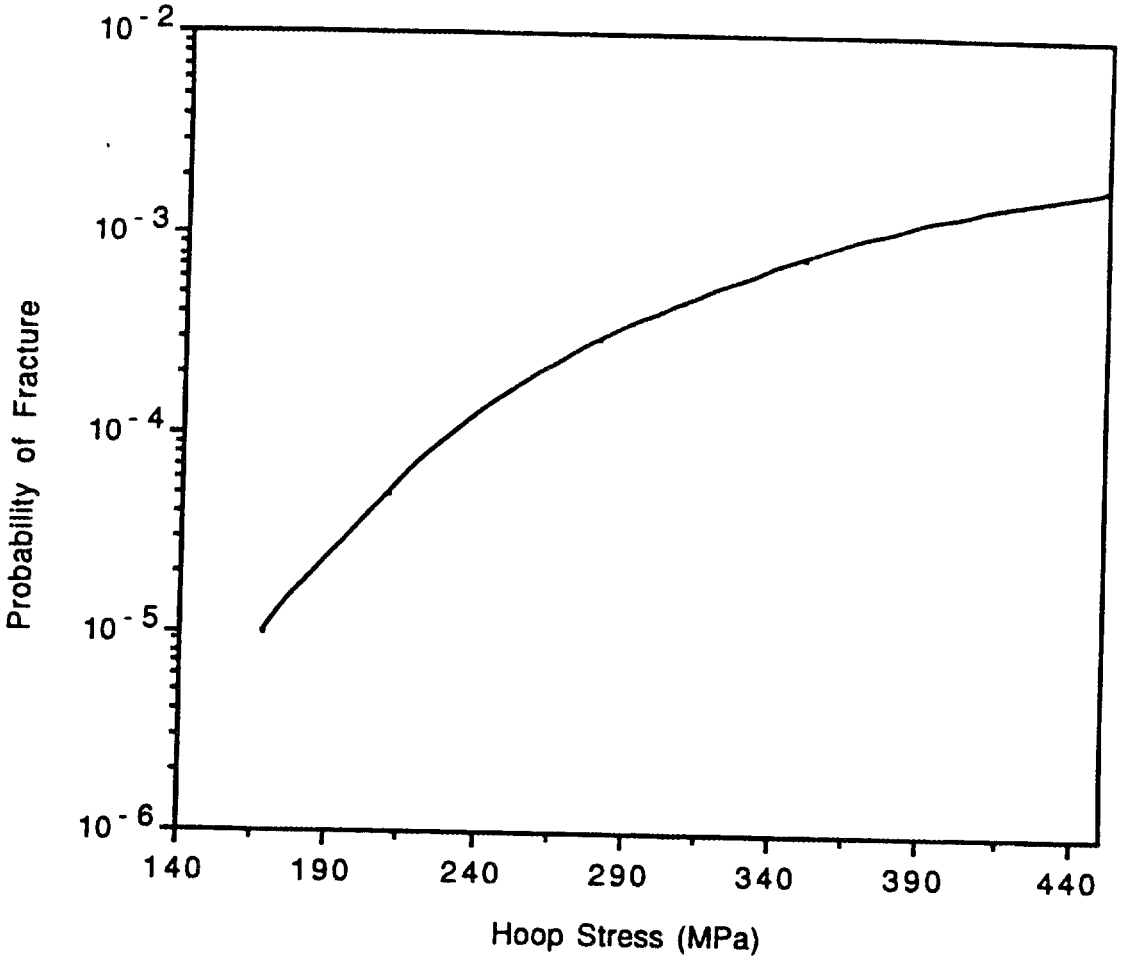

Fig. H.3a Variation of HFIR Vessel Fracture Probability vs Hoop Stress (Crack Density = 0.007 cracks/ft^2)

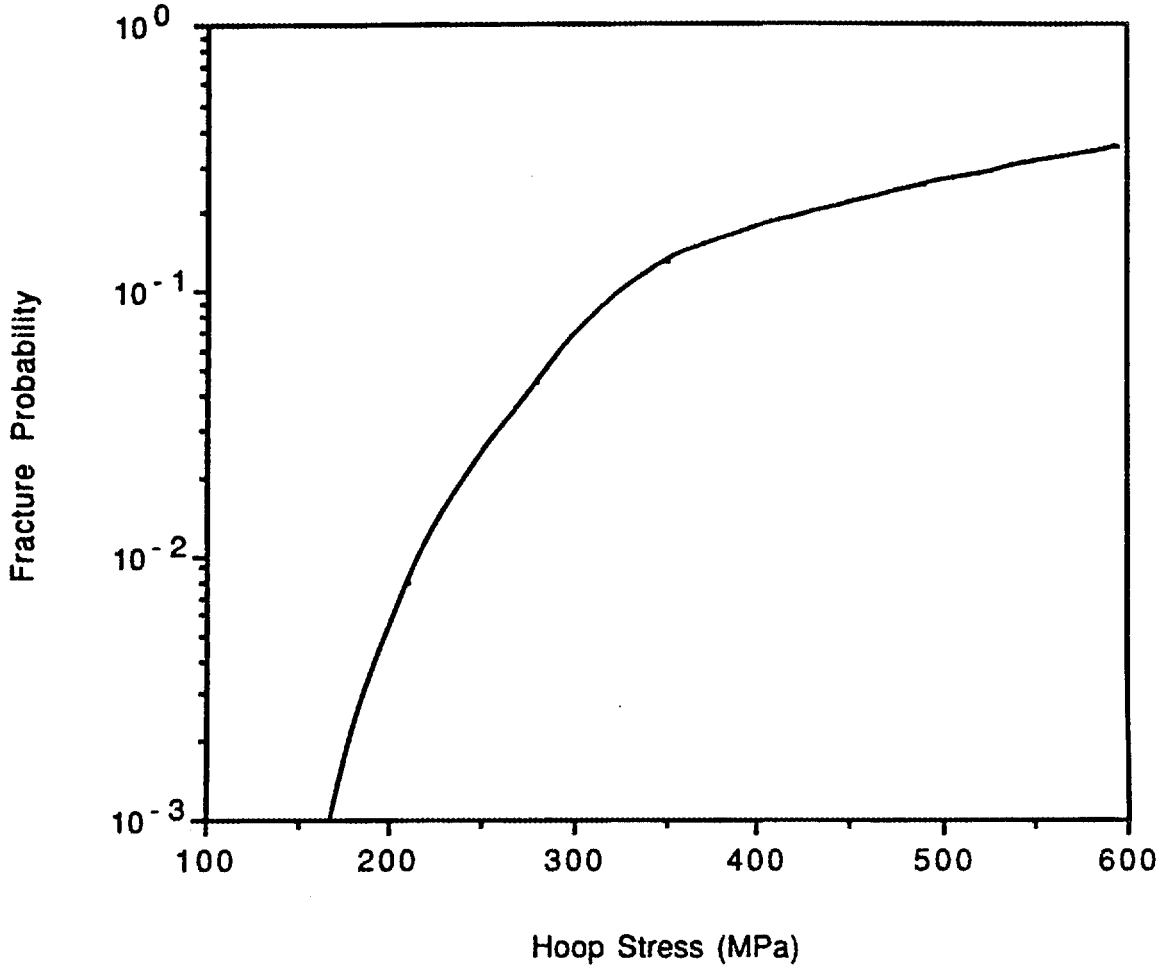

Fig. H.3b Variation of HFIR Vessel Fracture Probability vs Hoop Stress (Unit Crack Density)

APPENDIX I

Missile Transport Modeling and Analysis During Fuel-Coolant-Interaction (FCI) Events in HFIR

During energetic FCI events in the HFIR vessel, missiles may be generated. For the HFIR, that possible missile is the top head of the pressure vessel. This appendix describes salient aspects concerning top head missile transport modeling and analysis.

I.1 MODELING AND ASSUMPTIONS

The model formulation consists of setting up and solving a pair of ordinary differential equations describing the motion of the HFIR vessel top head upward through the reactor pool, upon bolt failure.

It was assumed that the top head can be represented as a circular disk, 2.5 m (8 ft) in diameter and 0.36 m (14 in.) thick, with a density of 8000 kg/m^3, launched upward with an initial velocity. The reactor pool is 4.27 m (14 ft) deep, filled with water with a density of 1000 kg/m^3. As the disk moves upward, it will experience a decelerating force caused by gravity and an accelerating force caused by the buoyancy of the disk. The effective mass of the disk is modeled as equal to the actual mass plus some multiple (Cv) of the mass of the water displaced by the disk. A force balance on the disk can then be written as

$$(m_s + C_v m_w)\, dv/dt = -m_s g + m_w g - 0.5\, C_d\, \rho_w A v^2 \ . \qquad \text{(I.1)}$$

where, m_s is the mass of disk, m_w is the mass of water displaced by disk, g is the acceleration caused by gravity, ρ_w is the density of the water, A is the cross-sectional area of the disk, v is the velocity of the disk, t is time, C_d is the drag coefficient, and C_v is the virtual mass coefficient.

The initial condition for the disk velocity is

$$v(0) = v_o \ , \tag{I.2}$$

where v_o is the initial velocity set as input by the user.

A stand-alone program was written, and Eq. (I.1) was numerically integrated to evaluate the position and velocity of the disk as it traverses through water as a function of time. In addition to the program, an analytical solution was also derived. Details of the derivation process are given in Ref. 50. This analytical solution was used to validate the numerical solution results.

Results were obtained for t_{break} (viz., the time when the disk reaches the top of the surface of the pool), v_{exit} (viz., the velocity of the disk at $t = t_{break}$), and h_{rise} (viz., the height above the reactor pool to which the disk would traverse before descending again). The estimation of h_{rise} was done simply by assuming traverse in a medium with no viscous dissipation which led to the simple expression,

$$h_{rise} = v^2_{exit}/2g. \tag{I.3}$$

Drag coefficients were taken from Ref. 51. The value for C_v is a conservative estimate equal to 0.9. Since the density of water is only one-eighth that of steel, this choice should have only a minor effect on the results.

I.2 RESULTS

With the input parameters mentioned above, the following estimates were made for the break time, exit speeds, and rise height:

Case 1: Drag Coefficient = 1.0

	Initial velocity (m/s) 20.0	35.0
t_{break} (s)	0.33	0.18
v_{exit} (m/s)	8.3	16.9
h_{rise} (m)	3.5	14.6

Case 2: Drag Coefficient = 1.4 (best estimate)

	Initial velocity (m/s) 20.0	35.0
t_{break} (s)	0.40	0.21
v_{exit} (m/s)	5.7	12.6
h_{rise} (m)	1.6	8.2

The initial velocities are estimates calculated from pressure pulses obtained in CTH calculations of FCI energetics as described in Appendix G.

Table D.1 Critical flow velocities for HFIR

Method/method	Element	Critical velocity (m/s)
Miller analogy	Inner	49.8
Miller analogy	Outer	47.1
Chapman*	Inner	77.7
Chapman*	Outer	71.6

*Calculations were done and documented in an internal letter from T. G. Chapman to J. R. McWherther, "Critical Velocity for HFIR Fuel Plates," April 24, 1962.

Internal Distribution List

1.	S. J. Chang	16.	T. S. Kress
2.	D. H. Cook	17.	B. L. Lepard
3.	W. G. Craddick	18.	R. H. Morris
4.	E. C. Fox	19.	D. L. Moses
5.	J. Freels	20.	L. J. Ott
6.	G. Flannagan	21.	J. Richard
7.	U. Gat	22.	D. L. Selby
8.	V. Georgevich	23.	D. B. Simpson
9.	S. R. Greene	24.	J. Stiegler
10.	R. C. Gwaltney	25-26.	R. P. Taleyarkhan
11.	R. M. Harrington	27.	S. Valenti
12.	S. A. Hodge	28.	C. D. West
13.	J. E. Jones Jr.	29.	ORNL Patent Section
14.	S. H. Kim	30.	Central Research Library
15.	J. Kirkpatrick	31-32.	Laboratory Records Department
		33.	Laboratory Records (RC)

External Distribution

30. J. Close, Idaho National Laboratories, P. O. Box 1625, EG&G, Idaho Falls, Idaho 83415
31. M. L. Corradini, Department of Nuclear Engineering, 1500 Johnson Drive, University of Wisconsin, Madison, Wisconsin, 53706-1687
32. F. Eltawila, USNRC, Division of Systems of Research, Office of Regulatory Research, Washington, D.C., 20555
33. M. L. Hyder, SRTC, Westinghouse Savannah River, Co., 1991 South Centennial Avenue, Bldg. 1, Aiken, South Carolina, 29803
34. R. T. Lahey, Nuclear Engineering and Engineering Physics, Rensselaer Polytechnic Institute, JEC 5048, Troy, New York, 12180-3590
35. M. Z. Podowoski, Nuclear Engineering and Engineering Physics, Rensselaer Polytechnic Institute, JEC 5048, Troy, New York, 12180-3590
36. J. Rsyskamp, Idaho National Laboratories, P. O. Box 1625, EG&G, Idaho Falls, Idaho 83415
37. R. Wright, USNRC, Division of Systems of Research, Office of Regulatory Research, Washington, D.C., 20555
38. DOE, Office of Scientific and Technical Information, P.O. Box 62, Oak Ridge, Tennessee 37831
39. AMERD, Richard Egli, U.S. Department of Energy, Oak Ridge Operations Office, P. O. Box 2001, Oak Ridge, Tennessee 37831-8600